ADVANCING THE STUDY OF INTRAMEMBRANE METALLOPROTEASES USING TWO MODELS FROM *BACILLUS SUBTILIS*

By

Daniel D Parrell

A DISSERTATION

Submitted to
Michigan State University
in partial fulfilment of the requirements
for the degree of

Microbiology and Molecular Genetics–Doctor of Philosophy

2019

ABSTRACT

ADVANCING THE STUDY INTRAMEMBRANE METALLOPROTEASES USING TWO MODELS FROM *BACILLUS SUBTILIS*

By

Daniel D Parrell

In recent years the field of intramembrane proteolysis has generated great discoveries about the unique process by which proteins are cut within cell membranes. The intramembrane metalloprotease (IMMP) family of intramembrane proteases has provided a number of excellent models for study in bacteria. The PDZ domain-containing IMMPs, RseP (*Escherichia coli*) and RasP (*Bacillus subtilis*) are the best understood IMMPs, and their study has have laid the groundwork for studying the role of IMMPs in a number of important bacterial pathogens. Work described in this dissertation has advanced the study of RasP. Better methods for heterologous expression of RasP and its substrates in *E. coli* are presented. Site-1 cleavage of the RasP substrate RsiW was required, while the substrate FtsL was cleaved directly in *E. coli*. Importantly, RasP is only the third IMMP to be purified and have *in vitro* activity demonstrated on a substrate (RsiW). Surprisingly, FtsL was not cleaved *in vitro*. The work also advanced knowledge about the cystathione beta synthase (CBS) domain-containing IMMP, SpoIVFB. IMMPs with CBS domains use ATP binding to regulate activity. To test for physiological conditions that change the ATP concentration, a luciferase-based ATP sensor was developed for *B. subtilis*. ATP levels change significantly during sporulation and in response to channels or "feeding tubes" present in *B. subtilis* cells during endospore formation. Interestingly, two different treatments that artificially lower ATP levels to the same extent affected processing of the substrate (Pro-σ^K) differently, suggesting other adenine nucleotides may bind the CBS domain. Indeed, an assay for conformational change upon ATP binding demonstrated that AMP may modulate SpoIVFB conformational changes. Critical residues of the CBS domain were identified by substitutional analysis in *E. coli* and *B. subtilis*, and additional residues of

interest were identified in a suppressor screen. Outstanding questions and future directions related to these projects are presented.

This dissertation is dedicated to my Parents, David and Carol Parrell, who showed me the value of hard work and dedication, and whose unwavering support taught me that I can achieve all things.

ACKNOWLEDGEMENTS

I would like to acknowledge my mentor Dr. Lee Kroos for his constant support during this work. His dedication to helping me grow as a scientist, to the scientific process, and to scientific integrity are what place him among some of the greatest mentors at Michigan State University. He will always be my professional model for taking care of your students, your colleagues, and your friends. Thank you so very much Lee!

I would like to thank my current, and past, mentors and peers for both academics and scientific research. Your guidance leading up to my time at Michigan State University shaped me into the scientist I am today. With each interpersonal interaction we grow and are shaped into more perfect citizens of science. I am honored to have more people to thank that would fit this page.

Finally, I wish to thank my friends and family for their support of (and often times effective distractions from) the work of my dissertation. Without your gentle reminders to experience the world and community around us I would have, no doubt, “worked much too hard.”

TABLE OF CONTENTS

LIST OF TABLES

LIST OF FIGURES

KEY TO ABBREVIATIONS

IMMP Intramembrane Metalloprotease

CBS Cystathione-β-Synthase

PDZ - Post synaptic density protein, Drosophila disc large tumor suppressor, and Zonula occludens-1 protein

ATP Adenosine Triphosphate

ADP Adenosine Diphosphate

AMP Adenosine Monophosphate

MC Mother Cell

FS Forespore

PS Post Starvation

S2P Site 2 Protease

SREBP - Sterol-regulatory element–binding proteins

ECF Extracytoplasmic Function

Mtb *Mycobacterium tuberculosis*

OPM Outer Membrane Protein

IP Immunoprecipitation

TMS Transmembrane Segment

RIP Regulated Intramembrane Protease

MBP Maltose Binding Protein

GFP Green Fluorescent Protein

YFP Yellow Fluorescent Protein

DM n-Decyl-β-D-Maltopyranoside

IPTG Isopropyl β-D-1-thiogalactopyranoside

LB Lysogeny Broth

PBS Phosphate Buffered Saline

Luc Luciferase

FCCP Carbonyl cyanide-4-(trifluoromethoxy)phenylhydrazone

CCCP Carbonyl cyanide m-chlorophenyl hydrazine

PCR Polymerase Chain Reaction

Cm Chloramphenicol

WT Wild Type

FRET Förster resonance energy transfer

SDS-PAGE sodium dodecyl sulfate–polyacrylamide gel electrophoresis

TBST Tris-buffered Saline plus Tween-20

HPR Horse Radish Peroxidase

CHAPTER 1: Lessons from the study of Intramembrane Metalloproteases in Bacteria

Introduction

There are circumstances in biology when gene regulation needs to be so tightly coupled to environmental or physiologic events that global regulators of gene expression are pre-produced and lay in waiting. The time it takes to transcribe and translate a transcription factor from gene to RNA to protein is too long for the required response. Instead, regulators are poised for activation, ready to generate a fast response to external threats and changing conditions, or in order to precisely couple gene expression with signaling cascades. An example of a bacterial system from bacteria includes the extensively studied response to starvation by the stress response sigma factor RpoS in *Escherichia coli* [1]. Under growth conditions RpoS is degraded by the ClpXP protease guided by the Clp-adapter protein RssB [2,3]. Upon entering the stationary phase, repression of RssB allows RpoS to stabilize, promoting global gene expression changes. RssB is regulated by phosphorylation as well as anti-adapter proteins in response to phosphate or magnesium starvation [4,5] and to DNA damage [6]. In the absence of these signals constant expression of RpoS is balanced by ClpXP-induced instability, but modulating any one of these signals has the effect of sequestering RssB and stabilizing RpoS, promoting fast expression of stress response genes. RpoS expression is highly regulated in many ways [1], providing an example of a fast response to external stimuli through posttranslational mechanisms.

In a more complex model for changes in gene regulation, the bacterium *Myxococcus xanthus* uses a network of gene regulation to carry out a fascinating example of coordinated expression changes [7]. During nutrient starvation a developmental process leads to aggregation of cells into mounds, and differentiation of cells in preparation for the production of dormant and highly stress-resistant cells called spores. During sporulation two transcriptional activators MrpC and FruA bind cooperatively DNA to re-program gene expression [8]. Through

cooperative binding MrpC and FruA can achieve more complex regulation of gene expression than either can by binding alone [9,10]. The ability to modulate one or more member of a binding partnership results in the potential for unique arrangements of factors that can quickly control gene expression. Cooperative binding of MrpC and FruA is reminiscent of systems for gene regulation in eukaryotic systems. While not directly homologous, the nuclear receptor protein family in eukaryotes is broadly responsible for directly sensing external signals and translating those into the dimerization of nuclear receptor pairs capable of DNA binding and changes in gene expression [11,12]. Study of nuclear receptor proteins has greatly advanced our understanding of the way eukaryotes achieve rapid changes in gene expression and shows that the requirement for such regulation is common among all forms of life.

A relatively recent breakthrough for fast activation of gene regulation has been established by the discovery of intramembrane proteases. These proteases, in general, activate transcriptional regulators following cleavage of a transmembrane segment of either an inhibitor that tethers the regulator to the membrane, or within the regulator itself. Once processed the regulator is released into the cytoplasm either for further processing, or in some cases directly activating them to alter gene expression. Four families of intramembrane proteases are widely studied, the Rhomboid proteases, the site-2 or intramembrane metalloproteases (IMMPs), the signal peptide peptidases or aspartyl proteases, and the glutamyl proteases [13,14]. The work of this dissertation is focused on the site-2 proteases or IMMPs from bacterial systems.

The first IMMP discovered, in fact the first intramembrane protease discovered, is the namesake protein site-2 protease (S2P), named for the canonical sequence of substrate cleavage events [15]. An IMMP, in most cases, requires a site-1 cleavage event, in the periplasm or extracellular space, prior to the intramembrane cleavage (site-2) by the IMMP. In the case of S2P, cleavage of intramembrane segments in sterol-regulatory element–binding proteins (SREBPs) leads to expression of cholesterol metabolism genes [16]. Following the

discovery of S2P, examples in bacteria were quickly identified. In *E. coli* the protein RseP was discovered and has become one of the best studied IMMPs [17]. Two proteins in *B. subtilis,* SpoIVFB [18,19] and RasP [20], were discovered as well. RasP appears to be a close homolog of RseP and part of the same broad family as S2P. SpoIVFB became the founding member of a new family of IMMPs. Since their discovery intramembrane proteases have been identified in all domains of life driving diverse biological processes and responses.

IMMPs are broadly defined as metalloproteases containing transmembrane helices with metalloprotease (HEXXH) and substrate binding (NPDG) motifs, named for critical amino acid residues that comprise these motifs [19,21]. As mentioned above, site-1 cleavage of an extracellular or periplasmic domain is typically required prior to processing by an IMMP. The signals leading to site-1 processing vary. This variation appears to be a window into the diversification of the physiologic signals to which IMMPs respond. Following site-2 cleavage and release from the membrane, further processing of anti-sigma factors by the ClpXP protease, or other proteases, is required in many bacterial cases. A notable exception to this general model is SpoIVFB. The substrate of SpoIVFB, Pro-σ^K, lacks the requirement for a site-1 cleavage event, and is directly activated by processing. Other notable differences in the SpoIVFB system will be reviewed below.

Despite the advances made in the years since the discovery of IMMPs, a number of questions remain about their regulation, evolution and mechanisms. Several of these outstanding questions will be discussed in the context of model IMMPs well-equipped to address these issues. Questions specifically addressed by work in this dissertation will be emphasized.

IMMPs belong to four broadly conserved classes

In the IMMP class of intramembrane proteases there are four broadly conserved families [21]. The first group are the PDZ (Named for: Post synaptic density protein, Drosophila disc

large tumor suppressor, and Zonula occludens-1 protein) domain-containing proteases such as RseP, S2P, and RasP. PDZ domain-containing IMMPs provide the greatest number of examples from the literature and are by far the best-studied class. PDZ domain-containing IMMPs are the most broadly-distributed among organisms based on available sequences and are defined by the presence of a PDZ domain which aids substrate recognition [22]. Another group, the cystathione-β-synthase (CBS) domain-containing IMMPs, founded by SpoIVFB [18,19], are the second most common in the literature. The only known crystal structure of an IMMP is a CBS domain-containing protein, however the CBS domain was removed from the protein in order to produce crystals [23]. CBS domains commonly drive conformational changes in proteins by binding adenosine-containing molecules [24,25]. The other families of IMMPs are less well known and have potential regulatory domains of unknown function [21]. The work described in this dissertation focuses on advancing knowledge about two IMMPs from *B. subtilis,* the PDZ domain-containing RasP and the CBS domain-containing SpoIVFB.

RseP is the best understood IMMP model

One of the first models in bacteria for the study of intramembrane proteolysis was RseP from *E. coli*. RseP is a PDZ domain-containing IMMP that activates the extracytoplasmic function (ECF) sigma factor σ^E. ECF sigma factors are commonly expressed in response to extracytoplasmic stress. The ECF response deals with unfolded or partially degraded proteins thereby maintaining extracytoplasmic proteins in the presence of extracytoplasmic stressors. In *E. coli*, RseP performs site-2 cleavage of the anti-σ^E protein RseA following site-1 proteolysis by DegS [26,27]. Site-1 processing of RseA happens in response to unfolding and partial degradation of outer membrane proteins (OMPs) during heat shock [28]. Degradation of OMPs is communicated to the site-1 protease (DegS) via a PDZ domain (not to be confused with the PDZ domain of RseP) [29,30]. PDZ domains are widely present protein-protein interaction

domains that play a role in diverse cell signaling processes [22]. Binding of OMP fragments modulates DegS activity on RseA, resulting in site-1 cleavage, preparing RseA for site-2 cleavage. The process by which unfolded OMPs signal site-1 cleavage and initiate site-2 cleavage is perhaps the best understood among the IMMPs.

The PDZ domain of RseP may act as a molecular sieve, excluding RseA prior to site-1 cleavage via size exclusion [31]. RseP contains a tandem repeat of PDZ domains that were reported to recognize DegS cleaved RseA [21,32,33]. However later work showed that RseP simply discriminates substrates sterically by size-exclusion, and not by a specific recognition sequence [31]. The lack of recognition sequence lends support to the novel ability of RseP to clear remnant signal peptides from the membrane [34]. Following DegS processing of rseA, site-2 processing by RseP involves a canonical HEXXH motif that defines part of the zinc-binding active site in IMMPs [19,21]. The importance of the HEXXH motif was demonstrated in RseP using mutational analyses in *E. coli* [17,27]. RseP was the first IMMP to be purified and shown to act on a physiologic substrate *in vitro* [35]. *In vitro* experiments were able to support the understanding that site-1 processing by DegS is required prior to RseP activity, using full-length RseA and truncated forms that mimic site-1 processing [35]. The ability to purify and show activity of an IMMP was a significant breakthrough. Since the work on RseP, activity of SpoIVFB was demonstrated using similar methods [36], and the purification and activity of a third protein, RasP, is demonstrated in this dissertation [37].

Following site-2 proteolysis, σ^E bound by processed RseA is released from the membrane into the cytoplasm [27]. However, ECF gene expression by σ^E is still inhibited by the remaining fragment of RseA. In a process that appears to be well-conserved, the ClpXP protease is required for final degradation of RseA [35,38]. In *E. coli*, the ClpXP adapter protein SspB targets RseA for the final step that leads to active σ^E [38]. This pathway for ECF activation has generated significant fundamental knowledge about how IMMPs are regulated

and process their substrates, and about how downstream gene expression occurs. Ideas and methods used in defining this IMMP model have been essential to the progress described in this dissertation.

RasP, an RseP homolog in *B. subtilis*

Building on the advancements in knowledge gained from RseP, work on the *B. subtilis* homolog RasP (formerly YluC) has accelerated. The anti-sigma factor, RsiW, which inhibits the *B. subtilis* ECF sigma factor σ^W, was the first of four RasP substrates to be discovered [20]. RsiW processing was elucidated by complementating *rasP* mutant *B. subtilis* with either wild-type *rasP* or *rasP* encoding an inactive E21A variant; however, the lack of complementation by *rasP* encoding E21A was unconfirmed due to a lack of antibodies against RasP [20,39]. Site-1 proteolysis is known to occur during envelope stress induced by alkaline shock or antimicrobial peptides [20,40,41]. In response to these stresses the protease PrsW is known to carry out the first step of site-1 processing (on RsiW) needed to allow RasP activity [40,41]. Deviating from what is known about RseA, additional extracytoplasmic processing of RsiW is required following cleavage by PrsW. Bulk proteases in the extracytoplasmic space are proposed to further process RsiW down to near the membrane before RasP cleaveage can occur [42], perhaps as a way to pass a size restriction for entry into the active site of RasP, imparted by its PDZ domain [31]. These results were obtained by heterologous expression of proteins in *E. coli*. However, two caveats of these experiments are that inactive RasP E21A was not used to control for effects of co-expression and that complete degradation or loss of RsiW was observed rather than the expected shortened form [42]. The results would benefit from use of an *in vitro* cleavage assay as well as from the development of a detection method for RasP (e.g., tagging and immunoblotting). Chapter 2 of this dissertation describes such progress [37]. Following RasP cleavage, RsiW must be further processed by the ClpXP and ClpEP proteases before σ^W becomes active [39], much like the case with *E. coli* σ^E.

Since the work demonstrating that RsiW is a substrate of RasP, three additional putative-substrates have been identified. The first is FtsL, which was demonstrated as a substrate concurrently with some work on RsiW [43]. FtsL is involved in regulating cell division, and indeed strains grown with truncated copies of FtsL are shorter than wild-type cells, similar to a RasP mutant [43]. Interestingly, FtsL processing does not appear to require site-1 proteolysis. Co-expression of RasP and full length FtsL does not appear to inhibit proteolysis [44], as is the case with RsiW and RseA. However, FtsL cleavage is inhibited by expression of the cell division protein DivIC [44]. Perhaps a site-1 cleavage like event must occur on DivIC, revealing or releasing FtsL for processing. The question of whether FtsL requires site-1 proteolysis would also benefit from an *in vitro* assay for RasP activity (see Chapter 2). Two other substrates for RasP are less well-studied. RsiV, another anti-sigma factor, is activated in response to lysozyme stress [45,46]. RsiV was demonstrated to directly bind lysozyme, suggesting a potential mechanism for signal transduction [47,48]. Finally, RasP has been implicated in the general process of clearing remnant signal peptide sequences of secreted proteins from the membrane [34], perhaps revealing a housekeeping function of RasP and IMMPs in general.

IMMPS have adapted to promote virulence in pathogenic bacteria

Several important human pathogens appear to use IMMPs to promote virulence. Examples from *Mycobacterium tuberculosis* (Rip1) and *Pseudomonas aeruginosa* (MucP) are reviewed below. Additional IMMPS of human pathogens that promote virulence are, YaeL of *Vibrio cholera* promotes cholera toxin production, Eep of *Enterococcus faecalis* promotes aggregation and biofilm formation and an RseP homolog in *Salmonella enterica* provides acid stress resistance, helping *S. enterica* evade host defenses [49,50]. IMMPs, especially homologs of RseP, seem to have been adapted for virulence mechanisms, possibly as a way to couple virulence with response to host stressors.

Rip1 of *M. tuberculosis*, an IMMP model of an important pathogen: Work on stress responses and virulence in the human pathogen *M. tuberculosis* (Mtb) has revealed an IMMP named Rip1, named for being a regulated intramembrane protease. Rip1 has quickly become one of the best models of an IMMP in a human pathogen. Rip1 was identified as a homolog of other IMMPs (notably RasP and RseP) and was targeted for study based on this homology [51]. Remarkably, Rip1 was required for persistence in the host, which is a hallmark trait that allows chronic Mtb infections [51]. During infection Mtb faces stress from host production of reactive oxygen and nitrogen species, as well as starvation for nutrients such as iron. This finding led to work demonstrating that Rip1 activates not one, but four ECF sigma factors. Much like RasP and RseP, Rip1 processes anti-sigma factors following a site-1 cleavage event, releasing sigma factors from the membrane into the cytoplasm (likely after final degradation of the anti-sigma factor by one or more Clp proteases). Each sigma factor controlled by Rip1 has a unique anti-sigma factor partner, σ^D/RsdA, σ^K/RslA, σ^L/RslA and σ^M/RsmA [52,53]. All four anti-sigma factors require a site-1 cleavage event, however the protease(s) responsible for site-1 cleavage remain unknown. Activation of σ^K and σ^L appears to induce expression of *katG,* an important component of the oxidative stress response, as well as *furA,* an important transcriptional repressor related to oxidative stress [52]. In addition to loss of persistence in the host and blocked oxidative stress response genes by σ^K and σ^L, the absence of Rip1 results in changes in envelope composition and colony morphology [51]. The four sigma factors activated by Rip1 present the possibility of redundant and/or combinatorial expression likely in response to diverse host-derived stress.

Further work on Rip1 and the substrate RsmA, the σ^M anti-sigma factor, has unveiled novel protein-protein interactions that may have broad implications for IMMPs. A proposed adapter protein, Ppr1, appears to couple binding of RsmA to the PDZ domain of Rip1 [54]. Ppr1 accelerates site-2 processing of site-1 cleaved RsmA, and not other substrates or the full length

RsmA. The proposed mechanism suggests that Ppr1 acts as an adapter protein, mediating interactions between the Rip1 PDZ domain and RsmA. This model raises interesting possibilities for other IMMPs. For instance, cleavage of FtsL by RasP appears to require no site-1 cleavage step, however, work described in Chapter 2 of this dissertation shows that we were unable to reconstitute cleavage of FtsL *in vitro* [37]. Perhaps reconstituting cleavage *in vitro* requires an as yet unidentified adapter protein from *B. subtilis*. Further work on Ppr1 may lead to the discovery of other adapter proteins providing critical new understanding about how potential substrates are recognized by IMMPs. Ppr1 is also be an interesting model to study the diversification of IMMP substrates and signal responses. The finding that Ppr1 interacts with the PDZ domain of Rip1 indicates that in this case the PDZ domain does not act simply as a molecular sieve monitoring site-1 cleavage of substrate, as proposed for *E. coli* RseP [31].

MucP of *P. aeruginosa*: MucP is a PDZ-containing IMMP that controls production of alginate and exopolysacharides [55–57], which promote growth as a biofilm. Biofilms of *P. aeruginosa* are of particular concern to individuals with a compromised immune system, such as cystic fibrosis (CF) patients, where *P. aeruginosa* is a major opportunistic pathogen. MucP provides an IMMP model for which there is a uniquely thorough understanding of site-1 proteolysis. An extracytoplasmic sigma factor, AlgU is held inactive at the membrane by the anti-sigma factor MucA [57]. Like other PDZ-containing IMMPS, MucP requires MucA to be processed by a site-1 protease. The site-1 protease for MucA is AlgW [55]. Triggering of site-1 proteolysis occurs in the presence of unfolded proteins in the periplasm and in the presence of antibiotics that target the cell wall [55,58]. The importance of studying site-1 cleavage in *P. aeruginosa* is underscored by the observation that in a number of *P. aeruginosa* clinical isolates *mucA* contains nonsense mutations that cause truncation after the AlgW site-1 cleavage site [56,59]. These truncations mimic site-1 cleavage, allowing MucP to cleave MucA without normal signaling or site-1 cleavage. The result is constitutive alginate production, stronger

biofilms, and more persistent infections. It is likely the advantage gained from producing biofilms that selects for adaptations such as the loss of a requirement for site-1 cleavage.

Additional substrates of MucP regulate iron uptake in *P. aeruginosa.* Production of siderophores, used to scavenge for iron, is regulated by the alternate sigma factors PvdS and Fpv1 [60,61]. These sigma factors are repressed by the membrane bound anti-sigma factor FpvR [62]. FpvR is cleaved by MucP in the membrane after processing by an unknown site-1 protease. FpvR bound to PvdS or Fpv1 is then released into the cytoplasm for further processing and activation of PvdS and Fpv1. In another example the sigma regulators FoxR and FuiR, which regulate the alternate sigma factors FoxI and FiuI respectively, are also substrates for MucP [62]. The site-1 proteases for this system are unknown as well, however the prospect of discovering the upstream regulators for these additional substrates of MucP is exciting. The signals leading to these site-1 cleavage events involve siderophores and iron binding to a cell surface receptor [62]. It is likely that these will be novel signal transduction mechanisms leading to IMMP activity. Because of this deviation from the common signals, MucP provides an interesting portrait of the diversification of IMMP responses.

SpoIVFB, a CBS domain-containing IMMP, is significantly different from other IMMP models

The best understood example of a CBS domain-containing IMMP is the *B. subtilis* protein SpoIVFB. Used to activate gene expression during the late stages of endospore formation, SpoIVFB and its known substrate Pro-σ^K are unique among the IMMPs in the literature. Pro-σ^K is an unusual substrate because it is a sigma factor containing a membrane-associated pro-domain, which inhibits function [63,64]. This is analogous, in function, to the anti-sigma factors of other IMMP models that are cleaved in the membrane and released to the cytoplasm for further processing, usually by the ClpXP protease [49]. Pro-σ^K differs in that once

processed by SpoIVFB it is released from the membrane and immediately active in the cytoplasm [64]. Recently, evidence from *P. putida* revealed an IMMP substrate that contains both the site-1 and site-2 proteolysis sites [65]. These findings suggest that IMMP substrates deviating from the majority may be more common than evidence from the current literature suggests, and argues for continued study of Pro-σ^K processing.

Another difference between SpoIVFB and other IMMP models is in the way SpoIVFB is regulated. Cleavage of Pro-σ^K does not require site-1 cleavage prior to processing by SpoIVFB. Instead SpoIVFB is directly inactivated by two proteins, SpoIVFA and BofA [66–70]. Degradation of SpoIVFA and BofA is required to allow SpoIVFB activity [71–74]. This results in a seemingly flipped model where a site-1 cleavage-like event must occur in the inhibitors of SpoIVFB rather than its substrate, before a site-2 cleavage-like event can occur in Pro-σ^K. Studying these inhibitors of SpoIVFB will likely lead to important breakthroughs in understanding IMMP regulation, and may lead to the development of strategies aimed at inhibiting their activity.

Another form of regulation of SpoIVFB is provided by its CBS domain. Previous work has shown that SpoIVFB activity requires ATP [36]. Additionally, in an experiment where the CBS domain of SpoIVFB was incubated with ^{32}P-labeled ATP, a monomer form of the CBS domain was observed to bind ATP under non-denaturing PAGE conditions [36]. A better understanding of the critical residues in the CBS domain and how they affect ATP binding is needed, and this is the topic of research described in Chapter 4. Recently, efforts to model the enzyme-substrate complex formed between catalytically-inactive SpoIVFB and Pro-σ^K have provided important insights into their possible interaction surfaces [75]. This work was made possible by purification of the complex, and several different approaches suggested the complex is composed of four SpoIVFB monomers and two Pro-σ^K monomers [76]. Even more recent evidence suggests that an F66A substitution locks SpoIVFB into an open conformation promoting unregulated proteolysis of Pro-σ^K even in the presence of BofA and SpoIVFA [77].

An important outstanding question is how ATP binding to the CBS domain contributes to SpoIVFB regulation. CBS domains commonly induce conformational changes in the proteins they regulate [24,25]. It has been proposed that extensive interaction between SpoIVFB and Pro-σ^K allows coordination between ATP binding by the SpoIVFB CBS domain and Pro-σ^K cleavage by the SpoIVFB membrane domain [75]. Chapter 3 and 4 present new insights into the role of adenine nucleotides in regulating SpoIVFB activity.

The timing of SpoIVFB expression during sporulation correlates with the production of a set of channel proteins that span the mother cell (MC) and forespore (FS) membranes during endospore formation [78]. These channels were deemed "feeding tubes" because they are required for gene expression in the FS compartment after engulfment, even by expression of the exogenous T7-RNAP [79,80]. These channels are composed of a multi-protein complex in the MC membrane interacting with a pore-forming protein in the FS membrane. The MC complex has homology to bacterial secretion systems, contributing to the leading hypothesis that the MC actively provides essential molecules to the FS [79,81]. It is interesting to consider whether these channels provide metabolites to the FS during sporulation in a way that affects the ATP concentration in the MC, and whether this may constitute a signal to the CBS domain of SpoIVFB. Chapter 3 describes the development of an *in vivo* ATP sensor to measure relative ATP concentrations in the MC and FS, which provided new insights into the role of the channels and energetics, as well as the role of ATP in regulating SpoIVFB activity. Understanding how these roles are connected will provide novel paradigms about how cellular events can be communicated to an IMMP.

Less well-understood models from *B. subtilis*

In addition to genes encoding *spoIVFB* and *rasP*, the *B. subtilis* genome contains two other IMMP-encoding genes, *yydH* and *ywhC*. There is no known function for YwhC, and no conserved domain architecture is present in its coding sequence other than the HEXXH and

NPDG motifs. YydH, however, has been implicated in the response to lysozyme stress [82]. The genes of the *yyd* operon encode an ABC transporter which appears to work in concert with a two-component regulator, LiaRS. Together these processes function to export YydF, a peptide that elicits cell envelope stress [82]. More recently, YydG was shown to be a two [4Fe–4S]-cluster radical S-adenosyl-L-methionine (SAM) dependent enzyme that converts L-amino acids in YydF to the D-form [83]. These D-amino acids are necessary for bioactivity of the modified YydF peptide, which inhibits growth of *B. subtilis* and induces expression of LiaRS, a two-component signal transduction system that senses cell-envelope stress and presumably activates genes whose products respond appropriately. To fully understand the role of Yyd proteins in envelope stress response, further work must be done. These examples from *B. subtilis* demonstrate that while we understand the processes and physiologic responses for PDZ- and CBS-domain containing IMMPs fairly well, we have limited knowledge about additional IMMP models.

Conclusions

IMMPs control a wide range of processes and are present in nearly all forms of life [49]. Through their study important fundamental knowledge has been gained about how IMMPs control gene expression in a wide variety of ways. Additionally, IMMP researchers have generated a number of tools useful not only for studying these proteases, but broadly for studying membrane proteins and gene regulation as well. This dissertation describes advances in the study of two IMMPs, RasP and SpoIVBF. I have demonstrated *in vitro* activity of RasP and addressed outstanding questions about RasP and its substrates, as well as generated some new questions. I have explored the role of ATP binding to the SpoIVFB CBS domain and how events during sporulation may be integrated with SpoIVFB activity by virtue of modulating cellular adenine nucleotide levels. Through my studies, I have advanced the field of IMMP research by generating new tools and fundamental knowledge.

REFERENCES

REFERENCES

1. Battesti A, Majdalani N, Gottesman S. The RpoS-mediated general stress response in *Escherichia coli*. Annu Rev Microbiol. 2011;65: 189–213. doi:10.1146/annurev-micro-090110-102946

2. Schweder T, Lee KH, Lomovskaya O, Matin A. Regulation of *Escherichia coli* starvation sigma factor (sigma s) by ClpXP protease. J Bacteriol. 1996;178: 470–6.

3. Muffler A, Fischer D, Altuvia S, Storz G, Hengge-Aronis R. The response regulator RssB controls stability of the sigma(S) subunit of RNA polymerase in *Escherichia coli*. EMBO J. 1996;15: 1333–9.

4. Bougdour A, Gottesman S. ppGpp regulation of RpoS degradation via anti-adaptor protein IraP. Proc Natl Acad Sci U S A. 2007;104: 12896–901. doi:10.1073/pnas.0705561104

5. Groisman EA, Bougdour A, Tu X, Gottesman S, Latifi T. The PhoP/PhoQ two-component system stabilizes the alternative sigma factor RpoS in *Salmonella enterica*. Proc Natl Acad Sci. 2006;103: 13503–13508. doi:10.1073/pnas.0606026103

6. Merrikh H, Ferrazzoli AE, Bougdour A, Olivier-Mason A, Lovett ST. A DNA damage response in *Escherichia coli* involving the alternative sigma factor, RpoS. Proc Natl Acad Sci U S A. 2009;106: 611–6. doi:10.1073/pnas.0803665106

7. Kroos L. highly signal-responsive gene regulatory network governing myxococcus development. Trends Genet. 2017;33: 3–15. doi:10.1016/J.TIG.2016.10.006

8. Mittal S, Kroos L. A combination of unusual transcription factors binds cooperatively to control *Myxococcus xanthus* developmental gene expression. Proc Natl Acad Sci U S A. National Academy of Sciences; 2009;106: 1965–70. doi:10.1073/pnas.0808516106

9. Mittal S, Kroos L. Combinatorial regulation by a novel arrangement of FruA and MrpC2 transcription factors during *Myxococcus xanthus* development. J Bacteriol. American Society for Microbiology Journals; 2009;191: 2753–63. doi:10.1128/JB.01818-08

10. Son B, Liu Y, Kroos L. Combinatorial regulation by MrpC2 and FruA involves three sites in the fmgE promoter region during *Myxococcus xanthus* development. J Bacteriol. 2011;193: 2756–66. doi:10.1128/JB.00205-11

11. Tata JR. Signalling through nuclear receptors. Nat Rev Mol Cell Biol. 2002;3: 702–710. doi:10.1038/nrm914

12. Evans RM, Mangelsdorf DJ. Nuclear receptors, RXR, and the Big Bang. Cell. 2014;157: 255–66. doi:10.1016/j.cell.2014.03.012

13. Urban S. Mechanisms and cellular functions of intramembrane proteases. Biochim Biophys Acta - Biomembr. 2013;1828: 2797–2800. doi:10.1016/J.BBAMEM.2013.07.001

14. Brown MS, Ye J, Rawson RB, Goldstein JL. Regulated intramembrane proteolysis: a control mechanism conserved from bacteria to humans. Cell. 2000;100: 391–8. doi:10.1016/S0092-8674(00)80675-3

15. Rawson RB. The SREBP pathway — insights from insigs and insects. Nat Rev Mol Cell Biol. 2003;4: 631–640. doi:10.1038/nrm1174

16. Rawson RB, Zelenski NG, Nijhawan D, Ye J, Sakai J, Hasan MT, et al. Complementation cloning of S2P, a gene Encoding a putative metalloprotease required for intramembrane cleavage of SREBPs. Mol Cell. Cell Press; 1997;1: 47–57. doi:10.1016/S1097-2765(00)80006-4

17. Kanehara K, Akiyama Y, Ito K. Characterization of the *yaeL* gene product and its S2P-protease motifs in *Escherichia coli*. Gene. 2001;281: 71–79. doi:10.1016/S0378-1119(01)00823-X

18. Yu N., Kroos L. Evidence that SpoIVFB is a novel type of membrane metalloprotease governing intercompartmental communication during *Bacillus subtilis* sporulation. J Bacteriol. 2000;182: 3305–9. doi:10.1128/JB.184.19.5393-5401.2002

19. Rudner DZ, Fawcett P, Losick R. A family of membrane-embedded metalloproteases involved in regulated proteolysis of membrane-associated transcription factors. Proc Natl Acad Sci U S A. 1999;96: 14765–70. doi:10.1073/pnas.96.26.14765

20. Schöbel S, Zellmeier S, Schumann W, Wiegert T. The *Bacillus subtilis* σ^W anti-sigma factor RsiW is degraded by intramembrane proteolysis through YluC. Mol Microbiol. (10.1111); 2004;52: 1091–1105. doi:10.1111/j.1365-2958.2004.04031.x

21. Kinch LN, Ginalski K, Grishin N V. Site-2 protease regulated intramembrane proteolysis: sequence homologs suggest an ancient signaling cascade. Protein Sci. 2006;15: 84–93. doi:10.1110/ps.051766506

22. Jeleń F, Oleksy A, Smietana K, Otlewski J. PDZ domains - common players in the cell signaling. Acta Biochim Pol. 2003;50: 985–1017.

23. Feng L, Yan H, Wu Z, Yan N, Wang Z, Jeffrey PD, Shi Y. Structure of a site-2 protease family intramembrane metalloprotease. Science. 2007;318: 1608–12. doi:10.1126/science.1150755

24. Baykov AA, Tuominen HK, Lahti R. The CBS domain: A protein module with an emerging prominent role in regulation. ACS Chem Biol. 2011;6: 1156–1163. doi:10.1021/cb200231c

25. Ereño-Orbea J, Oyenarte I, Martínez-Cruz LA. CBS domains: Ligand binding sites and conformational variability. Arch Biochem Biophys. 2013;540: 70–81. doi:10.1016/j.abb.2013.10.008

26. Alba BM, Leeds JA, Onufryk C, Lu CZ, Gross CA. DegS and YaeL participate sequentially in the cleavage of RseA to activate the σ^E-dependent extracytoplasmic stress response. Genes Dev. 2002;16: 2156–2168. doi:10.1101/gad.1008902

27. Kanehara K, Ito K, Akiyama Y. YaeL (EcfE) activates the σ^E pathway of stress response through a site-2 cleavage of anti-σ^E, RseA. Genes Dev. 2002;16: 2147–2155. doi:10.1101/gad.1002302

28. Mecsas J, Rouviere PE, Erickson JW, Donohue TJ, Gross CA. The activity of sigma E, an *Escherichia coli* heat-inducible sigma-factor, is modulated by expression of outer membrane proteins. Genes Dev. 1993;7: 2618–28. doi:10.1101/GAD.7.12B.2618

29. Sohn J, Sauer RT. OMP peptides modulate the activity of DegS protease by differential binding to active and inactive conformations. Mol Cell. 2009;33: 64–74. doi:10.1016/j.molcel.2008.12.017

30. Walsh NP, Alba BM, Bose B, Gross CA, Sauer RT. OMP peptide signals initiate the envelope-stress response by activating DegS protease via relief of inhibition mediated by its PDZ domain. Cell. 2003;113: 61–71. doi:10.1016/S0092-8674(03)00203-4

31. Hizukuri Y, Oda T, Tabata S, Tamura-Kawakami K, Oi R, Sato M, Takagi J, Akiyama Y, Nogi T. A structure-based model of substrate discrimination by a noncanonical PDZ tandem in the intramembrane-cleaving protease RseP. Structure. Elsevier Ltd; 2014;22: 326–336. doi:10.1016/j.str.2013.12.003

32. Kanehara K, Ito K, Akiyama Y. YaeL proteolysis of RseA is controlled by the PDZ domain of YaeL and a Gln-rich region of RseA. EMBO J. 2003;22: 6389–6398. doi:10.1093/emboj/cdg602

33. Inaba K, Suzuki M, Maegawa KI, Akiyama S, Ito K, Akiyama Y. A pair of circularly permutated PDZ domains control RseP, the S2P family intramembrane protease of *Escherichia coli*. J Biol Chem. 2008;283: 35042–35052. doi:10.1074/jbc.M806603200

34. Saito A, Hizukuri Y, Matsuo E, Chiba S, Mori H, Nishimura O, et al. Post-liberation cleavage of signal peptides is catalyzed by the site-2 protease (S2P) in bacteria. Proc Natl Acad Sci. 2011;108: 13740–13745. doi:10.1073/pnas.1108376108

35. Akiyama Y, Kanehara K, Ito K. RseP (YaeL), an *Escherichia coli* RIP protease, cleaves transmembrane sequences. EMBO J. 2004;23: 4434–4442. doi:10.1038/sj.emboj.7600449

36. Zhou R, Cusumano C, Sui D, Garavito RM, Kroos L. Intramembrane proteolytic cleavage of a membrane-tethered transcription factor by a metalloprotease depends on ATP. Proc Natl Acad Sci. 2009;106: 16174–16179. doi:10.1073/pnas.0901455106

37. Parrell D, Zhang Y, Olenic S, Kroos L. *Bacillus subtilis* intramembrane protease RasP activity in *Escherichia coli* and in vitro. J Bacteriol. 2017;199. doi:10.1128/JB.00381-17

38. Flynn JM, Neher SB, Kim YI, Sauer RT, Baker TA. Proteomic discovery of cellular substrates of the ClpXP protease reveals five classes of ClpX-recognition signals. Mol Cell. 2003;11: 671–83.

39. Zellmeier S, Schumann W, Wiegert T. Involvement of Clp protease activity in modulating the *Bacillus subtilis* σw stress response. Mol Microbiol. (10.1111); 2006;61: 1569–1582. doi:10.1111/j.1365-2958.2006.05323.x

40. Heinrich J, Wiegert T. YpdC determines site-1 degradation in regulated intramembrane proteolysis of the RsiW anti-sigma factor of *Bacillus subtilis*. Mol Microbiol. 2006;62: 566–579. doi:10.1111/j.1365-2958.2006.05391.x

41. Ellermeier CD, Losick R. Evidence for a novel protease governing regulated intramembrane proteolysis and resistance to antimicrobial peptides in *Bacillus subtilis*. Genes Dev. 2006;20: 1911–22. doi:10.1101/gad.1440606

42. Heinrich J, Hein K, Wiegert T. Two proteolytic modules are involved in regulated intramembrane proteolysis of *Bacillus subtilis* RsiW. Mol Microbiol. 2009;74: 1412–1426. doi:10.1111/j.1365-2958.2009.06940.x

43. Bramkamp M, Weston L, Daniel RA, Errington J. Regulated intramembrane proteolysis of FtsL protein and the control of cell division in *Bacillus subtilis*. Mol Microbiol. 2006;62: 580–591. doi:10.1111/j.1365-2958.2006.05402.x

44. Wadenpohl I, Bramkamp M. DivIC stabilizes FtsL against RasP cleavage. J Bacteriol. 2010;192: 5260–5263. doi:10.1128/JB.00287-10

45. Ho TD, Hastie JL, Intile PJ, Ellermeier CD. The *Bacillus subtilis* extracytoplasmic function σ factor σ^V Is induced by lysozyme and provides resistance to lysozyme. J Bacteriol. 2011;193: 6215–6222. doi:10.1128/JB.05467-11

46. Hastie JL, Williams KB, Ellermeier CD. The Activity of V, an Extracytoplasmic Function Factor of *Bacillus subtilis*, Is controlled by regulated proteolysis of the Anti-σ Factor RsiV. J Bacteriol. 2013;195: 3135–3144. doi:10.1128/JB.00292-13

47. Hastie JL, Williams KB, Sepúlveda C, Houtman JC, Forest KT, Ellermeier CD. Evidence of a Bacterial Receptor for Lysozyme: Binding of lysozyme to the anti-σ factor RsiV controls activation of the ECF σ factor σV. PLoS Genet. 2014;10: e1004643. doi:10.1371/journal.pgen.1004643

48. Hastie JL, Williams KB, Bohr LL, Houtman JC, Gakhar L, Ellermeier CD. The Anti-sigma Factor RsiV Is a bacterial receptor for lysozyme: co-crystal structure determination and demonstration that binding of lysozyme to RsiV is required for σ^V activation. PLOS Genet. 2016;12: e1006287. doi:10.1371/journal.pgen.1006287

49. Urban S. Making the cut: Central roles of intramembrane proteolysis in pathogenic microorganisms. Nat Rev Microbiol. 2009;7: 411–423. doi:10.1038/nrmicro2130

50. Schneider JS, Glickman MS. Function of site-2 proteases in bacteria and bacterial pathogens. Biochim Biophys Acta - Biomembr. 2013;1828: 2808–2814. doi:10.1016/j.bbamem.2013.04.019

51. Makinoshima H, Glickman MS. Regulation of *Mycobacterium tuberculosis* cell envelope composition and virulence by intramembrane proteolysis. Nature. 2005;436: 406–409. doi:10.1038/nature03713

52. Sklar JG, Makinoshima H, Schneider JS, Glickman MS. *M. tuberculosis* intramembrane protease Rip1 controls transcription through three anti-sigma factor substrates. Mol Microbiol. 2010;77: 605–617. doi:10.1111/j.1365-2958.2010.07232.x

53. Schneider JS, Sklar JG, Glickman MS. The Rip1 protease of *Mycobacterium tuberculosis* controls the SigD regulon. J Bacteriol. 2014;196: 2638–2645. doi:10.1128/JB.01537-14

54. Schneider JS, Reddy SP, E HY, Evans HW, Glickman MS. Site-2 protease substrate specificity and coupling in trans by a PDZ-substrate adapter protein. Proc Natl Acad Sci. 2013;110: 19543–19548. doi:10.1073/pnas.1305934110

55. Qiu D, Eisinger VM, Rowen DW, Yu HD. Regulated proteolysis controls mucoid conversion in *Pseudomonas aeruginosa*. Proc Natl Acad Sci U S A. 2007;104: 8107–12. doi:10.1073/pnas.0702660104

56. Boucher JC, Yu H, Mudd MH, Deretic V. Mucoid *Pseudomonas aeruginosa* in cystic fibrosis: characterization of muc mutations in clinical isolates and analysis of clearance in a mouse model of respiratory infection. Infect Immun. 1997;65: 3838–46.

57. Schurr MJ, Yu H, Martinez-Salazar JM, Boucher JC, Deretic V. Control of AlgU, a member of the sigma E-like family of stress sigma factors, by the negative regulators MucA and MucB and *Pseudomonas aeruginosa* conversion to mucoidy in cystic fibrosis. J Bacteriol. 1996;178: 4997–5004.

58. Wood LF, Leech AJ, Ohman DE. Cell wall-inhibitory antibiotics activate the alginate biosynthesis operon in *Pseudomonas aeruginosa* : roles of σ^{22} (AlgT) and the AlgW and Prc proteases. Mol Microbiol. (10.1111); 2006;62: 412–426. doi:10.1111/j.1365-2958.2006.05390.x

59. Damron FH, Goldberg JB. Proteolytic regulation of alginate overproduction in *Pseudomonas aeruginosa*. Mol Microbiol. 2012;84: 595–607. doi:10.1111/j.1365-2958.2012.08049.x

60. Lamont IL, Beare PA, Ochsner U, Vasil AI, Vasil ML. Siderophore-mediated signaling regulates virulence factor production in *Pseudomon asaeruginosa*. Proc Natl Acad Sci U S A. 2002;99: 7072–7. doi:10.1073/pnas.092016999

61. Beare PA, For RJ, Martin LW, Lamont IL. Siderophore-mediated cell signalling in *Pseudomonas aeruginosa*: divergent pathways regulate virulence factor production and siderophore receptor synthesis. Mol Microbiol. 2003;47: 195–207. Available: http://www.ncbi.nlm.nih.gov/pubmed/12492864

62. Draper RC, Martin LW, Beare PA, Lamont IL. Differential proteolysis of sigma regulators controls cell-surface signalling in *Pseudomonas aeruginosa*. Mol Microbiol. 2011;82: 1444–1453. doi:10.1111/j.1365-2958.2011.07901.x

63. Zhang B, Hofmeister A, Kroos L. The prosequence of pro-σ^K promotes membrane association and inhibits RNA polymerase core binding. J Bacteriol. 1998;180: 2434–41.

64. Kroos L, Kunkel B, Losick R. Switch protein alters specificity of RNA polymerase containing a compartment-specific sigma factor. Science (80-). 1989;243: 526–529. doi:10.1126/science.2492118

65. Bastiaansen KC, Civantos C, Bitter W, Llamas MA. New insights into the regulation of

cell-surface signaling activity acquired from a mutagenesis screen of the pseudomonas putida IutY sigma/anti-sigma factor. Front Microbiol. 2017;8: 747. doi:10.3389/fmicb.2017.00747

66. Cutting S, Oke V, Driks A, Losick R, Lu S, Kroos L. A forespore checkpoint for mother cell gene expression during development in *Bacillus subtilis*. Cell. 1990;62: 239–250.

67. Cutting S, Roels S, Losick R. Sporulation operon *spoIVF* and the characterization of mutations that uncouple mother-cell from forespore gene expression in *Bacillus subtilis*. J Mol Biol. 1991;221: 1237–1256. doi:10.1016/0022-2836(91)90931-U

68. Ricca E, Cutting S, Losick R. Characterization of *bofA*, a gene involved in intercompartmental regulation of pro-σ^K processing during sporulation in *Bacillus subtilis*. J Bacteriol. 1992;174: 3177–84.

69. Rudner DZ, Losick R. A sporulation membrane protein tethers the pro-σ^K processing enzyme to its inhibitor and dictates its subcellular localization. Genes Dev. 2002;16: 1007–1018. doi:10.1101/gad.977702

70. Zhou R, Kroos L. BofA protein inhibits intramembrane proteolysis of pro-σ^K in an intercompartmental signaling pathway during *Bacillus subtilis* sporulation. Proc Natl Acad Sci U S A. 2004;101: 6385–90. doi:10.1073/pnas.0307709101

71. Cutting S, Driks A, Schmidt R, Kunkel B, Losick R. Forespore-specific transcription of a gene in the signal transduction pathway that governs Pro-σ^K processing in *Bacillus subtilis*. Genes Dev. 1991;5: 456–66. doi:10.1101/GAD.5.3.456

72. Wakeley PR, Dorazi R, Hoa NT, Bowyer JR, Cutting SM. Proteolysis of SpoIVB is a critical determinant in signalling of Pro-σ^K processing in *Bacillus subtilis*. Mol Microbiol. 2000;36: 1336–48. doi:10.1046/J.1365-2958.2000.01946.X

73. Zhou R, Kroos L. Serine proteases from two cell types target different components of a complex that governs regulated intramembrane proteolysis of pro-σ^K during *Bacillus subtilis* development. Mol Microbiol. 2005;58: 835–846. doi:10.1111/j.1365-2958.2005.04870.

74. Campo N, Rudner DZ. A branched pathway governing the activation of a developmental transcription factor by regulated intramembrane proteolysis. Mol Cell. 2006;23: 25–35. doi:10.1016/j.molcel.2006.05.019

75. Halder S, Parrell D, Whitten D, Feig M, Kroos L. Interaction of intramembrane metalloprotease SpoIVFB with substrate Pro-σ^K. Proc Natl Acad Sci. 2017;114: E10677–E10686. doi:10.1073/pnas.1711467114

76. Zhang Y, Halder S, Kerr RA, Parrell D, Ruotolo B, Kroos L. Complex formed between intramembrane metalloprotease SpoIVFB and Its substrate, Pro-σ^K. J Biol Chem. 2016;291: 10347–62. doi:10.1074/jbc.M116.715508

77. Ramírez-Guadiana FH, Rodrigues CDA, Marquis KA, Campo N, Barajas-Ornelas R del C, Brock K, Marks D, Kruse A, Rudner D. Evidence that regulation of intramembrane

proteolysis is mediated by substrate gating during sporulation in *Bacillus subtilis*. PLOS Genet. 2018;14: e1007753. doi:10.1371/journal.pgen.1007753

78. Morlot C, Rodrigues CDA. The New Kid on the Block: A specialized secretion system during bacterial sporulation. Trends Microbiol. 2018;26: 663–676. doi:10.1016/j.tim.2018.01.001

79. Camp AH, Losick R. A feeding tube model for activation of a cell-specific transcription factor during sporulation in *Bacillus subtilis*. Genes Dev. 2009;23: 1014–1024. doi:10.1101/gad.1781709

80. Camp AH, Losick R. A novel pathway of intercellular signalling in *Bacillus subtilis* involves a protein with similarity to a component of type III secretion channels. Mol Microbiol. 2008;69: 402–417. doi:10.1111/j.1365-2958.2008.06289.x

81. Doan T, Morlot C, Meisner J, Serrano M, Henriques AO, Moran CP, Rudner D. Novel secretion apparatus maintains spore integrity and developmental gene expression in *Bacillus subtilis*. PLoS Genet. 2009;5: e1000566. doi:10.1371/journal.pgen.1000566

82. Butcher BG, Lin Y-P, Helmann JD. The *yydFGHIJ* operon of *Bacillus subtilis* encodes a peptide that induces the LiaRS two-component system. J Bacteriol. 2007;189: 8616–8625. doi:10.1128/JB.01181-07

83. Benjdia A, Guillot A, Ruffié P, Leprince J, Berteau O. Post-translational modification of ribosomally synthesized peptides by a radical SAM epimerase in *Bacillus subtilis*. Nat Chem. 2017;9: 698–707. doi:10.1038/nchem.2714

CHAPTER 2: *Bacillus subtilis* Intramembrane Protease RasP Activity in *Escherichia coli* and *in Vitro*

This chapter was published in the *Journal of Bacteriology* and can be found at the following citation:

Parrell D, Zhang Y, Olenic S, Kroos L. *Bacillus subtilis* intramembrane protease RasP activity in *Escherichia coli* and *in vitro*. J Bacteriol. 2017;199. doi:10.1128/JB.00381-17

I contributed significantly to the writing and editing of this manuscript in addition to using strains and plasmids generated by Yang Zhang to prepare final figures and build from his preliminary work. Sandra Olenic performed experiments in a *clpP*$^{-}$ mutant of *E. coli* BL21(DE3).

 The publication reprint and supplemental data are provided on the following pages.

CHAPTER 2: *Bacillus subtilis* Intramembrane Protease RasP Activity in *Escherichia coli* and *in Vitro*

ABSTRACT

RasP is a predicted intramembrane metalloprotease of *Bacillus subtilis* that has been proposed to cleave the stress response anti-sigma factors RsiW and RsiV, the cell division protein FtsL, and remnant signal peptides, within their transmembrane segments. To provide evidence for direct effects of RasP on putative substrates, we developed a heterologous coexpression system. Since expression of catalytically-inactive RasP E21A inhibited expression of other membrane proteins in *Escherichia coli*, we added extra transmembrane segments to RasP E21A, which allowed accumulation of most other membrane proteins. A corresponding active version of RasP appeared to promiscuously cleave coexpressed membrane proteins, except those with a large periplasmic domain. However, stable cleavage products were not observed, even in *clpP* mutant *E. coli.* Fusions of transmembrane segment-containing parts of FtsL and RsiW to *E. coli* maltose-binding protein (MBP) also resulted in proteins that appeared to be RasP substrates upon coexpression in *E. coli*, including FtsL with a full-length C-terminal domain (suggesting prior cleavage by a site-1 protease is unnecessary) and RsiW designed to mimic the PrsW site-1 cleavage product (suggesting further trimming by extracytoplasmic protease is unnecessary). Purified RasP cleaved His_6-MBP-RsiW(73-118) *in vitro* within the RsiW transmembrane segment based on mass spectrometry analysis, demonstrating that RasP is an intramembrane protease. Surprisingly, purified RasP failed to cleave His_6-MBP-FtsL(23-117). We propose that the lack of α-helix-breaking residues in the FtsL transmembrane segment creates a requirement for the membrane environment and/or an additional protein(s) in order for RasP to cleave FtsL.

INTRODUCTION

Intramembrane proteases (IPs) are polytopic membrane proteins with active site residues in transmembrane segments (TMSs). IPs cleave their substrates within a TMS or near the membrane surface, and regulated intramembrane proteolysis (RIP) controls diverse signaling pathways in a wide variety of organisms (1, 2). There are four types of IPs based on whether they utilize a metal ion, a serine residue, or a pair of aspartyl or glutamyl residues to catalyze peptide bond hydrolysis. Here, we focus on intramembrane metalloproteases (IMMPs) of bacteria. IMMPs are often called site-2 proteases (S2Ps) because they are related to human S2P and in many cases they cleave a TMS after an initial cleavage outside the membrane by a site-1 protease (3, 4).

IMMPs of bacteria function in envelope stress responses, sporulation, pheromone production, polar morphogenesis, cell division, signal peptide removal from the cell membrane, and virulence of important human pathogens (4). Despite their diverse and important functions, only two IMMPs have been purified and shown to cleave a physiological substrate within its TMS (3). RseP of *E. coli* has been shown to cleave the anti-σ factor RseA *in vitro* (5). The purified RseA was a C-terminally truncated version designed to mimic prior site-1 cleavage by DegS, since site-1 cleavage is normally required for RseA to serve as a substrate of RseP *in vivo* (6, 7). The other IMMP that has been shown to cleave its substrate *in vitro* is *B. subtilis* SpoIVFB, which cleaves Pro-σ^K (8). Here, we report the purification of a third IMMP, RasP of *B. subtilis*, and cleavage of a C-terminally truncated substrate within its TMS.

RasP (formerly YluC) has been proposed to function much like *E. coli* RseP, as an IMMP in a RIP pathway that leads to activation of a σ factor and governs envelope stress responses (9). A model of the RasP-dependent σ^W activation pathway of *B. subtilis* is depicted in Figure 1. Envelope stressors such as alkaline shock or antimicrobial peptides cause the site-1 protease PrsW (also called YpdC) to cleave the C-terminal extracytoplasmic portion of the anti-σ factor

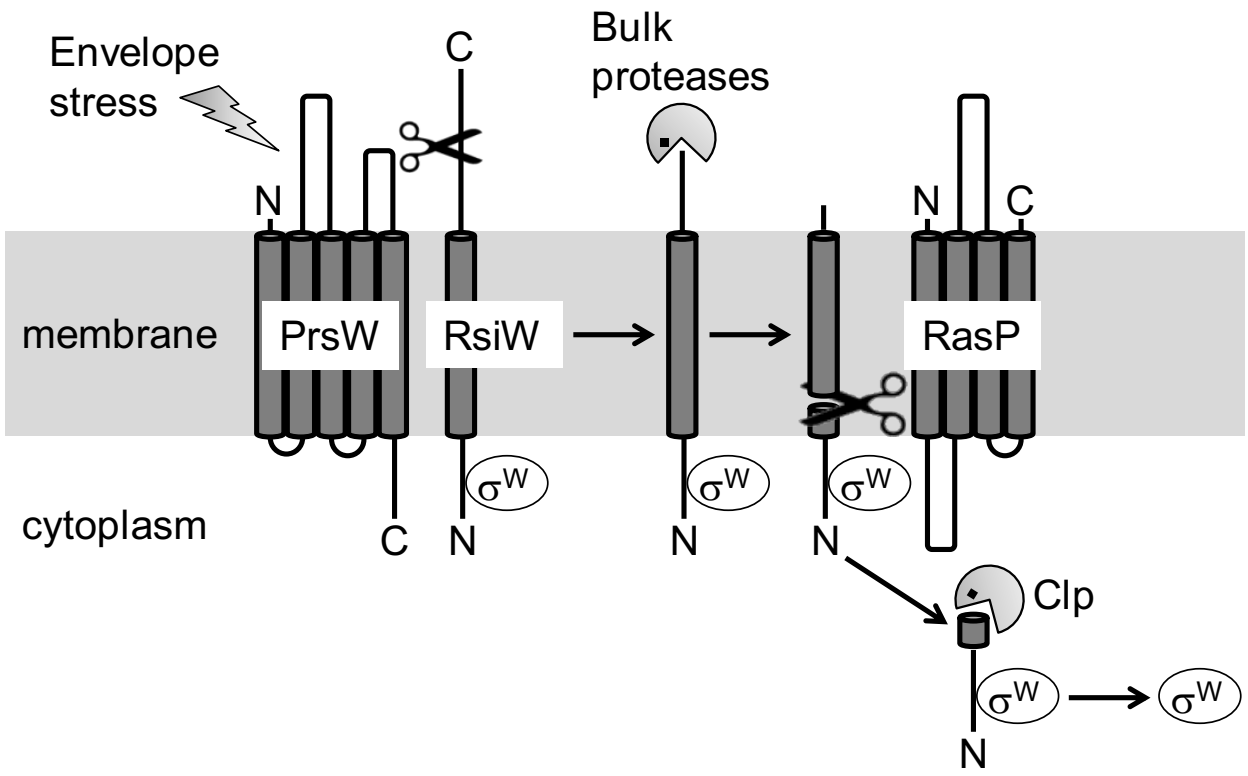

Figure 1 Model of the σ^W activation pathway. Envelope stress sensed by PrsW causes it to cleave the extracytoplasmic domain of the anti-σ, RsiW. The C-terminal end of RsiW is further degraded by one or more bulk proteases of unknown identity. This is proposed to allow RasP to cleave the TMS of RsiW. The N-terminal domain of RsiW, bound to σ^W, is released from the membrane into the cytoplasm, where Clp proteases degrade the rest of RsiW, freeing active σ^W. Scissors depict specific proteolytic cleavages and pacman symbols indicate processive degradation. The membrane topology of PrsW is from (11). The TMSs of RasP were predicted using TMpred (48) and its predicted membrane topology is based on analogy to *E. coli* RseP (49) and other IMMPs (30).

RsiW (10, 11). The remaining C-terminal extracytoplasmic portion of RsiW is susceptible to bulk proteases that trim it to within approximately 13 residues of the TMS (12). Next, RasP is proposed to cleave within the TMS of RsiW, releasing the N-terminal domain of RsiW bound to σ^W, into the cytoplasm (9). Finally, the N-terminal domain of RsiW is further degraded by ClpXP and ClpEP (13), allowing σ^W to direct transcription of ~60-90 genes whose products defend the cell against membrane-active antimicrobials (14).

Support for the proposed role of RasP in the σ^W activation pathway includes sequence similarity of RasP to IMMPs and analysis of a *B. subtilis rasP* null mutant that fails to activate σ^W (9). Complementation of the mutant with *rasP* restored σ^W activation. A *rasP E21A* allele failed to complement, consistent with the prediction that E21 in the HEXXH metalloprotease motif of the putative IMMP would be crucial for proteolytic activity. However, accumulation of RasP E21A was not verified since antibodies were not available. A subsequent study detected a RasP-dependent cleavage product of RsiW that was stabilized somewhat in *clpP* mutant *B. subtilis* (13), but the product was too unstable to allow the cleavage site to be mapped. Heterologous coexpression of PrsW and RsiW in *E. coli* resulted in C-terminally truncated RsiW that appeared to be trimmed further by Tsp (also called Prc), a periplasmic tail-specific protease of *E. coli*, and this shortened form of RsiW was no longer observed when RasP was also coexpressed (12). These results suggested that RasP cleaved the shortened form of RsiW; however, neither the cleavage product nor RasP was detected, and RasP E21A was not tested.

A second proposed substrate of RasP is the cell division protein FtsL. *B. subtilis* with a *rasP* mutation form shorter cells and FtsL is more stable, suggesting FtsL is normally limiting for cell division due to cleavage by RasP (15). Heterologous coexpression of S-tagged RasP and His-tagged FtsL in *E. coli* appeared to result in degradation of FtsL, whereas coexpression of RasP E21A with FtsL allowed it to accumulate, suggesting RasP directly cleaves FtsL. However, RasP of the expected size was not detected and accumulation of RasP E21A was not tested,

weakening the interpretation of this experiment, as well as heterologous coexpression experiments reported subsequently (16).

Evidence for additional substrates of RasP has come from experiments in *B. subtilis.* In one study, secreted proteins tagged at their N-terminus were further shortened in a RasP-dependent fashion after apparent initial cleavage by signal peptidase, suggesting that RasP, like *E. coli* RseP, removes remnant signal peptides from the cell membrane (17). Impressively, ectopic expression of RasP-His_6, but not RasP-His_6 E21A, restored further shortening in a *rasP* mutant, and both His-tagged forms of RasP accumulated similarly. The results support direct cleavage of signal peptides by RasP, but an indirect effect of RasP activity could not be excluded and the cleavage sites were not mapped. Another study implicated the anti-σ RsiV as a substrate of RasP, by comparing degradation of N-terminally GFP-tagged RsiV in wild-type and *rasP* mutant cells (18).

A limitation of RasP proteolysis studies in *B. subtilis* is that indirect effects cannot be ruled out. Heterologous coexpression of RasP and a potential substrate could provide evidence for a direct effect, since other *B. subtilis* proteins would be absent, but proof that RasP functions as an IMMP would require reconstitution *in vitro* of substrate cleavage within a TMS. Here, we report the development of a heterologous coexpression system in *E. coli* that allows detection of tagged RasP and RasP E21A, and provides evidence for RasP proteolytic activity on MBP fusions to TMS-containing parts of FtsL and C-terminally truncated RsiW. We also report purification of RasP-$FLAG_2$-His_6 and reconstitution *in vitro* of His_6-MBP-RsiW(73-118) cleavage within its TMS, demonstrating that RasP functions as an IMMP.

RESULTS

RasP can inhibit coexpression of other membrane proteins in *E. coli.* To coexpress RasP and potential substrates in *E. coli* (Fig. 2A), we engineered plasmids to express tagged proteins from T7 RNA polymerase promoters. The two plasmids were transformed separately

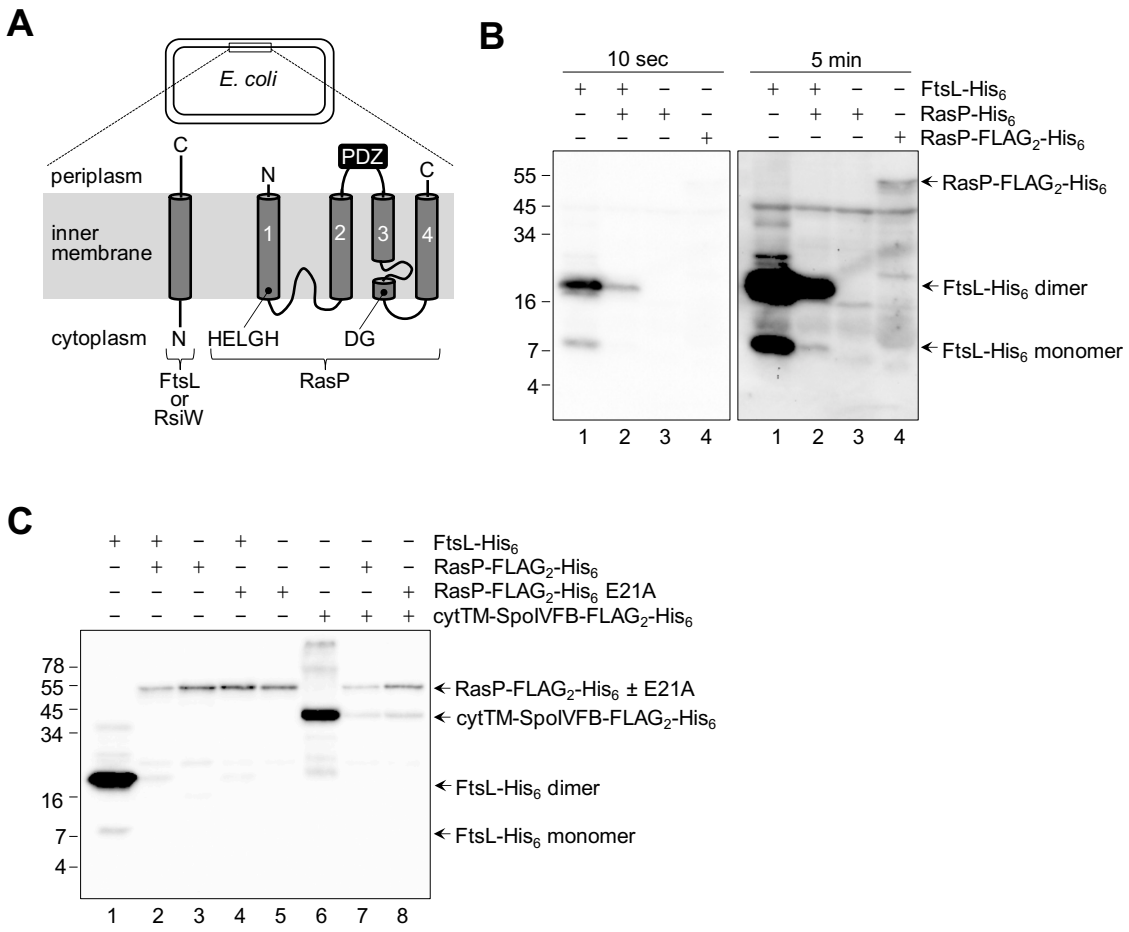

Figure 2 Effect of RasP on expression of other proteins in *E. coli*. (A) *E. coli* cell and an expanded view of the inner membrane, showing the predicted topology of RasP and its substrates. The topology of RasP was predicted as explained in the legend of Figure 1. Here, some additional features of RasP are depicted, including the HELGH motif with its catalytic E21 residue (9), a putative membrane-reentrant □-loop between TMS 1 and TMS 2 (28, 50), a PSD-95/Dgl/ZO-1 (PDZ) domain between TMS 2 and TMS 3 (30), and a short loop interrupting TMS 3 that is predicted on the basis of the structure of a *Methanocaldococcus janneschii* IMMP (51) and is followed by a conserved DG sequence whose D residue together with the two H residues of the HELGH motif are predicted to coordinate a zinc ion (30). The topology of RsiW was determined in *B. subtilis* (9) and is predicted to be the same in *E. coli*. The topology of FtsL has been predicted previously (52). (B) Effect of RasP-His_6 on accumulation of FtsL-His_6. *E. coli* bearing pYZ20 to express FtsL-His_6 and/or pYZ9 to express RasP-His_6 as indicated at the top were cultured (10 mL) and induced with IPTG. Extracts were subjected to immunoblot analysis with anti-His antibodies and two exposures are shown. *E. coli* bearing pYZ37 to express RasP-$FLAG_2$-His_6 was cultured and induced similarly for comparison. (C) Effect of RasP-$FLAG_2$-His_6 on accumulation of FtsL-His_6 and cytTM-SpoIVFB-$FLAG_2$-His_6. *E. coli* bearing pYZ20 to express FtsL-His_6, pYZ37 to express RasP-$FLAG_2$-His_6, pYZ44 to express RasP-$FLAG_2$-His_6 E21A, and/or pZR209 to express cytTM-SpoIVFB-$FLAG_2$-His_6 as indicated at the top were cultured, induced, and extracts were subjected to immunoblot analysis with anti-His antibodies (30 sec exposure). In panels B and C, migration of protein markers is indicated at the left and inferred identity of signals is indicated at the right, and a representative result from at least two biological replicates is shown.

or in combination into *E. coli* strain BL21(DE3), which can be induced to synthesize T7 RNA polymerase. Initially, plasmids designed to express RasP-His_6 and FtsL-His_6 were tested. Upon induction, transformants accumulated FtsL-His_6 abundantly in the absence of RasP-His_6 and much less abundantly in combination with RasP-His_6, although RasP-His_6 (46 kDa) could not be detected even in a long exposure of the immunoblot (Fig. 2B, lanes 1-3). We wanted to be able to detect RasP in order to strengthen the interpretation of experiments comparing active and inactive RasP coexpressed with potential substrates. We note that FtsL-His_6 (12 kDa) appeared to migrate primarily as a dimer (Fig. 2B, lane 1). SDS-resistant dimer formation was observed previously when *B. subtilis* FtsL and DivIC were coexpressed highly in *E. coli* (16).

To possibly improve detection of RasP, we engineered a plasmid to express RasP-$FLAG_2$-His_6. Surprisingly, RasP-$FLAG_2$-His_6 was detected by anti-His antibodies (Fig. 2B, lane 4), so it was unnecessary to use anti-FLAG antibodies, which are more sensitive. Plasmids engineered to express RasP-$FLAG_2$-His_6 and FtsL-His_6 were transformed separately or in combination into *E. coli* strain BL21(DE3). Both proteins accumulated separately, and in combination RasP-$FLAG_2$-His_6 accumulated slightly less abundantly and FtsL-His_6 was barely detectable (Fig. 2C, lanes 1-3). To test whether RasP proteolytic activity was responsible for the greatly reduced accumulation of FtsL, we catalytically-inactivated RasP by introducing an E21A substitution as described previously (9). Upon induction, RasP-$FLAG_2$-His_6 E21A accumulated, but in combination FtsL-His_6 was barely detectable (Fig. 2C, lanes 4-5). Therefore, RasP proteolytic activity was not responsible for reduced accumulation of FtsL. Rather, RasP, whether active or inactive, inhibited coexpression of FtsL. An effect of RasP on coexpression of FtsL was noted previously and was attributed to the burden of expressing multiple membrane proteins (16). To test this idea, we examined the effect of RasP on coexpression of *B. subtilis* SpoIVFB, an IMMP (19, 20) with 6 TMSs (21) that is not believed to be a substrate of RasP. We found that both active RasP-$FLAG_2$-His_6 and the inactive E21A version greatly reduced accumulation of cytTM-SpoIVFB-$FLAG_2$-His_6 (Fig. 2C, lanes 6-8). We conclude that RasP, whether active or inactive

proteolytically, can inhibit coexpression of other membrane proteins in *E. coli.* Below, we describe construction of an inactive RasP E21A variant with less inhibitory effect on coexpression of other membrane proteins.

Addition of TMSs to RasP allows evidence for proteolytic activity to be obtained in *E. coli.* Addition of cytTM to the N-terminus of SpoIVFB enhanced accumulation of cytTM-SpoIVFB-FLAG$_2$-His$_6$ expressed in *E. coli* (8). The rationale for adding cytTM, a TMS from rabbit cytochrome P450 2B4 (22), arose from the observation that the N-terminal TMS can affect the recognition and insertion process of the protein translocon (23). We reasoned that RasP might inhibit coexpression of other membrane proteins in *E. coli* by impairing the function of the protein translocon, and that adding cytTM might ameliorate this effect. To preserve the usual membrane orientation of cytTM, we also included the first TMS of SpoIVFB, whose C-terminal end is periplasmic when expressed in *E. coli* (21). This end was fused to the N-terminus of RasP, which was predicted to be periplasmic in *E. coli* (Fig. 2A). The resulting fusion protein, cytTM-SpoIVFBTM1-RasP-FLAG$_2$-His$_6$ (hereafter referred to as 2TM-RasP) (Fig. 3A), and a catalytically-inactive derivative, 2TM-RasP E21A, were expressed from T7 RNA polymerase promoters separately or in combination with FtsL-His$_6$. 2TM-RasP reduced accumulation of FtsL-His$_6$ much more than did 2TM-RasP E21A (Fig. 3B), suggesting that RasP proteolytic activity was primarily responsible for the reduced accumulation of FtsL-His$_6$. However, we did not detect a cleavage product (expected to be ~4 kDa smaller) even in a long exposure of the immunoblot. We reasoned that if 2TM-RasP cleaved FtsL-His$_6$ in its TMS, the C-terminal His$_6$-tagged fragment might be unstable.

FtsL was His$_6$-tagged at its N-terminus in previous work that suggested it can serve as a substrate for RasP proteolytic activity in *E. coli* (15, 16). Since Clp protease has been reported to degrade IMMP cleavage products released into the cytoplasm of *E. coli* and *B. subtilis* (13, 24), we reasoned that an N-terminal His$_6$ tag might allow detection of the N-terminal cleavage product of His$_6$-FtsL in *clpP* mutant *E. coli*. First, we engineered a plasmid to express His$_6$-FtsL

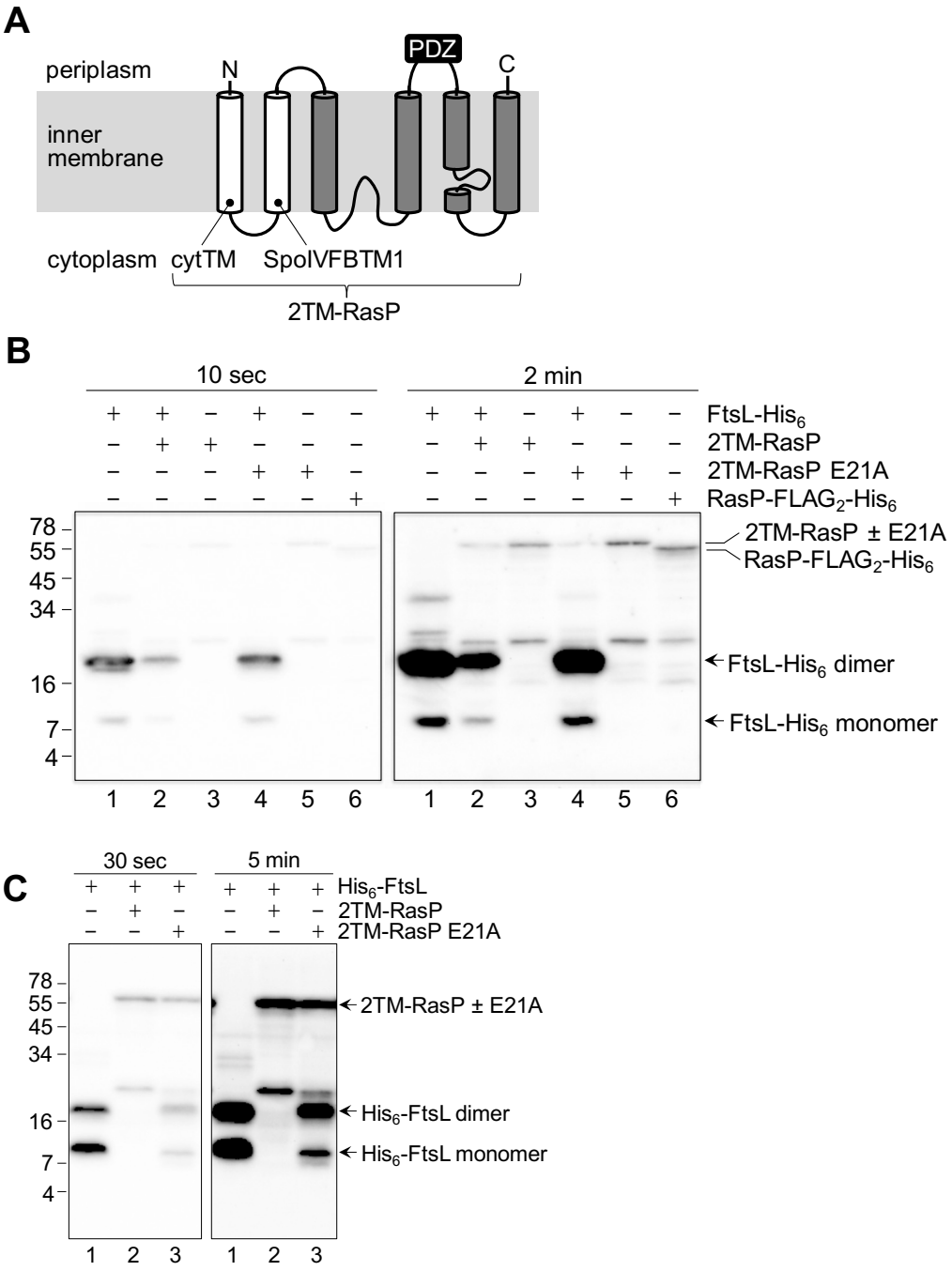

Figure 3 Activity of 2TM-RasP on FtsL in *E. coli*. (A) Predicted topology of 2TM-RasP. Two extra TM segments (cytTM and SpoIVFBTM1) were added to the N terminus of RasP, creating 2TM-RasP. (B) 2TM-RasP activity on FtsL-His6. *E. coli* bearing pYZ20 to express FtsL-His6, pYZ29 to express 2TM-RasP, pYZ53 to express 2TM-RasP E21A, and/or pYZ37 to express RasP-FLAG2-His6, as indicated at the top, was cultured (10 ml) and induced with IPTG. Extracts were subjected to immunoblot analysis with anti-His antibodies, and two exposures are shown. Migration of protein markers is indicated at the left, and the inferred identity of signals is indicated at the right. (C) 2TM-RasP activity on His6-FtsL. Wild-type (+) or *clpP* mutant (-) *E. coli*

Figure 3 (cont'd)
bearing pYZ66 to express His6-FtsL alone or in combination with pYZ29 or pYZ53 to express 2TM-RasP or 2TM-RasP E21A, respectively, as indicated at the top, was cultured and induced, and extracts were subjected to immunoblot analysis with anti-His antibodies (3- and 5-min exposures for the left and right blots, respectively). Migration of protein markers is indicated at the left or right, and the inferred identity of signals is indicated in the center. In panels B and C, a representative result from at least two biological replicates is shown.

from a T7 RNA polymerase promoter and tested expression alone or in combination with 2TM-RasP or 2TM-RasP E21A in *clpP*$^+$ *E. coli*. His_6-FtsL was barely detectable upon coexpression with 2TM-RasP and accumulated more abundantly upon coexpression with 2TM-RasP E21A, although not as abundantly as when expressed alone (Fig. 3C, lanes 1-3). This pattern of results suggests that 2TM-RasP is proteolytically active on His_6-FtsL, in agreement with the previous work (15, 16), and strengthening the conclusion since we show that 2TM-RasP E21A accumulates comparably to 2TM-RasP. However, no cleavage product was detected (expected to be ~4 kDa). Therefore, we constructed a *clpP* mutant derivative of *E. coli* strain BL21(DE3) and repeated the experiment, but still no cleavage product was detected even in a long exposure of the immunoblot (Fig. 3C, lanes 4-6).

Having established a system to detect RasP and obtain evidence for proteolytic activity in *E. coli*, we used the system to test for activity on C-terminally truncated RsiW. RasP normally cleaves RsiW after an initial cleavage in its C-terminal extracytoplasmic domain by PrsW (10, 11) and trimming by extracytoplasmic proteases (12) (Fig. 1). Although the exact extent of trimming is unknown, it was estimated to stop at about residue 118 of RsiW (12). Therefore, we engineered a plasmid to express His_6-RsiW(1-118) from a T7 RNA polymerase promoter and tested expression alone or in combination with 2TM-RasP or 2TM-RasP E21A. Expression of His_6-RsiW(1-118) alone resulted in a species migrating at the expected position (12 kDa), and this species was greatly diminished upon coexpression with 2TM-RasP, but only slightly more abundant upon coexpression with 2TM-RasP E21A (Fig. S1A). Although the small difference in accumulation of His_6-RsiW(1-118) was reproducible in multiple experiments, this pattern of results does not provide convincing evidence for proteolytic activity of 2TM-RasP on His_6-RsiW(1-118).

Our finding that catalytically-inactive 2TM-RasP E21A strongly inhibited coexpression of His_6-RsiW(1-118) (Fig. S1A) was reminiscent of the effect of RasP-$FLAG_2$-His_6 E21A on cytTM-SpoIVFB-$FLAG_2$-His_6 (Fig. 2C, lanes 6-8). Therefore, we examined the effects of 2TM-RasP

and 2TM-RasP E21A on coexpression of the putative nonsubstrate cytTM-SpoIVFB-$FLAG_2$-His_6. Surprisingly, 2TM-RasP greatly reduced accumulation of cytTM-SpoIVFB-$FLAG_2$-His_6 to a barely detectable level (Fig. S1B, lane 1). 2TM-RasP E21A allowed better accumulation of cytTM-SpoIVFB-$FLAG_2$-His_6, although not as much as when expressed alone (Fig. S1B, lanes 2 and 3). This pattern of results suggests that 2TM-RasP is proteolytically active on the putative nonsubstrate cytTM-SpoIVFB-$FLAG_2$-His_6, raising the possibility that 2TM-RasP is completely promiscuous (i.e., would cleave any coexpressed membrane protein) upon overexpression in *E. coli.*

We examined the effects of 2TM-RasP and 2TM-RasP E21A on coexpression of two other putative nonsubstrates, GFP-□27BofA and SpoIVFA. These proteins inhibit SpoIVFB activity during *B. subtilis* sporulation (25, 26). Both proteins are predicted to have a single TMS and a periplasmic C-terminal domain when expressed in *E. coli*, based on analysis of PhoA fusion proteins (21, 27). Hence, the membrane topology of GFP-□27BofA and SpoIVFA is expected to be the same as that of FtsL and RsiW (Fig. 2A). Interestingly, coexpression with 2TM-RasP reduced GFP-□27BofA accumulation and coexpression with 2TM-RasP E21A had little effect (Fig. S1C), suggesting that 2TM-RasP is proteolytically active on GFP-□27BofA. In contrast, neither 2TM-RasP nor 2TM-RasP E21A had much effect on accumulation of SpoIVFA (Fig. S1D), indicating that 2TM-RasP is not completely promiscuous when overexpressed in *E. coli*. We conclude that comparison of the effects of 2TM-RasP and 2TM-RasP E21A on accumulation of a potential substrate upon coexpression in *E. coli* can provide evidence for proteolytic activity, but 2TM-RasP appears to promiscuously cleave some putative nonsubstrates upon heterologous overexpression. Since SpoIVFA has a large extracytoplasmic domain and the extracytoplasmic parts of SpoIVFB and BofA are small, the size of the extracytoplasmic segments may primarily determine whether a membrane protein is cleaved by 2TM-RasP upon coexpression in *E. coli* (see Discussion).

In an effort toward reconstituting RasP cleavage of substrates *in vitro*, we tried to purify His_6-FtsL and His_6-RsiW(1-118), but the yields were very low (data not shown). To improve the yields and perhaps allow better accumulation of substrates upon coexpression with inactive 2TM-RasP E21A in our *E. coli* system, we fused the *E. coli* maltose-binding protein (MBP) to portions of FtsL and RsiW as described in the next section.

Evidence that 2TM-RasP is proteolytically active on His_6-MBP-FtsL and His_6-MBP-RsiW fusion proteins. We constructed two genes designed to fuse His_6-MBP to the 23rd residue of FtsL, which precedes the sequence KKRAS (residues 25-29) shown previously to be important for proteolytic activity of RasP on FtsL (15) (Fig. 4A). One gene was designed to fuse His_6-MBP to otherwise full-length FtsL, designated His_6-MBP-FtsL(23-117) (Fig. 4B). The other gene was designed to fuse His_6-MBP to C-terminally truncated FtsL, designated His_6-MBP-FtsL(23-68). The latter was designed to be comparable to RsiW(1-118), with the C-terminus 13-15 residues beyond the predicted TMS (Fig. 4A). It seemed possible that FtsL, like RsiW, might be subject to C-terminal trimming prior to RasP cleavage *in vivo* (12), so we wanted to produce comparable substrates to eventually test for RasP cleavage *in vitro*. First, though, we tested whether the fusion proteins (expressed from a T7 RNA polymerase promoter) appear to be substrates for 2TM-RasP in *E. coli*. Expression of His_6-MBP-FtsL(23-117) alone in *E. coli* resulted in three species (Fig. 4C, bottom panel, lane 1). The slowest-migrating species had an apparent molecular weight of about 52 kDa, as expected for the full-length protein. Presumably, the two faster-migrating species resulted from proteolysis upon overexpression (Fig. 4C, bottom panel, lane 1, dots). Interestingly, the fastest-migrating species co-migrated with a species observed when His_6-MBP-FtsL(23-68) alone was expressed in *E. coli* (Fig. 4C, bottom panel, lane 4, dot). This species appeared to be slightly smaller than full-length His_6-MBP-FtsL(23-68), suggesting it lacks nearly all of the C-terminal part predicted to be exposed to the periplasm (Fig. 4A). We considered the possibility that *E. coli* RseP was cleaving both His_6-MBP-FtsL proteins in their TMS, but this was not the case since an *rseP* mutant derivative of *E. coli* strain

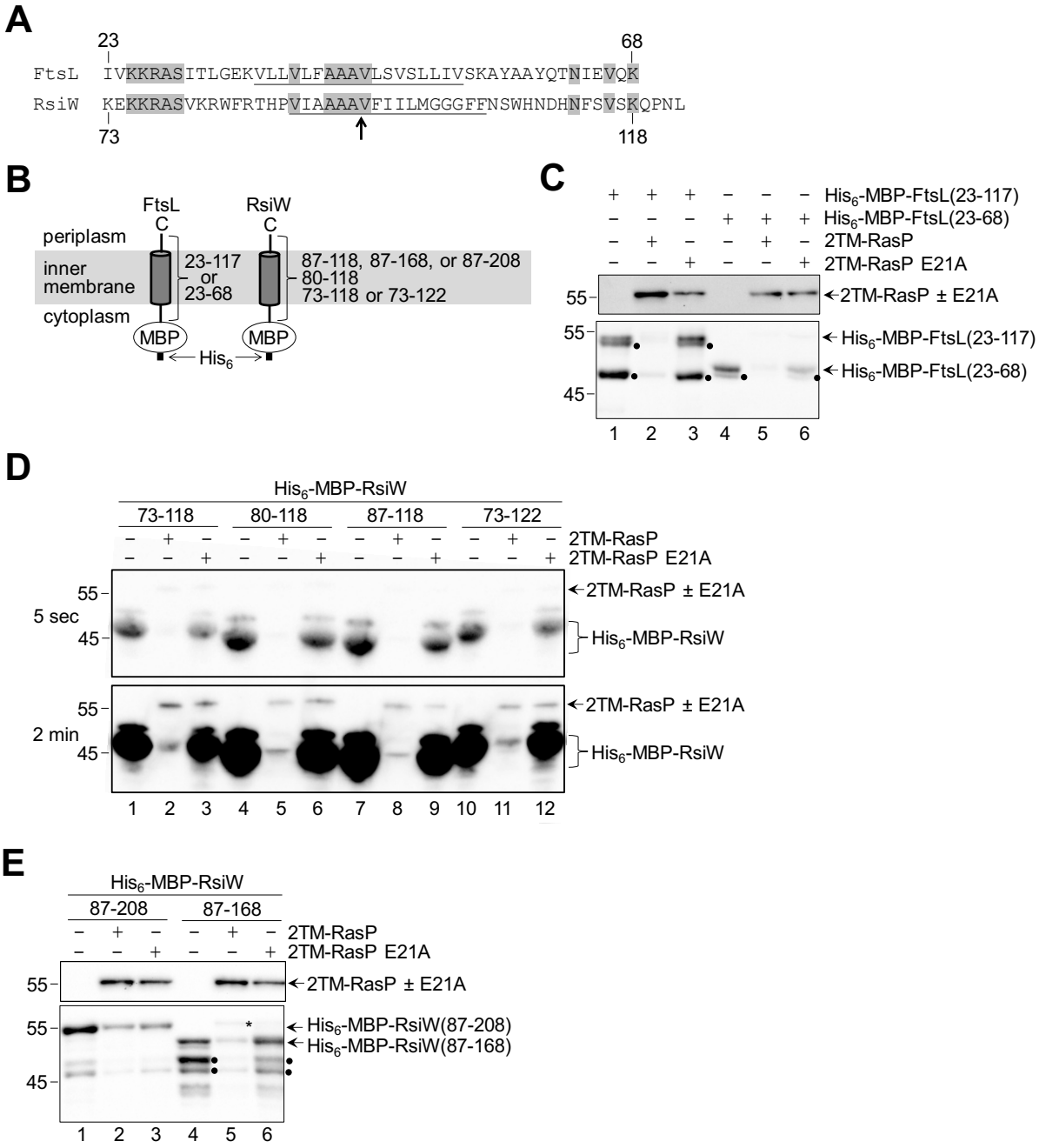

Figure 4 Activity of 2TM-RasP on MBP fusions to FtsL and RsiW in *E. coli*. (A) Sequences of FtsL and RsiW aligned at their KKRAS sequences. Gray background indicates identical residues. Predicted TM segments are underlined (15). Numbers indicate residues in FtsL and RsiW that were included in particular fusion proteins. The arrow indicates the cleavage site *in vitro* based on mass spectrometry analysis. (B) Predicted topology of His_6-MBP fusion proteins. Two fusions to FtsL and six fusions to RsiW were created as potential substrates for RasP. (C) 2TM-RasP activity on His_6-MBP-FtsL fusion proteins. *E. coli* bearing pYZ112 or pYZ111 to express His_6-MBP-FtsL(23–117) or His_6-MBP-FtsL(23–68), respectively, alone or in combination with pYZ29 or pYZ53 to express 2TM-RasP or 2TM-RasP E21A, respectively, as indicated at the top, was cultured (10 ml) and induced with IPTG. Extracts were subjected to

Figure 4 (cont'd)

immunoblot analysis with anti-FLAG (5-min exposure) or anti-His (1.5-min exposure) antibodies in the top and bottom panels, respectively. The dots indicate presumed proteolytic breakdown products independent of RasP activity. (D) 2TM-RasP activity on His_6-MBP-RsiW fusion proteins. The procedure was as for panel C except that *E. coli* bearing pYZ69, pYZ75, pYZ76, or pYZ115 to express His_6-MBP-RsiW(73–118), His_6-MBP-RsiW(80–118), His_6-MBP-RsiW(87–118), or His_6-MBP-RsiW(73–122), respectively, was cultured and induced, and extracts were subjected to immunoblot analysis with anti-His antibodies. Two exposures are shown. (E) 2TM-RasP activity on additional His_6-MBP-RsiW fusion proteins. The procedure was as for panel C except that *E. coli* bearing pDP56 or pDP57 to express His_6-MBP-RsiW(87–168) or His_6-MBP-RsiW(87–208), respectively, was cultured and induced, and extracts were subjected to immunoblot analysis with anti-FLAG (5-min exposure) or anti-His (30-s exposure) antibodies in the top and bottom panels, respectively. The dots indicate abundant presumed proteolytic breakdown products independent of RasP activity. The asterisk indicates 2TM-RasP ± E21A, which is weakly detected by anti-His antibodies in lanes 5 and 6 and comigrates with strongly detected His_6-MBP-RsiW(87–208) in lanes 2 and 3. In panels C to E, migration of protein markers is indicated at the left and the inferred identity of signals is indicated at the right, and a representative result from at least two biological replicates is shown.

BL21(DE3) expressing His_6-MBP-FtsL(23-117) alone produced the same species (Fig. S2, lanes 1 and 2). Coexpression of 2TM-RasP with either His_6-MBP-FtsL fusion protein greatly diminished the abundance of all species, and coexpression with 2TM-RasP E21A had much less effect (Fig. 4C, bottom panel), suggesting that all species are substrates of 2TM-RasP, although no apparent cleavage products were detected. We note that 2TM-RasP and 2TM-RasP E21A are undetectable with anti-His antibodies in the exposure shown in the bottom panel of Figure 4C, and that 2TM-RasP reproducibly accumulated better than 2TM-RasP E21A when each was coexpressed with His_6-MBP-FtsL(23-117), as detected with anti-FLAG antibodies (Fig. 4C, top panel, lanes 2 and 3). However, 2TM-RasP and 2TM-RasP E21A accumulated similarly upon coexpression with His_6-MBP-FtsL(23-117) in *clpP* mutant *E. coli*, although still no cleavage product (expected to be ~7 kDa smaller) was detected (Fig. S3, lanes 2 and 3). Likewise, 2TM-RasP and 2TM-RasP E21A accumulated similarly upon coexpression with His_6-MBP-FtsL(23-68) in *clpP*$^+$ *E. coli* and no cleavage product (expected to be ~2 kDa smaller) was detected (Fig. 4C, lanes 5 and 6). 2TM-RasP E21A reproducibly accumulated better than 2TM-RasP upon coexpression with His_6-MBP-FtsL(23-68) in *clpP* mutant *E. coli*, yet only active 2TM-RasP caused complete loss of His_6-MBP-FtsL(23-68) and still no cleavage product was detected (Fig. S3, lanes 5 and 6).

We also constructed genes designed to fuse His_6-MBP to portions of RsiW. One gene was designed to fuse His_6-MBP to the 73rd residue of C-terminally truncated RsiW, designated His_6-MBP-RsiW(73-118) (Fig. 4A and 4B). This fusion protein (expressed from a T7 RNA polymerase promoter) was almost undetectable upon coexpression with 2TM-RasP, but it accumulated considerably upon coexpression with 2TM-RasP E21A (Fig. 4D, lanes 2 and 3). The difference in accumulation of His_6-MBP-RsiW(73-118) upon coexpression with active versus inactive 2TM-RasP strongly suggests that His_6-MBP-RsiW(73-118) is a substrate. As for the other apparent substrates, a detectable cleavage product (expected to be ~2 kDa smaller) failed to accumulate even in *clpP* mutant *E. coli* (Fig. S4).

We also tested three variants of His_6-MBP-RsiW(73-118) that had deletions of the sequence KKRAS (leaving residues 80-118 of RsiW) or KKRASVKRWFRT (leaving residues 87-118 of RsiW) preceding the predicted TMS, or had four additional residues at the C-terminus (QPNL, hence residues 73-122 of RsiW) (Fig. 4A and 4B). The three variants were indistinguishable from His_6-MBP-RsiW(73-118); almost undetectable upon coexpression with 2TM-RasP, but accumulating considerably upon coexpression with 2TM-RasP E21A (Fig. 4D, lanes 4-12), suggesting they are substrates of 2TM-RasP. Detectable cleavage products failed to accumulate. For His_6-MBP-RsiW(87-118), we varied the growth temperature and the time of sample collection post-induction, but still a detectable cleavage product (expected to be ~2 kDa smaller) failed to accumulate (Fig. S5). We conclude that in *E. coli*, the KKRAS sequence of RsiW is not important for proteolytic activity of RasP. Also, leaving an additional 4 residues on the C-terminal end of RsiW did not interfere with RasP activity.

Having established that His_6-MBP-RsiW(87-118) appeared to be a substrate of 2TM-RasP in our *E. coli* system, we tested two derivatives with different C-terminal ends. His_6-MBP-RsiW(87-208) has a full-length C-terminal end and, as expected, was not cleaved by 2TM-RasP (Fig. 4E, bottom panel, lanes 1-3). In contrast, His_6-MBP-RsiW(87-168), which was designed to mimic the C-terminal end after cleavage by PrsW, appeared to be largely cleaved by 2TM-RasP, although some uncleaved His_6-MBP-RsiW(87-168) remained (Fig. 4E, bottom panel, lanes 4-6). Two prominent faster-migrating species also appeared to be substrates for 2TM-RasP (Fig. 4E, bottom panel, dots). The faster-migrating species are not due to *E. coli* RseP (Fig. S2, lanes 3 and 4), but may result from trimming by Tsp and/or activity of other periplasmic proteases in *E. coli*, as reported previously for RsiW upon coexpression with PrsW (12). However, in the previous study, His_6-RsiW cleaved by PrsW failed to accumulate as it was immediately trimmed by Tsp, whereas His_6-MBP-RsiW(87-168) accumulated in our system if 2TM-RasP was absent or catalytically-inactive (Fig. 4E, bottom panel, lanes 4 and 6). We

conclude that His_6-MBP-RsiW(87-168), but not His_6-MBP-RsiW(87-208), appears to serve as a substrate for 2TM-RasP in our *E. coli* system.

Taken together, our results with N-terminal His_6-MBP fusions to TMS-containing parts of FtsL and RsiW provide strong evidence that RasP is proteolytically active on the fusion proteins upon heterologous coexpression in *E. coli*, with the notable exception that His_6-MBP-RsiW(87-208) with a full-length C-terminal end resists cleavage.

RasP cleaves His_6-MBP-RsiW(73-118) *in vitro.* 2TM-RasP did not accumulate significantly better than RasP-$FLAG_2$-His_6 when expressed in *E. coli* (Fig. 3B, right panel, lanes 3 and 6), so we opted to purify RasP-$FLAG_2$-His_6. We reasoned that the latter, lacking the 2 extra TMSs at the N-terminal end of 2TM-RasP, might be easier to solubilize from membranes and would likely be active. RasP-$FLAG_2$-His_6 was solubilized from *E. coli* membranes with the nonionic detergent DM and purified by cobalt-affinity chromatography followed by gel filtration. As a control, we purified RasP-$FLAG_2$-His_6 E21A, which was expected to be inactive. Similarly, we purified His_6-MBP-RsiW(73-118), His_6-MBP-FtsL(23-117), and His_6-MBP-FtsL(23-68) as potential substrates. Each potential substrate was incubated with RasP-$FLAG_2$-His_6, the E21A variant, and alone in separate reactions containing detergent (0.1% DM) and zinc acetate (6 μM). Only incubation of RasP-$FLAG_2$-His_6 with His_6-MBP-RsiW(73-118) resulted in a cleavage product (Fig. 5A, lanes 2 and 3). The cleavage product appeared to be produced by proteolytic activity of RasP-$FLAG_2$-His_6 rather than a contaminating protease from *E. coli* since it was not observed with the E21A variant or the substrate alone (Fig. 5A, lanes 4 and 1, respectively). RasP-$FLAG_2$-His_6 did not appear to cleave either of the potential His_6-MBP-FtsL substrates (Fig. 5B). We considered the possibility that a cleavage product co-migrated with the fastest-migrating species (marked with an asterisk); however, mass spectrometry analysis of the reactions shown in lanes 4 (substrate alone) and 5 (substrate plus enzyme) of Figure 5B produced nearly identical patterns in the mass range expected for the faster-migrating species (Fig. S6). The masses of the most abundant species in this range were consistent with the

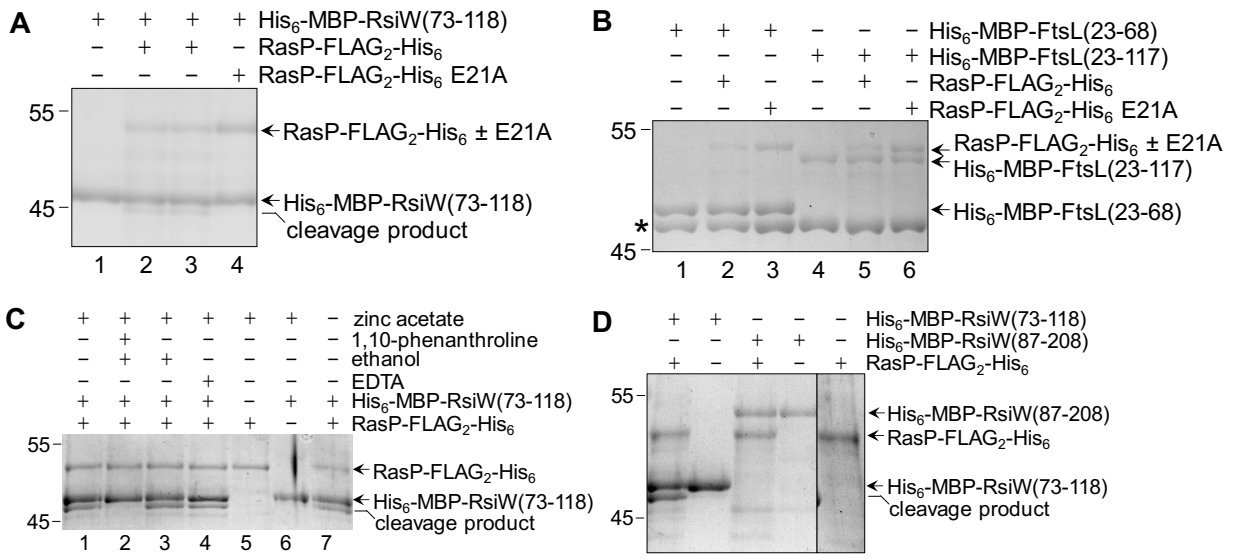

Figure 5 RasP cleaves His$_6$-MBP-RsiW(73–118) but not His$_6$-MBP-FtsL fusion proteins or His$_6$-MBP-RsiW(87– 208) *in vitro*. (A) Cleavage of His$_6$-MBP-RsiW(73–118) by RasP-FLAG$_2$-His$_6$. Purified His$_6$-MBP-RsiW(73–118) was incubated for 4 h alone or in combination with purified RasP-FLAG$_2$-His$_6$ or RasP-FLAG$_2$-His$_6$ E21A as indicated at the top. (B) RasP-FLAG$_2$-His$_6$ fails to cleave His$_6$-MBP-FtsL fusion proteins. Purified His$_6$-MBP- FtsL(23–68) or His$_6$-MBP-FtsL(23–117) was incubated for 12 h alone or in combination with purified RasP-FLAG$_2$-His$_6$ or RasP-FLAG$_2$-His$_6$ E21A as indicated at the top. (C) Dependence of His$_6$-MBP-RsiW(73– 118) cleavage by RasP-FLAG$_2$-His$_6$ on inhibitors and zinc. 1,10-Phenanthroline (5 mM) in ethanol, ethanol alone, or EDTA (5 mM) was added to the reaction mixture, or zinc acetate was omitted, as indicated. (D) RasP-FLAG$_2$ -His$_6$ fails to cleave His$_6$ -MBP-RsiW(87–208). Purified His$_6$ -MBP-RsiW(73–118) as a control or His$_6$-MBP-RsiW(87–208) was incubated with purified RasP-FLAG$_2$-His$_6$, or each protein was incubated separately as a control, as indicated at the top. The observed cleavage product from His$_6$-MBP-RsiW(73–118) (lane 1) is 6 residues longer than that expected if His$_6$-MBP-RsiW(87–208) were cleaved at the same position, but no cleavage product was observed (lane 3). The line indicates that intervening lanes were omitted from the image. For all panels, samples were subjected to SDS-PAGE followed by Coomassie blue staining. Migration of protein markers is indicated at the left, and purified proteins are indicated at the right. In panels A, C, and D, the location of the apparent cleavage product is indicated at the right. In panel B, the asterisk at the left indicates the faster-migrating species that copurified with both His$_6$-MBP-FtsL fusion proteins. A representative result from at least two independent *in vitro* reactions is shown.

predicted mass of His_6-MBP-FtsL(23-58) alone (44,860.2 Da) and with NaCl (44,918.7 Da). This corresponds to a C-terminus several residues beyond the end of the predicted FtsL TMS (Fig. 4A). Hence, the faster-migrating species may result from trimming by Tsp and/or activity of other periplasmic proteases in *E. coli*, but neither this species nor the longer potential His_6-MBP-FtsL substrates appear to be cleaved in their TMS by RasP-$FLAG_2$-His_6. Only His_6-MBP-RsiW(73-118) appeared to serve as a substrate of RasP-$FLAG_2$-His_6 *in vitro*.

To follow up on the apparent cleavage of His_6-MBP-RsiW(73-118) by RasP-$FLAG_2$-His_6 (Fig. 5A, lanes 2 and 3), a sample of the reaction was subjected to mass spectrometry analysis. Strikingly, the most abundant species had a mass of 43,626 ± 5 Da (Fig. 6), in excellent agreement with the predicted mass of His_6-MBP-RsiW(73-94) (43,625.6 Da). This result implies that RasP-$FLAG_2$-His_6 cleaved His_6-MBP-RsiW(73-118) between Ala-94 and Val-95 in the TMS (Fig. 4A). The second most abundant species had a mass of 46,366 ± 5 Da (Fig. 6), consistent with the predicted mass of uncleaved His_6-MBP-RsiW(73-118) (46,361.7 Da). The lower abundance of uncleaved substrate than cleavage product in the mass spectrometry analysis was unexpected based on their apparent abundance from the Coomassie Blue-stained gel (Fig. 5A, lanes 2 and 3). The presence of an intact TMS in the uncleaved substrate, but not in the cleavage product, might explain the discrepancy, since TMSs can impair ionization or other steps in the mass spectrometry analysis. As a control, the reaction in which His_6-MBP-RsiW(73-118) had been incubated alone (Fig. 5A, lane 1) was analyzed by mass spectrometry, and as expected the uncleaved substrate was observed, but not the cleavage product (Fig. S7). As a further control, a reaction in which RasP-$FLAG_2$-His_6 had been incubated alone was analyzed, and as expected neither the uncleaved substrate nor the cleavage product were observed (Fig. S8). Neither was RasP-$FLAG_2$-His_6 (50067.9 Da) observed (Fig. S8), presumably because its four TMSs impaired ionization or other steps, although a low abundance species at 50069 ± 5 Da was detected in the reaction of RasP-$FLAG_2$-His_6 with His_6-MBP-RsiW(73-118) (Fig. 6).

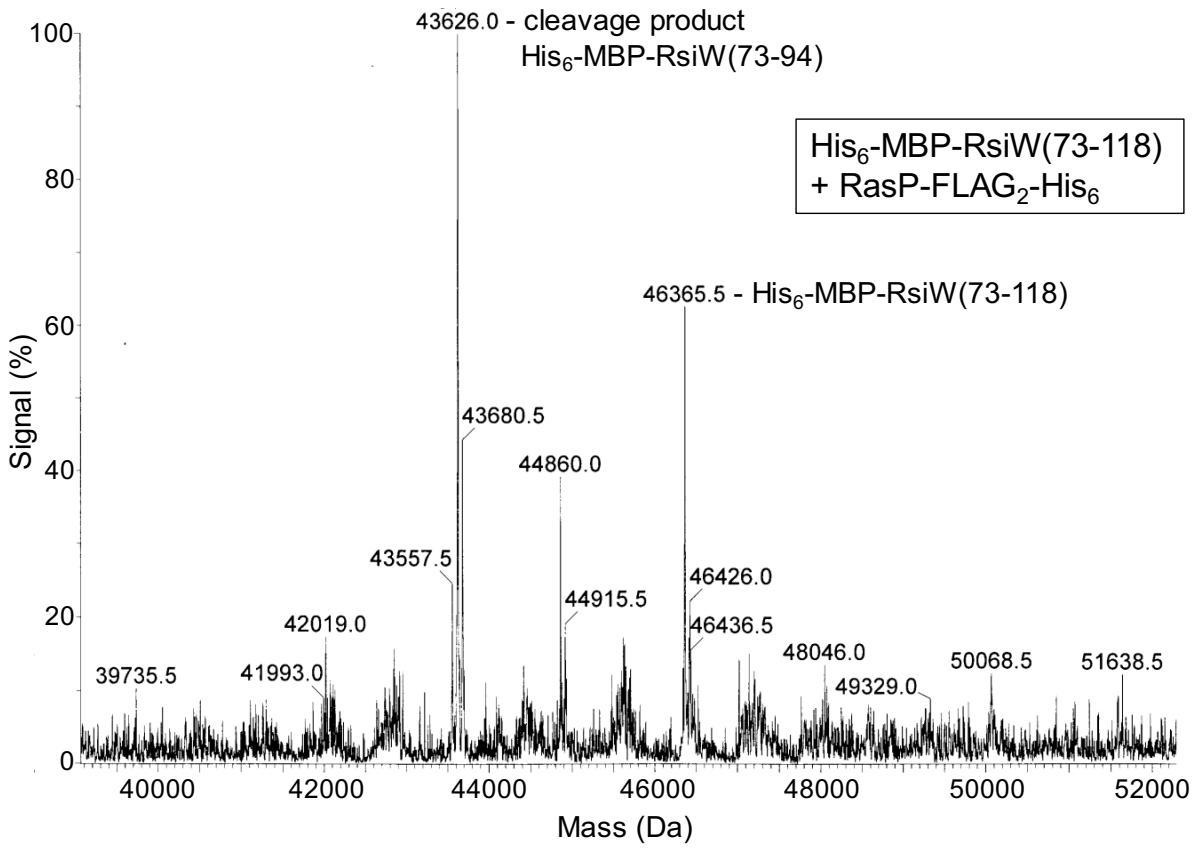

Figure 6 Mass spectrometry analysis of the reaction mixture containing His6-MBP-RsiW(73–118) plus RasP-FLAG2- His6. The zero charge state signal as a percentage of the maximum signal is plotted in the mass range from 39,000 to 52,000 Da. Numbers above peaks give the zero charge state mass (in daltons) at peak maxima. The implied cleavage product His6-MBP-RsiW(73–94) and uncleaved His6-MBP-RsiW(73–118) are indicated.

We conclude that purified RasP-FLAG$_2$-His$_6$ cleaved His$_6$-MBP-RsiW(73-118) within its TMS, demonstrating that RasP is an IMMP. RasP-FLAG$_2$-His$_6$ failed to cleave N-terminally His$_6$-MBP-tagged parts of FtsL beginning with residue 23, spanning the TMS, and ending with residue 117 (the last residue of native FtsL), residue 68 (designed to be comparable to C-terminally trimmed RsiW), or residue 58 (produced by *E. coli* proteolytic activity); possible reasons will be discussed.

Having established that purified RasP-FLAG$_2$-His$_6$ cleaved His$_6$-MBP-RsiW(73-118) within its TMS, we characterized the *in vitro* reaction further. Reducing the reaction temperature to 25°C nearly eliminated cleavage (Fig. S9A). The enzyme appeared to be slightly less active at high salt concentration (Fig. S9B). A time course showed that product accumulates steadily for at least 16 h at 37°C (Fig. S9C), so subsequent reactions were incubated under these conditions. A titration of the enzyme showed that product was approximately proportional to the amount of enzyme added to the reaction over the range tested (Fig. S9D), which covered the testable range given the concentrations of the enzyme and substrate that we purified. As expected, the reaction was inhibited by the metal chelator 1,10-phenanthroline (Fig. 5C, lane 2), as observed previously for *E. coli* RseP (5) and *B. subtilis* SpoIVFB (8). Interestingly, the reaction was not inhibited by EDTA (Fig. 5C, lane 4), perhaps because this metal chelator is highly charged and unable to access the RasP active site. Also, the reaction did not require zinc addition (Fig. 5C, lane 7), as did SpoIVFB (8), suggesting that RasP retained its metal ion during purification. Finally, His$_6$-MBP-RsiW(87-208) was not cleaved (Fig. 5D), consistent with our finding that the full-length C-terminal end blocks cleavage *in vivo* (Fig. 4E).

DISCUSSION

We have established a system for heterologous coexpression of *B. subtilis* RasP with putative substrates in *E. coli.* We have used the system to provide evidence that RasP cleaves FtsL, but putative nonsubstrates with comparably short extracytoplasmic segments also appeared to be cleaved. We found that C-terminally truncated His$_6$-MBP-RsiW fusion proteins

accumulate better than C-terminally truncated His_6-RsiW(1-118) upon coexpression with inactive RasP and provide stronger evidence for proteolysis by active RasP. Moreover, His_6-MBP fusion proteins could be purified, allowing us to demonstrate RasP intramembrane proteolytic activity *in vitro*. To our knowledge, this is only the third instance of an IMMP being purified and shown to cleave a physiological substrate in its TMS. Interestingly, purified RasP cleaved His_6-MBP-RsiW(73-118), but failed to cleave His_6-MBP-FtsL(23-117) or two C-terminally truncated derivatives (ending with residue 68 or residue 58). We conclude that the FtsL fusion proteins have one or more additional requirements for cleavage, which are unmet *in vitro*, but are satisfied upon coexpression in *E. coli.*

Heterologous coexpression of IMMPs and potential substrates. Our results reveal both potential pitfalls and potential solutions in efforts to provide evidence for proteolytic cleavage by IMMPs using heterologous coexpression approaches. First, we found that RasP-His_6 did not accumulate detectably despite overexpression using the powerful T7 RNA polymerase system. In a previous study, overexpression of S-tagged RasP in *E. coli* led to accumulation of a species much smaller than expected, suggesting that RasP was susceptible to degradation (15). We found that addition of $FLAG_2$ to RasP-His_6 allowed detection of RasP-$FLAG_2$-His_6 of the expected size (Fig. 2B). We do not understand why $FLAG_2$ improved accumulation of RasP-$FLAG_2$-His_6, but we note that the same C-terminal tags permitted accumulation of another IMMP, SpoIVFB (8).

Unfortunately, RasP-$FLAG_2$-His_6 inhibited coexpression of potential substrate and non-substrate membrane proteins irrespective of the catalytically-inactivating E21A substitution (Fig. 2C). These results highlight a second potential pitfall in heterologous coexpression experiments. Loss of potential substrate might be misinterpreted as evidence for IMMP-mediated proteolysis unless a control experiment with a catalytically-inactive IMMP is performed. The addition of two TMSs to RasP-$FLAG_2$-His_6 E21A partially or completely relieved inhibition of coexpression of most other membrane proteins. A notable exception was His_6-

RsiW(1-118), which prevented us from obtaining convincing evidence for RasP proteolytic activity on this potential substrate (Fig. S1A). This problem was overcome by fusing N-terminal His_6-MBP to C-terminally truncated RsiW (Fig. 4D).

A third potential pitfall of heterologous coexpression is that cleavage products may be less stable in the heterologous host than in the native organism. In prior work, neither immunoblot nor pulse-chase immunoprecipitation analysis revealed a RasP cleavage product of RsiW upon coexpression in *E. coli*, suggesting the putative cleavage product was unstable (12). In agreement, we were unable to detect RasP cleavage products in *E. coli*, including in a *clpP* mutant (Fig. 3C, S3, and S4). Additional mutations in *E. coli* protease genes might overcome this limitation of our current system.

Our experiments with putative nonsubstrates uncovered promiscuity as a fourth potential pitfall of heterologous coexpression. Since the effect of a *rasP* mutation on stability of SpoIVFB and BofA during *B. subtilis* sporulation has not been reported, we cannot be certain whether the apparent proteolytic activity of 2TM-RasP on cytTM-SpoIVFB-$FLAG_2$-His_6 (Fig. S1B) and GFP-□27BofA (Fig. S1C) is nonphysiological. SpoIVFB appears to have three short (3-8 residue) periplasmic loops (21) and BofA appears to have a short (31 residue) C-terminal periplasmic domain (27) based on analysis of PhoA fusion proteins expressed in *E. coli*, and based on a homology model of SpoIVFB (28). In contrast, SpoIVFA appears to have a long (173 residue) C-terminal extracytoplasmic domain (21, 29), and resisted cleavage by 2TM-RasP (Fig. S1D). Conceivably, the single PDZ domain of RasP (30) (Fig. 2A) acts as a size-exclusion filter as proposed for *E. coli* RseP (31, 32), which has a pair of circularly permuted PDZ domains in tandem, located in a periplasmic loop (33). Recent studies support a model in which the tandem PDZ domains prevent substrate RseA in complex with RseB from entering the RseP active site (31, 32). RseB interacts with a glutamine-rich region of the RseA periplasmic domain, creating a sizable complex (34, 35). Site-1 cleavage by DegS in the RseA periplasmic domain is proposed to reduce its size and release RseB, allowing C-terminally trucated RseA to

enter the active site of RseP (32). Since RseA with its intact 98-residue periplasmic domain can enter the active site of RseP if RseB is absent (36), it seems possible that RasP promiscuously allows coexpressed membrane proteins with small extracytoplasmic domains to enter its active site and be cleaved. Promiscuity may be an important feature of RseP and RasP that allows them to indiscriminately remove remnant signal peptides from membranes (17). Perhaps promiscuity also permits IMMPs with PDZ domains to clear excess subunits of membrane proteins that are normally found in complexes. During *B. subtilis* sporulation, SpoIVFB, BofA, and SpoIVFA form a complex that resists proteolysis, but the absence of any protein from the complex destabilizes the other two proteins (26). Whether the observed instability of SpoIVFB and BofA depends on RasP is unknown. In any case, the results of heterologous coexpression experiments must be interpreted with caution, not only because partner proteins may be missing but because expression levels and other factors may differ from the native organism.

Taken together with previous studies, our results reveal strategies that may apply broadly to the development of systems for heterologous coexpression of IMMPs and potential substrates. Addition of N-terminal cytTM (with proper attention to preserve its usual membrane topology, as was done by also adding SpoIVFBTM1 in the case of 2TM-RasP) and C-terminal $FLAG_2$-His_6 proved beneficial for both RasP in this study (Fig. 2 and 3) and for SpoIVFB in a previous study (8). Addition of N-terminal His_6-MBP to potential substrates was beneficial in this study, because such fusion proteins accumulated better than their N-terminally His_6-tagged counterparts upon coexpression with 2TM-RasP E21A and thus provided stronger evidence for proteolysis by 2TM-RasP (Fig. 4). Also, the His_6-MBP fusion proteins could be purified for *in vitro* studies (Fig. 5 and 6). Efforts to develop *E. coli* coexpression systems for other IMMPs and potential substrates, as well as work toward reconstituting proteolysis *in vitro*, might benefit by taking similar approaches.

Evidence that RasP cleaves full-length FtsL and C-terminally truncated RsiW *in vivo.* Part of the motivation for this study was to further investigate whether RasP cleaves full-length

FtsL without prior site-1 cleavage. This was suggested by the absence of a detectable site-1 cleavage product in *rasP* mutant *B. subtilis* (15). Given that RseP can cleave full-length RseA with its 98-residue periplasmic domain if RseB is absent (36), it seemed possible that full-length FtsL with its 64-residue extracytoplasmic domain might be cleaved by RasP. Indeed, full-length FtsL-His_6 (Fig. 3B) and His_6-FtsL (Fig. 3C), and His_6-MBP-FtsL(23-117) with an intact extracytoplasmic domain (Fig. 4C) all appeared to be cleaved by 2TM-RasP in *E. coli*. How then is FtsL cleavage by RasP regulated in *B. subtilis*? It has been suggested that a RasP recognition sequence, KKRAS, in the N-terminal cytoplasmic domain of FtsL (Fig. 4A) is shielded from RasP when FtsL interacts with other proteins in the divisome, and it was shown that DivIC interacts with FtsL and stabilizes FtsL against RasP cleavage upon heterologous coexpression in *E. coli* (16). In *B. subtilis*, divisome disassembly after division would uncover the KKRAS sequence of FtsL, allowing cleavage by RasP. In *E. coli* that are not coexpressing DivIC, the KKRAS sequence would be exposed, and our results (Fig. 3B, 3C, and 4C) support the notion that RasP can cleave full-length FtsL without prior site-1 cleavage (15, 16).

In contrast to FtsL, there is strong evidence from *in vivo* studies that RsiW undergoes site-1 cleavage by PrsW (10, 11). PrsW appears to remove 40 residues from the 103-residue C-terminal extracytoplasmic domain of RsiW (12). The remaining 63-residue extracytoplasmic portion is similar in length to the 64-residue extracytoplasmic domain of full-length FtsL, yet in a previous study it was concluded that RsiW must be further trimmed by extracytoplasmic proteases in order to be cleaved by RasP (12). The authors engineered *E. coli* to coexpress His_6-RsiW and PrsW. A 14 kDa form of His_6-RsiW accumulated, unless an *E. coli tsp* mutant was used, in which case a 19 kDa form accumulated. Further experiments provided evidence that the 19 kDa form was the PrsW cleavage product, the 14 kDa form resulted from trimming by Tsp, and only the 14 kDa form could be cleaved by RasP.

Our results support the requirement for site-1 cleavage of RsiW, but not the need for further trimming by extracytoplasmic proteases, prior to cleavage by RasP in our *E. coli* system. The

requirement for site-1 was demonstrated by our finding that His_6-MBP-RsiW(87-208) was not cleaved by 2TM-RasP (Fig. 4E). In contrast, His_6-MBP-RsiW(87-168), which was designed to mimic the product of site-1 cleavage by PrsW, appeared to be cleaved by 2TM-RasP without the need for further trimming by extracytoplasmic proteases. In the context of a model in which the PDZ domain acts as a size-exclusion filter (31, 32), our results suggest that the RasP PDZ domain excludes the full-length 103-residue extracytoplasmic domain of RsiW, but not the 63-residue extracytoplasmic portion after PrsW cleavage.

Perhaps the high level of expression using T7 RNA polymerase in our *E. coli* system accounts for the differences between our results and the previous study (12). Our site-1 cleavage mimic, His_6-MBP-RsiW(87-168), accumulated despite the presence of Tsp (Fig. 4E), whereas in the previous study Tsp immediately trimmed the 19 kDa form of His_6-RsiW resulting from site-1 cleavage by PrsW to a 14 kDa form (12). We observed two abundant breakdown products of His_6-MBP-RsiW(87-168) that may result from Tsp trimming (Fig. 4E, lane 4, dots). The larger and smaller breakdown products may result from Tsp trimming that stops prior to reaching the membrane and upon reaching the membrane, respectively. The smaller breakdown product might correspond to the 14 kDa form of His_6-RsiW observed previously (12). In addition to the high level of expression in our *E. coli* system, the addition of MBP likely contributes to stability of His_6-MBP-RsiW(87-168) and its breakdown products. High level coexpression of 2TM-RasP may account for the apparent cleavage of His_6-MBP-RsiW(87-168) and its breakdown products that we observed (Fig. 4E, lane 5).

It is unlikely that the PDZ domain of RasP must bind to a particular residue at the C-terminus of RsiW or FtsL, as had been proposed for the second of the tandem PDZ domains of *E. coli* RseP after site-1 cleavage of RseA by DegS based on *in vitro* results (37). These results did not agree with a subsequent *in vivo* study (31). Moreover, structural analysis of the tandem PDZ domains of *Aquifex aeolicus* RseP revealed tryptophan and proline residues lining the ligand-binding groove, that would likely be unfavorable for binding the C-terminal end of the

substrate, and these residues are conserved in the tandem PDZ domains of *E. coli* RseP (32) and in the PDZ domain of RasP (W237 and P288). Also, His_6-MBP fusions to FtsL or RsiW with several different C-terminal ends all appeared to be cleaved by 2TM-RasP in *E. coli* (Fig. 4).

In addition to the apparent difference between RsiW and FtsL in terms of a requirement for site-1 cleavage, another apparent difference relates to the KKRAS sequence. This sequence appears to be important for recognition of FtsL by RasP both in *B. subtilis* (15) and upon heterologous coexpression in *E. coli* (16). In contrast, the KKRAS sequence in RsiW did not appear to be important for cleavage by 2TM-RasP in our *E. coli* system (Fig. 4A, 4D, and 4E). It remains to be tested whether the KKRAS sequence would be dispensable for RsiW cleavage by RasP in *B. subtilis.* Also, it remains to be tested whether the KKRAS sequence would be dispensable for His_6-MBP-FtsL cleavage by 2TM-RasP in our *E. coli* system.

RasP cleaves the TMS of RsiW *in vitro*, but not that of FtsL. Our results indicate that purified RasP-$FLAG_2$-His_6 cleaved His_6-MBP-RsiW(73-118) within its TMS between Ala-94 and Val-95 (Fig. 4A, 5A, and 6), demonstrating that RasP is an IMMP. Only two other IMMPs, RseP (5) and SpoIVFB (8), have been shown to cleave a physiological substrate *in vitro*. In both cases, the cleavage site *in vitro* was the same as that *in vivo*. We were unable to map the *in vivo* cleavage site of RsiW due to instability of the cleavage product, even in *clpP* mutant *E. coli* (Fig. 3C, S3, and S4). However, previous mutational analysis of the four consecutive alanine residues preceding the *in vitro* cleavage site (Fig. 4A) suggested that RasP cleaves RsiW somewhere after alanine residues 92-94 in *B. subtilis* (13). These observations agree with the cleavage site we mapped between Ala-94 and Val-95 by mass spectrometry analysis of *in vitro* reaction products (Fig. 4A, 5A, and 6).

Neither full-length His_6-MBP-FtsL(23-117) nor two C-terminally truncated derivatives (ending with residue 68 or residue 58) appeared to be cleaved by RasP-$FLAG_2$-His_6 *in vitro* (Fig. 5B and S6). We hypothesize that a lack of □-helix-destabilizing residues in the TMS of FtsL prevents cleavage (Fig. 4A). Helix-destabilizing residues have been shown to be important for cleavage

of RseA by RseP *in vivo* and *in vitro* (5). The helix-destabilizing residues in RseA stabilize its interaction with RseP (38). The predicted TMS of RsiW is immediately preceded by a proline residue and contains three consecutive glycine residues (Fig. 4A), which might destabilize the TMS enough to allow cleavage by RasP *in vitro*. By substituting helix-stabilizing residues such as leucine into the predicted TMS of His_6-MBP-RsiW(73-118), and helix-destabilizing residues into the predicted TMS of His_6-MBP-FtsL(23-117), we plan to test the importance of helix stability in cleavage by RasP-$FLAG_2$-His_6 *in vitro.*

Since full-length His_6-MBP-FtsL(23-117) and C-terminally truncated derivatives do appear to be cleaved by 2TM-RasP upon coexpression in *E. coli* (Fig. 4C), we favor the idea that the membrane environment overcomes the lack of □-helix-breaking residues in the FtsL TMS to permit cleavage, although we cannot rule out the possibility that one or more additional protein conserved between *E. coli* and *B. subtilis* is required. Incorporation of SpoIVFB into liposomes enhanced cleavage of Pro-σ^K, relative to SpoIVFB in detergent micelles (8). This approach was facilitated by the finding that Pro-σ^K in detergent micelles associated stably with liposomes. Unlike the TMS of FtsL, the pro-sequence of Pro-σ^K associates peripherally with membranes (39, 40). It would likely be necessary to incorporate FtsL and RasP into the same liposome, either by co-incorporation or by liposome fusion, in order to test whether a membrane environment would allow cleavage.

Purified RasP-$FLAG_2$-His_6 cleaved His_6-MBP-RsiW(73-118) slowly (Fig. S9C), consistent with the behavior of RseP (5, 33) and SpoIVFB (8) *in vitro*. In addition to these IMMPs, other types of IPs including rhomboids (41, 42) and □-secretase (43, 44) exhibit slow rates of catalysis. Substrate gating (i.e., substrate access to the active site) rather than substrate affinity appears to be rate limiting in the case of the rhomboid GlpG (41). Whether a similar mechanism explains the kinetic properties of RasP and other IPs remains to be determined.

RasP-FLAG$_2$-His$_6$ behaved differently *in vitro* than most soluble metalloproteases in that His$_6$-MBP-RsiW(73-118) cleavage was not inhibited by the metal chelator EDTA (Fig. 5C, lane 4). It will be interesting to see whether this is a general characteristic of IMMPs. The effect of EDTA on RseP and SpoIVFB activity has not been reported. Addition of zinc acetate was important for SpoIVFB activity *in vitro*, perhaps because this IMMP required the harsh ionic detergent sarkosyl for solubilization from membranes, thus depleting the enzyme of zinc (8). Omission of zinc has not been reported for RseP, but like RasP, RseP can be solubilized from membranes with a mild detergent (5) so it may retain zinc during purification.

Purified RasP-FLAG$_2$-His$_6$ discriminated between potential His$_6$-MBP-RsiW substrates with different C-terminal ends, cleaving a truncated one ending with residue 118 but not a full-length one ending with residue 208 (Fig. 5D), consistent with our heterologous coexpression results (Fig. 4D and 4E). RseP likewise discriminated between truncated and full-length His$_6$-MBP-RseA substrates *in vitro* (33). Discrimination was lost by an RseP variant with substitutions in TMS 2 (A115V) and the first PDZ domain (G214E) that together appear to alter the conformation of the periplasmic region containing the tandem PDZ domains, based on trypsin sensitivity. Hence, biochemical experiments, as well as genetic and structural studies, support the model that the PDZ domains of RseP act as a size-exclusion filter for substrate discrimination (31-33). Our results are consistent with the PDZ domain of RasP playing a similar role. The methods we have established for investigation of RasP proteolytic activity in *E. coli* and *in vitro* can be used to further explore the role of the PDZ domain, as well as many other questions that remain to be addressed.

MATERIALS AND METHODS

Plasmids. The plasmids used in this study are described in Table S1 in the supplemental material, and primers are listed in Table S2. DNA sequencing was used to confirm the desired

sequences in cloned PCR products and genes subjected to site-specific mutagenesis (QuikChange kit; Stratagene).

Cotransformation and induction. Two plasmids with different antibiotic resistance genes and different genes fused to the T7 RNA polymerase promoter were cotransformed into *E. coli* BL21(DE3) and gene expression was induced with isopropyl β-D-thiogalactopyranoside (IPTG) as described previously (45) except cultures were shaken at 250 rpm. Briefly, transformants were grown in Luria-Bertani (LB) liquid medium containing 50 μg/mL kanamycin sulfate and 200 μg/mL ampicillin overnight at 37°C, then diluted 50-fold with fresh LB containing antibiotics, and grown until the culture reached the mid-log phase (about 60 Klett units), at which time IPTG (0.5 mM) was added and the culture was induced for 2 h. In one experiment, the growth temperature and induction time was varied. As controls, plasmids were transformed singly into *E. coli* and cultures were induced in parallel experiments. In some experiments, plasmids were transformed into a derivative of *E. coli* BL21(DE3) with a null mutation in *clpP*. This strain, designated EDP55, was constructed by using bacteriophage $P1_{vir}$ to transduce a *clpP* allele with a chloramphenicol resistance insertion (46) from strain MC4100 *clpP*::*cat* (a gift from Tania Baker) into BL21(DE3). Likewise, strain EZR489 was constructed by using $P1_{vir}$ to transduce an *rseP* allele with a kanamycin resistance insertion and an *rseA* allele with a chloramphenicol resistance insertion from strain KK377 (5) into BL21(DE3).

Immunoblot analysis. An equivalent amount of cells (based on the optical density of the culture at 600 nm) were collected from 0.5 to 1.0 mL of culture by centrifugation (12,000 × *g*) and cell extracts were prepared, mixed with an equal volume of 2× sample buffer (50 mM Tris·HCl pH 6.8, 4% SDS, 20% glycerol, 200 mM DTT, and 0.03% bromophenol blue), and boiled for 3 min as described previously (45). Equal volumes were subjected to SDS-PAGE and immunoblotting as described previously (47). SeeBlue Plus2 Prestained Standard (Invitrogen) was used to judge migration of protein species. Antibodies that recognize His_6 (penta-His,

Qiagen, catalog #34460), FLAG (M2 monoclonal antibody-peroxidase conjugate, Sigma, catalog #A8592), or green fluorescent protein (GFP) (47) were used at 1:10,000 dilution. Antibodies that recognize SpoIVFA (47) were used at 1:3000 dilution. A goat anti-rabbit immunoglobulin-horseradish peroxidase conjugate (Bio-Rad, catalog #170-6515 was used at 1:10,000 dilution to detect the anti-GFP and anti-SpoIVFA antibodies. Signals were detected using a ChemiDoc MP imager (Bio-Rad).

Large-scale overexpression of proteins for purification. For RasP-$FLAG_2$-His_6 ± E21A, the appropriate plasmids were transformed into *E. coli* BL21 (DE3) and transformants were selected, grown in a fermentor with vigorous aeration and pH control, induced with IPTG, collected, and stored as described previously (8). For potential substrates, the appropriate plasmids were transformed into *E. coli* BL21 (DE3) and induction was performed as described above, with cells grown in 4 L LB in flasks.

Protein purification. For RasP-$FLAG_2$-His_6 ± E21A, cells (10 g) were resuspended in 30 mL of lysis buffer (PBS containing 0.1 mg/mL lysozyme, 1 mg/mL RNase A, 2 mg/mL DNase I, 1 mM PMSF, 10 mM 2-mercaptoethanol, and 10% glycerol), incubated at 37°C for 10 min, and passed 3 times through a French pressure cell (SLM Aminco) at 14,000 psi (96 MPa). The cell lysate was centrifuged at low speed (15,000 × *g* for 15 min at 4°C) to sediment cell debris. The supernatant was centrifuged at high speed (150,000 × *g* for 90 min at 4°C) to sediment membrane vesicles. The pellet was dispersed in 30 mL of resuspension buffer (PBS containing 1 mM Pefabloc SC, 5 mM 2-mercaptoethanol, and 10% glycerol) using a motorized dounce homogenizer. The suspension was treated with *n*-decyl-β-D-maltoside (DM) (1%) (Anatrace, Maumee, OH) by rotating the mixture for 1 h at 4°C in order to solubilize membrane proteins. The mixture was then centrifuged at 150,000 × *g* for 75 min at 4°C to sediment insoluble material. The supernatant was mixed with 1 mL Talon superflow metal affinity resin (Clontech) that had been equilibrated with buffer (PBS containing 1% DM, 5 mM 2-mercaptoethanol, and 10% glycerol). The mixture was rotated for 1 h at 4°C. The cobalt resin was sedimented by

centrifugation at 708 × *g* for 2 min at 4°C. The cobalt resin was washed 3 times with PBS containing 150 mM NaCl, 10% glycerol, and the following (5 mL with 0.5% DM; 5 mL with 0.1% DM; 3.5 mL with 0.1% DM and 10 mM imidazole) by rotating briefly then sedimenting the resin as above. To elute the protein, the resin was mixed with 1 mL PBS containing 150 mM NaCl, 10% glycerol, 0.1% DM, and 400 mM imidazole by rotating the mixture for 5 min at room temperature, then the resin was sedimented as above. The supernatant was applied to a 1.0 cm × 30 cm Superdex 200 gel filtration column equilibrated with PBS containing 150 mM NaCl, 5% glycerol, and 0.1% DM. The column was eluted with the same buffer at 0.4 mL/min and 0.5-mL fractions were collected. Fractions were analyzed by SDS-PAGE followed by Coomassie Blue staining of proteins and detection of RasP-FLAG$_2$-His$_6$ ± E21A by immunoblot, and 3 or 4 fractions containing the highest concentration of the desired protein were concentrated to 0.5 mL using an Amicon Ultra centrifugal device with a 10-kDa cut-off (Millipore). The final concentration of both enzymes was 0.3 mg/ml as determined using the Bio-Rad Protein Assay with bovine IgG as the standard. The enzymes were either added immediately to reaction mixtures for *in vitro* proteolysis as described below, or glycerol was added to a final concentration of 10% and the enzymes were stored at -80° in aliquots until use. One freeze/thaw cycle did not detectably change activity.

For potential substrates, the desired proteins were purified as described above with the following modifications: cells (7.5 g) were resuspended in 23 mL of lysis buffer containing 3 tablets of Roche cOmplete Mini protease inhibitors instead of 1 mM PMSF; the pellet containing membrane vesicles was dispersed in 15 mL of resuspension buffer containing 1 tablet of Roche cOmplete Mini protease inhibitors instead of 1 mM Pefabloc SC; the cobalt resin was washed 2 times with PBS containing 150 mM NaCl, 10% glycerol, and the following (5 mL with 0.5% DM; 5 mL with 0.1% DM); the protein was eluted stepwise by mixing the resin with 1 mL of PBS containing 150 mM NaCl, 10% glycerol, 0.1% DM and 30-450 mM imidazole in 30 mM increments. Fractions were analyzed by SDS-PAGE followed by Coomassie Blue staining of

proteins and detection of the desired protein by immunoblot. The fraction containing the highest concentration of the desired protein was further purified by gel filtration, fractions were analyzed, and the desired protein was concentrated as described above. The final concentration of each potential substrate was 1 mg/ml as determined using the Bio-Rad Protein Assay with bovine IgG as the standard. The potential substrates were either added immediately to reaction mixtures for *in vitro* proteolysis as described below, or glycerol was added to a final concentration of 10% and the potential substrates were stored at -80° in aliquots until use. One freeze/thaw cycle did not detectably change the result.

Reaction mixtures for *in vitro* proteolysis with purified proteins. Reaction mixtures contained purified RasP-FLAG$_2$-His$_6$ (2 μg) or RasP-FLAG$_2$-His$_6$ E21A (3 μg) and purified His$_6$-MBP-RsiW(87-208) (2 μg), His$_6$-MBP-RsiW(73-118) (4 μg), His$_6$-MBP-FtsL(23-117) (6 μg), or His$_6$-MBP-FtsL(23-68) (8 μg) in 30 μL PBS, pH 7.2, 150 mM NaCl, 10% glycerol, 0.1% DM, and 6 μM zinc acetate, unless indicated otherwise. Reaction mixtures were incubated at 37°C for 16 h unless indicated otherwise, then terminated by the addition of an equal volume of 2× sample buffer and boiling for 3 min before SDS-PAGE followed by Coomassie Blue staining of proteins.

Mass spectrometry analysis. Samples of reaction mixtures for *in vitro* proteolysis were submitted to the Mass Spectrometry and Metabolomics Core of the Research Technology Support Facility at Michigan State University. The samples were subjected to desalting on a 10 mm × 1.0 mm BetaBasic CN column (5 μm particles; Thermo). Protein was eluted from the column by a gradient using solvent A = 0.1% aqueous formic acid and solvent B = acetonitrile, starting at A/B = 99/1, and increasing to A/B = 30/70 at 5 min after injection and holding at this composition for an additional 5 min. Analysis employed electrospray ionization (positive polarity) and a Xevo G2-S QTof mass spectrometer (Waters). Electrospray ionization mass spectra were deconvoluted to a zero charge state spectrum using the Waters MaxEnt1 software tool.

ACKNOWLEDGMENTS

We thank Benjamin Pursley for constructing pBP2, Dexin Sui and R. Michael Garavito for the gift of p17b-H6-TEV-MCS, Lee Alexander and R. Mark Worden of the Michigan State University Protein Expression Lab for performing the large-scale overexpression of proteins, and Lijun Chen and A. Daniel Jones of the Mass Spectrometry and Metabolomics Core of the Research Technology Support Facility at Michigan State University for performing the mass spectrometry analysis and for helpful comments on that section of the manuscript.

FUNDING INFORMATION

Research reported in this publication was supported by the National Institute of General Medical Sciences of the National Institutes of Health under award number R01GM43585. The content is solely the responsibility of the authors and does not necessarily represent the official views of the National Institutes of Health. Partial salary support for L.K. was provided by Michigan State University AgBioResearch and for D.P. by the Eleanor L. Gilmore Endowed Excellence Award administered by the Department of Microbiology and Molecular Genetics at Michigan State University.

APPENDIX A

SUPPLEMENTAL MATERIAL

Table S1. Plasmids used in this study

Plasmid[a]	Description[b]	Construction	Reference
p17b-H6-TEV-MCS	Ap^R; expression vector	Coding sequences for H6 and a TEV protease cleavage site were cloned into NdeI-BamHI-digested pET17b	D. Sui and R.M. Garavito, unpublished data
pBP2	Ap^R; MBP-RsiW(1-122)	Part of *rsiW* was amplified by PCR using *B. subtilis* PY79 (53) chromosomal DNA as template and primers LK2581 and LK2582, the fragment was digested with NotI and XhoI, then cloned into NotI-XhoI-digested pRMG-*Eco*MBP	This study
pCR2.1-TOPO	Ap^R/Km^R; PCR cloning vector		Invitrogen
pDP56	Ap^R; H6-MBP-RsiW(87-168)	A DNA fragment encoding MBP-RsiW(87-118) was amplified by PCR using pYZ76 as template and primers PDP147 and PDP148. A fragment of *rsiW* encoding residues 119-168 was amplified from *B. subtilis* PY79 chromosomal DNA (53) using primers PDP 149 and PDP153. The two fragments were used as templates for sequence overlap extension with primers PDP147 and PDP 153 to amplify a fragment encoding MBP-RsiW (87-168). This fragment was digested with NdeI and XhoI, and cloned into NdeI-XhoI-digested pYZ76.	This study
pDP57	Ap^R; H6-MBP-RsiW(87-208)	A DNA encoding MBP-RsiW(87-118) was amplified by PCR using pYZ76 as template and primers PDP147 and PDP148. A fragment of *rsiW* encoding residues 119-208) was amplified from *B. subtilis* PY79 chromosomal DNA (53) using primers PDP 149 and PDP152. These two fragments were used as templates for sequence overlap extension with primers PDP147 and PDP 152 to amplify a fragment encoding MBP-RsiW (87-208). This fragment was digested with NdeI and XhoI, and cloned into NdeI-XhoI-digested pYZ76.	This study
pET-17b	Ap^R; expression vector		Novagen
pET-21b	Ap^R; expression vector		Novagen
pET-29b	Km^R; expression vector		Novagen
pLW01	Ap^R; expression vector		(54)
pRMG-*Eco*MBP	Ap^R; T7 RNA polymerase promoter fused to the *E. coli malE* gene for expression of MBP fusion proteins	Coding sequence for *E. coli* MalE (MBP) residues 29-390 was cloned between the NcoI and NotI sites of the pLW01 MCS, and the coding sequence of a TEV protease cleavage site and a BamHI recognition site were cloned between the NotI and XhoI sites of the pLW01 MCS	(55)

Table S1 (cont'd)

pYZ5	Ap^R/Km^R; RasP	*rasP* was amplified by PCR using *B. subtilis* PY79 (53) chromosomal DNA as template and primers LK2566 and LK2567, then cloned into pCR2.1-TOPO	This study
pYZ9	Km^R; RasP-H6	NdeI-HindIII fragment from pYZ5 was subcloned into NdeI and HindIII digested pET-29b vector	This study
pYZ16	Ap^R/Km^R; FtsL	*ftsL* was amplified by PCR using *B. subtilis* PY79 (53) chromosomal DNA as template and primers LK2632 and LK2633, then cloned into pCR2.1-TOPO	This study
pYZ20	Ap^R; FtsL-H6	NdeI-XhoI fragment from pYZ16 was ligated to NdeI-XhoI-digested pET-21b	This study
pYZ29	Km^R; cytTM-SpoIVFBTM1-RasP-F2-H6	NdeI-HindIII fragment from pYZ5 was ligated to NdeI-HindIII-digested pZR236	This study
pYZ37	Km^R; RasP-F2-H6	NdeI-XhoI fragment from pYZ29 was ligated to NdeI-XhoI-digested pET-29b	This study
pYZ44	Km^R; RasP-F2-H6 E21A	pYZ37 was subjected to site-directed mutagenesis using primers YZ110 and YZ111	This study
pYZ47	Ap^R; H6-RsiW(1-118)	Part of *rsiW* was amplified by PCR using pBP2 as template and primers YZ116 and YZ92, the fragment was digested with BamHI and XhoI, and ligated to BamHI-XhoI-digested p17b-H6-TEV-MCS	This study
pYZ52	Ap^R; H6-RsiW(1-118)	pYZ47 was subjected to site-directed mutagenesis using primers YZ112 and YZ113 to introduce a *lac* operator after the T7 RNA polymerase promoter	This study
pYZ53	Km^R; cytTM-SpoIVFBTM1-RasP-F2-H6 E21A	pYZ29 was subjected to site-directed mutagenesis using primers YZ110 and YZ111	This study
pYZ57	Ap^R; H6-FtsL	*ftsL* was amplified by PCR using pYZ20 as template and primers YZ107 and YZ96, the fragment was digested with BamHI and XhoI, and ligated to BamHI-XhoI-digested pYZ52	This study
pYZ66	Ap^R; H6-FtsL	*H6-ftsL* was amplified by PCR using pYZ57 as template and primers YZ95 and YZ96, the fragment was digested with NdeI and XhoI, and ligated to NdeI-XhoI digested pET-21b	This study
pYZ69	Ap^R; H6-MBP-RsiW(73-118)	*malE* was amplified by PCR using pBP2 as template and primers YZ89 and YZ90, part of *rsiW* was amplified by PCR using pYZ52 as template and YZ91 and YZ92 as primers, the two fragments were used as template for sequence overlap extension PCR with primers YZ89 and YZ92, the fragment was digested with NdeI and XhoI, and ligated to NdeI-XhoI-digested pET-21b	This study

Table S1 (cont'd)

pYZ75	Ap^R; H6-MBP-RsiW(80-118)	pYZ69 was subjected to site-directed mutagenesis using primers YZ83 and YZ84	This study
pYZ76	Ap^R; H6-MBP-RsiW(87-118)	pYZ69 was subjected to site-directed mutagenesis using primers YZ81 and YZ82	This study
pYZ111	Ap^R; H6-MBP-FtsL(23-68)	Part of *ftsL* was amplified by PCR using pYZ66 as template and primers YZ35 and YZ36, the fragment was digested with NotI and XhoI, and ligated to NotI-XhoI-digested pYZ69	This study
pYZ112	Ap^R; H6-MBP-FtsL(23-117)	Part of *ftsL* was amplified by PCR using pYZ66 as template and primers YZ35 and YZ96, the fragment was digested with NotI and XhoI, and ligated to NotI-XhoI-digested pYZ69	This study
pYZ115	Ap^R; H6-MBP-RsiW(73-122)	Part of *rsiW* was amplified by PCR using pBP2 as template and primers YZ124 and YZ91, the fragment was digested with NotI and XhoI, and ligated to NotI-XhoI-digested pYZ69	This study
pZR62	Ap^R; GFP-□27BofA		(45)
pZR73	Ap^R; SpoIVFA		(45)
pZR209	Ap^R; cytTM-SpoIVFB-F2-H6		(8)
pZR236	Km^R; cytTM-SpoIVFB-F2-H6		(8)

[a] All plasmids used for protein expression have the pBR322 origin of replication.
[b] Abbreviations: Ap^R, ampicillin-resistant; Km^R, kanamycin-resistant; cytTM, transmembrane segment from rabbit Cytochrome P450 2B4; MBP, maltose-binding protein; MCS, multiple cloning site; F2, two FLAG epitopes; H6, 6 His residues; SpoIVFBTM1, first transmembrane segment of SpoIVFB; TEV, Tobacco Etch Virus.

Table S2. Primers used in this study

Primer	Sequence
LK2566	CATATGTTCGTGAATACAGTTATAGC
LK2567	AAGCTTCAAAAACAGCCGCTGGATATC
LK2581	GCGGCCGCCATGAGCTGTCCTGAACAAATTGT
LK2582	CTCGAGTTAAAGATTCGGCTGCTTGGACAC
LK2632	CATATGAGCAATTTAGCTTACCAACC
LK2633	CTCGAGTTCCTGTATGTTTTTCACTTTTTTATC
PDP147	TTAACTTTAAGAAGGAGATATACATATGGCACAAGCTTAAGGAGATATACATATGCACCA
PDP148	CTTGGACACGCTGAAATTGTG
PDP149	CACAATTTCAGCGTGTCCAAG
PDP152	GTGGTGCTCGAGTTACTCTTCTCCGTTCGGATTG
PDP153	GTGGTGCTCGAGTTAGGCCATATACTTTTCGCCGTT
YZ35	GGATGCGGCCGCCATTGTCAAGAAAAGGGCTTCCAT
YZ36	GCAACTCGAGTCACTTTTGCACCTCAATATTGGTTT
YZ81	GAAGCCCTGAAAGACGCGCATCCCGTTATCGCAGCT
YZ82	AGCTGCGATAACGGGATGCGCGTCTTTCAGGGCTTC
YZ83	GAAGCCCTGAAAGACGCGGTAAAAAGATGGTTCAGA
YZ84	TCTGAACCATCTTTTTACCGCGTCTTTCAGGGCTTC
YZ89	CAGAGTCATATGCACCACCACCACCACCACGAAACTGAAGAAGGTAAACTGGTAATC
YZ90	TCTTTTTACAGAAGCTCTTTTCTTCTCCTTGGCGGCCGCGTCTTTCAGGGCTTCATCGAC
YZ91	GTCGATGAAGCCCTGAAAGACGCGGCCGCCAAGGAGAAGAAAAGAGCTTCTGTAAAAAGA
YZ92	CAGGCTCGAGTTACTTGGACACGCTGAAATTGTG
YZ95	CAGAGTCATATGCACCACCACCACCACCACATGAGCAATTTAGCTTACCAAC
YZ96	GCAACTCGAGTCATTCCTGTATGTTTTTCACTTTTTTATC
YZ107	GAGCGGATCCATGAGCAATTTAGCTTACCAAC
YZ110	CGCTCGTTTTCTTCCATGCGCTGGGCCATTTATTGC
YZ111	GCAATAAATGGCCCAGCGCATGGAAGAAAACGAGCG
YZ112	AATACGACTCACTATAGGGGAATTGTGAGCGGATAACAATTCCCCTCTAGAAATAATTTTG
YZ113	CAAAATTATTTCTAGAGGGGAATTGTTATCCGCTCACAATTCCCCTATAGTGAGTCGTATT
YZ116	GCTCGGATCCATGAGCTGTCCTGAACAAATTGTG
YZ124	GTGGTGGTGCTCGAGTTAAAGATTCGGCTGCTTGGACACGCTGAAATT

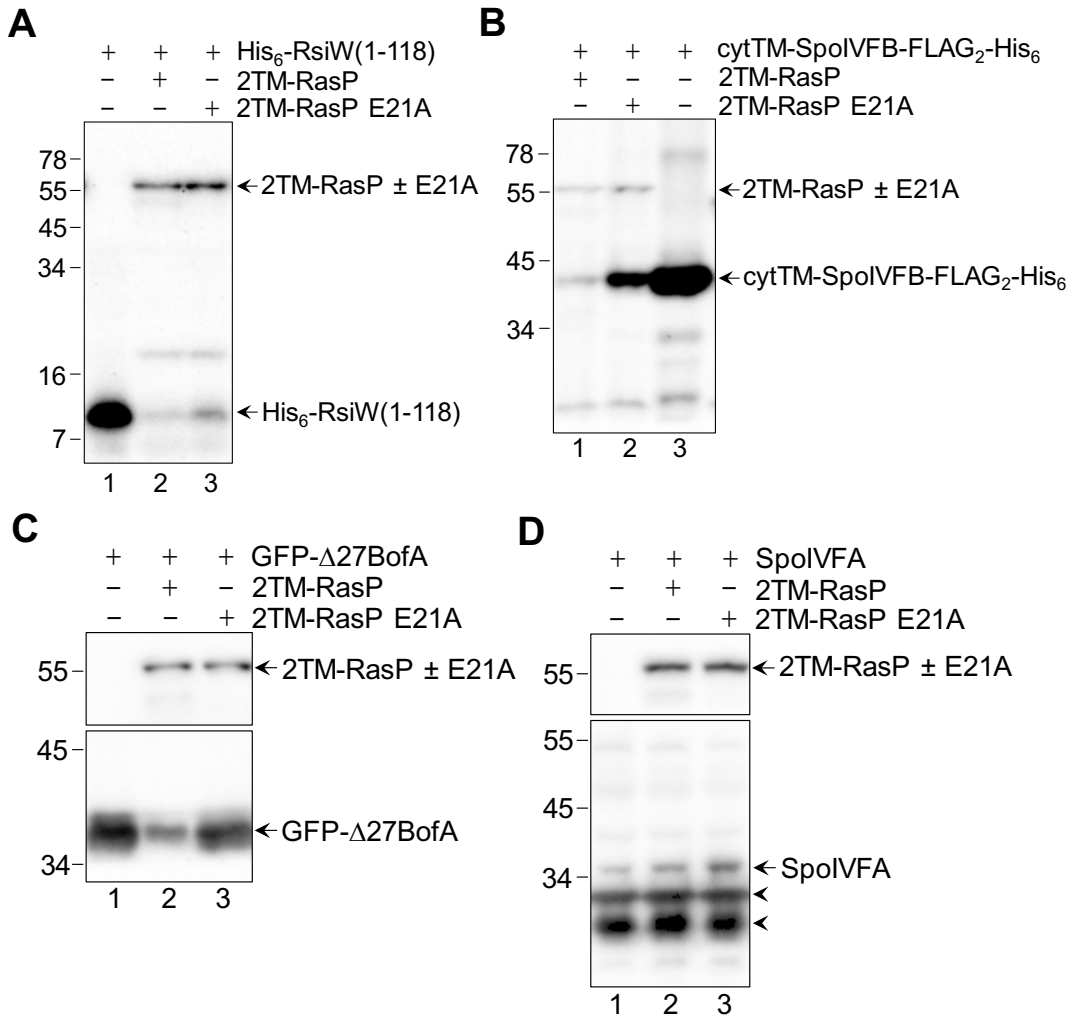

Figure S1 Activity of 2TM-RasP on His_6-RsiW(118) and putative nonsubstrates in *E. coli*. (A) 2TM-RasP activity on His_6-RsiW(118). *E. coli* bearing pYZ52 to express His_6-RsiW(1-118) alone or in combination with pYZ29 or pYZ53 to express 2TM-RasP or 2TM-RasP E21A, respectively, as indicated at the top were cultured, induced, and extracts were subjected to immunoblot analysis with anti-His antibodies (3 min exposure). (B) RasP activity on cytTM-SpoIVFB-$FLAG_2$-His_6. The experiment was carried out as in panel A except *E. coli* bearing pZR209 to express cytTM-SpoIVFB-$FLAG_2$-His_6 was used and a 30 sec exposure of the blot is shown. (C) RasP activity on GFP-□27BofA. As in panel A except *E. coli* bearing pZR62 to express GFP-□27BofA was used and extracts were subjected to immunoblot analysis with anti-FLAG (30 sec exposure) or anti-GFP antibodies (5 sec exposure) in the top and bottom panels, respectively. (D) RasP activity on SpoIVFA. As in panel A except *E. coli* bearing pZR73 to express SpoIVFA was used and extracts were subjected to immunoblot analysis with anti-FLAG (10 sec exposure) or anti-SpoIVFA antibodies (10 sec exposure) in the top and bottom panels, respectively. In each panel, migration of protein markers is indicated at the left and inferred identity of signals is indicated at the right, and a representative result from at least two biological replicates is shown. In panel D, arrowheads indicate *E. coli* proteins that crossreact strongly with the antibodies.

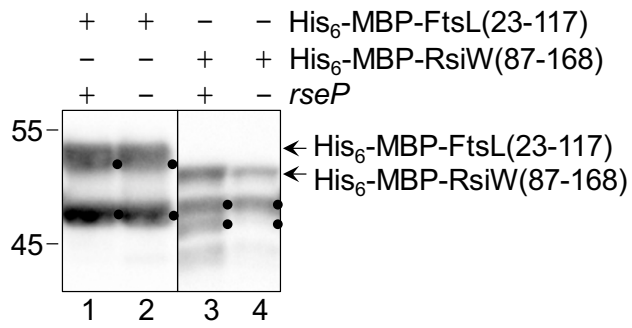

Figure S2 Expression of His_6-MBP fusion proteins in *rseP* mutant *E. coli*. Wild-type (+) or *rseP* mutant (-) *E. coli* bearing pYZ112 to express His_6-MBP-FtsL(23-117) or pDP56 to express His_6-MBP-RsiW(87-168) as indicated at the top were cultured (10 mL) and induced with IPTG. Extracts were subjected to immunoblot analysis with anti-His antibodies (5 sec exposure). Migration of protein markers is indicated at the left and inferred identity of signals is indicated at the right. The dots indicate presumed proteolytic breakdown products. A representative result from at least two biological replicates is shown.

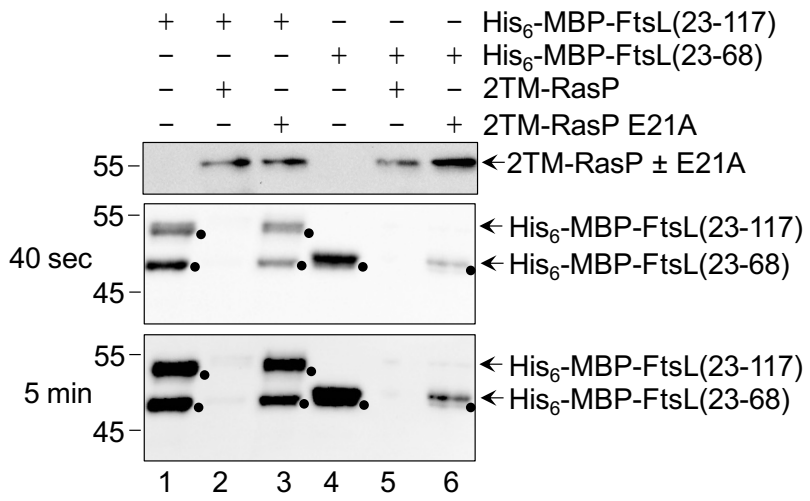

Figure S3 2TM-RasP activity on His_6-MBP-FtsL fusion proteins in *clpP* mutant *E. coli*. *E. coli* bearing pYZ111 or pYZ112 to express His_6-MBP-FtsL(23-117) or His_6-MBP-FtsL(23-68), respectively, alone or in combination with pYZ29 or pYZ53 to express 2TM-RasP or 2TM-RasP E21A, respectively, as indicated at the top were cultured (10 mL) and induced with IPTG. Extracts were subjected to immunoblot analysis with anti-FLAG (top panel, 2.5 min exposure) or anti-His (middle and bottom panels, two exposures) antibodies. The dots indicate presumed proteolytic breakdown products independent of RasP activity. Migration of protein markers is indicated at the left and inferred identity of signals is indicated at the right. The RasP-dependent cleavage products were expected to be ~7 kDa smaller than His_6-MBP-FtsL(23-117) and ~2 kDa smaller than His_6-MBP-FtsL(23-68) in lanes 2 and 5, respectively, but were not observed. A representative result from at least two biological replicates is shown.

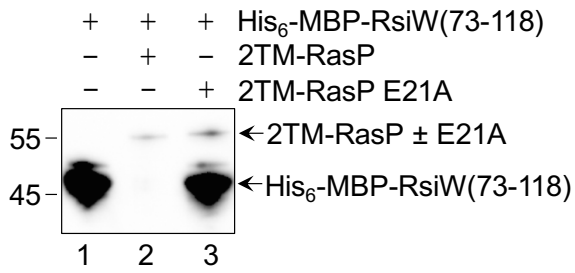

Figure S4 2TM-RasP activity on His_6-MBP-RsiW(73-118) in *clpP* mutant *E. coli*. *E. coli* bearing pYZ69 to express His_6-MBP-RsiW(73-118) alone or in combination with pYZ29 or pYZ53 to express 2TM-RasP or 2TM-RasP E21A, respectively, as indicated at the top were cultured (10 mL) and induced with IPTG. Extracts were subjected to immunoblot analysis with anti-His antibodies (1.5 min exposure). Migration of protein markers is indicated at the left and inferred identity of signals is indicated at the right. The cleavage product is expected to be ~2 kDa smaller than His_6-MBP-RsiW(73-118), but was not observed. A representative result from at least two biological replicates is shown.

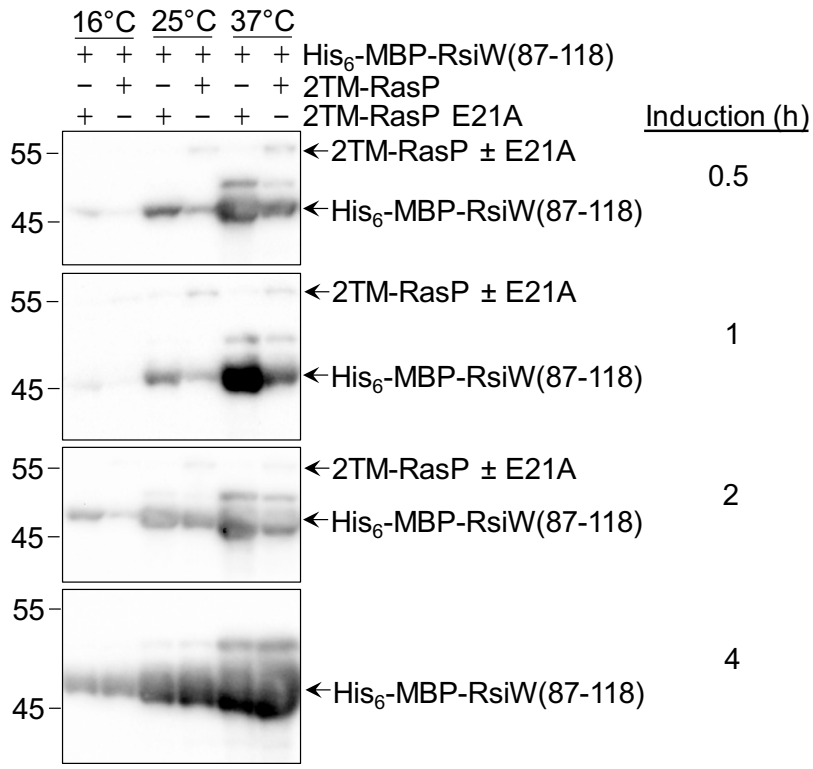

Figure S5 2TM-RasP activity on His_6-MBP-RsiW(87-118) at various temperatures and times post-induction. *E. coli* bearing pYZ76 to express His_6-MBP-RsiW(87-118) in combination with pYZ29 or pYZ53 to express 2TM-RasP or 2TM-RasP E21A, respectively, were cultured (10 mL) at different growth temperatures as indicated at the top and induced with IPTG for the periods indicated at the right. Extracts were subjected to immunoblot analysis with anti-His antibodies (10 sec exposure, all panels are from the same blot). Migration of protein markers is indicated at the left and inferred identity of signals is indicated at the right. The cleavage product is expected to be ~2 kDa smaller than His_6-MBP-RsiW(87-118), but was not observed. A representative result from at least two biological replicates is shown.

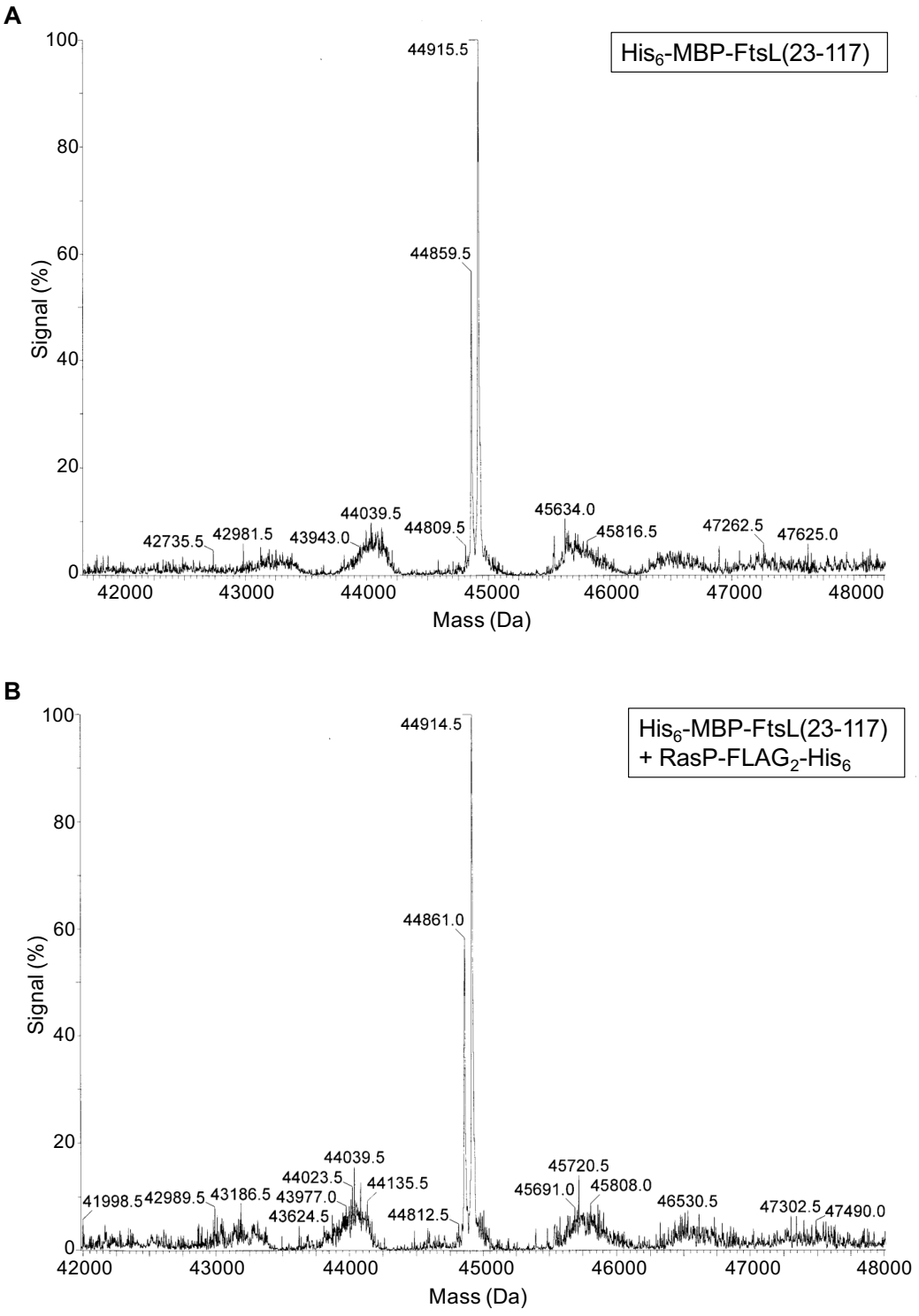

Figure S6 Mass spectrometry analysis of the reaction containing His_6-MBP-FtsL(23-117) alone (A) or in combination with RasP-$FLAG_2$-His_6 (B). The zero charge state signal as a percentage of the maximum signal is plotted in the mass range from 42,000–48,000 Da. Numbers above peaks give the zero charge state mass (in Da) at peak maxima.

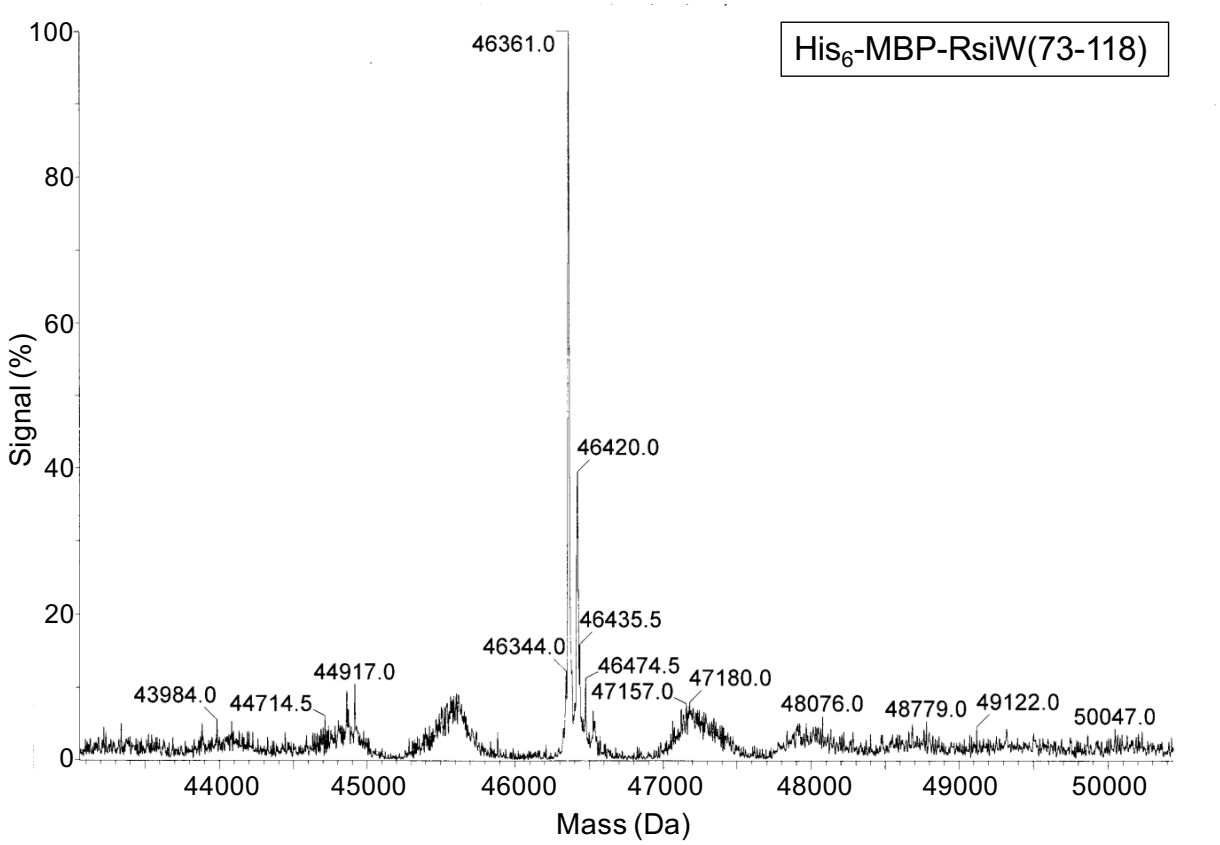

Figure S7 Mass spectrometry analysis of the reaction containing only His_6-MBP-RsiW(73-118). The zero charge state signal as a percentage of the maximum signal is plotted in the mass range from 43,100–50,400 Da. Numbers above peaks give the zero charge state mass (in Da) at peak maxima.

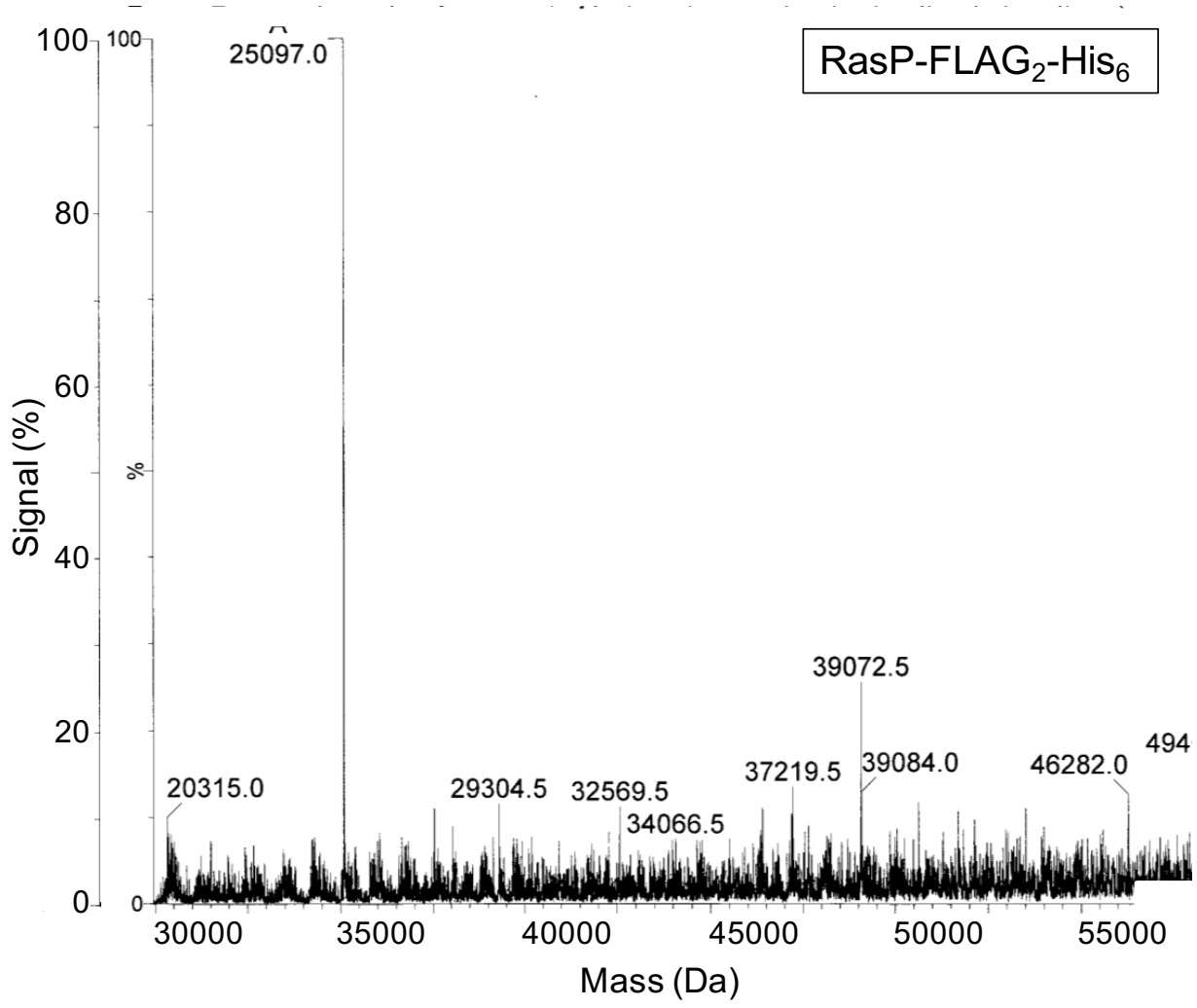

Figure S8 Mass spectrometry analysis of the reaction containing only RasP-FLAG$_2$-His$_6$. The zero charge state signal as a percentage of the maximum signal is plotted in the mass range from 27,500–55,000 Da. Numbers above peaks give the zero charge state mass (in Da) at peak maxima.

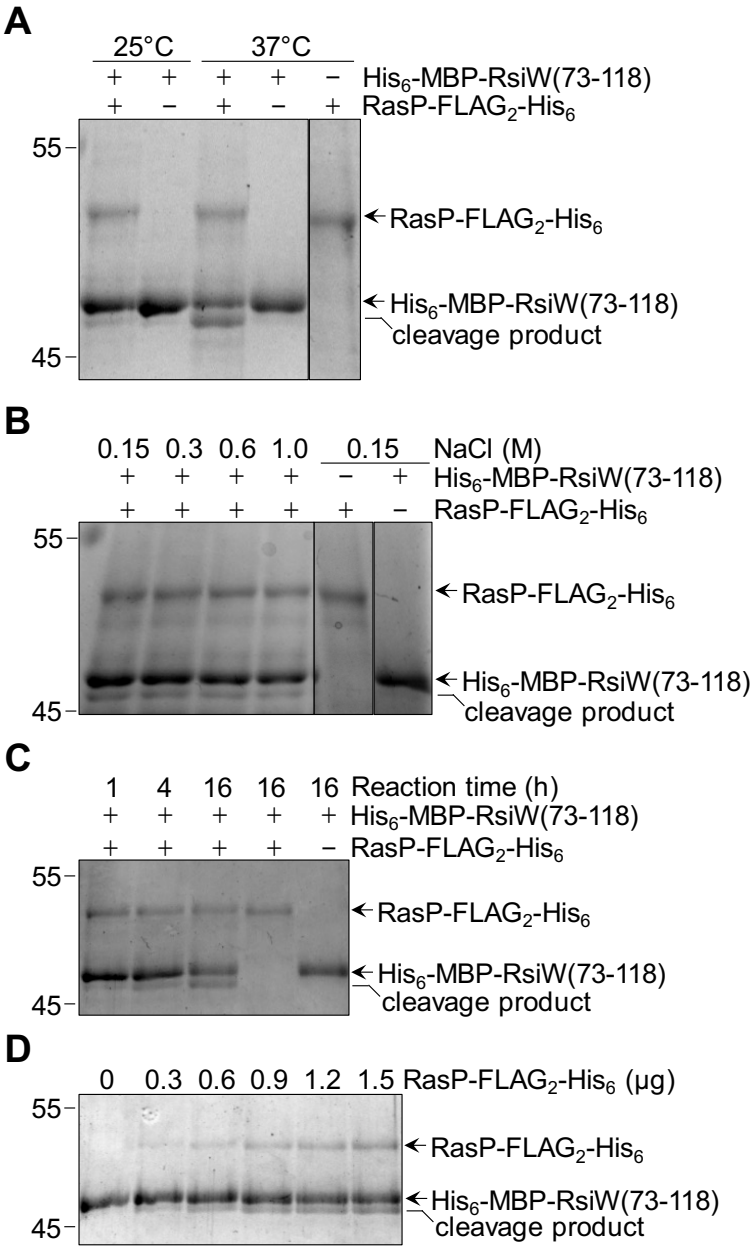

Figure S9 Cleavage of His_6-MBP-RsiW(73-118) by RasP-$FLAG_2$-His_6 under various conditions *in vitro*. (A) Dependence on temperature. Reactions were incubated for 16 h at the indicated temperatures. (B) Dependence on salt concentration. The concentration of NaCl in the reaction was varied as indicated. (C) Time course. Reactions were incubated at 37°C for the times indicated. As controls, enzyme and substrate were incubated separately. (D) Dependence on enzyme. His_6-MBP-RsiW(73-118) (2.5 μg) was incubated with the indicated amount of RasP-$FLAG_2$-His_6 in 15 □L reactions. In panels A and B, lines indicate that intervening lanes were removed from the image.

REFERENCES

REFERENCES

1. Brown MS, Ye J, Rawson RB, Goldstein JL. Regulated intramembrane proteolysis: a control mechanism conserved from bacteria to humans. 2000. Cell 100:391-398.

2. Urban S. Mechanisms and cellular functions of intramembrane proteases. Biochim. Biophys. Acta - Biomembr. 2013. 1828:2797-2800.

3. Kroos L, Akiyama Y. Biochemical and structural insights into intramembrane metalloprotease mechanisms. Biochim. Biophys. Acta - Biomembr. 2013. 1828:2873-2885.

4. Schneider JS, Glickman MS. Function of site-2 proteases in bacteria and bacterial pathogens. Biochim. Biophys. Acta - Biomembr. 2013. 1828:2808-2814.

5. Akiyama Y, Kanehara K, Ito K. RseP (YaeL), an *Escherichia coli* RIP protease, cleaves transmembrane sequences. EMBO J. 2004. 23:4434-4442.

6. Alba BM, Leeds JA, Onufryk C, Lu CZ, Gross CA. DegS and YaeL participate sequentially in the cleavage of RseA to activate the s^E-dependent extracytoplasmic stress response. Genes Dev. 2002. 16:2156-2168.

7. Kanehara K, Ito K, Akiyama Y. YaeL (EcfE) activates the s^E pathway of stress response through a site-2 cleavage of anti-s^E, RseA. Genes Dev. 2002. 16:2147-2155.

8. Zhou R, Cusumano C, Sui D, Garavito RM, Kroos L. Intramembrane proteolytic cleavage of a membrane-tethered transcription factor by a metalloprotease depends on ATP. Proc. Natl. Acad. Sci. USA 2009. 106:16174-16179.

9. Schobel S, Zellmeier S, Schumann W, Wiegert T. The *Bacillus subtilis* s^W anti-sigma factor RsiW is degraded by intramembrane proteolysis through YluC. Mol. Microbiol. 2004. 52:1091-1105.

10. Ellermeier CD, Losick R. Evidence for a novel protease governing regulated intramembrane proteolysis and resistance to antimicrobial peptides in *Bacillus subtilis*. Genes Dev. 2006. 20:1911-1922.

11. Heinrich J, Wiegert T. YpdC determines site-1 degradation in regulated intramembrane proteolysis of the RsiW anti-sigma factor of *Bacillus subtilis*. Mol. Microbiol. 2006. 62:566-579.

12. Heinrich J, Hein K, Wiegert T. Two proteolytic modules are involved in regulated intramembrane proteolysis of *Bacillus subtilis* RsiW. Mol. Microbiol. 2009. 74:1412-1426.

13. Zellmeier S, Schumann W, Wiegert T. Involvement of Clp protease activity in modulating the *Bacillus subtilis* s^W stress response. Mol. Microbiol. 2006. 61:1569-1582.

14. Helmann JD. *Bacillus subtilis* extracytoplasmic function (ECF) sigma factors and defense of the cell envelope. Curr. Opin. Microbiol. 2016. 30:122-132.

15. Bramkamp M, Weston L, Daniel RA, Errington J. Regulated intramembrane proteolysis of FtsL protein and the control of cell division in *Bacillus subtilis*. Mol. Microbiol. 2006. 62:580-591.

16. Wadenpohl I, Bramkamp M. DivIC stabilizes FtsL against RasP cleavage. J. Bacteriol. 2010. 192:5260-5263.

17. Saito A, Hizukuri Y, Matsuo E, Chiba S, Mori H, Nishimura O, Ito K, Akiyama Y. Post-liberation cleavage of signal peptides is catalyzed by the site-2 protease (S2P) in bacteria. Proc. Natl. Acad. Sci. USA. 2011. 108:13740-13745.

18. Hastie JL, Williams KB, Ellermeier CD. The activity of s^V, an extracytoplasmic function s factor of *Bacillus subtilis*, is controlled by regulated proteolysis of the anti-s factor RsiV. J. Bacteriol. 2013. 195:3135-3144.

19. Rudner D, Fawcett P, Losick R. A family of membrane-embedded metalloproteases involved in regulated proteolysis of membrane-associated transcription factors. Proc. Natl. Acad. Sci. USA. 1999. 96:14765-14770.

20. Yu Y-TN, Kroos L. Evidence that SpoIVFB is a novel type of membrane metalloprotease governing intercompartmental communication during *Bacillus subtilis* sporulation. J. Bacteriol. 2000. 182:3305-3309.

21. Green D, Cutting S. Membrane topology of the *Bacillus subtilis* Pro-s^K processing complex. J. Bacteriol. 2000. 182:278-285.

22. Saribas AS, Gruenke L, Waskell L. Overexpression and purification of the membrane-bound cytochrome P450 2B4. Protein Expr. Purif. 2001. 21:303-309.

23. Hessa T, Kim H, Bihlmaier K, Lundin C, Boekel J, Andersson H, Nilsson I, White SH, von Heijne G. Recognition of transmembrane helices by the endoplasmic reticulum translocon. Nature. 2005. 433:377-381.

24. Flynn JM, Levchenko I, Sauer RT, Baker TA. Modulating substrate choice: the SspB adaptor delivers a regulator of the extracytoplasmic-stress response to the AAA+ protease ClpXP for degradation. Genes Dev. 2004. 18:2292-2301.

25. Cutting S, Oke V, Driks A, Losick R, Lu S, Kroos L. A forespore checkpoint for mother-cell gene expression during development in *Bacillus subtilis*. 1990. Cell 62:239-250.

26. Rudner DZ, Losick R. A sporulation membrane protein tethers the pro-s^K processing enzyme to its inhibitor and dictates its subcellular localization. Genes Dev. 2002. 16:1007-1018.

27. Varcamonti M, Marasco R, De Felice M, Sacco M. Membrane topology analysis of the *Bacillus subtilis* BofA protein involved in pro-s^K processing. Microbiol. 1997. 143:1053-1058.

28. Zhang Y, Luethy PM, Zhou R, Kroos L. Residues in conserved loops of intramembrane metalloprotease SpoIVFB interact with residues near the cleavage site in Pro-s^K. J. Bacteriol. 2013. 195:4936-4946.

29. Cutting S, Roels S, Losick R. Sporulation operon *spoIVF* and the characterization of mutations that uncouple mother-cell from forespore gene expression in *Bacillus subtilis*. J. Mol. Biol. 1991. 221:1237-1256.

30. Kinch LN, Ginalski K, Grishin NV. Site-2 protease regulated intramembrane proteolysis: sequence homologs suggest an ancient signaling cascade. Protein Sci. 2006. 15:84-93.

31. Hizukuri Y, Akiyama Y. PDZ domains of RseP are not essential for sequential cleavage of RseA or stress-induced s^E activation *in vivo*. Mol. Microbiol. 2012. 86:1232-1245.

32. Hizukuri Y, Oda T, Tabata S, Tamura-Kawakami K, Oi R, Sato M, Takagi J, Akiyama Y, Nogi T. A structure-based model of substrate discrimination by a noncanonical PDZ tandem in the intramembrane-cleaving protease RseP. Structure. 2014. 22:326-336.

33. Inaba K, Suzuki M, Maegawa K, Akiyama S, Ito K, Akiyama Y. A pair of circularly permutated PDZ domains control RseP, the S2P family intramembrane protease of *Escherichia coli*. J. Biol. Chem. 2008. 283:35042-35052.

34. Kanehara K, Ito K, Akiyama Y. YaeL proteolysis of RseA is controlled by the PDZ domain of YaeL and a Gln-rich region of RseA. EMBO J. 2003. 22:6389-6398.

35. Kim DY, Kwon E, Choi J, Hwang HY, Kim KK. Structural basis for the negative regulation of bacterial stress response by RseB. Protein Sci. 2010. 19:1258-1263.

36. Grigorova IL, Chaba R, Zhong HJ, Alba BM, Rhodius V, Herman C, Gross CA. Fine-tuning of the *Escherichia coli* s^E envelope stress response relies on multiple mechanisms to inhibit signal-independent proteolysis of the transmembrane anti-sigma factor, RseA. Genes Dev. 2004. 18:2686-2697.

37. Li X, Wang B, Feng L, Kang H, Qi Y, Wang J, Shi Y. Cleavage of RseA by RseP requires a carboxyl-terminal hydrophobic amino acid following DegS cleavage. Proc. Natl. Acad. Sci. USA. 2009. 106:14837-14842.

38. Koide K, Ito K, Akiyama Y. Substrate recognition and binding by RseP, an *Escherichia coli* intramembrane protease. J. Biol. Chem. 2008. 283:9562-9570.

39. Zhang B, Hofmeister A, Kroos L. The pro-sequence of pro-s^K promotes membrane association and inhibits RNA polymerase core binding. J. Bacteriol. 1998. 180:2434-2441.

40. Zhou R, Chen K, Xiang X, Gu L, Kroos L. Features of Pro-s^K important for cleavage by SpoIVFB, an intramembrane metalloprotease. J. Bacteriol. 2013. 195:2793-2806.

41. Dickey SW, Baker RP, Cho S, Urban S. Proteolysis inside the membrane is a rate-governed reaction not driven by substrate affinity. Cell. 2013. 155:1270-1281.

42. Strisovsky K, Sharpe HJ, Freeman M. Sequence-specific intramembrane proteolysis: identification of a recognition motif in rhomboid substrates. Mol. Cell. 2009. 36:1048-1059.

43. Bolduc DM, Montagna DR, Gu YL, Selkoe DJ, Wolfe MS. Nicastrin functions to sterically hinder g-secretase-substrate interactions driven by substrate transmembrane domain. Proc. Natl. Acad. Sci. USA. 2016. 113:E509-E518.

44. Kamp F, Winkler E, Trambauer J, Ebke A, Fluhrer R, Steiner H. Intramembrane proteolysis of b-amyloid precursor protein by g-secretase is an unusually slow process. Biophys. J. 2015. 108:1229-1237.

45. Zhou R, Kroos L. BofA protein inhibits intramembrane proteolysis of pro-s^K in an intercompartmental signaling pathway during *Bacillus subtilis* sporulation. Proc. Natl. Acad. Sci. USA. 2004. 101:6385-6390.

46. Maurizi MR, Clark WP, Katayama Y, Rudikoff S, Pumphrey J, Bowers B, Gottesman S. Sequence and structure of ClpP, the proteolytic component of the ATP-dependent Clp protease of *Escherichia coli*. J. Biol. Chem. 1990. 265:12536-12545.

47. Kroos L, Yu YT, Mills D, Ferguson-Miller S. Forespore signaling is necessary for pro-s^K processing during *Bacillus subtilis* sporulation despite the loss of SpoIVFA upon translational arrest. J. Bacteriol. 2002. 184:5393-5401.

48. Hofmann K, Stoffel W. TMbase - A database of membrane spanning proteins segments. Biol. Chem. Hoppe-Seyler. 1993. 374:166.

49. Kanehara K, Akiyama Y, Ito K. Characterization of the *yaeL* gene product and its S2P-protease motifs in *Escherichia coli*. Gene. 2001. 281:71-79.

50. Akiyama K, Mizuno S, Hizukuri Y, Mori H, Nogi T, Akiyama Y. Roles of the membrane-reentrant b-hairpin-like loop of RseP protease in selective substrate cleavage. eLIFE 2015. 4:e08928.

51. Feng L, Yan H, Wu Z, Yan N, Wang Z, Jeffrey PD, Shi Y. Structure of a site-2 protease family intramembrane metalloprotease. Science. 2007. 318:1608-1612.

52. Daniel RA, Errington J. Intrinsic instability of the essential cell division protein FtsL of *Bacillus subtilis* and a role for DivIB protein in FtsL turnover. Mol. Microbiol. 2000. 36:278-289.

53. Youngman P, Perkins JB, Losick R. Construction of a cloning site near one end of Tn*917* into which foreign DNA may be inserted without affecting transposition in *Bacillus subtilis* or expression of the transposon-borne *erm* gene. Plasmid 1984. 12:1-9.

54. Bridges A, Gruenke L, Chang YT, Vakser IA, Loew G, Waskell L. Identification of the binding site on cytochrome P450 2B4 for cytochrome b5 and cytochrome P450 reductase. J. Biol. Chem. 1998. 273:17036-17049.

55. Zhang Y, Gao X, Garavito RM. Structural analysis of the intracellular domain of (pro)renin receptor fused to maltose-binding protein. Biochem. Biophys. Res. Commun. 2011. 407:674-679.

CHAPTER 3: Channels and ionophores impact compartment-specific ATP concentrations and Pro-σ^K cleavage during *Bacillus subtilis* sporulation

Abstract

Starvation of the bacterium *Bacillus subtilis* initiates a process of sporulation involving the formation of mother cell (MC) and forespore (FS) compartments. During engulfment, the MC membrane migrates around the FS, and the MC is proposed to "feed" the FS metabolites through protein channels. The channels are necessary for post-engulfment FS gene expression, which initiates a proteolytic cascade that relieves inhibition of SpoIVFB, an intramemebrane protease that cleaves Pro-σ^K and releases σ^K to direct MC gene expression. SpoIVFB has an ATP-binding cystathionine-β-synthase (CBS) domain exposed to the MC cytoplasm, but the role of ATP in regulating Pro-σ^K cleavage has been unclear, as has the impact of the channels on MC and FS ATP levels. Using compartment-specific expression of the ATP-dependent enzyme luciferase to measure relative ATP concentrations during sporulation, we found that the MC ATP concentration rises nearly twofold coincident with completion of engulfment, decreasing levels of channel proteins, and increasing cleavage of Pro-σ^K. Surprisingly, the FS ATP concentration did not decline. Treatment with ionophores lowered the MC and FS ATP concentrations during and after engulfment, suggesting that proton gradients drive ATP synthesis in both compartments. Ionophores inhibited Pro-σ^K cleavage, but not simply by lowering the MC ATP concentration. Rather, the MC energy status (ratio of ATP to ADP and/or AMP) may be sensed by the SpoIVFB CBS domain to regulate Pro-σ^K cleavage. Mutants lacking a channel protein exhibited higher MC and lower FS ATP concentrations during engulfment. However, ATP did not appear to be the limiting factor for post-engulfment FS gene expression in channel mutants or for MC cleavage of Pro-σ^K in wild type cells. We propose that during engulfment the channels transport amino acids and/or nucleotides (other than ATP)

necessary for post-engulfment FS gene expression, which relieves inhibition of SpoIVFB, allowing Pro-σ^K cleavage commensurate with the MC energy status.

Introduction

Endospore formation by the bacterium *Bacillus subtilis* has long been a model system for studies of cell-to-cell communication in bacteria [1]. In a remarkably complex process, *B. subtilis* enters sporulation upon encountering starvation conditions, after which a number of events are set in motion [2]. Initially, a polar septum is formed, creating a large compartment referred to as the mother cell (MC) and a smaller compartment destined to become the forespore (FS). After septation, the FS is engulfed by the MC as the MC membrane migrates around the FS, eventually pinching off the FS within the MC (Fig. 3.1). At this stage, the FS compartment is surrounded by two membranes, with an intermembrane space between them. Following engulfment, a modified peptidoglycan layer called the cortex is produced in the intermembrane space and a protective protein coat is produced by the MC around the FS. Once FS development is complete, the MC lyses, releasing a dormant spore.

The process of endospore formation by *B. subtilis* is controlled by differential gene expression in the two compartments or "cell types", driven by the activation of alternative sigma factors [3, 4]. Several mechanisms ensure activation of σ^F in the FS shortly after polar septum formation [5]. Activity of σ^F initiates a signaling pathway that leads to proteolytic activation of Pro-σ^E in the MC [6]. During the ensuing engulfment process, σ^F activity produces SpoIIQ that inserts in the inner FS membrane and σ^E activity produces SpoIIIA proteins that insert in the engulfing MC membrane (Fig. 3.1), forming channels between the two compartments that are required for full activity of σ^G in the FS [7-13]. The activation of σ^G coincides with completion of engulfment and initiates a signaling pathway that leads to proteolytic cleavage of Pro-σ^K to active σ^K in the MC [6, 14].

Intercellular communication is an essential function for multicellularity. In animals and plants, gap junctions and plasmodesmata, respectively, provide channels for passage of small molecules between cells. The channels that form between the MC and the FS during the

Fig. 3.1

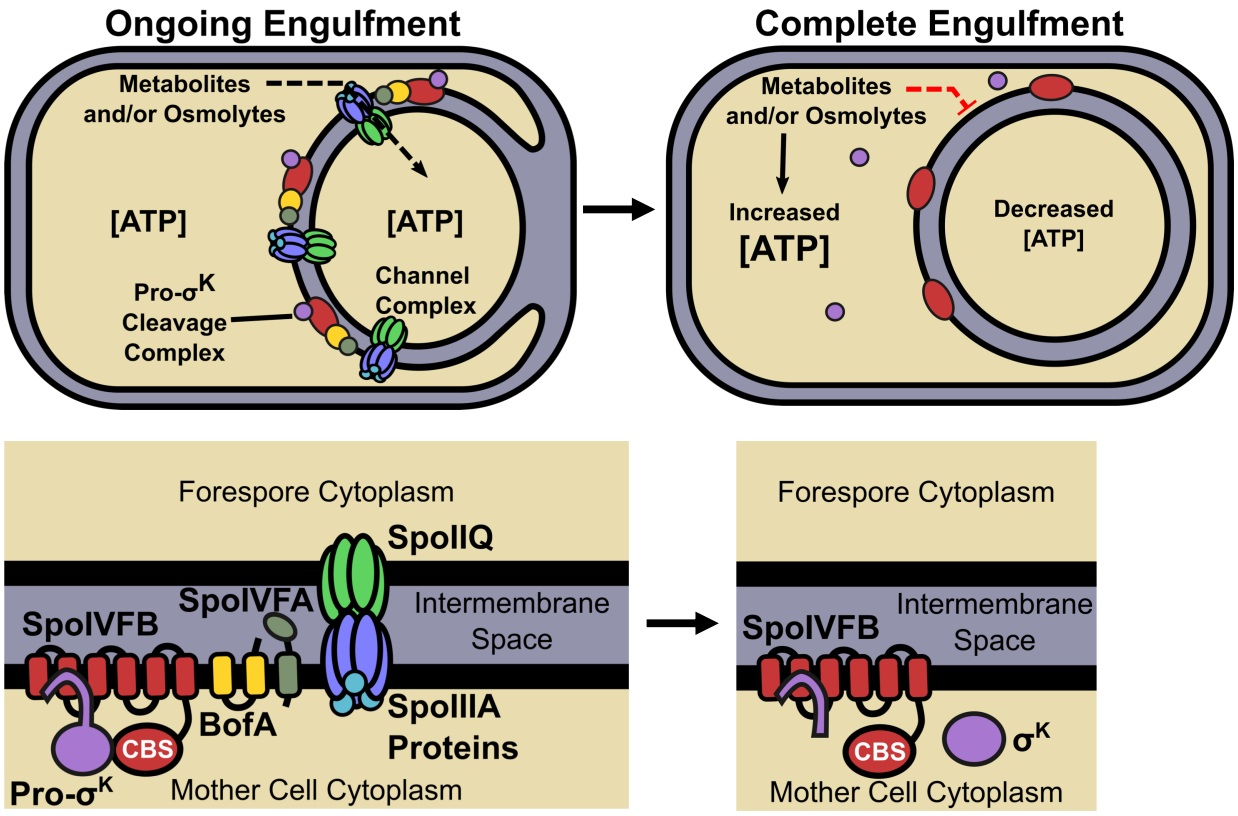

Figure 3.1 How channels may impact ATP concentrations and Pro-σ^K cleavage. The top left illustrates ongoing engulfment, during which the MC membrane migrates around the FS. Channel complexes are proposed to transport metabolites and/or osmolytes from the MC to the FS. ATP may be maintained at a similar concentration in the two compartments. Inactive Pro-σ^K cleavage complexes are associated with channel complexes. The bottom left indicates the proteins in each complex. The top right illustrates complete engulfment. The FS has been pinched off within the MC. Channel complexes are inactive or absent (the latter is depicted), thus halting transport. The lack of transport may cause the MC ATP concentration to increase. Gene expression in the FS may cause the ATP concentration to decrease. SpoIVB and CtpB produced under σ^G control in the FS (not shown) are secreted into the intermembrane space and cleave SpoIVFA and BofA (depicted as absent), relieving inhibition of SpoIVFB. The CBS domain of SpoIVFB (bottom right) may sense the elevated ATP concentration in the MC, so that Pro-σ^K is cleaved and σ^K is released into the MC.

engulfment stage of *B. subtilis* sporulation have been proposed to function analogously, acting as “feeding tubes” [11]. Specifically, the MC is proposed to provide small molecules through the channels that support biosynthesis in the FS. Evidence for the feeding tube model is that the channels are required for persistent activity of σ^F in the FS, as well as for full activity of σ^G. Moreover, heterologous phage T7 RNA polymerase produced in the FS exhibited channel-dependent activity [11]. Hence, dependence on the channels is not limited to σ^G activity. However, the identity of the molecule(s) that transit the channels remains a mystery.

The extracellular domains of SpoIIQ and SpoIIIAH interact directly, forming a channel in the intermembrane space surrounding the FS [7, 8]. The channel appears to be gated on the MC (SpoIIIAH) side by other SpoIIIA proteins and open on the FS (SpoIIQ) side [10]. SpoIIIAA may function in substrate secretion since it resembles secretion ATPases [10] and its ATPase motifs appear to be required for σ^G activation [12]. The eight SpoIIIA proteins and SpoIIQ form a multimeric complex that appears to be a novel secretion apparatus [9, 10, 15] for metabolites and/or osmolytes (Fig. 3.1) that maintain the integrity of the FS and allow σ^G to become fully active [11-13]. Assembly of the channels requires peptidoglycan hydrolysis [7, 16] and GerM [17]. Structural determination and modeling of channel protein complexes support the notion that they form large, stacked rings capable of mediating communication between the MC and FS [18-22].

Upon completion of engulfment, the channels likely cease to function. SpoIIQ is released from immobile complexes and cleaved by SpoIVB [23]. SpoIIIAH is rapidly degraded [10]. The levels of SpoIIIAA and SpoIIIAE decline [12].

How does channel function during engulfment prepare the FS for post-engulfment biosynthetic activity and maintenance of FS integrity? The feeding tube model [11] and its extension [12] propose that the MC feeds metabolites and/or osmolytes to the FS through the channels. If so, the channels may impact the energy status of the two compartments, which

may affect the ATP levels. This possibility is illustrated in Figure 1. During engulfment, channel function would maintain the ATP concentration in the FS at the expense of the MC. Upon completion of engulfment, loss of channel function may allow the MC ATP concentration to rise (due to the FS no longer draining energy), and the FS ATP concentration would presumably decline due to energy utilization for expression of the σ^G regulon. To investigate these possibilities, we devised a method to measure the relative ATP concentration in each compartment during sporulation. The method relies on compartment-specific expression of firefly luciferase (Luc), which catalyzes ATP-dependent oxidation of luciferin, producing light [24]. Luc has been used to measure the relative ATP concentration in *Escherichia coli* [25], and as a reporter of promoter activity during *B. subtilis* growth and sporulation [26], but Luc has not been used to measure relative ATP levels in the two compartments.

How does channel function impact the MC? In addition to possibly lowering the MC ATP concentration during engulfment (Fig. 3.1), channel function is necessary for σ^G activation in the FS upon completion of engulfment [7-13], which leads to σ^K activation in the MC. The activation of σ^K involves proteolytic cleavage of Pro-σ^K by SpoIVFB, an intramembrane metalloprotease [27, 28] whose activity depends not only on a signaling pathway initiated by σ^G, but also on binding of ATP to a domain of SpoIVFB located in the MC [29].

The σ^G-dependent signaling pathway involves two serine proteases, SpoIVB and CtpB, produced in the FS under σ^G control and secreted into the intermembrane space [30-34]. SpoIVB and CtpB cleave SpoIVFA and BofA, which form an inhibitory complex with SpoIVFB [35-39] (Fig. 3.1). Recent evidence suggests that relief from inhibition induces a conformational change in SpoIVFB that promotes interaction with Pro-σ^K and cleavage to produce σ^K [40]. Interestingly, the Pro-σ^K cleavage complexes co-localize with the channel complexes composed of SpoIIIA proteins and SpoIIQ [8, 41] (Fig. 3.1). Interactions between proteins in the two

complexes aid in recruitment to the membranes surrounding the FS, but neither the molecular details of the interactions nor whether they play a role beyond recruitment is known.

In addition to relief from inhibition by SpoIVFA and BofA, activity of SpoIVFB may depend on the MC ATP concentration. Cleavage of Pro-σ^K by SpoIVFB *in vitro* depends on ATP and SpoIVFB has a cystathionine-β-synthase (CBS) domain that binds ATP [29]. The CBS domain of SpoIVFB is predicted to be exposed to the MC cytoplasm (Fig. 3.1), based on membrane topological analysis in *E. coli* [42]. CBS domains in a variety of proteins regulate activity in response to energy status by undergoing a conformational change upon ligand binding [43, 44]. Hence, it was proposed that the CBS domain of SpoIVFB senses the ATP concentration in the MC and regulates Pro-σ^K cleavage appropriately [29]. Deletion of the SpoIVFB CBS domain resulted in no cleavage of Pro-σ^K upon coexpression in *E. coli* [29, 45]. Coexpression in *E. coli* of full-length, catalytically-inactive SpoIVFB with C-terminally truncated Pro-σ^K (which is cleaved by active SpoIVFB) resulted in formation of a 4:2 SpoIVFB·Pro-σ^K complex that was stable during purification [46]. Cross-linking of the two proteins following coexpression in *E. coli* [47] and purification [45, 46] provided constraints to build a homology model of the complex, and it was proposed that extensive interaction between the two proteins allows ATP-induced movement of the SpoIVFB CBS domain to position Pro-σ^K for cleavage by the SpoIVFB membrane domain [45]. However, in a recent study, a SpoIVFB-YFP fusion protein lacking the CBS domain cleaved Pro-σ^K during sporulation of *B. subtilis* [40]. Cleavage was reduced, suggesting that the CBS domain of SpoIVFB plays an important, but nonessential, role. It remains to be established whether the SpoIVFB CBS domain senses the MC ATP concentration and regulates Pro-σ^K cleavage.

Here, we report the use of compartment-specific expression of Luc, mutants lacking channel proteins, and ionophores that uncouple oxidative phosphorylation and lower the cellular ATP concentration, to address several outstanding questions. Do ATP concentrations in the MC and

FS change during sporulation? Does loss of channel proteins impact the MC and FS ATP concentrations? Does the ATP concentration regulate cleavage of Pro-σ^K by SpoIVFB?

Results

A luciferase variant can detect changes in the ATP concentration in the mother cell and forespore during sporulation

DNA constructs were built in which the gene for Luc or an H245F variant (Luc H245F, which increases the K_m for Mg-ATP from 160 μM to 830 μM) [24] were fused to the mother cell-specific *spoIID* promoter or the forespore-specific *spoIIQ* promoter [48] in plasmids that allow gene replacement by homologous recombination at the chromosomal *amyE* locus of *B. subtilis* [49]. The resulting strains were used to test the sensitivity of Luc and Luc H245F in each compartment to decreases in the ATP concentration brought about by treatment with the ionophore carbonyl cyanide *p*-trifluoromethoxyphenylhydrazone (FCCP) at 3.5 h poststarvation (PS). As controls, aliquots from the same cultures were left untreated. All the aliquots contained the Luc substrate luciferin and were used to measure both the luminescence and the Luc level by immunoblot analysis at 3.75 h PS (i.e., 15 min later).

For native Luc expressed in the MC or FS, neither luminescence (Fig. 3.2A) nor the protein level (Fig. 3.2B) changed much after treatment with FCCP (100 μM), although both luminescence and the Luc level were lower in the FS than the MC. When luminescence was divided by the Luc level to yield normalized values, the values were similar for the MC and FS, although unexpectedly the value in the MC after FCCP treatment was slightly higher than the other values (Fig. 3.3A).

In contrast to native Luc, when Luc H245F was expressed in the MC or FS, luminescence decreased by about seven fold after FCCP treatment (Fig. 3.2C). Even without FCCP

Fig. 3.2

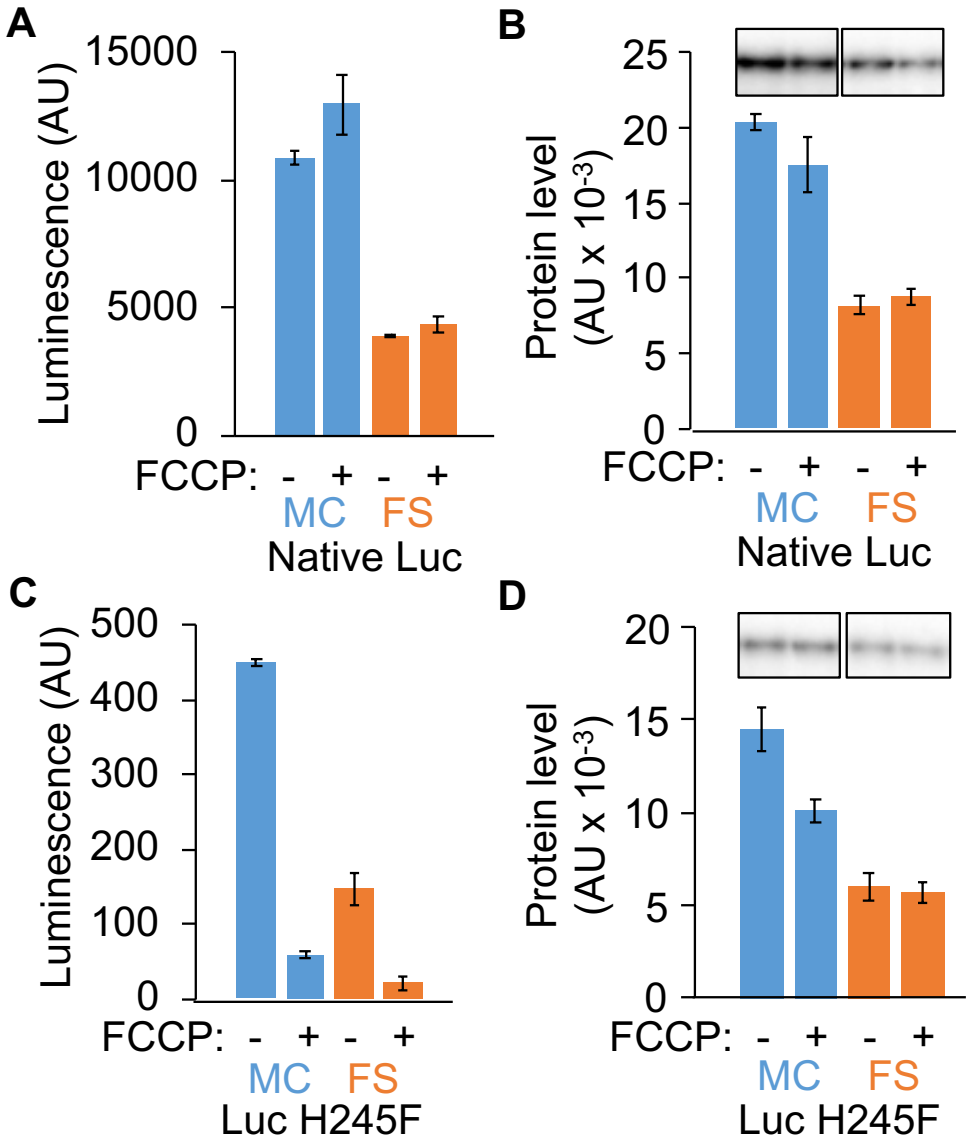

Figure 3.2 *B. subtilis* strains engineered to express native Luc or Luc H245F in the MC or FS were starved to induce sporulation. At 3.5 h PS, culture aliquots were transferred to a 96-well plate with luciferin. Aliquots were left untreated as controls (-) or were treated with 100 μM FCCP (+) for 15 min, prior to measuring the luminescence and the Luc level by immunoblot analysis with anti-Luc antibodies. Graphs show the average of three biological replicates and error bars represent one standard deviation. Luminescence from native Luc **(A)** and Luc H245F **(C)** in arbitrary units (AU). Levels of native Luc **(B)** and Luc H245F **(D)**. Representative immunoblots are shown at the top and quantification of replicates is shown below.

treatment, luminescence from Luc H245F was much lower than from native Luc (Fig. 3.2A), as expected

since Luc H245F has a higher K_m for Mg-ATP and a 16-fold lower turnover number (k_{cat}) than native Luc [24]. The Luc H245F levels (Fig. 3.2D) were only slightly lower than the native Luc levels (Fig. 3.2B). Importantly, after FCCP treatment, the normalized values (i.e., luminescence/Luc H245F level) decreased about fivefold on average for the MC and nearly sevenfold for the FS (Fig. 3.3B). Hence, the decreased luminescence from Luc H245F appeared to indicate significantly reduced concentrations of ATP in both the MC and the FS after FCCP treatment.

Taken together, our results are consistent with the expectation that the K_m for Mg-ATP of Luc H245F is closer than that of native Luc to cellular ATP concentrations and therefore a more sensitive indicator of changes in the ATP concentration *in vivo*. Hence, all subsequent experiments utilized Luc H245F. Because the normalized values of luminescence/Luc H245F level appear to reflect the ATP concentration *in vivo*, we refer to the normalized value as the "relative ATP concentration" hereafter.

The ATP concentration rises nearly twofold in the mother cell during sporulation but is unchanged in the forespore

To test for changes in ATP concentration during sporulation, strains expressing Luc H245F in the MC or FS were starved to induce sporulation and the luminescence and Luc H245F levels were measured at various times PS. The luminescence rose more in the MC than in the FS by 3 h PS and remained higher in the MC than in the FS until 6 h PS (Fig. 3.4A). The Luc H245F levels were similar in the MC and FS, reaching maxima at 3.5 h and 4 h, respectively (Fig. 3.4B), as expected for expression from the *spoIID* and *spoIIQ* promoters [48].

The relative ATP concentration (i.e., luminescence/Luc H245F level) showed an upward trend in the MC from 3.5 to 6 h PS (Fig. 3.5). The increases from 3.5 to 5 h (1.4-fold, P = 0.031

Fig. 3.3

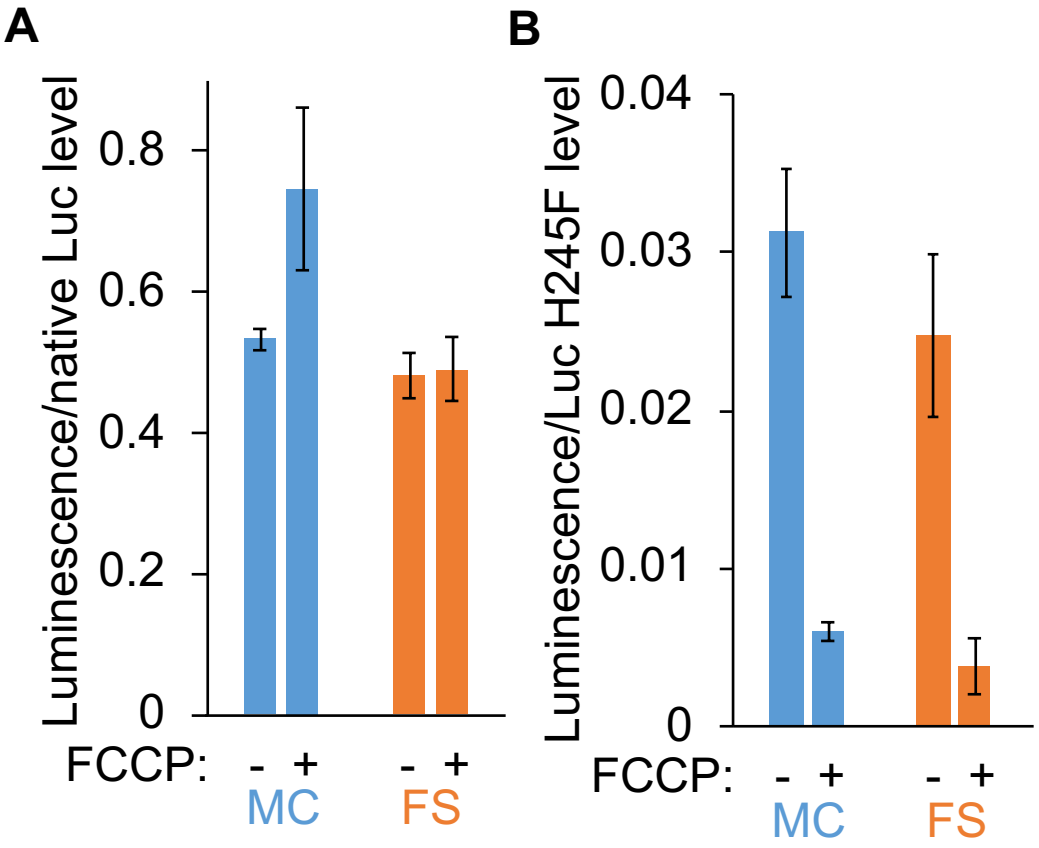

Figure 3.3 Luc H245F detects decreases in compartment-specific ATP concentrations after FCCP treatment during sporulation. *B. subtilis* strains engineered to express native Luc or Luc H245F in the MC or FS were starved to induce sporulation. At 3.5 h PS, culture aliquots were transferred to a 96-well plate with luciferin. Aliquots were left untreated as controls (-) or were treated with 100 μM FCCP (+) for 15 min, prior to measuring the luminescence and the Luc level by immunoblot analysis with anti-Luc antibodies. The luminescence was divided by the Luc level to yield a normalized value for each strain and treatment. Graphs show the average of three biological replicates and error bars represent one standard deviation. **(A)** Luminescence/native Luc level. **(B)** Luminescence/Luc H245F level.

Fig. 3.4

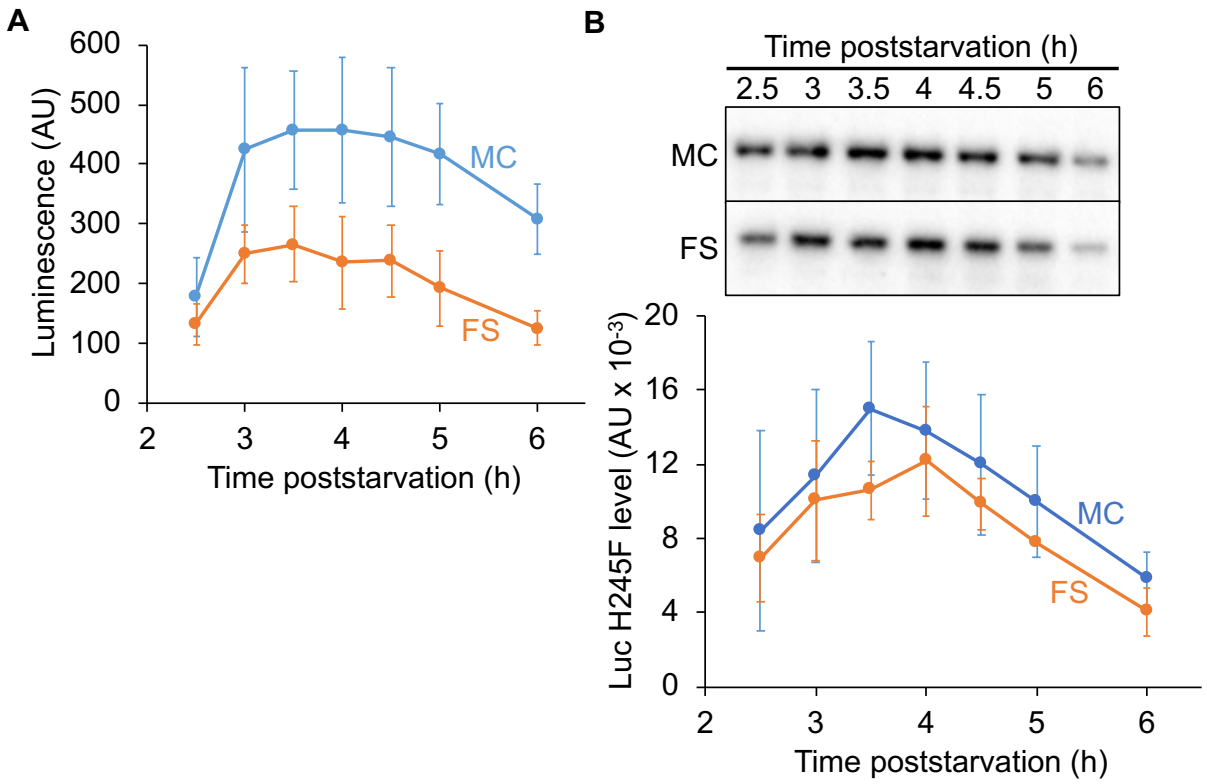

Figure 3.4 Luminescence and Luc H245F levels during sporulation. *B. subtilis* strains engineered to express Luc H245F in the MC or FS were starved to induce sporulation. At 2 h PS, culture aliquots were transferred to a 96-well plate, prior to measuring the luminescence and the Luc H245F level by immunoblot analysis with anti-Luc antibodies at the indicated times PS. Graphs show the average of three biological replicates and error bars represent one standard deviation. **(A)** Luminescence in arbitrary units (AU). **(B)** Luc H245F level. Representative immunoblots are shown at the top and quantification of replicates is shown below.

in a paired two-tailed *t*-test) and from 3.5 to 6 h (1.8-fold, P = 0.033) are statistically significant at the 95% confidence level, and the increase from 3.5 to 4.5 h (1.2-fold, P = 0.053) is nearly so. These results are consistent with the possibility that loss of channel function upon completion of engulfment allows the MC ATP concentration to rise (Fig. 3.1).

The relative ATP concentration in the FS did not change significantly from 2.5 to 6 h PS (Fig. 3.5). In particular, we did not observe a decline in the FS ATP concentration, which we thought might accompany loss of channel function upon engulfment completion (Fig. 3.1). Although Luc H245F detected a decreased ATP concentration in the FS after FCCP treatment at 3.5 h PS (Fig. 3.3B), our results in Figure 3.5 raised the question of whether Luc H245F remains a sensitive indicator of decreased ATP concentrations at later times. Therefore, the effects of 100 μM FCCP treatment on luminescence and the Luc H245F level were measured to determine the relative ATP concentration after FCCP treatment as a percentage of the untreated control from 4 to 6 h PS. FCCP treatment lowered the ATP concentration to 9-23% that of the untreated control at all times in both compartments (Fig. 3.6), supporting the use of Luc H245F to measure decreases in ATP concentration in the FS and MC during sporulation.

Taken together, our results suggest that the ATP concentration rises nearly twofold in the MC between 3.5 and 6 h PS, while the concentration of ATP in the FS does not change significantly. To interpret these observations, we examined morphological changes and the levels of key sporulation proteins in samples collected during the experiments to measure ATP.

The rising mother cell ATP concentration correlates with progression of engulfment, cleavage of Pro-σ^K, and decreasing levels of channel proteins

To examine morphological changes during sporulation, confocal fluorescence microscopy was used to track the progression from formation of flat polar septa to curved septa, through the early and late stages of engulfment, and finally completion of engulfment (Fig. 3.7). For

Fig. 3.5

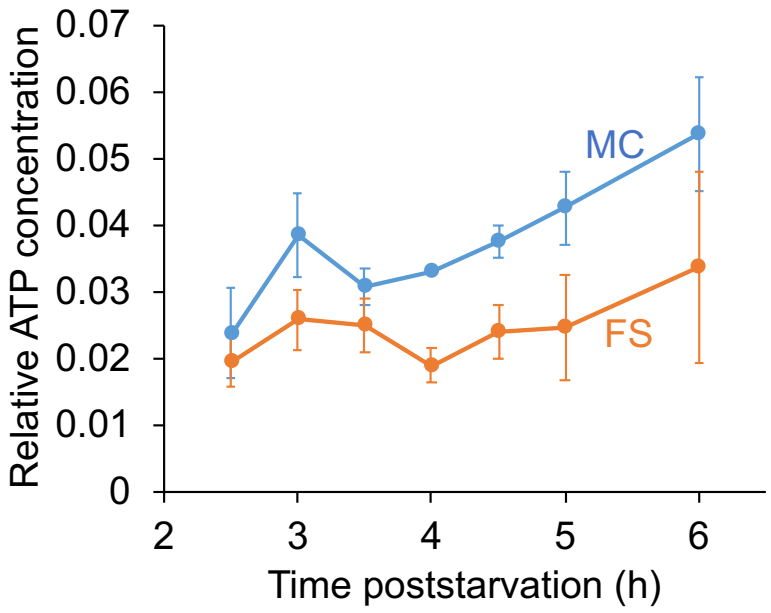

Figure 3.5 The ATP concentration rises in the MC but not in the FS. *B. subtilis* strains engineered to express Luc H245F in the MC or FS were starved to induce sporulation. At 2 h PS, culture aliquots were transferred to a 96-well plate, prior to measuring the luminescence and the Luc H245F level by immunoblot analysis with anti-Luc antibodies at the indicated times PS. The luminescence was divided by the Luc H245F level to yield a normalized value representing the relative ATP concentration. The graph shows the average of three biological replicates and error bars represent one standard deviation.

Fig. 3.6

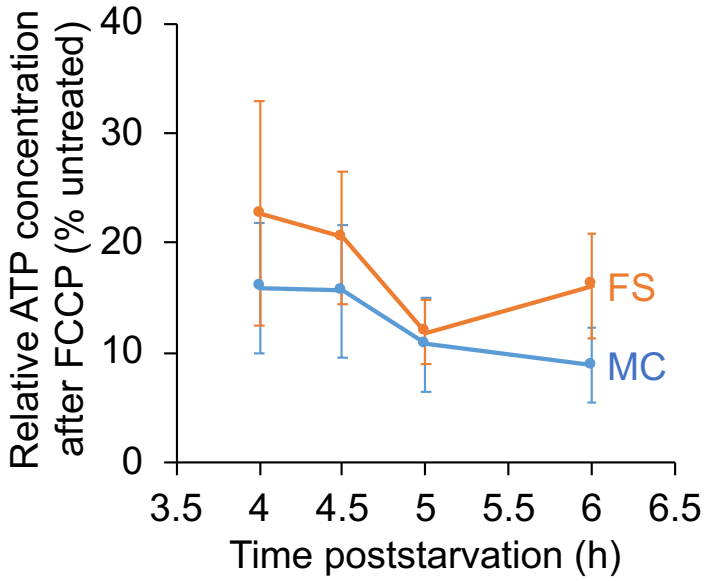

Figure 3.6 Luc H245F detects decreases in compartment-specific ATP concentrations after FCCP treatment at later times during sporulation. *B. subtilis* strains engineered to express Luc H245F in the MC or FS were starved to induce sporulation. At 2 h PS, culture aliquots were transferred to a 96-well plate with luciferin. Aliquots were treated with FCCP (100 μM) for 15 min or left untreated as controls, prior to measuring the luminescence and the Luc H245F level by immunoblot analysis with anti-Luc antibodies at the indicated times PS. The luminescence was divided by the Luc H245F level to yield a normalized value. The normalized value after FCCP treatment was divided by the normalized value of the untreated control to yield the relative ATP concentration after FCCP treatment as a percentage of the untreated control. The graph shows the average relative ATP concentration for three biological replicates and error bars represent one standard deviation.

Fig. 3.7

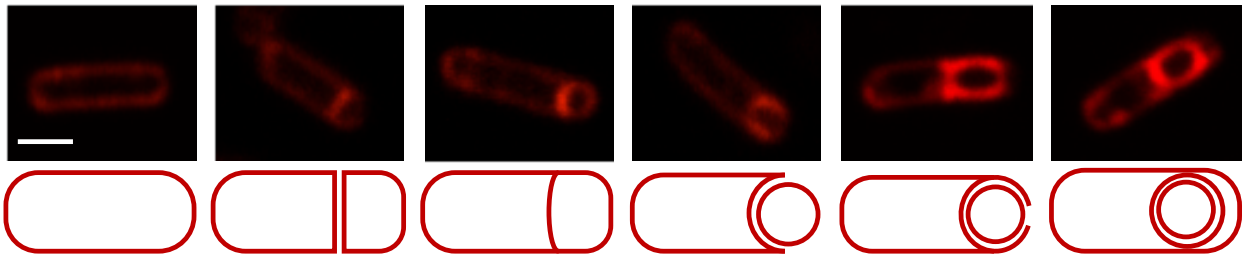

Time PS (h)	Flat septa	Curved septa	Early engulfment	Late engulfment	Complete engulfment
2.5	43	25	16	16	0
3	35	21	23	21	0
3.5	10	6	13	71	0
4	6	5	9	75	5
4.5	13	4	14	68	1
5	8	3	10	67	12
6	4	4	5	45	42

Figure 3.7 Morphological changes during sporulation. *B. subtilis* strains engineered to express Luc H245F in the MC or FS were starved to induce sporulation. At 2 h PS, culture aliquots were transferred to a 96-well plate with FM 4-64 to stain membranes. Images were collected at the indicated times PS using confocal fluorescence microscopy. A representative rod-shaped cell (top, left panel; scale bar = 1 μm) and sporangia representative of each stage (top row; same scale) are shown, with cartoon depictions of membranes below. The percentage of sporangia (150-250 counted; rod-shaped cells were not counted) at each morphological stage is listed at each time PS for the strain expressing Luc H245F in the MC. Gray fill indicates >20%. Similar results were observed for the strain expressing Luc H245F in the FS, and for the wild-type parental strain PY79 which does not express Luc H245F.

simplicity, only the counts for the strain expressing Luc H245F in the MC are shown. The strain expressing Luc H245F in the FS exhibited no significant difference. The majority of sporangia formed flat or curved septa at 2.5 and 3 h PS. From 3.5 to 5 h, most sporangia were at the late stage of engulfment, and by 6 h the majority of sporangia were about evenly split between the late stage and completion of engulfment. In this experiment and in all of our other sporulation time course experiments in which luminescence was measured (Fig. 3.4 and see below), culture aliquots were transferred to a 96-well plate at 2 h PS in order to facilitate subsequent luminescence measurements. We note that the late stage of engulfment was prolonged after transfer to the 96-well plate, as compared with continued incubation and vigorous agitation in flasks. Interestingly, progression through the late stage and completion of engulfment from 3.5 to 6 h PS (Fig. 3.7) correlated with the rise in ATP concentration in the MC (Fig. 3.5).

To examine changes in protein levels, samples were subjected to immunoblot analysis. The levels of SpoIVFA, SpoIVFB, and Pro-σ^K/σ^K suggested that sporulation was delayed by approximately 1 h in 96-well plates (Fig. 3.8) as compared with flasks [45]. Nevertheless, cleavage of Pro-σ^K was observed at 4.5 h PS and the σ^K level rose thereafter (Fig. 3.8), indicative of SpoIVFB protease activity and coincident with the MC rise in ATP concentration (Fig. 3.5). The levels of SpoIVFA (a negative regulator of SpoIVFB) [36, 38] and SpoIVFB decreased at 5 and 6 h (Fig. 3.8). The levels of the channel proteins SpoIIQ and SpoIIIAH peaked at 3 to 3.5 h and decreased thereafter (Fig. 3.8), consistent with reported degradation of channels [10, 23, 41] and coincident with the rise in ATP concentration in the MC (Fig. 3.5).

Altogether, our results suggest that a nearly twofold rise in the MC ATP concentration correlates with progression through the late stage and completion of engulfment, and with rising SpoIVFB cleavage of Pro-σ^K to σ^K and falling levels of the SpoIIQ and SpoIIIAH channel proteins. These correlations support the possibility that channel destruction upon engulfment completion causes the MC ATP concentration to rise (Fig. 3.1). Importantly, cleavage of Pro-σ^K

Fig. 3.8

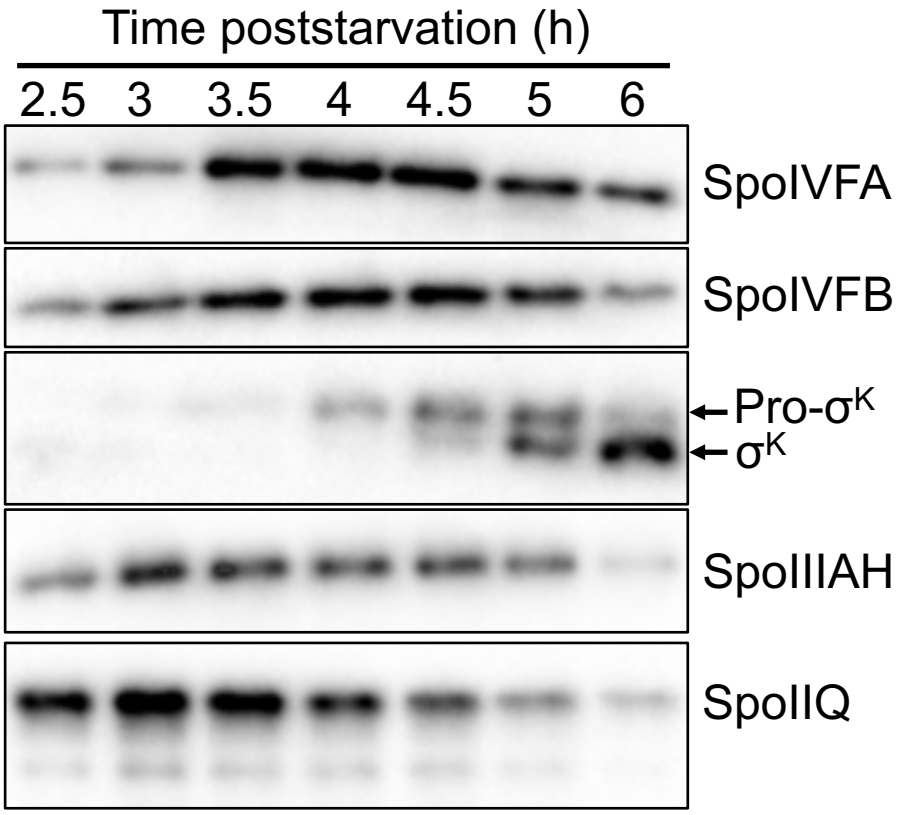

Figure 3.8 Cleavage of Pro-σ^K and decreasing levels of channel proteins correlate with the rise in MC ATP concentration during sporulation. *B. subtilis* strains engineered to express Luc H245F in the MC or FS were starved to induce sporulation. At 2 h PS, culture aliquots were transferred to a 96-well plate. Samples collected from aliquots at the indicated times PS were subjected to immunoblot analysis using antibodies against SpoIVFA, SpoIVFB, Pro-σ^K, SpoIIIAH, and SpoIIQ. Representative immunoblots are shown. Similar results were observed for at least two biological replicates of strains expressing Luc H245F in the MC or FS.

to σ^K at 4.5 to 6 h PS (Fig. 3.8) indicates that σ^G is active in the FS during that period, yet the FS ATP concentration did not decline (Fig. 3.5), despite Luc H245F remaining a sensitive indicator of decreases in ATP concentration after ionophore addition (Fig. 3.6). To gain further insight, we next examined the effects of deletion mutations in genes encoding channel proteins.

Loss of channel proteins affects the ATP concentration in the mother cell and the forespore To test whether channel proteins impact the ATP concentration in either compartment during sporulation, deletion mutations in *spoIIQ, spoIIIAH*, and *spoIIIAA* were transformed into the strains that express Luc H245F in the MC or FS. We chose these mutations because SpoIIQ and SpoIIIAH form the channel [7, 8], and SpoIIIAA ATPase may control substrate secretion through the channel on the MC side [10, 12], whereas the functions of the other SpoIIIA proteins are less well-defined. To determine the relative ATP concentrations during sporulation, we measured the luminescence and Luc H245F levels of the mutants that express Luc H245F in the MC or FS. Like the wild-type (WT) strains (Fig. 3.4A), the luminescence in the mutants rose more in the MC than in the FS by 3 h PS and remained higher in the MC than in the FS by 6 h PS (Fig. 3.9A). On average, the maximum luminescence in the MC was slightly higher in the *spoIIQ* mutant and slightly lower in the *spoIIIAH* mutant as compared with WT and the *spoIIIAA* mutant. The maximum Luc H245F level on average was about two fold lower in the FS of the *spoIIQ* mutant and in both compartments of the *spoIIIAA* mutant as compared with WT and the *spoIIIAH* mutant (Fig. 3.4B and Fig 3.9B). The twofold lower Luc H245F level in the FS of the *spoIIQ* and *spoIIIAA* mutants was unexpected because the *spoIIQ* promoter we used to drive FS-specific expression of Luc H245F depends solely on σ^F (not on σ^G) [50] and expression of *lacZ* fused to the *spoIIQ* promoter was indistinguishable from WT in *spoIIQ* and *spoIIIAA-AH* mutants [11]. The two fold lower level of Luc H245F in the MC of the *spoIIIAA* mutant was also surprising, since the *spoIID* promoter we used to drive MC-

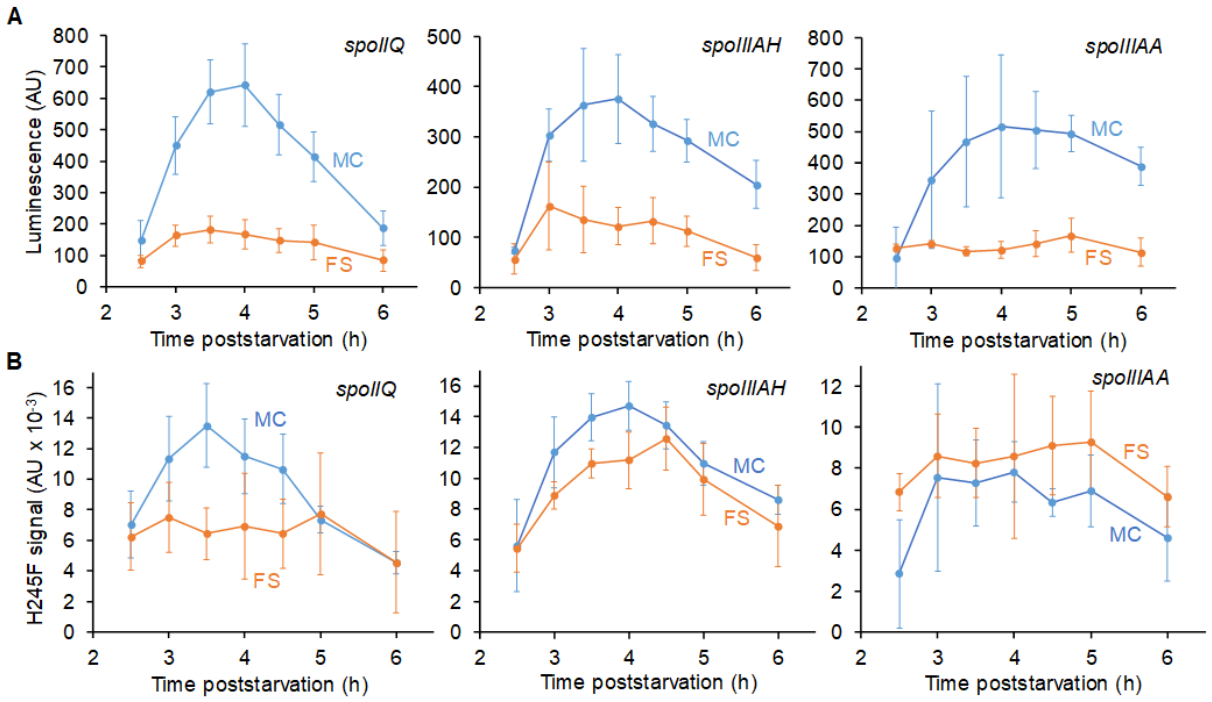

Figure 3.9 Luminescence and Luc H245F levels during sporulation of channel mutants. *B. subtilis* mutants with a deletion in the indicated gene and engineered to express Luc H245F in the MC or FS were starved to induce sporulation. At 2 h PS, culture aliquots were transferred to a 96-well plate, prior to measuring the luminescence and the Luc H245F level by immunoblot analysis with anti-Luc antibodies at the indicated times PS. Graphs show the average of three biological replicates and error bars represent one standard deviation. **(A)** Luminescence of the indicated mutants in arbitrary units (AU). **(B)** Luc H245F levels of the indicated mutants.

specific expression of Luc H245F depends solely on σ^E (not on σ^K) [51] and expression of *lacZ* fused to the *spoIID* promoter was indistinguishable from WT in *spoIIIA* mutants [52]. Perhaps the mutants differ from WT in posttranscriptional regulation of Luc H245F levels. Although the Luc H245F level was only two fold lower in the mutants, Luc H245F could become limiting in the reaction that produces luminescence, leading to an underestimate of the relative ATP concentration (see below).

The relative ATP concentration (i.e., luminescence/Luc H245F level) in the MC was higher on average in the *spoIIQ* and *spoIIIAA* mutants than in WT from 3.5 to 5 h PS (Fig 3.10A), and the difference was statistically significant at 3.5 to 4.5 h for both mutants and at 6 h for the *spoIIIAA* mutant ($P < 0.05$ in Student's two-tailed *t*-tests). As noted above, the Luc H245F level is twofold lower in the *spoIIIAA* mutant than in WT, so Luc H245F could become limiting for luminescence in the mutant, leading to an underestimate of the relative ATP concentration. The average value of 0.092 for the *spoIIIAA* mutant at 6 h PS (Fig 3.10A) was the highest average value observed in any of our experiments with Luc H245F. We cannot rule out the possibility that Luc H245F is saturated for ATP binding in the MC of the *spoIIIAA* mutant at 6 h PS, so the average relative ATP concentration of 0.092 is a minimum estimate. In any case the results suggest that the MC ATP concentration rises earlier in the *spoIIQ* and *spoIIIAA* mutants than in WT (Fig 3.10A), consistent with the hypothesis that functional channels normally decrease the ATP concentration in the MC (Fig. 3.1). However, the MC ATP concentration did not rise significantly in the *spoIIIAH* mutant (Fig 3.10A). Rather, the concentration was lower on average than in WT at all times measured, and the difference was significant at 4.5 to 6 h ($P < 0.05$), owing to the rise in relative ATP levels for WT. One possible explanation of this result is that the SpoIIIA proteins other than SpoIIIAH form a secretion system that functions aberrantly, lowering the MC ATP concentration. The *spoIIQ* mutant may likewise form a secretion system that functions aberrantly, but in a delayed fashion that only lowers the MC ATP concentration

Fig. 3.10

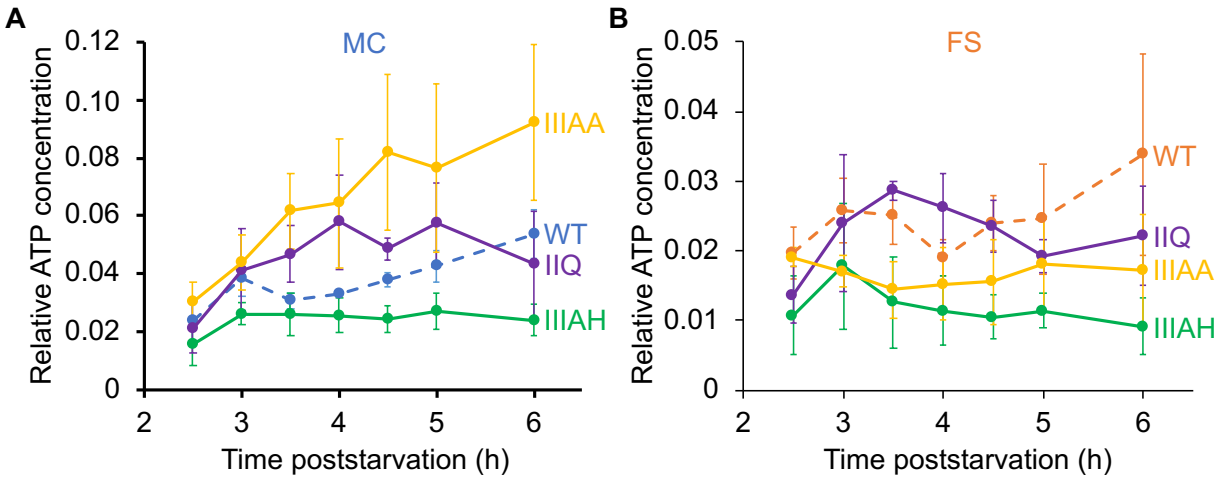

Figure 3.10 Compartment-specific ATP concentration is altered in channel mutants. *B. subtilis* mutants unable to produce the indicated channel protein and engineered to express Luc H245F in the MC or FS were starved to induce sporulation. At 2 h PS, culture aliquots were transferred to a 96-well plate, prior to measuring the luminescence and the Luc H245F level by immunoblot analysis with anti-Luc antibodies at the indicated times PS. The luminescence was divided by the Luc H245F level to yield a normalized value representing the relative ATP concentration in the MC **(A)** or FS **(B)**. Graphs show the average of three or four biological replicates and error bars represent one standard deviation. The results for Wild type (WT) are shown for comparison (same data as Fig. 3.5).

after 4 h, whereas the *spoIIIAA* mutant may form channels that are completely inactive for secretion and never lower the MC ATP concentration (see Discussion).

The FS ATP concentration did not change significantly during sporulation of WT (Fig. 3.5), which was inconsistent with the hypothesis that the FS ATP concentration would decrease after the channels were degraded (Fig. 3.1). Our results suggest that in WT the ATP concentration is maintained in the FS at least until 6 h PS (Fig. 3.5), when engulfment is complete or nearly so in the majority of cells (Fig. 3.7), Pro-σ^K has been cleaved to σ^K (Fig. 3.8), and the levels of the SpoIIQ and SpoIIIAH channel proteins have fallen markedly (Fig. 3.8). These observations do not rule out a possible role of the channels in maintaining the FS ATP concentration during engulfment. In support of a role, the FS ATP concentration in the *spoIIIAA* and *spoIIIAH* mutants was lower on average than in WT at 3 h PS and thereafter (Fig 3.10B). The difference was statistically significant for both mutants at 3 to 3.5 h, and for the *spoIIIAH* mutant at 4 to 6 h as well ($P < 0.05$ in Student's two-tailed *t*-tests). However, the FS ATP concentration in the *spoIIQ* mutant did not differ significantly from that of WT. A possible explanation of these results is that SpoIIQ allows leakage of ATP from the FS due to impaired channel assembly in the *spoIIIAA* and *spoIIIAH* mutants (see Discussion).

We characterized the membrane morphology of the mutant strains we created. The *spoIIQ* and *spoIIIAH* mutants were impaired for engulfment. Unlike WT, the majority of mutant sporangia were in the early stage of engulfment when examined at 6 h PS (Table 3.1). Approximately half of the sporangia that had advanced farther, to the late stage or completion of engulfment, exhibited a FS that appeared to be smaller than usual or misshapen, as reported previously [12]. Additionally, a few disporic cells were observed. In contrast, the *spoIIIAA* mutants (i.e., the two strains with the same *spoIIIAA* mutation, but expressing Luc H245F in the MC or FS) were similar to WT at 6 h PS; the majority of cells were about evenly split between the late stage and completion of engulfment (Table 3.1). However, as expected, at 24 h PS the

Table 3.1 Morphology of bacterial strains after 6 h of starvation

Strain[a]	Flat septa	Curved septa	Early engulfment	Late engulfment	Complete engulfment
WT	4	4	5	45	42
spoIIQ	13	7	59	19	2
spoIIIAH	9	12	42	26	11
spoIIIAA	8	5	4	41	42

[a]*B. subtilis* wild type (WT) or mutant strains that express Luc H245F in the MC or FS were starved to induce sporulation. At 2 h PS, culture aliquots were transferred to a 96-well plate with FM 4-64 to stain membranes. Images were collected at 6 h PS using confocal fluorescence microscopy. The percentage of sporangia (150-250 counted; rod-shaped cells were not counted) at each morphological stage is listed for the strains expressing Luc H245F in the MC. Data for WT are from Figure 3.7. Gray fill indicates >40%. Similar results were observed for the strains expressing Luc H245F in the FS.

efficiency of heat-resistant spore formation by the *spoIIIAA* mutants was less than 1% that of WT.

We also characterized the mutants with respect to protein levels using immunoblot analysis as for WT. The levels of SpoIVFA, SpoIVFB, and Pro-σ^K were similar to those in WT, albeit with slightly less SpoIVFA in the *spoIIQ* and *spoIIIAA* mutants (Fig. 3.8 and 3.11). Also, in all three mutants, the SpoIVFB level was higher than in WT at 6 h PS, presumably because sporulation was blocked. As expected [41], no σ^K was observed in the *spoIIQ* and *spoIIIAA* mutants (Fig. 3.11). A very small amount of σ^K was seen in the *spoIIIAH* mutants, which may explain why *spoIIIAH* mutants form heat-resistant spores with higher efficiency than other *spoIIIA* mutants [12]. The level of SpoIIIAH was lower in the *spoIIQ* mutant than in WT, and accumulation of SpoIIIAH was delayed by about 30 min in the *spoIIQ* and *spoIIIAA* mutants (Fig. 3.8 and 3.11). The level of SpoIIQ was lower in the *spoIIIAA* and *spoIIIAH* mutants than in WT, although the temporal pattern of accumulation was similar.

In sum, our results provide evidence that loss of channel proteins can impact the ATP concentration in both the MC and the FS, and that loss of one channel protein can influence the level of other channel proteins.

Fig. 3.11

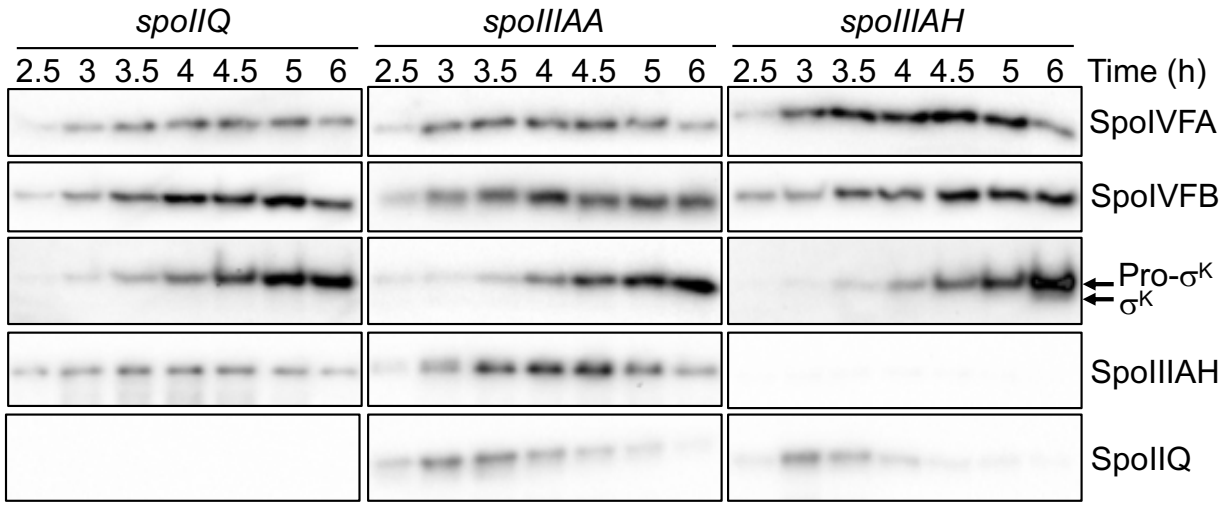

Figure 3.11 Loss of channel proteins impairs cleavage of Pro-σ^K and affects the level of other channel proteins. *B. subtilis* mutants with a deletion in the indicated gene and engineered to express Luc H245F in the MC or FS were starved to induce sporulation. At 2 h PS, culture aliquots were transferred to a 96-well plate. Samples collected from aliquots at the indicated times PS were subjected to immunoblot analysis using antibodies against SpoIVFA, SpoIVFB, Pro-σ^K, SpoIIIAH, and SpoIIQ. Representative immunoblots are shown. Similar results were observed for at least two biological replicates of mutants expressing Luc H245F in the MC or FS.

Bypass mutants lacking channel proteins do not accumulate more σ^K than a bypass mutant with channel proteins

The *spoIIQ*, *spoIIIAH*, and *spoIIIAA* mutants exhibited little or no accumulation of σ^K (Fig. 3.11), as expected since these mutants fail to activate σ^G in the FS [7-12] and σ^G activity is necessary to relieve inhibition of SpoIVFB by SpoIVFA and BofA, allowing cleavage of Pro-σ^K [30-40]. However, the dependence of Pro-σ^K cleavage on σ^G activity can be bypassed by mutations in *spoIVFA* or *bofA* [35-37]. We reasoned that a bypass mutation in combination with a null mutation in *spoIIQ* or *spoIIIAA* might result in earlier and/or elevated accumulation of σ^K, because *spoIIQ* and *spoIIIAA* mutations increased the MC ATP concentration relative to WT (Fig 3.10A) and the CBS domain of SpoIVFB may sense the MC ATP concentration and stimulate Pro-σ^K cleavage [29, 45]. We combined the *bofB8* bypass mutation in *spoIVFA* with null mutations in *spoIIQ*, *spoIIIAH*, and *spoIIIAA*. All strains with the *bofB8* mutation also have a null mutation in *spoIIIG*, which codes for σ^G [53]. The *spoIIIG* mutation blocks SpoIVB expression [30], but the *bofB8* mutation bypasses the need for SpoIVB to relieve inhibition of SpoIVFB [35]. We measured the Pro-σ^K and σ^K levels during sporulation. As expected [35], the *bofB8* mutation advanced the timing of accumulation of σ^K, but in combination with the other mutations, σ^K accumulation was barely detectable (*spoIIQ*), reduced (*spoIIIAH*), or similar to *bofB8* alone (*spoIIIAA*) (Fig. 3.12A). Hence, mutants lacking channel proteins did not accumulate σ^K earlier or at an elevated level. These results suggest that the MC ATP concentration is not limiting for SpoIVFB cleavage of Pro-σ^K under these conditions. Below, we consider two other factors that may have limited SpoIVFB cleavage of Pro-σ^K in this experiment.

First, we examined accumulation of SpoIVFB, because previously a bypass mutation (*bofAΔ*) in combination with a null mutation in *spoIIQ* was shown to greatly reduce SpoIVFB accumulation and σ^K was undetectable during sporulation [54]. In contrast, the *bofB8* mutation in combination with a null mutation in *spoIIQ* did not impair SpoIVFB accumulation as compared

Fig. 3.12

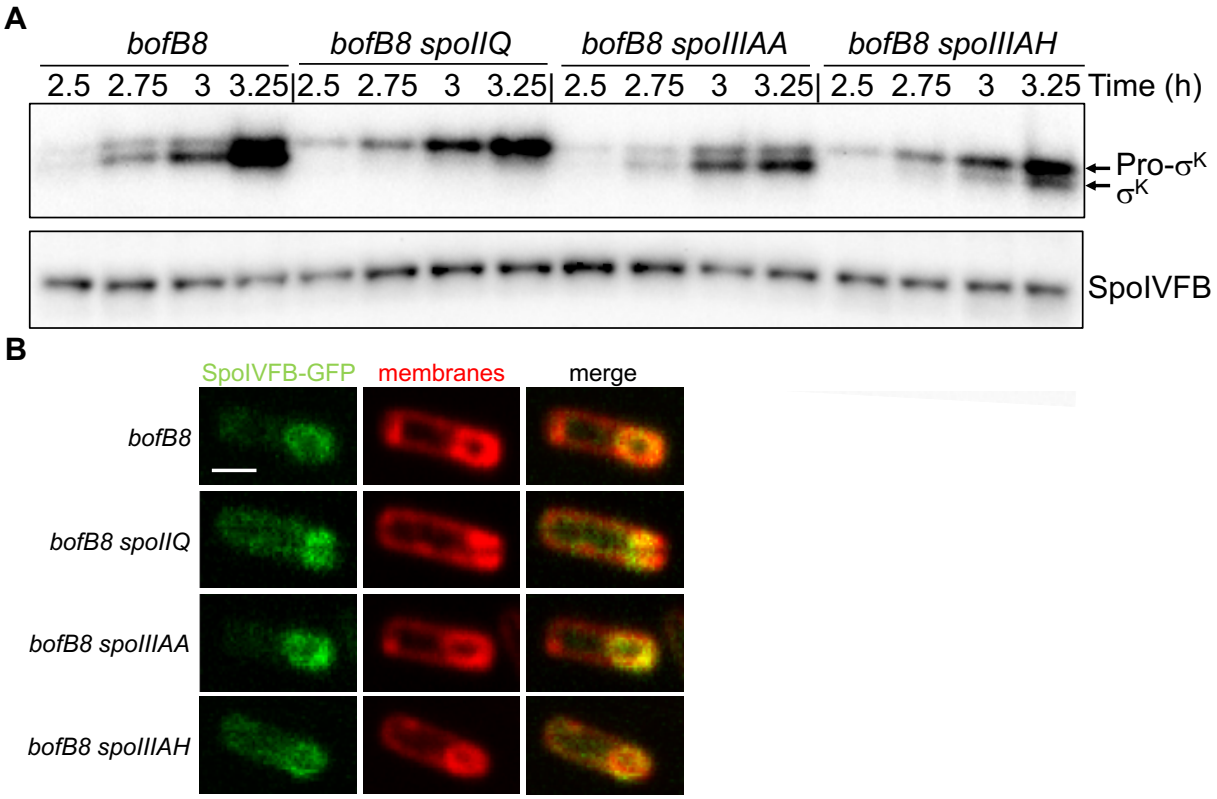

Figure 3.12 Bypass mutants lacking channel proteins differ in cleavage of Pro-σ^K and SpoIVFB-GFP localization. *B. subtilis* strains bearing the *bofB8* mutation alone or in combination with a deletion of *spoIIQ*, *spoIIIAA*, or *spoIIIAH* were starved to induce sporulation. All these strains have a null mutation in *spoIIIG*, which is bypassed by the *bofB8* mutation [35]. **(A)** Immunoblot analysis. Samples collected at the indicated times PS were subjected to immunoblot analysis using antibodies against Pro-σ^K and SpoIVFB. Representative immunoblots are shown. Similar results were observed for at least two biological replicates. **(B)** Confocal fluorescence microscopy. The native *spoIVFB* gene was C-terminally fused to *gfp* in the indicated strains, samples were collected at 3 h PS, and FM 4-64 was added to stain membranes. Images of fluorescence from SpoIVFB-GFP and membranes, and the merged images, are shown in the indicated columns, for a representative sporangium. In the top, left panel the scale bar = 1 μm.

with the *bofB8* mutation alone (Fig. 3.12A). SpoIVFB accumulation was also similar for the *bofB8* mutation in combination with a null mutation in *spoIIIAH* or *spoIIIAA.*

Since SpoIVFB accumulated, we considered the possibility that it was mislocalized. Previously, null mutations in *spoIIQ* or *spoIIIAH-G* (i.e., deletion of both *spoIIIAG* and *spoIIIAH*) were reported to prevent localization of SpoIVFB-GFP to the engulfing membrane, although SpoIVFB-GFP appeared to accumulate in the outer FS membrane after completion of engulfment [41]. We created strains in which the native *spoIVFB* gene was C-terminally fused to *gfp*. Immunoblot analysis of all the strains with antibodies against GFP revealed that SpoIVFB-GFP migrated at the expected position, with very little or no free GFP due to degradation (Fig. 3.13). Therefore, we examined SpoIVFB-GFP localization using confocal fluorescence microscopy. The *bofB8* mutation alone or in combination with the null mutation in *spoIIIAA*, allowed predominantly FS localization of SpoIVFB-GFP (presumably to the outer FS membrane) (Fig. 3.12B), consistent with their similar σ^K accumulation (Fig. 3.12A). In contrast, the *bofB8* mutation in combination with a null mutation in *spoIIQ* or *spoIIIAH* resulted in considerable MC fluorescence (Fig. 3.12B), suggesting that SpoIVFB-GFP was partially mislocalized, which may explain why σ^K accumulation was impaired (Fig. 3.12A).

We conclude that SpoIIIAA is not required for proper localization of SpoIVFB-GFP or for normal accumulation of SpoIVFB in the context of the *bofB8* bypass mutation (Fig. 3.12). Yet, loss of SpoIIIAA does not elevate σ^K accumulation in the bypass mutant (Fig. 3.12A), even though loss of SpoIIIAA does elevate the MC ATP concentration relative to WT (Fig 3.10A). Together, these results strongly suggest that the MC ATP concentration is not limiting for SpoIVFB cleavage of Pro-σ^K under these conditions. Moreover, in the strains with the *bofB8* mutation alone or in combination with the *spoIIIAA* mutation, σ^K accumulates as soon as Pro-σ^K is detected (Fig. 3.12A), suggesting that the MC ATP concentration is sufficient for SpoIVFB cleavage of Pro-σ^K before the ATP concentration rises in the MC (Fig 3.10A).

Fig. 3.13

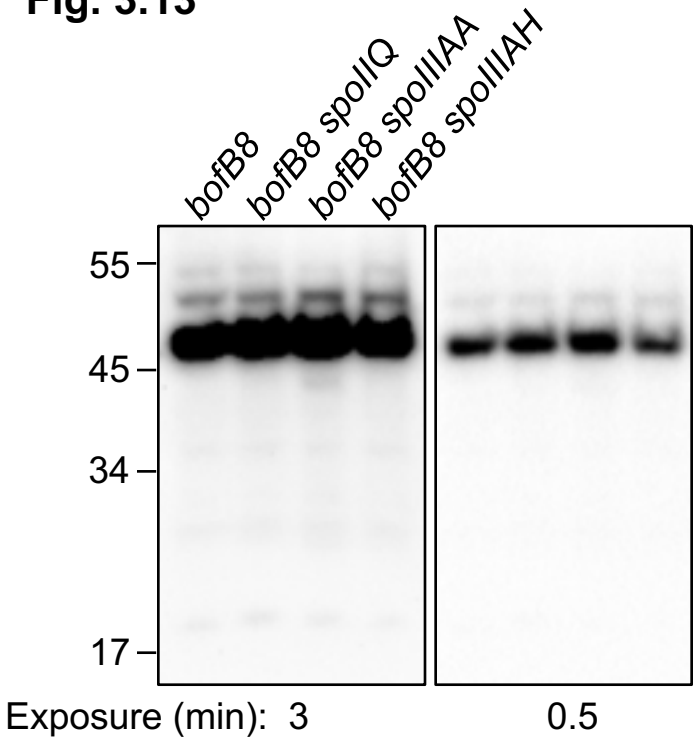

Figure 3.13 SpoIVFB-GFP accumulates similarly in bypass mutants. *B. subtilis* strains with the *bofB8* mutation alone or in combination with a deletion of *spoIIQ*, *spoIIIAA*, or *spoIIIAH*, and with *gfp* fused to *spoIVFB*, were starved to induce sporulation. All these strains have a null mutation in *spoIIIG*, which is bypassed by the *bofB8* mutation [35]. Samples collected at 3 h PS were subjected to immunoblot analysis using antibodies against GFP. The left panel shows a long exposure to demonstrate that very little or no free GFP (27 kDa) accumulated. The molecular weight (kDa) and migration of marker proteins is indicated. The right panel shows a short exposure of the same blot to demonstrate that the SpoIVFB-GFP level was similar in all the strains.

Both ionophores and chloramphenicol decrease the mother cell ATP concentration, but only ionophores inhibit Pro-σ^K cleavage

Since SpoIVFB did not appear to sense the rise in MC ATP concentration, we tested whether SpoIVFB would be inhibited by a decrease in ATP concentration brought about by treatment with an ionophore. In a previous study, the ionophore carbonyl cyanide *m*-chlorophenylhydrazone (CCCP) was shown to inhibit cleavage of Pro-σ^K during *B. subtilis* sporulation, but the inhibition appeared to be primarily due to decreased synthesis of SpoIVB [55]. SpoIVB cleaves the extracytoplasmic domain of SpoIVFA in the space between the membranes surrounding the FS, relieving inhibition of SpoIVFB [31-33, 40]. The *spoIVB* gene is transcribed by σ^G RNA polymerase [30], which is the primary reason that σ^G activity is required for Pro-σ^K cleavage [35], as mentioned above. Using the same *bofB8 spoIIIG* bypass mutant as in the experiments shown in Figure 3.12, the inhibition of Pro-σ^K cleavage by CCCP (5 μM) was partially overcome [55]. This result raised the question whether 5 μM CCCP treatment substantially lowered the ATP level in the MC during *B. subtilis* sporulation. Therefore, we compared the effects of different ionophores at different concentrations on the relative ATP concentration in the MC.

We compared the effects of CCCP and FCCP treatments at 5 and 100 μM at 3.5 h PS. As observed for treatment with 100 μM FCCP, the other treatments primarily decreased the luminescence (Fig. 3.14A) and had little impact on the Luc H245F level (Fig. 3.14B), resulting in normalized values that indicate all four treatments decreased the relative ATP concentration in the MC after 15 min (Fig. 3.15A). The decrease brought about by 5 μM CCCP (~57%) was less than for 5 μM FCCP (~71%), and 100 μM CCCP (~81%) or FCCP (~94%) brought about greater decreases.

Since treatment with ionophores decreased the relative ATP concentration in the MC, we tested whether cleavage of Pro-σ^K by SpoIVFB was inhibited by ionophores. We used the same

Fig. 3.14

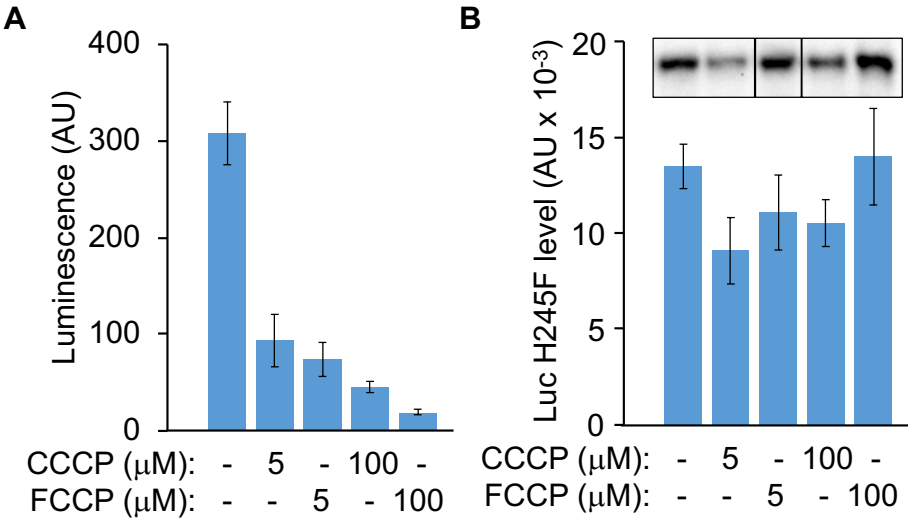

Figure 3.14 MC luminescence and Luc H245F levels after treatment with ionophores during sporulation. *B. subtilis* engineered to express Luc H245F in the MC was starved to induce sporulation. At 3.5 h PS, culture aliquots were transferred to a 96-well plate with luciferin. Aliquots were left untreated as controls (-) or were treated with an ionophore as indicated for 15 min, prior to measuring the luminescence and the Luc H245F level by immunoblot analysis with anti-Luc antibodies. Graphs show the average of three biological replicates and error bars represent one standard deviation. **(A)** Luminescence in arbitrary units (AU). **(B)** Luc H245F level. A representative immunoblot is shown at the top (vertical lines indicate intervening lanes were removed) and quantification of replicates is shown below.

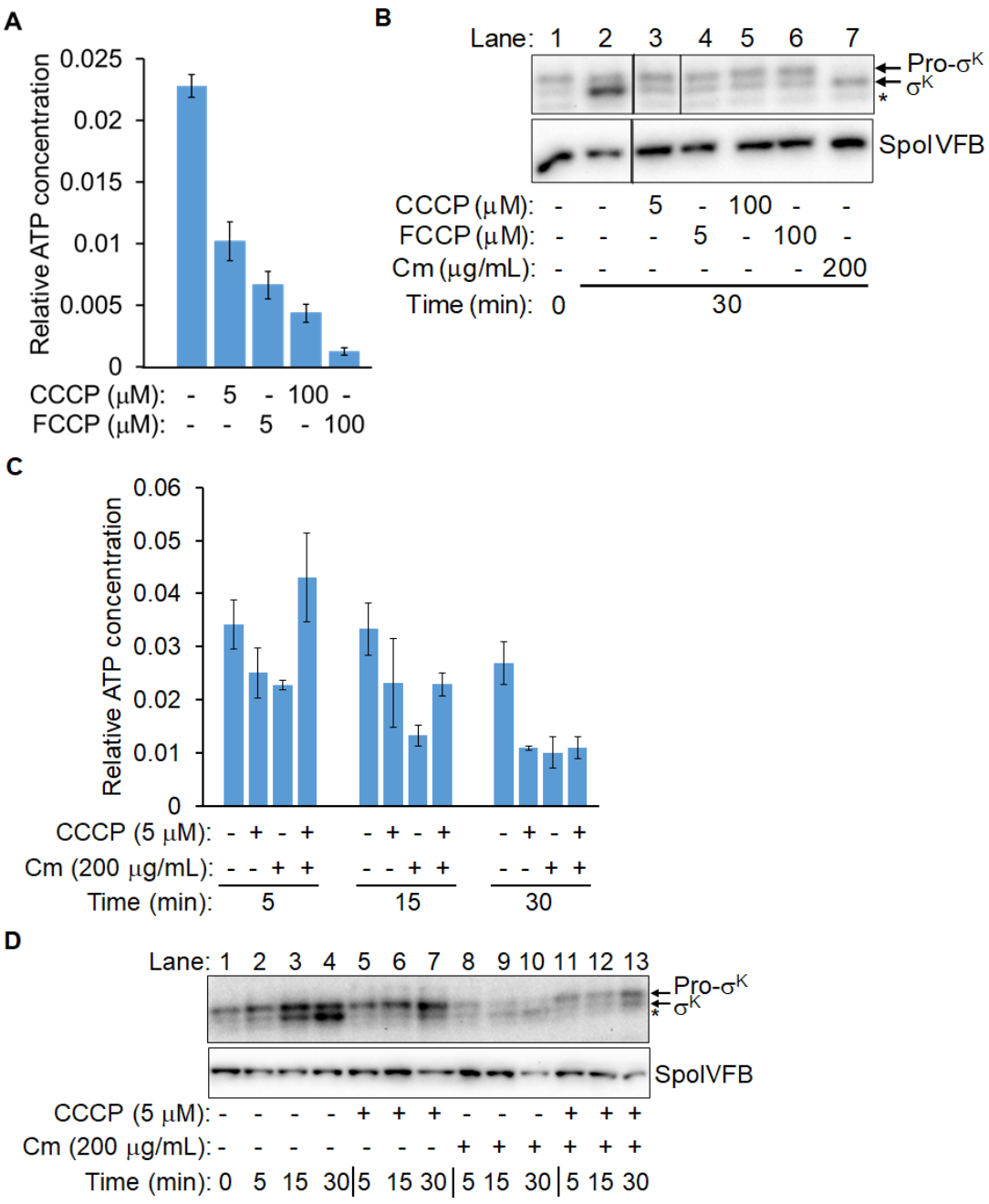

Figure 3.15 Ionophores decrease the MC ATP concentration and inhibit Pro-σ^K cleavage. **(A)** Relative ATP concentration in the MC after ionophore treatment. *B. subtilis* engineered to express Luc H245F in the MC was starved to induce sporulation. At 3.5 h PS, culture aliquots were transferred to a 96-well plate with luciferin. Aliquots were left untreated as controls (-) or were treated with an ionophore as indicated for 15 min, prior to measuring the luminescence and the Luc H245F level by immunoblot analysis with anti-Luc antibodies. The luminescence was divided by the Luc H245F level to yield a normalized value representing the relative ATP concentration. The graph shows the average of three or four biological replicates and error bars represent one standard deviation. **(B)** Cleavage of Pro-σ^K after ionophore or Cm treatment. *B. subtilis* with a null mutation in *spoIIIG* and the *bofB8* mutation that bypasses the need for

Figure 3.15 (cont'd)

spoIIIG [35] was starved to induce sporulation. At 2.25 h PS, the culture was split, and at 2.5 h, the cultures were left untreated as a control (-) or were treated with an ionophore or Cm as indicated for 30 min. Samples were subjected to immunoblot analysis with antibodies against Pro-σ^K and SpoIVFB. A representative immunoblot is shown (vertical lines indicate intervening lanes were removed). The asterisk indicates a breakdown product of Pro-σ^K or a cross-reactive protein. Similar results were observed for at least two biological replicates. **(C)** Relative ATP concentration in the MC after CCCP and/or Cm treatment. The experiment was performed as described for panel A, except cultures were treated at 2.5 h to match panel B, prior to measuring the luminescence and the Luc H245F level at 5, 15, and 30 min after treatment (Fig. 3.17). The luminescence was divided by the Luc H245F level to yield a normalized value representing the relative ATP concentration. The graph shows the average of three biological replicates and error bars represent one standard deviation. **(D)** Cleavage of Pro-σ^K after CCCP and/or Cm treatment. This experiment was performed as described for panel B, except cultures were treated as indicated for 5, 15, and 30 min.

bofB8 spoIIIG bypass mutant as in the experiments shown in Figure 3.12 and in the previous study [55]. As explained above, the *bofB8* mutation bypasses the need for σ^G-dependent expression of SpoIVB, which normally is required to relieve inhibition of SpoIVFB and allow Pro-σ^K cleavage [30, 35, 36]. We anticipated that ionophores would inhibit protein synthesis [55], so it was necessary to bypass the need for synthesis of SpoIVB. As a control, we tested the effect of the protein synthesis inhibitor chloramphenicol (Cm) on Pro-σ^K cleavage in the bypass mutant, expecting to observe cleavage based on the previous study [55]. In the bypass mutant at 2.5 h PS, Pro-σ^K is more abundant than σ^K (Fig. 3.15B, lane 1), but by 3 h, σ^K is more abundant (lane 2), due to cleavage of Pro-σ^K by SpoIVFB. In contrast, treatment at 2.5 h with CCCP or FCCP at 5 or 100 μM appeared to substantially inhibit Pro-σ^K cleavage by 3 h since the ratio of σ^K to Pro-σ^K changed very little in comparison with lane 1 (lanes 3-6). As expected, the ionophores appeared to inhibit protein synthesis, as the combined accumulation of Pro-σ^K and σ^K in lanes 3-6 was only slightly more than in lane 1, and less than in lane 2. However, the inhibition of Pro-σ^K cleavage by ionophores was not due to inhibition of protein synthesis, since treatment with Cm did not inhibit cleavage (lane 7). Neither was the inhibition of Pro-σ^K cleavage by ionophores due to loss of SpoIVFB, whose abundance was similar at 2.5 h and at 3 h under all conditions (Fig. 3.15B, bottom panel).

Taken together, our results show that ionophores decrease the ATP concentration in the MC and inhibit Pro-σ^K cleavage, whereas Cm treatment does not inhibit Pro-σ^K cleavage (Fig. 3.15).

We did not expect Cm treatment to decrease the MC ATP concentration, since Cm treatment of growing *E. coli* increased the relative ATP concentration about two fold after 10 min, presumably since less ATP was being utilized for protein synthesis [25]. However, our measurements were in *B. subtilis* and the MC ATP concentration was measured 15 min after treatment with ionophores at 3.5 h PS (Fig. 3.15A). Therefore, we measured the effect of Cm

under the same conditions. We found that Cm also decreases the luminescence and has little effect on the Luc H245F level, hence decreasing the relative MC ATP concentration (Fig. 3.16). The decrease (53%) was comparable to that brought about by 5 μM CCCP (57%) (Fig. 3.15A) and less than that brought about by 100 μM FCCP (73%) in the same experiment (Fig. 3.16). We note that the decrease brought about by 100 μM FCCP varied from 94% (Fig. 3.15A) to 81% (Fig. 3.3B) in other experiments, but was consistently greater than that brought about by Cm or 5 μM CCCP. Therefore, we focused on treatments with Cm and/or 5 μM CCCP in order to understand their strikingly different effects on Pro-σ^K cleavage (Fig. 3.15B).

We reasoned that the 5 μM CCCP treatment might cause the MC ATP concentration to decrease more rapidly than the Cm treatment, explaining the observed inhibition of Pro-σ^K cleavage by CCCP but not Cm (Fig. 3.15B). However, we found that Cm caused the MC ATP concentration to decrease at least as rapidly as CCCP after treatment at 2.5 h PS (Fig. 3.15C and Fig 3.17). Interestingly, the treatment with both CCCP and Cm did not cause the MC ATP concentration to decrease after 5 min and caused a similar decrease as CCCP alone after 15 min. The treatments were performed at 2.5 h to match the time of treatments in the experiment shown in Figure 3.12. We repeated the experiment in order to also examine Pro-σ^K cleavage at earlier times post-treatment. We again observed that CCCP inhibited Pro-σ^K cleavage more than Cm after 30 min (Fig. 3.15D, compare lanes 7 and 10). The difference was already evident after 15 min (compare lanes 6 and 9), when the MC ATP concentration was on average lower after treatment with Cm than CCCP (Fig. 3.15C). Importantly, combined treatment with Cm and CCCP (Fig. 3.15D, lanes 11-13) inhibited Pro-σ^K cleavage comparably to treatment with CCCP alone (lanes 5-7), and as expected the combined treatment inhibited protein synthesis more than CCCP alone and comparably to Cm alone (lanes 8-10). Hence, the MC ATP concentration does not explain the inhibition of Pro-σ^K cleavage that we observe after CCCP treatment or

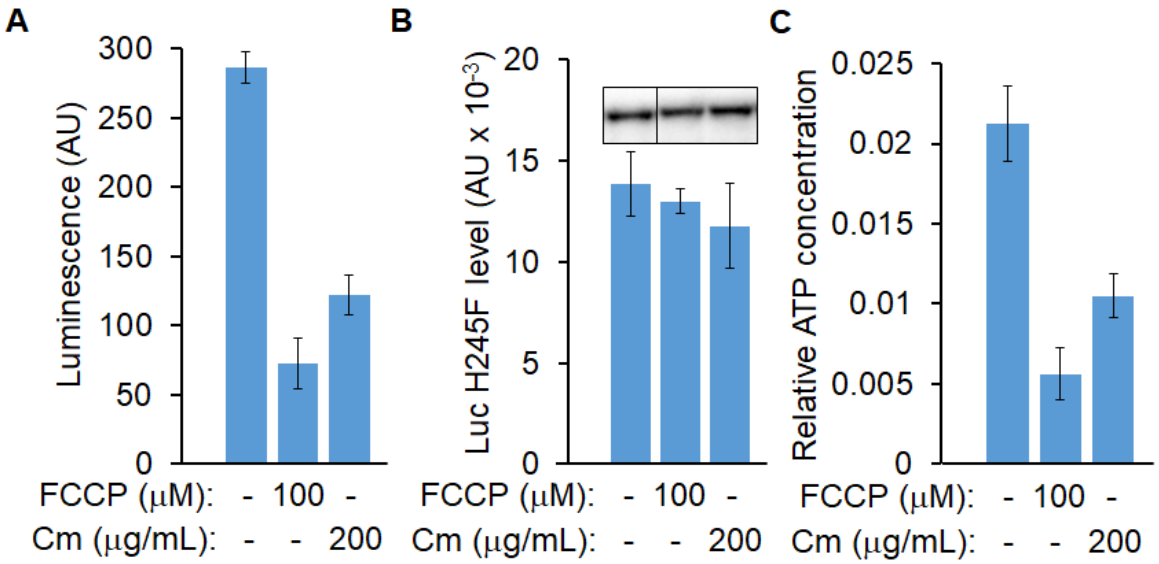

Figure 3.16 Cm decreases the MC ATP concentration. *B. subtilis* engineered to express Luc H245F in the MC was starved to induce sporulation. At 3.5 h PS, culture aliquots were transferred to a 96-well plate with luciferin. Aliquots were left untreated as controls (-) or were treated with FCCP or Cm as indicated for 15 min, prior to measuring the luminescence and the Luc H245F level by immunoblot analysis with anti-Luc antibodies. **(A)** Luminescence in arbitrary units (AU). **(B)** Luc H245F level. A representative immunoblot is shown at the top (vertical line indicates intervening lanes were removed) and quantification of replicates is shown below. **(C)** Relative ATP concentration. The luminescence was divided by the Luc H245F level to yield a normalized value representing the relative ATP concentration. Graphs show the average of three biological replicates and error bars represent one standard deviation.

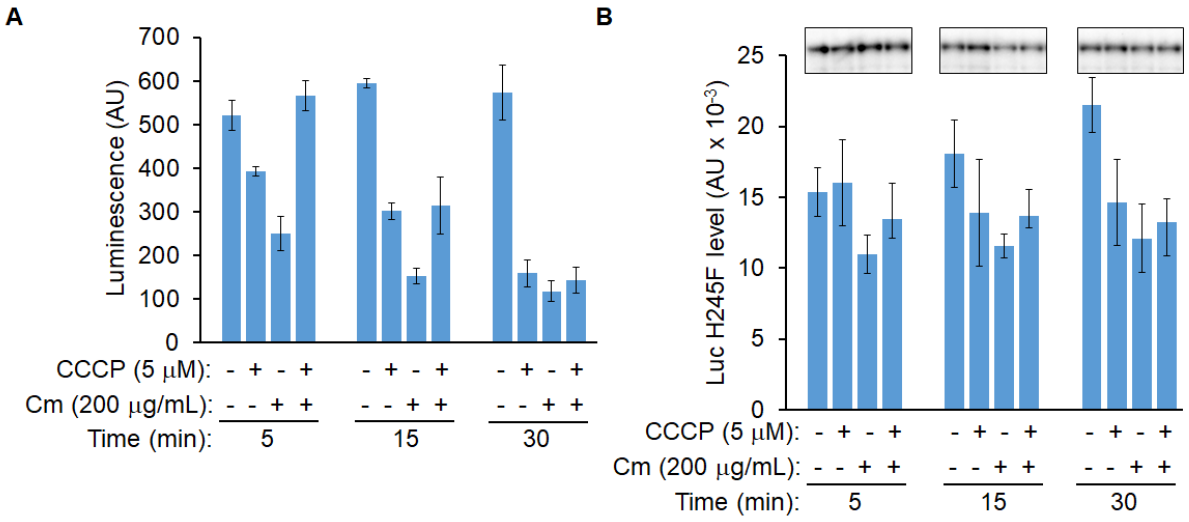

Figure 3.17 MC luminescence and Luc H245F levels after CCCP and/or Cm treatment. *B. subtilis* engineered to express Luc H245F in the MC was starved to induce sporulation. At 2.25 h PS, culture aliquots were transferred to a 96-well plate with luciferin, and at 2.5 h, aliquots were left untreated as controls (-) or were treated with CCCP and/or Cm (+) as indicated, prior to measuring the luminescence and the Luc H245F level by immunoblot analysis with anti-Luc antibodies at 5, 15, and 30 min after treatment. Graphs show the average of three biological replicates and error bars represent one standard deviation. **(A)** Luminescence in arbitrary units (AU). **(B)** Luc H245F level. A representative immunoblot is shown at the top (panels were cropped from the same immunoblot) and quantification of replicates is shown below.

combined treatment with CCCP and Cm. Rather, we suggest that CCCP alone or in combination with Cm alters the MC energy status differently than Cm alone, as reflected in the ratio of ATP to ADP and/or AMP, and that the CBS domain of SpoIVFB senses the MC energy status and regulates Pro-σ^K cleavage appropriately.

Discussion

We devised a method to measure the relative ATP concentration in each compartment during sporulation and used the method to show that the ATP concentration rises nearly twofold in the MC coincident with progression through the late stage and completion of engulfment, SpoIVFB-dependent cleavage of Pro-σ^K, and decreasing levels of the channel proteins SpoIIQ and SpoIIIAH. The coincidence of these events suggests that engulfment completion and ensuing channel destruction cause the MC ATP concentration to rise (Fig. 3.1). However, the rise in MC ATP concentration does not appear to be necessary for Pro-σ^K cleavage, based on our analysis of mutants that bypass the normal requirement for the σ^G-dependent signaling pathway from the FS to relieve inhibition of SpoIVFB. On the other hand, a drop in the MC ATP concentration brought about by ionophore treatment inhibited Pro-σ^K cleavage, but cleavage was not inhibited by at least as great a drop in ATP concentration due to protein synthesis inhibition. A plausible explanation based on CBS domain function in other proteins is that the SpoIVFB CBS domain senses the ratio of adenine nucleotides (i.e., energy status) in the MC rather than sensing only the ATP concentration.

Surprisingly, the FS ATP concentration did not decline during sporulation, suggesting that ATP can be synthesized in the FS after completion of engulfment, when σ^G becomes fully active. Because treatment with an ionophore rapidly decreased the FS ATP concentration late during sporulation, a proton gradient across the inner FS membrane may drive ATP synthesis after channel destruction. Earlier, during engulfment, proper assembly of the channels appears

to be important for maintaining the normal concentration of ATP in the FS, unless SpoIIQ is absent. SpoIIQ may allow leakage of ATP from the FS of mutants with impaired channel assembly. We propose that properly assembled channels allow the MC to feed the FS amino acids and/or nucleotides (other than ATP) that are used both directly for post-engulfment gene expression and indirectly for ATP synthesis.

Luciferase H245F detects changes in ATP concentration over a broad range

Relative ATP concentrations (i.e., luminescence/Luc H245F level) ranged from as high as 0.092 (on average) in the MC of the *spoIIIAA* mutant at 6 h PS (Fig 3.10A) to as low as 0.0013 in the MC of WT at 15 min after treatment with 100 μM FCCP at 3.5 h PS (Fig. 3.15A), a 71-fold range. The latter value of 0.0013 was lower than in two comparable experiments (0.0060 and 0.0056 in Fig. 3.3B and S7C Fig, respectively), but values of ≤ 0.0031 were observed in the MC and FS of WT at 15 min after treatment with 100 μM FCCP at 5 or 6 h PS (data not shown) in the experiment summarized in Fig. 3.6. Therefore, values reproducibly ranged at least ~30-fold (from 0.0031 to 0.092). This range is broader than the ~10-fold range observed for an *E. coli* purine auxotroph grown in minimal medium supplemented with adenine or guanine [25]. In their pioneering study, Schneider and Gourse [25] noted that Luc H245F reports ATP available to an enzyme *in vivo*, which is less than the total ATP pool measured by extraction methods because the total pool includes ATP tightly associated with other macromolecules (i.e., unavailable to Luc H245F). They inferred that the available ATP concentration is either less than 3 mM (i.e., the estimated total ATP concentration) or that cytoplasmic conditions increase the apparent K_m of Luc H245F for Mg-ATP (830 μM *in vitro*), since they demonstrated that Luc H245F was not saturated for ATP *in vivo*. These considerations highlight the caveats of comparing relative ATP concentrations measured with Luc H245F *in vivo* and the total ATP pool measured by extraction methods. Therefore, we did not attempt to make such comparisons, particularly since methods

to separate the MC and FS compartments are time-consuming, raising concern that the total ATP pools might change during the separation procedure. Rather, we focused on using Luc H245F to measure the relative ATP concentration in each compartment, and our results demonstrate the utility of Luc H245F to detect relative changes over a broad range. We note that Luc H245F has been expressed in *Rhodospirillum rubrum* and large changes in luminescence were observed after treatment with ionophores, but the Luc H245F level was not measured [56]. Also, large changes in luminescence were observed when Luc H245F was expressed during growth of a purine auxotroph in minimal medium supplemented with different concentrations of adenine, but the inferred changes in ATP level did not correlate well quantitatively with trichloroacetic acid extraction of ATP, further highlighting the caveats of comparing ATP measurements with Luc H245F *in vivo* and with extraction methods.

A limitation of using Luc H245F is the inability to observe individual cells microscopically because light production is too low. In an effort to measure relative changes in ATP concentration at single-cell resolution, we attempted expression of a codon-optimized variant of the FRET-based ATP sensor AT1.03 [57] in *B. subtilis*. However, we were unable to generate a strain with sufficient expression to allow measurements (see Appendix 3.1).

Channel destruction upon engulfment completion correlates with a nearly twofold rise in the mother cell ATP concentration, but this does not appear to be necessary for Pro-σ^K cleavage The findings that SpoIVFB has an ATP-binding CBS domain and that cleavage of Pro-σ^K by SpoIVFB *in vitro* depends on ATP led to the suggestion that the SpoIVFB CBS domain senses the MC ATP concentration and regulates Pro-σ^K cleavage appropriately [29]. In particular, it was attractive to propose that channel destruction upon completion of engulfment [10, 12, 23] causes the MC ATP concentration to rise and that this is sensed by the CBS

domain of SpoIVFB, triggering cleavage of Pro-σ^K [6, 14]. Our data support some aspects of this model, but not others.

Our data strongly support the hypothesis that channel destruction upon completing engulfment causes a nearly twofold rise in the MC ATP concentration. We used MC-expressed Luc H245F to measure a rise in the relative ATP concentration from an average of 0.031 at 3.5 h PS to 0.054 at 6 h (Fig. 3.5). Both values are well within the range (0.092 to 0.0013) observed in our study. Most of the rise in MC ATP concentration occurred at 5 and 6 h, coincident with an increasing percentage of sporangia that had completed engulfment (Fig. 3.7), and with increased cleavage of Pro-σ^K to σ^K and decreased levels of channel proteins (Fig. 3.8).

Our data also support the hypothesis that channel function during engulfment normally decreases the MC ATP concentration (Fig. 3.1). The relative ATP concentration increased earlier in the MC of *spoIIQ* and *spoIIIAA* mutants than in WT (Fig 3.10A). The mutants reached average values of 0.058 (*spoIIQ*) and 0.064 (*spoIIIAA*) at 4 h PS, whereas WT reached only 0.033. Interestingly, the MC ATP concentration plateaued in the *spoIIQ* mutant, but continued to rise in the *spoIIIAA* mutant until 6 h. This difference may reflect different roles of SpoIIQ and SpoIIIAA in channel function after 4 h. In the absence of SpoIIQ, the SpoIIIAH [7] and SpoIIIAG [12] proteins mislocalize to the MC membrane. Perhaps the SpoIIIA proteins eventually assemble to some extent in the MC membrane and secrete something from the MC cytoplasm, preventing the ATP concentration from continuing to rise after 4 h in the *spoIIQ* mutant. In the absence of SpoIIIAA, channels may assemble but completely fail to secrete something from the MC due to the lack of SpoIIIAA ATPase activity [12], so the ATP concentration continues to rise after 4 h in the *spoIIIAA* mutant.

Why did the MC ATP concentration remain low in the *spoIIIAH* mutant? We propose an explanation similar to that for the *spoIIQ* mutant, but with more rapid assembly of SpoIIIA proteins capable of secreting something from the MC, so the ATP concentration never rises (Fig 3.10A). In support of this explanation, SpoIIIAG is less severely mislocalized in the *spoIIIAH*

mutant than in the *spoIIQ* mutant [12]. Also, the *spoIIIAH* mutant forms spores at 5% the efficiency of WT, whereas mutants lacking any other SpoIIIA protein [12] or SpoIIQ [58, 59] exhibit much more severe sporulation defects. These observations suggest that in the absence of SpoIIIAH, the other SpoIIIA proteins can still interact weakly with SpoIIQ [12]. In any case, we propose that the other SpoIIIA proteins assemble efficiently and secrete something from the MC so that the MC ATP concentration remains low in the *spoIIIAH* mutant.

Our data do not support the hypothesis that in WT the rise in MC ATP concentration triggers Pro-σ^K cleavage. Rather, relief from inhibition by SpoIVFA and BofA appears to be sufficient to allow SpoIVFB to cleave Pro-σ^K before the rise in MC ATP concentration. We used the *bofB8* mutation, which prematurely truncates SpoIVFA by just six residues [36], to relieve inhibition of SpoIVFB. We found that σ^K accumulates as soon as Pro-σ^K is detected, by 2.75 h PS (Fig. 3.12A), well before the rise in MC ATP concentration at 5 to 6 h in WT (Fig. 3.5), even if we assume the rise would have occurred 1 h earlier if culture aliquots had not been transferred from flasks to 96-well plates at 2 h PS. Also, the ratio of σ^K to Pro-σ^K was not higher in the *bofB8 spoIIIAA* double mutant than in the *bofB8* single mutant (Fig. 3.12A), although the MC ATP concentration was expected to be higher in the double mutant, based on the elevated concentration in the *spoIIIAA* mutant compared with WT at 3 and 4 h (Fig 3.10A). These observations suggest that the concentration of ATP in the MC is sufficient for SpoIVFB activity prior to the rise that accompanies engulfment completion and channel destruction.

The SpoIVFB CBS domain may sense the mother cell energy status and regulate Pro-σ^K cleavage appropriately

If the CBS domain of SpoIVFB does not sense the rise in MC ATP concentration, then what is its purpose? We reasoned that ATP dependence of SpoIVFB might instead reduce the cleavage of Pro-σ^K if the energy status is too low to support expression of the σ^K regulon. It was

proposed previously that the SpoIVFB CBS domain senses the MC energy status [29], based on analogy with CBS domains that bind adenine nucleotides and function as sensors of cellular energy status to regulate activity of metabolic enzymes, kinases, and channels [44]. This idea was also favored in a recent study that showed YFP could substitute for the CBS domain of SpoIVFB, stabilizing the N-terminal protease domain and allowing partial activity that was adequate for efficient sporulation [40]. Even in the complete absence of SpoIVFB, overproduction of Pro-σ^K allows a very small amount of σ^K to accumulate (presumably due to cleavage by one or more proteases other than SpoIVFB), which is sufficient for about 25% the normal level of sporulation [60]. Hence, in order to impact the formation of heat-resistant spores, the proposed energy sensing by the SpoIVFB CBS domain would need to strongly inhibit Pro-σ^K cleavage.

We used ionophore treatment to lower the MC ATP concentration and we measured the effect on Pro-σ^K cleavage. We found that a modest decrease of about twofold in the MC ATP concentration by 15 min after treatment with 5 μM CCCP (Fig. 3.15A) partially inhibited Pro-σ^K cleavage (Fig. 3.15B). In contrast, treatment with the protein synthesis inhibitor Cm did not inhibit cleavage of Pro-σ^K (Fig. 3.15B and 9D), despite causing the MC ATP concentration to decrease at least as rapidly as treatment with 5 μM CCCP (Fig. 3.15C). Because the MC ATP concentration does not explain the strikingly different effects of ionophores and Cm on Pro-σ^K cleavage, we propose that ionophores and Cm differentially alter the MC energy status as reflected in the ratio of adenine nucleotides (i.e. AMP:ATP ratio), and that the SpoIVFB CBS domain senses the ratio of ATP to ADP and/or AMP in the MC and regulates cleavage of Pro-σ^K appropriately. We plan to test the effects of adenine nucleotides on Pro-σ^K cleavage by SpoIVFB *in vitro.*

The available ATP concentration in the forespore does not decline despite σ^G activity

The FS ATP concentration did not change significantly from 2.5 to 6 h PS (Fig. 3.5). This result was surprising since the ATP concentration in dormant spores of *B. subtilis*, as well as *Bacillus megaterium* and *Bacillus cereus*, were reported to be very low [61], and forespores isolated from *B. megaterium* exhibited a sharp decline in extractable ATP between 3 and 5 h PS [62]. However, there are numerous differences between these earlier studies and our approach, as discussed above, so we did not attempt to separate the FS and MC compartments of *B. subtilis*, and measure the ATP pools by extraction methods.

Our results suggest that the available ATP concentration is maintained in the FS at least until 6 h PS (Fig. 3.5), when many sporangia have completed engulfment (Fig. 3.7) and σ^G activity in the FS has led to efficient Pro-σ^K cleavage in the MC (Fig. 3.8). We infer that σ^G activity does not rapidly deplete the available ATP in the FS after completion of engulfment. We propose that reserves in the FS generate a proton gradient across the inner FS membrane that drives ATP synthesis after engulfment completion and channel destruction. In support of this model, ionophore treatment at 6 h PS dramatically lowered the relative FS ATP concentration by about 84% after 15 min (Fig. 3.6). This result indicates both that FS ATP synthesis depends on a proton gradient and that FS ATP utilization is high at a time when many sporangia have completed engulfment (Fig. 3.7) and channel proteins have declined (Fig. 3.8). Presumably, expression of the σ^G regulon (including *spoIVB*, which relieves inhibition of SpoIVFB, as evidenced by cleavage of Pro-σ^K to σ^K, Fig. 3.8) accounts for some of the high utilization of ATP in the FS.

What reserves in the FS could generate a proton gradient? Biochemical analysis of *B. megaterium* forespores has provided some possible clues. Several metabolites (i.e. 3-phosphoglycerate, arginine, glutamate) accumulate in forespores by 3 h PS (the earliest they could be isolated) or shortly thereafter [62]. Enzymes for 3-phosphoglycerate utilization are

present [62], perhaps accounting for some ATP synthesis, but 3-phosphoglycerate continues to accumulate for later utilization during spore germination [61]. In forespores, the 3-phosphoglycerate is not expected to feed into the citric acid cycle since several enzymes are low or absent [62], so reduced substrates like NAD(P)H would not be generated. In contrast, catabolism of arginine and/or glutamate could produce NAD(P)H for respiratory chain activity to generate a proton gradient and ATP synthesis. This hypothesis is based on studies of *B. megaterium* forespores and will need to be tested by analyzing *B. subtilis* forespores.

Importantly, a crucial portion of whatever FS reserves drive ATP synthesis after engulfment completion must be acquired through the channels during engulfment, because channel function is required for σ^G to become fully active post-engulfment [11-13].

Impaired channel assembly may allow ATP to leak from the forespore through SpoIIQ

The loss of SpoIIIAA or SpoIIIAH lowered the FS ATP concentration at 3 h PS and thereafter, whereas the loss of SpoIIQ did not have this effect during engulfment (Fig 3.10B). We propose that in WT proper channel assembly during engulfment prevents ATP leakage from the FS. In the *spoIIIAH* mutant, the extracellular domains of SpoIIIAH and SpoIIQ would fail to interact in the intermembrane space [7, 8]. We propose that incomplete channel assembly allows ATP to leak from the FS through SpoIIQ. In WT the SpoIIQ end of the channel is open since *E. coli* BirA (37 kDa) made in the FS can access the C-terminal extracellular domains of SpoIIQ and SpoIIIAH [10]. Such a large opening across the inner FS membrane likely requires one or more proteins in addition to SpoIIQ, since the membrane-associated N-terminal domain of SpoIIQ is small (43-residues) and contains a single transmembrane segment (TMS) [58]. The SpoIIQ TMS may interact generically with one or more other proteins to create an opening across the inner FS membrane since the N-terminal 38-residue TMS-containing part of *E. coli* MalF can substitute for the N-terminal domain of SpoIIQ [11]. In the absence of SpoIIIAH, SpoIIQ localization is only slightly defective, because other proteins (SpoIID, SpoIIM, SpoIIP, BofA,

SpoIVFA, GerM) help localize SpoIIQ [7, 8, 16, 17, 41, 63]. Therefore, it is reasonable to propose that SpoIIQ and one or more partners assemble a pore through which ATP leaks from the FS of the *spoIIIAH* mutant due to incomplete channel assembly.

We propose a similar explanation for the lower FS ATP concentration in the *spoIIIAA* mutant as compared with WT (Fig 3.10B). However, the defect in channel assembly may be less severe in the *spoIIIAA* mutant than in the *spoIIIAH* mutant, resulting in less ATP leakage from the FS late during development (Fig 3.10B). In a *spoIIIAA* mutant, the initial localization of SpoIIIAH to the polar septum is delayed [7]. We propose that delayed assembly of SpoIIIA proteins in the MC membrane of the polar septum allows transient leakage of ATP through a pore in the FS membrane created by timely assembly of SpoIIQ and its putative partner(s) at 3 and 3.5 h PS (Fig 3.10B). Later during development, the extracellular domains of SpoIIQ and SpoIIIAH interact, preventing further ATP leakage from the FS. Notably, the progression of engulfment by 6 h PS was similar to WT for the *spoIIIAA* mutant, but less efficient for the *spoIIIAH* (Table 3.1). Also, the *spoIIIAH* mutation, but not the *spoIIIAA* mutation, caused partial mislocalization of SpoIVFB-GFP (Fig. 3.15B). Both these observations are consistent with a more severe defect in the *spoIIIAH* mutant than in the *spoIIIAA* mutant, in terms of assembly of the channels and associated proteins.

In the absence of SpoIIQ, we propose that no pore forms across the inner FS membrane, so ATP does not leak out of the FS. This would explain why the FS ATP concentration in the *spoIIQ* mutant did not differ significantly from that of WT during engulfment (Fig 3.10B). Why then does σ^G fail to become fully active in the *spoIIQ* mutant? The TMS of SpoIIQ regulates expression of the anti-σ^G factor CsfB [64] and several features of the *sigG* promoter, mRNA leader sequence, and start codon dampen expression [13], but these findings do not explain a more general requirement of SpoIIQ and SpoIIIA proteins for macromolecular synthesis in the FS [11]. Our data suggest that available ATP is not the limiting factor for FS gene expression in

the *spoIIQ* mutant (Fig 3.10B). Moreover, the available FS ATP concentration in the *spoIIIAA* mutant is similar to that of the *spoIIQ* mutant by 6 h PS (Fig 3.10B), when many *spoIIIAA* mutant sporangia have completed engulfment (Table 3.1) and σ^G is active in WT as evidenced by cleavage of Pro-σ^K to σ^K (Fig. 3.8). Yet σ^G fails to become fully active in the *spoIIIAA* mutant [12] and Pro-σ^K is not cleaved (Fig. 3.11). We propose that inactive channels in the *spoIIIAA* mutant and incomplete channels in the *spoIIQ* and *spoIIIAH* mutants fail to transport metabolites (e.g., amino acids and/or nucleotides other than ATP) from the MC to the FS during engulfment that become necessary for full σ^G-dependent gene expression post-engulfment. Interestingly, it was suggested that amino acids for protein synthesis in the FS would be obtained from the MC because key amino acid biosynthetic enzymes are low or absent in *B. megaterium* forespores [62] and/or mature spores [65]. Perhaps in WT the channels transport amino acids from the MC into the FS during engulfment, and the amino acids are both used directly in protein synthesis and catabolized to maintain the FS ATP concentration after the completion of engulfment as discussed above.

Conclusions and future directions

Our results demonstrate the utility of Luc H245F for measuring the relative ATP concentration over a broad range in the *B. subtilis* MC and FS during sporulation. They demonstrate a nearly twofold rise in the MC ATP concentration that correlates with channel destruction upon engulfment completion, but suggest that the concentration of other adenine nucleotides may also be sensed by the SpoIVFB CBS domain to regulate Pro-σ^K cleavage in response to the MC energy status. We discovered that the FS ATP concentration does not decline after engulfment completion and σ^G activation, but declines rapidly after ionophore treatment at that time, suggesting that a proton gradient across the inner FS membrane is driving ATP synthesis. Finally, our analysis of mutants lacking channel proteins suggests that ATP is not the limiting

factor for FS gene expression. Rather, we propose that transport of other nucleotides and/or amino acids from the MC through the channels to the FS during engulfment is necessary for full σ^G-dependent gene expression post-engulfment. How the channels impact nucleotide and amino acid pools in both compartments appears to be key to understanding σ^G and σ^K activity in the FS and MC, respectively.

Materials and methods

Bacterial strains, plasmids, primers, and media

Strains, plasmids, and primers used in this study are listed in Table 3.2 (appendix 3 A). Genes cloned after polymerase chain reaction (PCR) or subjected to site-directed mutagenesis were verified by DNA sequencing. *B. subtilis* strains were derived from the wild-type strain PY79 or the *bofB8 spoIIIG* mutant SC777. Plasmids for compartment-specific expression of Luc were transformed *via* natural competence using the Gröningen method [66] and selecting for chloramphenicol resistance (5 μg/mL). Gene replacements at *amyE* were identified by loss of amylase activity on 1% potato starch medium with Gram's iodine solution [49]. The resulting strains were then transformed (using the Gröningen method) with chromosomal DNA to introduce a mutation in *spoIIQ, spoIIIAA*, or *spoIIIAH* by selecting for genetically linked phleomycin resistance (0.5 μg/mL) and screening for a sporulation defect on DSM [67] 1.5% agar. Sporulation was induced by the Sterlini-Mandelstam method [68], initially in flasks with shaking (400 rpm) at 37°C, and in some experiments culture aliquots were transferred to 96-well plates as described below, and vigorous shaking at 37°C was continued.

Using Luc to measure the relative ATP concentration after treatment with ionophores

Sporulation was induced in flasks and at 3.5 h PS culture aliquots (200 μL) were transferred to a 96-well plate (black walls, clear bottom) with D-luciferin (4.5 mM), a concentration 300-fold higher than the K_m for luciferin of native Luc and 50-fold higher than that of Luc H245F [24]. In a

control experiment, luminescence was similar whether luciferin was present from the beginning or within a few minutes of adding it later, indicating this concentration of exogenous luciferin rapidly establishes an intracellular concentration that is not significantly depleted by Luc activity, as observed previously [26]. For each strain, aliquots were either treated with FCCP (100 μM) or left untreated as a control. After 15 min, luminescence was measured on a Filtermax F5 plate reader (Molecular Devices), then the samples were centrifuged at 14100 X *g* for 3 min, the supernatants were removed, and the pellets were stored at -80°C for subsequent immunoblot analysis with anti-Luc antibodies. Each Luc signal was quantified and normalized to a control sample (from BDP85 at 3.5 h PS) on the same blot. The luminescence was divided by the Luc level to yield a normalized value representing the relative ATP concentration, assuming that culture aeration provided a constant concentration of dissolved O_2.

In related experiments, culture aliquots in 96-well plates (for luminescence and immunoblot measurements) or subcultures in flasks (for immunoblots only; Fig. 3.15BD) were treated with FCCP, CCCP, or Chloramphenicol (Cm) alone or in combination at different times PS for 5, 15, and/or 30 min as indicated.

Using Luc H245F to measure the relative ATP concentration in the MC or the FS during sporulation

Sporulation was induced in flasks and at 2 h PS culture aliquots were transferred to a 96-well plate as described above. For each biological replicate, three aliquots were added to wells with luciferin for measurement of luminescence as described above. Luminescence was measured at intervals and averaged for the three wells. In parallel for each biological replicate, seven aliquots were added to wells lacking luciferin (as a cost-saving measure since luciferin is expensive) and, at intervals, a sample was collected for subsequent immunoblot analysis with anti-Luc antibodies as described above. A control experiment showed that luciferin did not affect the Luc H245F level. At each interval, the average luminescence was divided by the Luc

H245F level to yield a normalized value representing the relative ATP concentration for that biological replicate. The graphs show the average of relative ATP level ratios for three or four biological replicates and error bars represent one standard deviation.

Immunoblot analysis

Whole-cell extracts were prepared as described previously for *E. coli* [39], except 25 μL each of lysis buffer and 2× sample buffer were used for cell pellets from 200 μL samples collected from 96-well plates, and samples were incubated at 55°C for 5 min rather than boiling for 3 min. For experiments in flasks (Fig. 3.12A and 3.15BD, 3.13 and Fig. 3.17), equivalent amounts of cells based on the optical density at 600 nm of the culture were collected from 0.5-1.0 mL by centrifugation at 14100 × *g* for 3 min, the supernatants were removed, and the pellets were stored at -80°C. Whole-cell extracts were prepared as described above, except using 50 μL each of lysis buffer and 2× sample buffer. Proteins were separated by SDS-PAGE using 14% Prosieve-50 (Lonza) polyacrylamide gels and electroblotted to Immobilon-P membranes (Millipore). Blots were blocked with 5% nonfat dry milk in TBST (20 mM Tris-HCl [pH 7.5], 0.5 M NaCl, 0.1% Tween) for 1 h at 25°C with shaking. Blots were probed with anti-Luc-horse radish peroxidase (HRP) conjugate (1:10,000) (Rockland catalog #200-103-150-0100) or antibodies against SpoIVFA (1:3000) [55], SpoIVFB (1:5000) [45], Pro-σ^K (1:3000) [69], SpoIIQ (1:10,000) [54], SpoIIIAH (1:10,000) [70], or GFP (1:10,000) [55] diluted in TBST with 1% milk and incubated overnight at 4°C with shaking. Antibodies not conjugated to HRP were detected with a goat anti-rabbit-HRP antibody (Bio-Rad catalog #170-6515) at a 1:10,000 dilution in TBST with 1% milk for 1 h at 25°C with shaking. Signals were generated using the Western Lightning Plus ECL reagent (PerkinElmer) and signals were detected using a ChemiDoc MP imaging system (Bio-Rad), with exposure times short enough to ensure that signals were not saturated. Signal intensities were quantified using Image Lab 5.1 software (Bio-Rad) volume tools.

Fluorescence microscopy

Imaging of *B. subtilis* morphological changes during sporulation was performed on an Olympus FluoView FV-1000 filter-based confocal microscope. The lipophilic dye FM 4-64 (AAT Bioquest) was used to stain membranes. Sporulation was induced in flasks and at 2 h PS seven 250 μL culture aliquots were transferred to a 96-well plate with FM 4-64 (1 μg/mL), which does not affect sporulation. At intervals, an aliquot was collected and frozen in liquid nitrogen. FM 4-64 (ex/em ~515/640 nm) was excited using a 515 nM argon laser and fluorescence was captured using a BA560IF band pass filter. A differential interference contrast image was also captured in order to score cells based on presence of a phase-bright forespore, indicative of completed engulfment. For each sample, 150-250 cells were classified according to their morphological stage. For the channel mutants, only a sample at 6 h PS was examined, to determine the stage at which sporulation was blocked.

Acknowledgments

We thank Emily Frankman for constructing pEF1 and pEF2. We are grateful to David Rudner for providing antibodies against SpoIIQ and SpoIIIAH, several strains of *B. subtilis*, and pDR110. We also thank Kit Pogliano, Stephen Leppla, and Hiromi Imamura for sending plasmids. We thank Amy Camp for helpful discussions and Kristin Parent for use of her plate reader. Fluorescence microscopy was performed at the Michigan State University Center for Advanced Microscopy.

APPENDICES

APPENDIX A

Additional Results for Chapter 3

Efforts to build a FRET-based ATP sensor

Our initial effort to measure cellular ATP concentrations aimed to use a Fluorescence Resonance Energy Transfer (FRET) biosensor. In recent years, fluorescence-based biomolecule sensors have provided many useful tools for researchers. These sensors have often relied on FRET between pairs of florescent proteins linked to a "sensor" protein which brings the FRET pair together or apart in response to a particular biomolecule. One such sensor is the ATP sensor AT1.03 [72]. This sensor uses a blue (mseCFP) and yellow (cp173-mVenus) pair of fluorescent proteins fused to the ATP-binding domain of the epsilon subunit of *B. subtilis* ATP synthase. When ATP is bound, the FRET pair is brought close enough that FRET can occur. By using AT1.03 and a confocal microscope, we hoped to achieve measurements of cellular ATP levels at single-cell resolution. An additional benefit to using AT1.03 was that variants developed by Imamura *et al.* [72] work at different ranges of ATP concentrations, allowing the sensor to be tuned to specific applications. AT1.03 was successfully used to measure ATP levels in human cell lines [72, 73], however, no studies to our knowledge have successfully used AT1.03 in bacteria.

DNA constructs were built in which the gene for AT1.03 was fused to the mother cell-specific *spoIID* promoter or the forespore-specific *spoIIQ* promoter [71] in plasmids that allow gene replacement by homologous recombination at the chromosomal *amyE* locus of *B. subtilis* [49]. Additionally, the gene for AT1.03 was codon optimized (designated $AT1.03_{opt}$) for expression in *B. subtilis* (sequence available on request) and fused to the *spoIIQ* promoter or the IPTG-inducible *spank* promoter in plasmids that allow gene replacement at *amyE*, or fused to the IPTG-inducible *spac* promoter in an autonomously replicating multicopy plasmid (see Table 3.2 for plasmid construction details and resulting bacterial strains).

B. subtilis strains with a compartment-specific promoter fused to AT1.03 or $AT1.03_{opt}$ were starved to induce sporulation (see Materials and Methods). Strains with an IPTG-inducible promoter fused to $AT1.03_{opt}$ were grown in LB medium [74] at 37°C with shaking until an optical

density at 600 nm of 0.5-0.6 was reached, then IPTG (0.5 mM) was added and incubation continued for 2 h. For comparison, *B. subtilis* strains with a multicopy plasmid in which the gene for CFP_{opt} or YFP_{opt} (codon optimized for expression in *Bacillus anthracis*) was fused to the constitutive *B. anthracis pagA* promoter (Table 3.2), were grown in LB medium at 37°C with shaking until an optical density at 600 nm of 0.5-0.6 was reached. These strains express fluorescent proteins highly and fluoresce brightly. Samples for microscopy were collected and flash frozen in liquid nitrogen. These samples were later thawed and observed using an Olympus FluoView FV1000 confocal laser scanning microscope. Blue fluorescent proteins were excited using a 514 nm argon laser and emission was detected in the first channel using a 510 nm cut-off dichroic mirror, followed by a 480-495 nm band pass filter. Yellow fluorescent proteins were excited using a 458 nm argon laser and emission was detected in the second channel using a 535-565 nm band pass filter. Samples to compare expression of fluorescent proteins were prepared from equivalent amounts of cells based on the optical density at 600 nm of the culture [39] and immunoblot analysis was performed using anti-GFP antibodies (see Materials and Methods).

All of the strains designed to express AT1.03 or $AT1.03_{opt}$ showed little or no fluorescence above background. A representative cell from the strain with IPTG-inducible $AT1.03_{opt}$ on a multicopy plasmid demonstrates the low signal-to-noise ratio under conditions that allowed us to see fluorescence from cells (Fig. 3.18, top panels). Additionally, the presence of fluorescent foci and filamentous cells upon IPTG induction suggests that the sensor protein forms inclusion bodies and may be toxic. IPTG induction from a single chromosomal copy during growth or expression from a compartment-specific promoter during sporulation yielded similar low fluorescence and also displayed foci indicative of inclusion bodies (data not shown). In contrast, the strains expressing CFP_{opt} or YFP_{opt} constitutively exhibited relatively high fluorescence, as expected (Fig. 3.18, bottom panels). Immunoblot analysis using anti-GFP antibodies confirmed poor accumulation of $AT1.03_{opt}$ in the IPTG-inducible strains (Fig. 3.18). Similar accumulation

was observed during sporulation of strains with compartment-specific promoters fused to AT1.03 or AT1.03$_{opt}$ (data not shown). As expected, CFP$_{opt}$ and YFP$_{opt}$ accumulated abundantly in the strains that expressed these proteins constitutively (Fig. 3.18B). Taken together, these results show that AT1.03 and AT1.03$_{opt}$ are poorly expressed in *B. subtilis*.

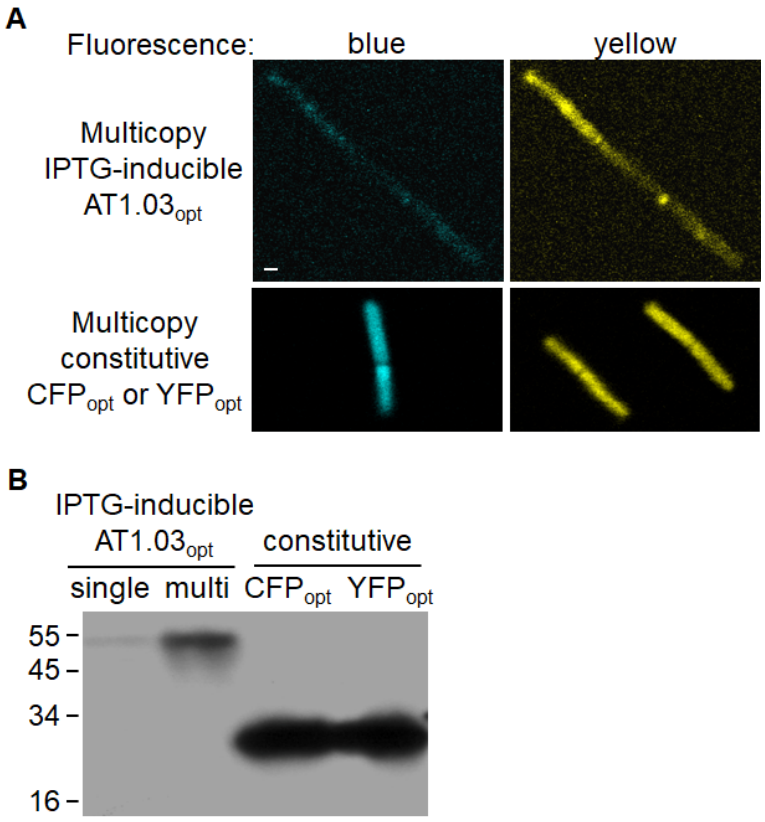

Figure 3.18 Analysis of *B. subtilis* designed to express a FRET-based ATP sensor. (A) Fluorescence microscopy. The top panels show a single filamentous cell after induction with IPTG for 2 h to express AT1.03$_{opt}$ from a multicopy plasmid. The bottom panels show dividing cells constitutively expressing CFP$_{opt}$ (left) or YFP$_{opt}$ (right) from a multicopy plasmid. The photomultiplier tube high voltage setting was adjusted to be more sensitive in order to visualize the cell shown in the top panels, which explains the higher background fluorescence than in the bottom panels. All panels are at the same scale and in the top, left panel the scale bar = 1 μm. **(B)** Immunoblot analysis. *B. subtilis* designed to express AT1.03$_{opt}$ from a single copy at the chromosomal *amyE* locus or from a multicopy plasmid were induced with IPTG for 2 h. For comparison, *B. subtilis* designed to express CFP$_{opt}$ or YFP$_{opt}$ constitutively from a multicopy plasmid were grown to the mid-log phase. Samples were subjected to immunoblot analysis using antibodies against GFP. The molecular weight (kDa) and migration of marker proteins is indicated.

APPENDIX B

Strains, Plasmids, and Primers for Chapter 3

Table 3.2 Bacterial strains, plasmids, and primers

Strain	Genotype	Construction	Citation
PY79	Prototrophic wild-type strain		[75]
BTD117	Δ*spoIIIAAΩpDT21 (phleo^r)*		[12]
BTD125	Δ*spoIIIAHΩpDT21 (phleo^r)*		[12]
BTD141	*spoIIQ::spec^r*		[12]
SC777	*spoIIIG::cm^r bofB8*		[76]
BDR347	*spoIVFBΩpdr68 [spoIVFB-gfp(mut2) (tet^r)]*		[38]
BDP1	*amyE::P$_{spoIIQ}$-AT1.03 (cm^r)*	PY79 was transformed with pEF1	This study
BDP2	*amyE::P$_{spoIID}$-AT1.03 (cm^r)*	PY79 was transformed with pEF2	This study
BDP34	*amyE::P$_{spoIIQ}$-AT1.03$_{opt}$ (cm^r)*	PY79 was transformed with pDP4	This study
BDP36	*amyE::P$_{spank}$-AT1.03 (spec^r)*	PY79 was transformed with pDP5	This study
BDP38		PY79 was transformed with pDP6	This study
BDP40		PY79 was transformed with pSW4-CFP$_{opt}$	This study
BDP41		PY79 was transformed with pSW4-YFP$_{opt}$	This study
BDP84	*amyE::P$_{spoIID}$-luc (cm^r)*	PY79 was transformed with pDP58	This study
BDP85	*amyE::P$_{spoIID}$-luc H245F (cm^r)*	PY79 was transformed with pDP77	This study
BDP86	*amyE::P$_{spoIIQ}$-luc (cm^r)*	PY79 was transformed with pDP59	This study
BDP87	*amyE::P$_{spoIIQ}$-luc H245F (cm^r)*	PY79 was transformed with pDP78	This study
BDP92	*amyE::P$_{spoIID}$-luc H245F (cm^r), ΔspoIIIAAΩpDT21 (phleo^r)*	BDP85 was transformed with BTD117 DNA	This study
BDP93	*amyE::P$_{spoIID}$-luc H245F (cm^r), ΔspoIIIAHΩpDT21 (phleo^r)*	BDP85 was transformed with BTD125 DNA	This study
BDP94	*amyE::P$_{spoIID}$-luc H245F (cm^r), spoIIQ::spec^r*	BDP85 was transformed with BTD141 DNA	This study
BDP99	*amyE::P$_{spoIIQ}$-luc H245F (cm^r), ΔspoIIIAHΩpDT21 (phleo^r)*	BDP87 was transformed with BTD125 DNA	This study
BDP100	*amyE::P$_{spoIIQ}$-luc H245F (cm^r), spoIIQ::spec^r*	BDP87 was transformed with BTD141 DNA	This study
BDP105	*amyE::P$_{spoIIQ}$-luc H245F (cm^r), ΔspoIIIAAΩpDT21 (phleo^r)*	BDP87 was transformed with BTD117 DNA	This study
BDP106	*spoIIIG::cm^r, bofB8, spoIIQ::spec^r*	SC777 was transformed with BTD141 DNA	This study
BDP107	*spoIIIG::cm^r, bofB8, ΔspoIIIAAΩpDT21 (phleo^r)*	SC777 was transformed with BTD117 DNA	This study

Table 3.2 (cont'd)

BDP108	*spoIIIG::cm^r, bofB8, ΔspoIIIAHΩpDT21 (phleo^r)*	SC777 was transformed with BTD125 DNA	This study
BDP109	*spoIIIG::cm^r, bofB8, spoIVFBΩpdr68 [spoIVFB-gfp(mut2) (tet^r)]*	SC777 was transformed with BDR347 DNA	This study
BDP110	*spoIIIG::cm^r, bofB8, spoIIQ::spec^r, spoIVFBΩpdr68 [spoIVFB-gfp(mut2) (tet^r)]*	BDP106 was transformed with BDR347 DNA	This study
BDP111	*spoIIIG::cm^r, bofB8, ΔspoIIIAAΩpDT21 (phleo^r), spoIVFBΩpdr68 [spoIVFB-gfp(mut2) (tet^r)]*	BDP107 was transformed with BDR347 DNA	This study
BDP112	*spoIIIG::cm^r, bofB8, ΔspoIIIAHΩpDT21 (phleo^r), spoIVFBΩpdr68 [spoIVFB-gfp(mut2) (tet^r)]*	BDP108 was transformed with BDR347 DNA	This study

Plasmid	Description	Construction	Citation
pGL2-control vector	contains the firefly luciferase gene *luc*		Promega
pMDS13	pDG1662 containing *amyE::P_{spoIIQ}-gfp* (cm^r)		[71]
pMDS14	pDG1662 containing *amyE::P_{spoIID}-gfp (cm^r)*		[71]
pcDNA-AT1.03	contains the FRET-based ATP sensor gene *AT1.03*		[57]
pSW4-CFP_{opt}	contains *P_{pagA}-ecfp$_{opt}$*		[77]
pSW4-YFP_{opt}	contains *P_{pagA}-eyfp$_{opt}$*		[77]
pDG148	vector for autonomous replication in *B. subtilis*		[53]
pDG364	vector for gene replacement at *amyE*		[78]
pDR110	vector for *P_{spank}* fusion and gene replacement at *amyE*		David Rudner
pEF1	pDG364 containing *amyE::P_{spoIIQ}-AT1.03 (cm^r)*	*P_{spoIIQ}* and the first 5 codons of *spoIIQ* were amplified by PCR using pMDS13 as template and primers EF01 and EF02. The fragment was digested with BglII and XhoI. AT1.03 was amplified by PCR using pcDNA-AT1.03 as template and primers DH03 and DH04. The fragment was digested with XhoI and HindIII. The fragments were included in a three-way ligation with BamHI-HindIII-digested pDG364.	This study

Table 3.2 (cont'd)

pEF2	pDG364 containing *amyE::P_{spoIID}-AT1.03 (cm^r)*	P_{spoIID} and the first 4 codons of *spoIID* were amplified by PCR using pMDS14 as template and primers DH02 and EF07. The fragment was digested with BglII and XhoI. AT1.03 was amplified by PCR using pcDNA-AT1.03 as template and primers DH03 and DH04. The fragment was digested with XhoI and HindIII. The fragments were included in a three-way ligation with BamHI-HindIII-digested pDG364.	This study
pDP3	pUCminusMCS containing the FRET-based ATP sensor gene $AT1.03_{opt}$	pDP3 was constructed by Blue Heron Biotech. $AT1.03_{opt}$ is codon optimized for expression in *B. subtilis* and is preceded by SalI, ribosome binding, and XhoI sites, and followed by HindIII and SphI sites.	This study
pDP4	pDG364 containing *amyE::P_{spoIIQ}-$AT1.03_{opt}$ (cm^r)*	P_{spoIIQ} and the first 5 codons of *spoIIQ* were amplified by PCR using pMDS13 and primers EF01 and EF02. The fragment was digested with BglII and XhoI. pDP3 was digested with XhoI and HindIII to produce a fragment with $AT1.03_{opt}$. The fragments were included in a three-way ligation with BamHI-HindIII-digested pDG364.	This study
pDP5	pDR110 containing *amyE::P_{spank}-$AT1.03_{opt}$ ($spec^r$)*	pDP3 was digested with SalI and SphI to produce a fragment with a ribosome binding site and $AT1.03_{opt}$. The fragment was ligated with SalI-SphI-digested pDR110.	This study
pDP6	pDG148 containing P_{spac}-$AT1.03_{opt}$ (kan^r)	pDP3 was digested with SalI and SphI to produce a fragment with a ribosome binding site and $AT1.03_{opt}$. The fragment was ligated with SalI-SphI-digested pDG148.	This study
pDP58	pDG364 containing *amyE::P_{spoIID}-luc (cm^r)*	P_{spoIID} and the first 4 codons of *spoIID* were amplified by PCR using pMDS14 as template and primers PDP141 and PDP175. The *luc* gene was amplified by PCR using pGL2 as template and primers PDP145 and PDP146. The fragments were used in a Gibson assembly reaction [10] with HindIII-digested pDG364.	This study
pDP59	pDG364 containing *amyE::P_{spoIIQ}-luc (cm^r)*	P_{spoIIQ} and the first 5 codons of *spoIIQ* were amplified by PCR using pMDS13 as template and primers	This study

Table 3.2 (cont'd)

		PDP139 and PDP174. The *luc* gene was amplified by PCR using pGL2 as template and primers PDP145 and PDP146. The fragments were used in a Gibson assembly reaction [10] with HindIII-digested pDG364.	
pDP77	pDG364 containing *amyE::P_{spoIID}-luc H245F (cm^r)*	pDP58 was subjected to site-directed mutagenesis using the QuikChange kit (Stratagene) and primers PDP160 and 161.	This study
pDP78	pDG364 containing *amyE::P_{spoIIQ}-luc H245F (cm^r)*	pDP59 was subjected to site-directed mutagenesis using the QuikChange kit (Stratagene) and primers PDP160 and 161.	This study

Primer	Sequence
DH02	CTGATCACTAGTGGATCCTGCGAATTGTTTCATATTCAGCTGC
DH03	GCGACTAGTATGGTGAGCAAGGGCGAGG
DH04	CTTAAGCTTACTCGATGTTGTG
EF01	GCCTCGAGTTTTCTTCCTCTCTCATTGTTTCATC
EF02	GCCTCGAGGCGAATTGTTTCATATTCAGCTGC
EF07	GTACAGCTTCAGGGAGCTGAAG
PDP139	GACCGGCGCTCAGGGATCCTAGAAGTTCGCTAGCGCCATAAGTGAGCGGATGCCAAG
PDP141	GACCGGCGCTCAGGGATCCTAGAAGTTCGCTAGCGTTGATTTAGCAAACTATATC
PDP145	ATGGAAGACGCCAAAAACATAAAG
PDP146	AGCTGTCAAACATGAGAATTCGATATTACAATTTGGACTTTCCGCC
PDP160	AGTGTTGTTCCATTCCATTTCGGTTTTGGAATGTTTACT
PDP161	AGTAAACATTCCAAAACCGAAATGGAATGGAACAACACT
PDP174	TCTTTATGTTTTTGGCGTCTTCTTCTTCCTCTCTCATTGTTTC
PDP175	TCTTTATGTTTTTGGCGTCTTCTGCGAATTGTTTCATATTC

REFERENCES

REFERENCES

1. Losick R, Stragier P. Crisscross regulation of cell-type-specific gene expression during development in *B. subtilis*. Nature. 1992;355:601-4.

2. Tan IS, Ramamurthi KS. Spore formation in *Bacillus subtilis*. Environ Microbiol Rep. 2014;6(3):212-25. doi: 10.1111/1758-2229.12130.

3. Higgins D, Dworkin J. Recent progress in *Bacillus subtilis* sporulation. FEMS Microbiol Rev. 2012;36(1):131-48. doi: 10.1111/j.1574-6976.2011.00310.x.

4. Kroos L. The *Bacillus* and *Myxococcus* developmental networks and their transcriptional regulators. Annu Rev Genet. 2007;41:13-39.

5. Bradshaw N, Losick R. Asymmetric division triggers cell-specific gene expression through coupled capture and stabilization of a phosphatase. eLife. 2015;4:e08145. doi: 10.7554/eLife.08145.

6. Konovalova A, Sogaard-Andersen L, Kroos L. Regulated proteolysis in bacterial development. FEMS Microbiol Rev. 2014;38:493-522.

7. Blaylock B, Jiang X, Rubio A, Moran CP, Jr., Pogliano K. Zipper-like interaction between proteins in adjacent daughter cells mediates protein localization. Genes Dev. 2004;18(23):2916-28.

8. Doan T, Marquis KA, Rudner DZ. Subcellular localization of a sporulation membrane protein is achieved through a network of interactions along and across the septum. Mol Microbiol. 2005;55(6):1767-81.

9. Camp AH, Losick R. A novel pathway of intercellular signalling in *Bacillus subtilis* involves a protein with similarity to a component of type III secretion channels. Mol Microbiol. 2008;69:402-17.

10. Meisner J, Wang X, Serrano M, Henriques AO, Moran CP, Jr. A channel connecting the mother cell and forespore during bacterial endospore formation. Proc Natl Acad Sci USA. 2008;105(39):15100-5.

11. Camp AH, Losick R. A feeding tube model for activation of a cell-specific transcription factor during sporulation in *Bacillus subtilis*. Genes Dev. 2009;23(8):1014-24.

12. Doan T, Morlot C, Meisner J, Serrano M, Henriques AO, Moran CP, Rudner D. Novel secretion apparatus maintains spore integrity and developmental gene expression in *Bacillus subtilis*. PLoS Genet. 2009;5(7):e1000566. doi: 10.1371/journal.pgen.1000566.

13. Mearls EB, Jackter J, Colquhoun JM, Farmer V, Matthews AJ, Murphy LS, et al. Transcription and translation of the *sigG* gene is tuned for proper execution of the switch from early to late gene expression in the developing *Bacillus subtilis* spore. PLoS Genet. 2018;14(4):e1007350. doi: 10.1371/journal.pgen.1007350.

14. Kroos L, Akiyama Y. Biochemical and structural insights into intramembrane metalloprotease mechanisms. Biochim Biophys Acta - Biomembr. 2013;1828(12):2873-85.

15. Zeytuni N, Flanagan KA, Worrall LJ, Massoni SC, Camp AH, Strynadka NCJ. Structural characterization of SpoIIIAB sporulation-essential protein in *Bacillus subtilis*. J Struct Biol. 2018;202(2):105-12. doi: 10.1016/j.jsb.2017.12.009.

16. Rodrigues CD, Marquis KA, Meisner J, Rudner DZ. Peptidoglycan hydrolysis is required for assembly and activity of the transenvelope secretion complex during sporulation in *Bacillus subtilis*. Mol Microbiol. 2013;89(6):1039-52. doi: 10.1111/mmi.12322.

17. Rodrigues CD, Ramirez-Guadiana FH, Meeske AJ, Wang X, Rudner DZ. GerM is required to assemble the basal platform of the SpoIIIA-SpoIIQ transenvelope complex during sporulation in *Bacillus subtilis*. Mol Microbiol. 2016;102(2):260-73. doi: 10.1111/mmi.13457.

18. Rodrigues CD, Henry X, Neumann E, Kurauskas V, Bellard L, Fichou Y, et al. A ring-shaped conduit connects the mother cell and forespore during sporulation in *Bacillus subtilis*. Proc Natl Acad Sci USA. 2016;113(41):11585-90. doi: 10.1073/pnas.1609604113.

19. Zeytuni N, Hong C, Flanagan KA, Worrall LJ, Theiltges KA, Vuckovic M, et al. Near-atomic resolution cryoelectron microscopy structure of the 30-fold homooligomeric SpoIIIAG channel essential to spore formation in *Bacillus subtilis*. Proc Natl Acad Sci USA. 2017;114(34):E7073-E81. doi: 10.1073/pnas.1704310114.

20. Levdikov VM, Blagova EV, McFeat A, Fogg MJ, Wilson KS, Wilkinson AJ. Structure of components of an intercellular channel complex in sporulating *Bacillus subtilis*. Proc Natl Acad Sci USA. 2012;109(14):5441-5. doi: 10.1073/pnas.1120087109.

21. Trouve J, Mohamed A, Leisico F, Contreras-Martel C, Liu B, Mas C, et al. Structural characterization of the sporulation protein GerM from *Bacillus subtilis*. J Struct Biol. 2018;204(3):481-90. doi: 10.1016/j.jsb.2018.09.010.

22. Meisner J, Maehigashi T, Andre I, Dunham CM, Moran CP, Jr. Structure of the basal components of a bacterial transporter. Proc Natl Acad Sci USA. 2012;109(14):5446-51. doi: 10.1073/pnas.1120113109.

23. Chiba S, Coleman K, Pogliano K. Impact of membrane fusion and proteolysis on SpoIIQ dynamics and interaction with SpoIIIAH. J Biol Chem. 2007;282(4):2576-86.

24. Branchini BR, Magyar RA, Murtiashaw MH, Anderson SM, Helgerson LC, Zimmer M. Site-directed mutagenesis of firefly luciferase active site amino acids: a proposed model for bioluminescence color. Biochemistry. 1999;38(40):13223-30.

25. Schneider DA, Gourse RL. Relationship between growth rate and ATP concentration in *Escherichia coli*: a bioassay for available cellular ATP. J Biol Chem. 2004;279(9):8262-8. doi: 10.1074/jbc.M311996200.

26. Mirouze N, Prepiak P, Dubnau D. Fluctuations in *spo0A* transcription control rare developmental transitions in *Bacillus subtilis*. PLoS Genet. 2011;7(4):e1002048. doi: 10.1371/journal.pgen.1002048.

27. Rudner D, Fawcett P, Losick R. A family of membrane-embedded metalloproteases involved in regulated proteolysis of membrane-associated transcription factors. Proc Natl Acad Sci USA. 1999;96:14765-70.

28. Yu Y-TN, Kroos L. Evidence that SpoIVFB is a novel type of membrane metalloprotease governing intercompartmental communication during *Bacillus subtilis* sporulation. J Bacteriol. 2000;182:3305-9.

29. Zhou R, Cusumano C, Sui D, Garavito RM, Kroos L. Intramembrane proteolytic cleavage of a membrane-tethered transcription factor by a metalloprotease depends on ATP. Proc Natl Acad Sci USA. 2009;106:16174-9.

30. Cutting S, Driks A, Schmidt R, Kunkel B, Losick R. Forespore-specific transcription of a gene in the signal transduction pathway that governs pro-σ^K processing in *Bacillus subtilis*. Genes Dev. 1991;5:456-66.

31. Wakeley PR, Dorazi R, Hoa NT, Bowyer JR, Cutting SM. Proteolysis of SpoIVB is a critical determinant in signalling of Pro-σ^K processing in *Bacillus subtilis*. Mol Microbiol. 2000;36(6):1336-48.

32. Zhou R, Kroos L. Serine proteases from two cell types target different components of a complex that governs regulated intramembrane proteolysis of pro-σ^K during *Bacillus subtilis* development. Mol Microbiol. 2005;58(3):835-46.

33. Campo N, Rudner DZ. A branched pathway governing the activation of a developmental transcription factor by regulated intramembrane proteolysis. Mol Cell. 2006;23(1):25-35.

34. Campo N, Rudner DZ. SpoIVB and CtpB are both forespore signals in the activation of the sporulation transcription factor sigmaK in *Bacillus subtilis*. J Bacteriol. 2007;189(16):6021-7.

35. Cutting S, Oke V, Driks A, Losick R, Lu S, Kroos L. A forespore checkpoint for mother-cell gene expression during development in *Bacillus subtilis*. Cell. 1990;62:239-50.

36. Cutting S, Roels S, Losick R. Sporulation operon *spoIVF* and the characterization of mutations that uncouple mother-cell from forespore gene expression in *Bacillus subtilis*. J Mol Biol. 1991;221:1237-56.

37. Ricca E, Cutting S, Losick R. Characterization of *bofA*, a gene involved in intercompartmental regulation of pro-σ^K processing during sporulation in *Bacillus subtilis*. J Bacteriol. 1992;174:3177-84.

38. Rudner DZ, Losick R. A sporulation membrane protein tethers the pro-σ^K processing enzyme to its inhibitor and dictates its subcellular localization. Genes Dev. 2002;16(8):1007-18.

39. Zhou R, Kroos L. BofA protein inhibits intramembrane proteolysis of pro-s^K in an intercompartmental signaling pathway during *Bacillus subtilis* sporulation. Proc Natl Acad Sci USA. 2004;101(17):6385-90.

40. Ramirez-Guadiana FH, Rodrigues CDA, Marquis KA, Campo N, Barajas-Ornelas RDC, Brock K, et al. Evidence that regulation of intramembrane proteolysis is mediated by substrate gating during sporulation in *Bacillus subtilis*. PLoS Genet. 2018;14(11):e1007753. doi: 10.1371/journal.pgen.1007753.

41. Jiang X, Rubio A, Chiba S, Pogliano K. Engulfment-regulated proteolysis of SpoIIQ: evidence that dual checkpoints control sigma activity. Mol Microbiol. 2005;58(1):102-15.

42. Green D, Cutting S. Membrane topology of the *Bacillus subtilis* Pro-σ^K processing complex. J Bacteriol. 2000;182:278-85.

43. Baykov AA, Tuominen HK, Lahti R. The CBS domain: a protein module with an emerging prominent role in regulation. ACS Chem Biol. 2011;6(11):1156-63. doi: 10.1021/cb200231c.

44. Scott JW, Hawley SA, Green KA, Anis M, Stewart G, Scullion GA, et al. CBS domains form energy-sensing modules whose binding of adenosine ligands is disrupted by disease mutations. J Clin Invest. 2004;113(2):274-84.

45. Halder S, Parrell D, Whitten D, Feig M, Kroos L. Interaction of intramembrane metalloprotease SpoIVFB with substrate Pro-σ^K. Proc Natl Acad Sci USA. 2017;114:E10677-E86.

46. Zhang Y, Halder S, Kerr R, Parrell D, Ruotolo B, Kroos L. Complex formed between intramembrane metalloprotease SpoIVFB and its substrate, Pro-σ^K. J Biol Chem. 2016;291:10347-62.

47. Zhang Y, Luethy PM, Zhou R, Kroos L. Residues in conserved loops of intramembrane metalloprotease SpoIVFB interact with residues near the cleavage site in Pro-σ^K. J Bacteriol. 2013;195(21):4936-46. doi: JB.00807-13.

48. Sharp MD, Pogliano K. Role of cell-specific SpoIIIE assembly in polarity of DNA transfer. Science. 2002;295(5552):137-9. doi: 10.1126/science.1066274.

49. Shimotsu H, Henner DJ. Construction of a single-copy integration vector and its use in analysis of regulation of the *trp* operon of *Bacillus subtilis*. Gene. 1986;43:85-94.

50. Londono-Vallejo JA. Mutational analysis of the early forespore/mother-cell signalling pathway in *Bacillus subtilis.* Microbiol. 1997;143:2753-61.

51. Eichenberger P, Fujita M, Jensen ST, Conlon EM, Rudner DZ, Wang ST, et al. The program of gene transcription for a single differentiating cell type during sporulation in *Bacillus subtilis*. PLoS Biol. 2004;2(10):e328.

52. Clarke S, Lopez-Diaz I, Mandelstam J. Use of *lacZ* fusions to determine the dependence pattern of the sporulation gene *spoIID* in *spo* mutants of *Bacillus subtilis*. J Gen Microbiol. 1986;132:2987-94.

53. Karmazyn-Campelli C, Bonamy C, Savelli B, Stragier P. Tandem genes encoding σ-factors for consecutive steps of development in *Bacillus subtilis*. Genes & Dev. 1989;3:150-7.

54. Doan T, Rudner DZ. Perturbations to engulfment trigger a degradative response that prevents cell-cell signalling during sporulation in *Bacillus subtilis*. Mol Microbiol. 2007;64(2):500-11. doi: 10.1111/j.1365-2958.2007.05677.x.

55. Kroos L, Yu YT, Mills D, Ferguson-Miller S. Forespore signaling is necessary for pro-σ^K processing during *Bacillus subtilis* sporulation despite the loss of SpoIVFA upon translational arrest. J Bacteriol. 2002;184(19):5393-401.

56. Zhang Y, Pohlmann EL, Roberts GP. Effect of perturbation of ATP level on the activity and regulation of nitrogenase in *Rhodospirillum rubrum*. J Bacteriol. 2009;191(17):5526-37. doi: 10.1128/JB.00585-09.

57. Imamura H, Nhat KP, Togawa H, Saito K, Iino R, Kato-Yamada Y, et al. Visualization of ATP levels inside single living cells with fluorescence resonance energy transfer-based genetically encoded indicators. Proc Natl Acad Sci USA. 2009;106(37):15651-6. doi: 10.1073/pnas.0904764106.

58. Londono-Vallejo JA, Frehel C, Stragier P. SpoIIQ, a forespore-expressed gene required for engulfment in *Bacillus subtilis*. Mol Microbiol. 1997;24(1):29-39.

59. Sun YL, Sharp MD, Pogliano K. A dispensable role for forespore-specific gene expression in engulfment of the forespore during sporulation of *Bacillus subtilis*. J Bacteriol. 2000;182(10):2919-27.

60. Lu S, Kroos L. Overproducing the *Bacillus subtilis* mother-cell sigma factor precursor, pro-σ^K, uncouples σ^K-dependent gene expression from dependence on intercompartmental communication. J Bacteriol. 1994;176(13):3936-43.

61. Setlow P, Kornberg A. Biochemical studies of bacterial sporulation and germination. XXII. Energy metabolism in early stages of germination of *Bacillus megaterium* spores. J Biol Chem. 1970;245(14):3637-44.

62. Singh RP, Setlow B, Setlow P. Levels of small molecules and enzymes in the mother cell compartment and the forespore of sporulating Bacillus megaterium. J Bacteriol. 1977;130:1130-8.

63. Fredlund J, Broder D, Fleming T, Claussin C, Pogliano K. The SpoIIQ landmark protein has different requirements for septal localization and immobilization. Mol Microbiol. 2013;89(6):1053-68. doi: 10.1111/mmi.12333.

64. Flanagan KA, Comber JD, Mearls E, Fenton C, Wang Erickson AF, Camp AH. A membrane-embedded amino acid couples the SpoIIQ channel protein to anti-sigma factor transcriptional repression during *Bacillus subtilis* sporulation. J Bacteriol. 2016;198(9):1451-63. doi: 10.1128/JB.00958-15.

65. Setlow P, Primus G. Protein metabolism during germination of *Bacillus megaterium* spores. I. Protein synthesis and amino acid metabolism. J Biol Chem. 1975;250(2):623-30.

66. Bron S. Plasmids. In: Harwood CR, Cutting SM, editors. Molecular Biological Methods for *Bacillus*. New York: John Wiley & Sons; 1990. p. 75-174.

67. Harwood CR, Cutting SM. Molecular Biological Methods for *Bacillus*. Chichester, England: John Wiley & Sons; 1990. 581 p.

68. Sterlini JM, Mandelstam J. Commitment to sporulation in *Bacillus subtilis* and its relationship to development of actinomycin resistance. Biochem J. 1969;113:29-37.

69. Lu S, Halberg R, Kroos L. Processing of the mother-cell s factor, σ^K, may depend on events occurring in the forespore during *Bacillus subtilis* development. Proc Natl Acad Sci USA. 1990;87:9722-6.

70. Campo N, Marquis KA, Rudner DZ. SpoIIQ anchors membrane proteins on both sides of the sporulation septum in *Bacillus subtilis*. J Biol Chem. 2008;283(8):4975-82. doi: 10.1074/jbc.M708024200.

71. Sharp MD, Pogliano K. Role of cell-specific SpoIIIE assembly in polarity of DNA transfer. Science. 2002;295(5552):137-9. doi: 10.1126/science.1066274.

72. Imamura H, Nhat KP, Togawa H, Saito K, Iino R, Kato-Yamada Y, et al. Visualization of ATP levels inside single living cells with fluorescence resonance energy transfer-based genetically encoded indicators. Proc Natl Acad Sci USA. 2009;106(37):15651-6. doi: 10.1073/pnas.0904764106.

73. Ando T, Imamura H, Suzuki R, Aizaki H, Watanabe T, Wakita T, et al. Visualization and measurement of ATP levels in living cells replicating hepatitis C virus genome RNA. PLoS Pathog. 2012;8(3):e1002561. doi: 10.1371/journal.ppat.1002561.

74. Sambrook J, Fritsch EF, Maniatis T. Molecular cloning: a laboratory manual, 2nd ed. Cold Spring Habor, NY: Cold Spring Harbor Laboratory Press; 1989.

75. Youngman P, Perkins JB, Losick R. Construction of a cloning site near one end of Tn*917* into which foreign DNA may be inserted without affecting transposition in *Bacillus subtilis* or expression of the transposon-borne *erm* gene. Plasmid. 1984;12:1-9.

76. Cutting S, Oke V, Driks A, Losick R, Lu S, Kroos L. A forespore checkpoint for mother-cell gene expression during development in *Bacillus subtilis*. Cell. 1990;62:239-50.

77. Sastalla I, Chim K, Cheung GY, Pomerantsev AP, Leppla SH. Codon-optimized fluorescent proteins designed for expression in low-GC gram-positive bacteria. Appl Environ Microbiol. 2009;75(7):2099-110. doi: 10.1128/AEM.02066-08.

78. Gibson DG, Young L, Chuang RY, Venter JC, Hutchison CA, 3rd, Smith HO. Enzymatic assembly of DNA molecules up to several hundred kilobases. Nat Methods. 2009;6(5):343-5. doi: 10.1038/nmeth.1318.

CHAPTER 4: ATP-induced conformational change in the SpoIVFB·Pro-σ^K complex and the role of the CBS domain in SpoIVFB activity and stability

Abstract:

Bacillus subtilis endospore formation provides an excellent model system to study signaling and gene regulatory mechanisms. During sporulation, asymmetric cell division and an engulfment process produce a mother cell and a forespore. After the forespore becomes engulfed, a signaling pathway from the forespore relieves inhibition of the intramembrane metalloprotease SpoIVFB, which is mediated by two other proteins that form a complex with SpoIVFB in the outer forespore membrane. Active SpoIVFB cleaves membrane-associated Pro-σ^K, releasing it into the mother cell to direct cell-type-specific transcription. Intramembrane metalloproteases like SpoIVFB are broadly conserved and control many important signaling pathways, however a better understanding of their regulatory mechanisms is needed. SpoIVFB has a CBS domain that binds ATP and is required for SpoIVFB to cleave Pro-σ^K *in vitro*. We present an ATP-dependent crosslinking assay that utilizes proximity of SpoIVFB and Pro-σ^K residues near the active site, and different length chemical crosslinkers, to detect an apparent conformational change of the complex upon ATP binding, and inhibition of the change by AMP. CBS domains commonly regulate activity of proteins *via* conformational changes. A model for an ATP-induced conformational change in SpoIVFB that positions Pro-σ^K for cleavage will be discussed. A number of amino acid substitutions for CBS domain residues were made. Several of these changes have an effect on Pro-σ^K cleavage upon heterologous expression in *Escherichia coli*. Surprisingly, many of these changes destabilize SpoIVFB when expressed in sporulating *B. subtilis*. A suppressor screen led to isolation of strains that reverse the destabilizing effects of CBS domain substitutions. Suppressor isolates had novel SpoIVFB substitutions. Possible mechanistic roles for substituted residues of the CBS domain and the interdomain linker of

SpoIVFB are discussed. By studying regulated intramembrane proteolysis in *B. subtilis*, we hope to elucidate fundamental principles of how these broadly conserved proteins function in signaling pathways that govern sporulation and many other important processes.

Introduction

During endospore formation *Bacillus subtilis* forms two cell types, a small cell called the forespore (FS) and larger cell called the mother cell (MC). These cells achieve differential gene expression throughout the sporulation process [1]. In response to starvation *B. subtilis* cells undergo an asymmetric cell division resulting in the cellular compartments destined to become the MC and FS. These processes are driven by SpoIIE, FtsZ and DivIB expressed by the sporulation master regulator Spo0A-P, as well as σ^A and σ^H [2,3]. After asymmetric cell division occurs, gene expression is controlled by σ^F in the FS after its release from SpoIIAB [4]. σ^F produces a signal that activates σ^E in the MC by proteolysis of Pro-σ^E [5]. The σ^F and σ^E regulons set up a number of events including an engulfmen-like process where the MC membrane surrounds the FS, resulting in a FS engulfed within the MC, surrounded by inner and outer FS membranes. Following engulfment differential gene expression continues as another FS sigma factor (σ^G) is expressed as part of the σ^F regulon, but σ^G remains inactive until the completion of engulfment by processes that are beginning to be better understood [6]. σ^G expression leads to signaling across the inner FS membrane to the intermembrane space and activate SpoIVFB. SpoIVBF, an intramembrane metalloprotease (IMMP) in the outer FS membrane, processes membrane-associated Pro-σ^K and releases active σ^K to drive the final stages of sporulation in the MC resulting in mature spores [7–9].

Activation of σ^K by intramembrane proteolysis led to the discovery of SpoIVFB, an important member of a novel family of IMMPs [8,9]. The IMMPs are one of four major classes of intramembrane proteases that drive important processes in nearly all organisms [10]. The typical signal transduction pathway for IMMPs involves pre-processing of the IMMP substrate, usually an anti-sigma factor, by a site-1 protease in the periplasm or extracellular space, followed by site-2 cleavage by an IMMP and release of the substrate into the cytoplasm [11]. Once in the cytoplasm further processing of anti-sigma factors by the Clp protease typically is

required to relieve inhibition of the sigma factor. SpoIVFB deviates from this process significantly. SpoIVFB directly cleaves Pro-σ^K without site-1 cleavage [12]. However, SpoIVFB is inhibited by BofA and SpoIVFA [13–17]. Signals from the FS relieve inhibition of SpoIVFB by proteolysis of SpoIVFA and BofA. The serine proteases SpoIVB and CtpB are secreted into the intermembrane space where they cleave regions of SpoIVFA and BofA, relieving inhibition of SpoIVFB [18–21].

In addition to regulation by SpoIVFA and BofA, SpoIVFB has an additional regulatory element, an ATP-binding CBS domain. SpoIVFB requires zinc and ATP for *in vitro* processing of Pro-σ^K [12]. Additionally, the purified CBS domain appears to bind ATP [12]. What might be the role of ATP in controlling SpoIVFB activity? Binding of ATP to CBS domains typically causes a conformational change in proteins [22,23]. Therefore, it has been proposed that binding of ATP to CBS domains of tetrameric SpoIVFB causes a conformational change that positions Pro-σ^K for cleavage [12]. In support of this model, Pro-σ^K appears to interact extensively with the SpoIVFB interdomain linker and CBS domain, so ATP-induced movement of the CBS domains may be transmitted through the linker so as to shift the position of Pro-σ^K in the SpoIVFB active site [24]. Recent evidence suggests that SpoIVFB also undergoes conformational change when SpoIVB cleaves SpoIVFA, shifting from a closed conformation to a more open one that allows Pro-σ^K binding [12,25]. Perhaps ATP binding modulates these conformational changes.

Our results using a luciferase-based ATP sensor system suggest that lowering ATP concentration via ionophores or chloramphenicol differentially impacts Pro-σ^K processing (Chapter 3). Perhaps the ratio of ATP to other adenine nucleotides is altered differently under the two conditions, creating cells with different energy status. CBS domains often bind adenine nucleotides other than ATP in order to measure energy status in a cell [22]. Exploring whether other adenine nucleotides bind the CBS domain would address a critical knowledge gap surrounding SpoIVFB regulation.

Additionally, limited knowledge exists about what residues in the CBS domain are critical for SpoIVFB function. Comparing the SpoIVFB CBS domain to canonical CBS domain motifs [23] and using sequence analysis of SpoIVFB orthologs could guide substitutional analysis of the CBS domain in SpoIVFB. Here, we report a novel assay for testing conformational changes in SpoIVFB. We use the assay to show that AMP interferes with an ATP-induced conformational change in a SpoIVFB·Pro-σ^K complex. Critical residues comprising putative ATP/AMP binding motifs are proposed and single amino acid substitutions are used to test the requirement of these residues for SpoIVFB activity. Finally, isolates that suppress destabilizing CBS domain substitutions were recovered and DNA sequencing revealed additional residues that affect the stability of SpoIVFB. Our results significantly advance the knowledge of SpoIVFB regulation and pose several interesting questions related to future work. More broadly, our findings provide new insights that contribute to a better understanding of IMMP function and protein regulation by ligand binding and CBS domain-mediated conformational change.

Materials and Methods

Bacterial strains, plasmids, primers, and media

A list of strains and plasmids used in this study, and descriptions of their construction, as well as a list of primers, is provided in Table 4.1. Plasmids constructed using PCR or site-directed mutagenesis were confirmed by DNA sequencing. *B. subtilis* strains were generated from the wild-type strain PY79 or a *spoIVFAB* mutant, BSL51. Plasmids for ectopic integration at *amyE* were transformed into *B. subtilis* using the Gröningen method [26] and resistance to spectinomycin (100 μg/mL) was selected. Gene replacement at *amyE* was screened for by loss of amylase activity on 1% potato starch medium with Gram's iodine solution [27]. Sporulation was induced by the Sterlini-Mandelstam "resuspension" method [28] unless indicated that nutrient exhaustion in DSM liquid medium was used [26]. Unless otherwise noted, *Escherichia*

Table 4.1: Bacterial strains, plasmids, and primers

Plasmid:	Description:	Construction:	Reference:
pZR27	KmR; Pro-σ^K (1-126)-His6		[17]
pZR209	Ap^R; TM-SpoIVFB-FLAG2-His6		[12]
pDR18a	Sp^R; amyE::spoIVF		[9]
pSGMU2	Cm^R; Plasmid Integration vector		[44]
pYZ2	Km^R; T7-Pro-σ^K(1-126)-His_6/T7-CytTM-SpoIVFB-$Flag_2$-His_6	pZR209 was digested with BglII and ZhoI to produce a CytTM-SpoIVFB-Flag2-His_6 fragment. The fragment was ligated with BglII-XhoI-digested pZR27.	This Study
pYZ107	Ap^R; cytTM-SpoIVFB-FLAG2-HIS6 C35S E44Q C165L C167L C172S C246S		[33]
pFB6	Km^R; Pro-σ^K(1-126)-His6 / CytTM	A fragment containing CytTM was amplified by PCR from pYZ2 using primers PFB13 and PFB14 (These primers destroy a BamHI cut site). A fragment containing Pro-σ^K(1-126)-HIS6 and the plasmid backbone was amplified by PCR from pYZ2 using primers PFB11 and PFB12. These fragments were joined with Gibson Assembly.	This Study
pDP9	Ap^R; TM-SpoIVFB-FLAG2-HIS6 F242A	pZR209 was subjected to site-directed mutagenesis using primers PDP37 and PDP38	This study
pDP10	Ap^R; TM-SpoIVFB-FLAG2-HIS6 H248A	pZR209 was subjected to site-directed mutagenesis using primers PDP47 and PDP48	This study
pDP11	Ap^R; TM-SpoIVFB-FLAG2-HIS6 D263A	pZR209 was subjected to site-directed mutagenesis using primers PDP49 and PDP50	This study
pDP12	Ap^R; TM-SpoIVFB-FLAG2-HIS6 E264A	pZR209 was subjected to site-directed mutagenesis using primers PDP51 and PDP52	This study
pDP13	Ap^R; TM-SpoIVFB-FLAG2-HIS6 N265A	pZR209 was subjected to site-directed mutagenesis using primers PDP53 and PDP54	This study
pDP14	Ap^R; TM-SpoIVFB-FLAG2-HIS6 E266A	pZR209 was subjected to site-directed mutagenesis using primers PDP39 and PDP40	This study
pDP15	Ap^R; TM-SpoIVFB-FLAG2-HIS6 K275A	pZR209 was subjected to site-directed mutagenesis using primers PDP41 and PDP42	This study
pDP16	Ap^R; TM-SpoIVFB-FLAG2-HIS6 R276A	pZR209 was subjected to site-directed mutagenesis using primers PDP43 and PDP44	This study
pDP17	Ap^R; TM-SpoIVFB-FLAG2-HIS6 E283A	pZR209 was subjected to site-directed mutagenesis using primers PDP45 and PDP46	This study

Table 4.1 (cont'd)

pDP20	pSGUM2 containing 5'-truncated *spoIVFB*(205-864) with 2xFLAG-His_6	A fragment from bp 205-864 of *spoIVFB* including a 2xFLAG-His_6 epitope tag was amplified by PCR from pZR209 using PDP60 and PDP61. The fragment was digested with SalI and BamHI and ligated with SalI-BamHI-digested pSGMU2.	This study
pDP25	Ap^R; TM-SpoIVFB-FLAG2-HIS6 S260G	pZR209 was subjected to site-directed mutagenesis using primers PDP70 and PDP71	This study
pDP26	Ap^R; TM-SpoIVFB-FLAG2-HIS6 S260A	pZR209 was subjected to site-directed mutagenesis using primers PDP68 and PDP69	This study
pDP27	Ap^R; TM-SpoIVFB-FLAG2-HIS6 E264D	pZR209 was subjected to site-directed mutagenesis using primers PDP72 and PDP73	This study
pDP30	pSGMU2 containing 5'- and 3'-truncated *spoIVFB*(205-666)	A *spoIVFB* fragment from 205bp to 666bp was amplified by PCR using primers PDP90 and PDP92. The fragment was HindIII digested and ligated with HindIII-digested pDP20. Sequencing with PDP14 confirmed correct orientation of the insert. PDP92 creates a stop codon before FLAG.	This study
pDP31	pSGMU2 containing 5'- and 3'-truncated *spoIVFB*(205-666) with 2xFLAG-His_6	A *spoIVFB* fragment from 205bp to 666bp was amplified by PCR using primers PDP90 and PDP91. The fragment was HindIII digested and ligated with HindIII-digested pDP20. Sequencing with PDP14 confirmed correct orientation of the insert.	This study
pDP32	Ap^R; TM-SpoIVFB-FLAG2-HIS6 E264Q	pZR209 was subjected to site-directed mutagenesis using primers PDP76 and PDP77	This study
pDP33	Ap^R; TM-SpoIVFB-FLAG2-HIS6 E264L	pZR209 was subjected to site-directed mutagenesis using primers PDP74 and PDP75	This study
pDP34	Ap^R; TM-SpoIVFB-FLAG2-HIS6 F272A	pZR209 was subjected to site-directed mutagenesis using primers PDP93 and PDP94	This study
pDP35	Ap^R; TM-SpoIVFB-STOP-FLAG2-HIS6	pZR209 was subjected to site-directed mutagenesis using primers LK2692 LK2693	This study
pDP50	pSGMU2 containing 5'-truncated *spoIVFB*(205-864)	A fragment from bp 205-864 of *spoIVFB* was amplified by PCR from pZR209 using primers PDP84 and PDP85. The fragment was digested with SalI and BamHI, and ligated with SalI-BamHI-digested pSGMU2. PDP84 introduces a stop codon before the *spoIVFB* fragment preventing expression from the downstream *spoIVFB* fragment after plasmid integration.	This study

Table 4.1 (cont'd)

pDP66	Sp^R; amyE::spoIVF with SpoIVFB H206A	pDR18a was subjected to site-directed mutagenesis using primers PDP47 and PDP48	This study
pDP67	Sp^R; amyE::spoIVFB S260A	pDR18a was subjected to site-directed mutagenesis using primers PDP68 and PDP69	This study
pDP68	Sp^R; amyE::spoIVFB S260G	pDR18a was subjected to site-directed mutagenesis using primers PDP70 and PDP71	This study
pDP69	Sp^R; amyE::spoIVFB E264A	pDR18a was subjected to site-directed mutagenesis using primers PDP51 and PDP52	This study
pDP70	Sp^R; amyE::spoIVFB E264D	pDR18a was subjected to site-directed mutagenesis using primers PDP72 and PDP73	This study
pDP71	Sp^R; amyE::spoIVFB E264Q	pDR18a was subjected to site-directed mutagenesis using primers PDP76 and PDP77	This study
pDP72	Sp^R; amyE::spoIVFB F272A	pDR18a was subjected to site-directed mutagenesis using primers PDP93 and PDP94	This study
pDP81	Km^R; Pro-σ^K(1-126)-HIS6 C109S	pFB6 was subjected to site-directed mutagenesis using primers LK1123 and LK1124	This study
pDP82	Km^R; Pro-σ^K(1-126)-HIS6 C109S/ CytTM-SpoIVFB-F2 E44C	A CytTM-SpoIVFB-F2 E44C fragment was amplified by PCR from pYZ107 using primers FB15 and FB18 and inserted into BamHI digested pDP81 using Gibson assembly.	This study
pDP83	Km^R; Pro-σ^K(1-126)-HIS6 C109S/ SpoIVFB-F2 E44C	pDP82 was subjected to site-directed mutagenesis using primers PDP174 and PDP175	This study

Strain:	**Description:**	**Construction:**	**Reference:**
PY79			[45]
BSL51			[37]
BDP42	*spoIVFBΩpDP20*	PY79 was transformed with pDP20	
BDP46	*spoIVFBΩpDP30*	PY79 was transformed with pDP30	
BDP48	*spoIVFBΩpDP31*	PY79 was transformed with pDP31	
BDP76	Sp^R; amyE::spoIVF with SpoIVFB H248A	BSL51 was transformed with pDP65	
BDP77	Sp^R; amyE::spoIVF with SpoIVFB S260A	BSL51 was transformed with pDP67	
BDP78	Sp^R; amyE::spoIVF with SpoIVFB S260G	BSL51 was transformed with pDP68	
BDP79	Sp^R; amyE::spoIVF with SpoIVFB E264A	BSL51 was transformed with pDP69	
BDP80	Sp^R; amyE::spoIVF with SpoIVFB E264D	BSL51 was transformed with pDP70	
BDP81	Sp^R; amyE::spoIVF with SpoIVFB E264Q	BSL51 was transformed with pDP71	

Table 4.1 (cont'd)

BDP82	Sp^R; amyE::spoIVF with SpoIVFB F272A	BSL51 was transformed with pDP72	

Primer:	Sequence
LK1123	GTATGCAGCGAGATCTATTGAAAATG
LK1124	CATTTTCAATAGATCTCGCTGCATAC
LK2692	CTGCTTCTGCCCTACTAAAAGCTTGATTACAAG
LK2693	CTTGTAATCAAGCTTTTAGTAGGGCAGAAGCAG
FB11	CGAAAACCTGTACTTCCAGGGCGGATCCGATCCGGCTGCTAACAAAG
FB12	TTAGTGGTGGTGGTGGTGGTGGAAGCCTTTTTTTGTTTTTTTCAATGCG
FB13	CGCATTGAAAAAAACAAAAAAAGGCTCCCACCACCACCACCACCACTAAGAT
FB14	CTTTGTTAGCAGCCGGATCGGATCCGCCCTGGAAGGTACAGGTTTTCG
FB15	CGAAAACCTGTACTTCCAGGG
FB18	CTTTGTTAGCAGCCGGATCGGATCCTTACTTGTCATCGTCATCCTTGTAATCC
PDP37	CTATCATGTGATGGCCGAGGCCAAACGTGGCTGTAAGCATC
PDP38	GATGCTTACAGCCACGTTTGGCCTCGGCCATCACATGATAG
PDP39	CAGCCAGCTTGACGAGAATGCAGTGCTGCACGCTTACTTTG
PDP40	CAAAGTAAGCGTGCAGCACTGCATTCTCGTCAAGCTGGCTG
PDP41	CACGCTTACTTTGCCGATGCGCGGACGAATTCTTCCATG
PDP42	CATGGAAGAATTCGTCCGCGCATCGGCAAAGTAAGCGTG
PDP43	GCTTACTTTGCCGATAAGGCGACGAATTCTTCCATGGAG
PDP44	CTCCATGGAAGAATTCGTCGCCTTATCGGCAAAGTAAGC
PDP45	GACGAATTCTTCCATGGAGGCACTGCTTCTGCCCTACAAG
PDP46	CTTGTAGGGCAGAAGCAGTGCCTCCATGGAAGAATTCGTC
PDP47	GTTCAAACGTGGCTGTAAGGCTCCGATTATTATAGAAAAATC
PDP48	GATTTTTCTATATATATCGGAGCCTTACAGCCACGTTTGAAC
PDP49	CAAAAGCTCAGCCAGCTTGCCGAGAATGAAGTGCTGCAC
PDP50	GTGCAGCACTTCATTCTCGGCAAGCTGGCTGAGCTTTTG
PDP51	AAGCTCAGCCAGCTTGACGCGAATGAAGTGCTGCACGCT
PDP52	AGCGTGCAGCACTTCATTCGCGTCAAGCTGGCTGAGCTT
PDP53	CTCAGCCAGCTTGACGAGGCTGAAGTGCTGCACGCTTAC
PDP54	GTAAGCGTGCAGCACTTCAGCCTCGTCAAGCTGGCTGAG
PDP60	GCAGTCGTCGACGGTCGAAGTGGAAGAGCACG
PDP61	GCAGTCGGATCCCTTTGTTAGCAGCCGGATCTCAG
PDP68	AAATCAGGCCAAAAGCTCGCCCAGCTTGACGAGAATGAA
PDP69	TTCATTCTCGTCAAGCTGGGCGAGCTTTTGGCCTGATTT
PDP70	AAATCAGGCCAAAAGCTCGGCCAGCTTGACGAGAATGAA
PDP71	TTCATTCTCGTCAAGCTGGCCGAGCTTTTGGCCTGATTT
PDP72	AAGCTCAGCCAGCTTGACGACAATGAAGTGCTGCACGCT
PDP73	AGCGTGCAGCACTTCATTGTCGTCAAGCTGGCTGAGCTT
PDP74	AAGCTCAGCCAGCTTGACCTGAATGAAGTGCTGCACGCT
PDP75	AGCGTGCAGCACTTCATTCAGGTCAAGCTGGCTGAGCTT
PDP76	AAGCTCAGCCAGCTTGACCAGAATGAAGTGCTGCACGCT
PDP77	AGCGTGCAGCACTTCATTCTGGTCAAGCTGGCTGAGCTT
PDP84	GCAGTCGTCGACTGAGGTCGAAGTGGAAGAGCACG

Table 4.1 (cont'd)

PDP85	GCAGTCGGATCCTCAGTAGGGCAGAAGCAGTTCCTCCATG
PDP90	GCAGTCAAGCTTTGAGGTCGAAGTGGAAGAGCACG
PDP91	GACTGCAAGCTTCTACAGAAGTTTCTCAGGCTCCCTG
PDP92	GACTGCAAGCTTCAGAAGTTTCTCAAGCTCCCTG
PDP93	GAATTCGTCCGCTTATCGGCAGCGTAAGCGTGCAGCACTTC
PDP94	GAAGTGCTGCACGCTTACGCTGCCGATAAGCGGACGAATTC
PDP174	CTTTAAGAAGGAGATATACCATGAATAAATGGCTCG
PDP175	CGAGCCATTTATTCATGGTATATCTCCTTCTTAAAG

coli strains were grown in Lysogeny Broth (LB) medium with either ampicillin (50 μg/mL) or kanamycin (50 μg/mL) or both for selection of plasmid maintenance. Induction of protein synthesis by *E. coli* BL21(DE3) derivatives was achieved by addition of IPTG at 0.5 mM for 2 hours.

Chemical crosslinking of the SpoIVFB·Pro-σ^K complex

The SpoIVFB·Pro-σ^K complex was purified as previously described [24]. Approximately 2 μg of complex was added to crosslinking reactions in PBS containing 150 mM NaCl, 10% glycerol, and 6 μM zinc acetate with or without 1 mM ATP. The crosslinkers *N*-(β-maleimidoacetoxy)succinimide ester (AMAS) (Thermo Fisher Scientific, catalog #22295) and sulfosuccinimidyl-4-(*N*-maleimidomethyl)cyclohexane-1-carboxylate (Sulfo-SMCC) (Thermo Fisher Scientific, catalog # 22322) were used at 0.2 mM and diluted from 5 mM stocks dissolved in DMSO (AMAS) or water (sulfo-SMCC). Nucleotides were added from 10 mM stocks, except a twofold dilution series of the ATP stock was used to vary the concentration. All reactions were incubated at 25°C for 1 h prior to addition of sample buffer (50 mM Tris-HCl, pH 6.8, 4% SDS, 20% vol/vol glycerol, 200 mM DTT, and 0.03% bromophenol blue) to quench crosslinking and followed by boiling for 3 min. Proteins were separated by SDS-PAGE using 14% Prosieve-50 (Lonza) polyacrylamide gels. Gels were stained with Coomassie blue for 45 min and destained until the background was clear of dye. Gel images were collected with a Chemidoc MP imaging system (BioRad) using automatic exposure settings.

SpoIVFB sequence analysis

Orthologs of *B. subtilis spoIVFB* were collected from the NCBI and Uniprot data bases by searching for genes annotated as *spoIVFB* in the genomes of other endospore-forming bacterial species. These orthologous protein sequences were aligned using the homology

extension algorithm of the T-Coffee multiple sequence alignment package [29]. Residues conserved in greater than 70% of sequences were considered for further investigation. The *B. subtilis* SpoIVFB CBS domain secondary structure was predicted using the Jpred 4 algorithm [30]. The consensus sequences of adenine-nucleotide-binding motifs in CBS domains [23] were manually mapped onto the *B. subtilis* SpoIVFB CBS domain based on location within predicted secondary structure regions and matching with motif residues.

Immunoblot analysis

Whole-cell extracts were prepared as previously described for *E. coli* [12] or *B. subtilis* [24]. Extracts were separated by SDS-PAGE using 14% Prosieve-50 (Lonza) polyacrylamide gels and electroblotted to Immobilon-P membranes (Millipore). Blots were blocked with 5% nonfat dry milk in TBST (20 mM Tris-HCl [pH 7.5], 0.5 M NaCl, 0.1% Tween) for 1 h at 25°C with shaking. Blots for *E. coli* coexpression were probed with HRP-linked antibodies against penta-His (1:10,000) (Qiagen, catalog # 34460) or FLAG (1:10,000) (Sigma, catalog #A8592-1MG) diluted in TBST with 1% milk and incubated 1 h at 25°C with shaking. Blots for *B. subtilis* samples were probed with primary antibodies against SpoIVFB (1:5000) [24] or Pro-σ^K (1:3000) [31] diluted in TBST with 1% milk and incubated overnight at 4°C with shaking. These antibodies were not conjugated to HRP and were detected with a goat anti-rabbit-HRP secondary antibody (Bio-Rad, catalog #170-6515) at a 1:10,000 dilution in TBST with 1% milk for 1 h at 25°C with shaking. Signals were generated using the Western Lightning Plus ECL reagent (PerkinElmer) and signals were detected using a ChemiDoc MP imaging system (Bio-Rad).

Suppressor Screen

A suppressor screen was performed on strains that express SpoIVFB H248A or E264A variants. Cultures were inoculated in 10 mL of DSM liquid medium using 4-5 isolated colonies

that grew on LB agar after streaking from freezer stocks. Cultures were grown for 24 h at 37°C and 400 rpm shaking. At 24 h, a 1 mL sample was collected for a freezer stock and stored at -80°C with 20% glycerol. A 2 mL sample was collected for dilution plating. A dilution series was carried out in 10 mM sodium phosphate buffer (pH 7.4) containing 50 mM KCl and 1 mM $MgSO_4$ by serially transferring 0.5 mL samples to 4.5 mL of buffer. Samples (100 μL) from 10^{-4}-10^{-8} dilutions were plated on LB agar to achieve 10^{-5}-10^{-9} dilutions of viable cells. The dilution series and the remaining 1.5 mL of culture sample were heat-treated in an 80°C water bath for 10 min to kill non-spore cells and 100 μL of each sample was plated to achieve 10^{-1}-10^{-9} dilutions of heat-resistant spores [26]. A new 10 mL DSM culture was started using 0.5 mL of heat-treated culture and returned to shaking at 37°C. Plates were incubated at 37°C overnight and colony forming units (CFUs) representing viable cells or heat-resistant spores were enumerated from plates containing between 30-300 CFUs. The resulting CFUs/mL were used to calculate the sporulation efficiency as the percent of spores over viable cells. This process was repeated for 5 days until sporulation efficiency had recovered by several orders of magnitude.

At the conclusion of the screen, 4 isolates from rounds 3-5 of selection were recovered for each strain by streaking for isolated colonies from the freezer stock and picking isolated colonies to an LB plate with spectinomycin selection (100 μg/mL). Plates were incubated overnight at 37°C and at 16 h colonies were used for PCR as follows. A single colony was picked into 50 uL of TE buffer (10 mM Tris-HCl pH 8.0, 0.5 mM EDTA) and boiled for 5 min. A sample (2 μL) of this cell lysate was used as template to amplify the *spoIVFB* gene in a 50 μL PCR reaction using primers PDP106 PDP103 and ACCUZYME high-fidelity DNA polymerase (Bioline, catalog #BIO-25028). Colony PCR products were purified using the Qiagen PCR cleanup kit and subjected to DNA sequencing using primer PDP103. Sequences were checked for intragenic mutations resulting in non-revertant amino acid changes.

Results

ATP binding induces a conformational change in the SpoIVFB·Pro-σ^K complex

The ability of purified SpoIVFB to cleave Pro-σ^K was found to depend on addition of zinc and ATP [12]. Radioactive ATP binding to a monomeric form of the CBS domain was demonstrated by native PAGE [12]. These observations led to the question of how ATP binding regulates SpoIVFB activity. Upon ligand binding, CBS domains typically cause conformational changes within proteins [22,23]. To test for a conformational change in SpoIVFB upon ATP binding, chemical crosslinkers of differing length were used to test for crosslinking between Pro-σ^K and catalytically-inactive SpoIVFB, to identify those forming a stable complex [32]. The chemicals used, AMAS (4.4 Å) and Sulfo-SMCC (8.3 Å), are heterobifunctional amine-to-sulfhydryl crosslinkers. The protein complex we purified was composed of cysteineless (Cysless) Pro-σ^K(1-127) and mono-Cys SpoIVFB E44C. Chemical crosslinking of Cysless Pro-σ^K(1-127) K24 to mono-Cys SpoIVFB E44C was predicted, based on prior studies showing that mono-Cys Pro-σ^K(1-127) K24C was crosslinked to mono-Cys SpoIVFB E44C both *in vivo* [33] and *in vitro* [32] disulfide crosslinking experiments. Chemical crosslinking was performed in the presence and absence of 1 mM ATP. Under both conditions (+/- ATP), the longer crosslinker Sulfo-SMCC was able to crosslink the two proteins, although less complex was observed in the presence of ATP (Fig. 4.1A, lanes 4 and 5). The shorter crosslinker AMAS was able to crosslink the two proteins in the absence of ATP, but very little of the complex was observed in the presence of ATP (Fig. 4.1A, lanes 1 and 2). These observations suggest that ATP binding induces a conformational change in the complex which moves E44 at the active site of SpoIVFB away from K24 near the cleavage site in Pro-σ^K. This movement would presumably position the peptide bond between S21 and Y22 of Pro-σ^K for cleavage, in order to explain the requirement of ATP for cleavage *in vitro* [12].

Fig. 4.1A

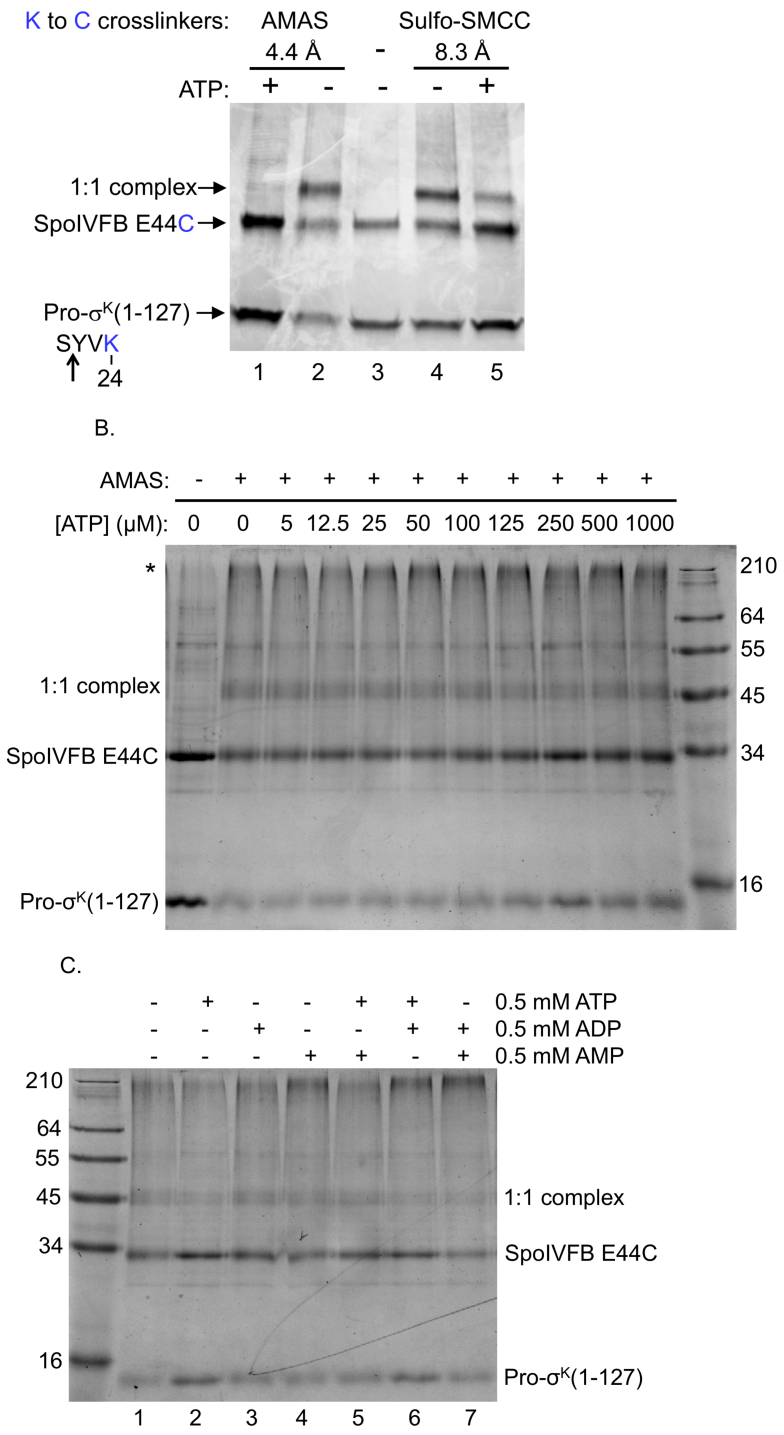

Figure 4.1 Chemical crosslinking demonstrates an ATP- and AMP-dependent conformational change. A purified complex of mono-Cys SpoIVFB-FLAG$_2$-His$_6$ E44C and Cys-less Pro-σ^K (1-127)-His$_6$ was incubated for 1 h at 25°C in the presence of 0.2 mM AMAS or Sulfo-SMCC. Samples were separated by SDS-PAGE and stained with Coomassie Blue. Proteins migrating at positions expected for the SpoIVFB E44C monomer, the Pro-σ^K (1-127)

Figure 4.1 (cont'd)

monomer, and a 1:1 complex of the two are indicated. **(A)** Effect of ATP. Crosslinking was performed in the presence or absence of 1 mM ATP. Shown below Pro-σ^K (1-127) is the amino acid sequence near the cleavage site (indicated by the upward arrow) with K24 in blue, the residue predicted to be crosslinked to SpoIVFB E44C in the complex. **(B)** ATP titration. The concentration of ATP was varied in the presence of AMAS. High molecular weight species in the presence of crosslinker and sample boiling are indicated with an asterisk. **(C)** Effects of ADP, AMP, and nucleotide mixtures. Crosslinking with AMAS was performed in the presence or absence of nucleotide(s).

To measure the dependence of AMAS crosslinking on ATP, the concentration of ATP in the reaction was varied. As expected, decreasing intensity of the crosslinked complex and increasing intensity of SpoIVFB and Pro-σ^K(1-127) monomers was observed as the ATP concentration was increased (Fig. 4.1B). Quantification of the Pro-σ^K(1-127) and SpoIVFB monomer signals yielded a typical binding curve and an estimated K_d of 100-120 μM (data not shown). However, quantification of the SpoIVFB·Pro-σ^K(1-127) complex signal did not yield a similar binding curve, perhaps due to crosslinking and aggregation of proteins into higher molecular weight species (Fig. 4.1B, asterisk). These species increase in the presence of AMAS. Preliminary evidence suggests that the species occur, in part, due to boiling the samples (data not shown). Therefore the experiment will be repeated without boiling of samples. Interestingly, the K_d for ATP binding of 100-120 μM, estimated from the monomer signals, is consistent with the binding constants of other CBS domains [22,34].

In addition to ATP binding, many CBS domains bind other adenine nucleotides to achieve more complex regulation based on cellular energy status [22,23]. To test whether other nucleotides affect the crosslink generated by AMAS, the protein complex was exposed to ADP or AMP alone, or in combination with each other or ATP. As expected, 0.5 mM ATP decreased formation of crosslinked complex (Fig. 4.1C, lanes 1 and 2). In contrast, neither ADP nor AMP alone at 0.5 mM affected complex formation (lanes 3 and 4). These results could mean either that ADP and AMP do not bind or that they promote the conformation that prevents crosslinking. To investigate these possibilities, the effects of adenine nucleotide mixtures were examined. The mixture of AMP and ATP yielded an intriguing result. AMP appeared to reverse the effect of ATP on crosslinking by AMAS (lane 5). ADP did not reverse the effect of ATP (lane 6), and the mixture of ADP and AMP had no effect on crosslinking. Taken together, these results, albeit preliminary due to boiling of samples and lack of repetition, suggest that ATP and AMP induce distinct conformational states of the SpoIVFB·Pro-σ^K(1-127) complex, as detected by chemical

crosslinking between a residue at the active site of SpoIVFB and a residue near the cleavage site in Pro-σ^K(1-127). Also, AMP is expected to have a lower binding constant than ATP, since AMP reversed the effect of ATP when the nucleotides were mixed at equimolar concentrations before addition to the complex.

Predicted nucleotide-binding motifs and conserved residues in the SpoIVFB CBS domain

The CBS domain of SpoIVFB appears to contain the canonical secondary structure motifs of a CBS domain. Structure prediction using Jpred 4 [30] predicts a β1-α1-β2-β3-α2 structure (Fig. 4.2A) common among CBS domains [22]. It additionally predicts an α0 helix and flexible linker preceding β1, and α3 following α2 [23,24]. Closer inspection of the CBS domain sequence reveals conserved residues and likely nucleotide-binding motifs. In a sequence alignment of 136 SpoIVFB orthologs from *Bacilli* and *Clostridia*, three residues were 70-90% conserved, F242, H248 and E264 (Fig. 4.2B). These residues fall within or near the proposed secondary structures and nucleotide-binding motifs (Fig. 4.2A).

Two CBS domain nucleotide-binding motifs appear to be present in SpoVIFB. An hxxhP consensus sequence near the start of β2 (h is any hydrophobic residue and x is any residue) mediates interaction with adenosyl groups while preventing guanosyl binding (Fig. 4.2A) [23]. This sequence aligns with the GCKHP sequence of SpoIVFB (Fig. 4.2A), which contains the 70% conserved H248 residue before the proline in the motif. The other consensus nucleotide-binding sequence is GhhT/SxxD/N, which is often found near β3 and α2 [23]. This sequence aligns with the GQKLSQLD sequence of SpoIVFB (Fig. 4.2A). The 90% conserved E264 residue of SpoIVFB immediately follows the aspartate at the end of the motif. Because aspartate and glutamate residues are highly similar, conservation of E264 may suggest a variation upon the theme of this motif. We note that the three residues (QKL) between G256 and S260 deviate from the consensus GhhS sequence. The GhhT/SxxD/N motif often

Fig 4.2A.

B.

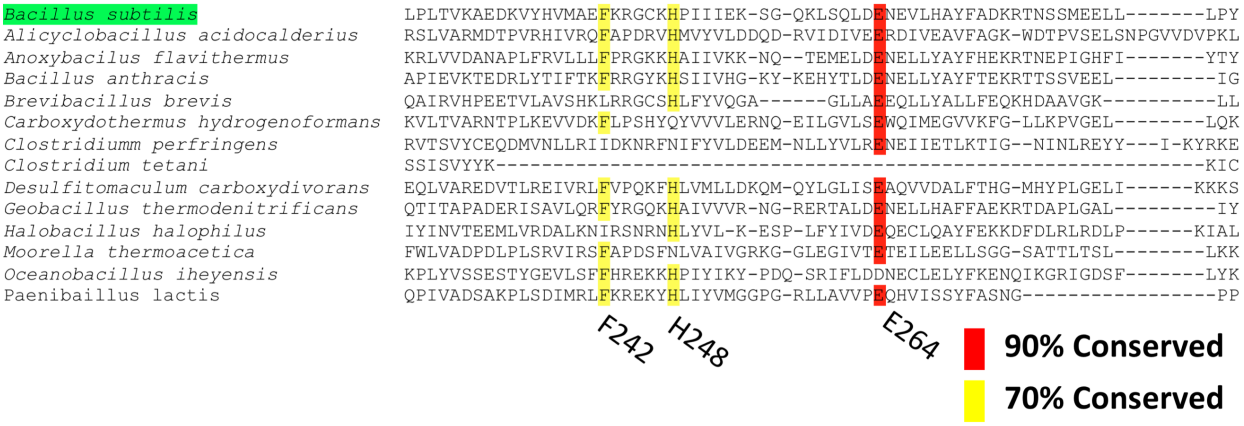

C.

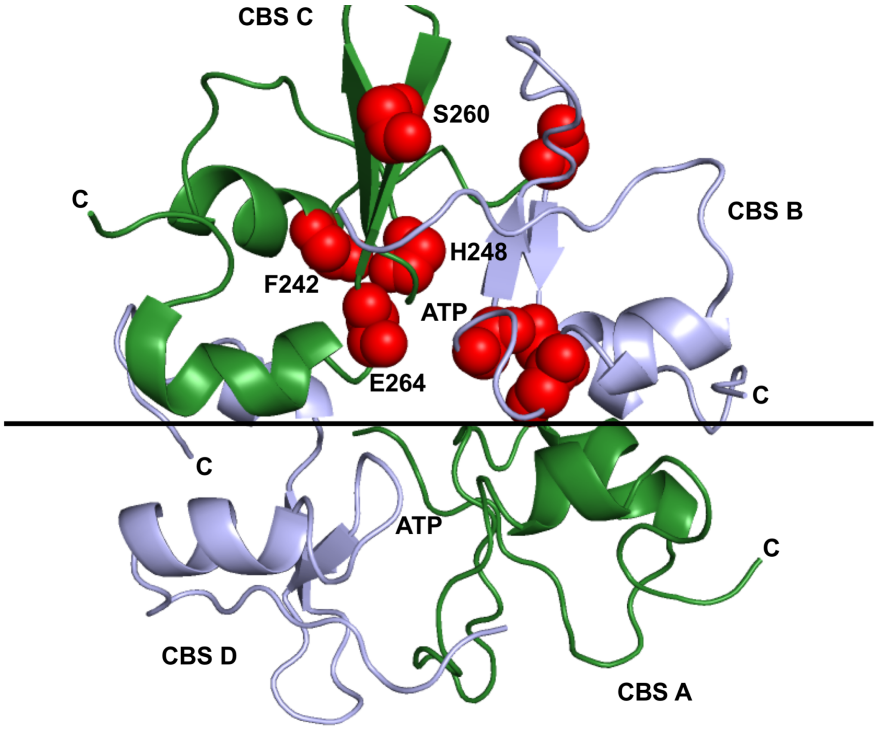

Figure 4.2 The SpoIVFB CBS domain contains conserved residues and predicted nucleotide-binding motifs. (A) Predicted secondary structure and nucleotide-binding motifs in the SpoIVFB C-terminal domain. The canonical CBS domain secondary structure of β1-α1-β2-β3-α2 is sometimes preceded by α0-linker and followed by α3 (top), and this appears to be the case in the C-terminal domain of SpoIVFB, for which residues 200-288 are aligned with the Jpred 4 secondary structure prediction (bottom). Green and blue indicate α-helices and β-sheets, respectively. Consensus sequences of adenine nucleotide-binding motifs are aligned with underlined similar sequences in SpoIVFB (h is any hydrophobic residue and x is any

Figure 4.2 (cont'd)

residue). Conserved residue F242 is indicated to help locate other residues mentioned in the text. **(B)** Conserved residues in the SpoIVFB CBS domain. A sequence alignment *of B. subtilis* SpoIVFB residues 225-288 with 13 representative orthologs from a large alignment that includes 136 orthologs. Three conserved residues are indicated with F242 and H248 at least 70% conserved (yellow) and E264 at least 90% conserved (red) in the large alignment. **(C)** Locations of residues and proposed ATP-binding pockets in a homology model of SpoIVFB CBS domains. Tetrameric SpoIVFB, as viewed from the "bottom" (i.e., the MC cytoplasm, looking upward toward the membrane) with only the CBS domains shown. CBS domain pairs, each proposed to bind ATP approximately where shown, are separated by a line. Conserved residues F242, H248, and E264, as well as S260 in the predicted GQKLSQLD nucleotide-binding sequence (panel A) are represented with red spheres in the CBS C and CBS B pair, and are labeled in CBS C. The C-terminus of each CBS domain is labeled.

promotes AMP-binding, and the conserved aspartate residue interacts with the 2' and/or 3' hydroxyl of ribose. In light of our observations that ATP and AMP induce distinct conformational states of the SpoIVFB·Pro-σ^K complex, the presence of predicted nucleotide-binding motifs and nearby conserved residues lends further support to a model in which ATP and AMP binding regulates SpoIVFB activity. To visualize the location of potentially crucial residues, we mapped them on a homology model of the SpoIVFB·Pro-σ^K complex recently generated by our group [24] (Fig. 4.2C). Many of the residues fall at the interface of two CBS domains in the proposed ATP-binding pocket [24]. Considering all of these observations it is likely that the highly conserved residues and predicted nucleotide-binding motifs play an important role in ATP binding and SpoIVFB activity. Therefore, we performed amino acid substitution analysis of the highly conserved residues, two residues within the predicted nucleotide-binding motifs, and three other residues (Table 4.2).

Table 4.2 Amino acid substitutions in the SpoIVFB CBS domain

Amino Acid	Substitutions
F242	A
H248	A
S260	A, G
D263	A
E264	A, D, L, Q
N265	A
E266	A
F272	A

Amino acid substitutions in the CBS domain affect Pro-σ^K cleavage in *E. coli*

The effects of amino acid substitutions in SpoIVFB were tested by coexpression with Pro-σ^K(1-127) in *E. coli*. Plasmids that express wild-type or variants of cytTM-SpoIVFB-$FLAG_2$-His_6 (ampicillin resistant) were co-transformed with a plasmid that expresses Pro-σ^K(1-127)-His_6 and a kanamycin resistance marker. This co-expression system reconstitutes SpoIVFB cleavage of Pro-σ^K *in vivo* and has been used previously to test the effects of amino acid changes in SpoIVFB or Pro-σ^K(1-127) [12,17,24,32,33,35]. In a first round of alanine substitutions in SpoIVFB, we found that the three highly conserved residues F242, H248, and E264 are important, since cleavage of Pro-σ^K(1-127) was impaired strongly (Fig. 4.3A). Accumulation of those three SpoIVFB variants appeared to be reduced, perhaps contributing to diminished Pro-σ^K(1-127) cleavage. The other substitutions had little effect on Pro-σ^K(1-127) cleavage or SpoIVFB accumulation. Interestingly, D263A had no effect despite the prediction that D263 at the end of the GQKLSQLD sequence may interact with the 2' and/or 3' hydroxyl of ribose. Perhaps E264 instead makes that interaction. F242 may interact with adenine via stacking interactions, as planar aromatic residues commonly do [22]. H248 is part of the GCKHP sequence that may favor adenosyl rather than guanosyl binding [23]. In any case, the three most conserved residues in the CBS domain clearly play critical roles in the activity and/or stability of SpoIVFB.

In an additional round of substitutions, other changes to E264, as well as changes to S260 in the GQKLSQLD sequence and F272 at the end of β-2 owing to its potential for stacking with adenine. Surprisingly, neither S260A nor S260G impaired Pro-σ^K(1-127) cleavage (Fig. 4.3B), despite the apparent match of S260 to the consensus sequence for nucleotide binding (Fig. 4.2A). These results suggest that S260 is not required for ATP binding or that alanine or glycine at this position allows SpoIVFB activity without ATP binding. F272A also had little effect on cleavage (Fig. 4.3B, lane 8). E264 tolerated conservative substitutions (D or Q) but like

Fig 4.3A.

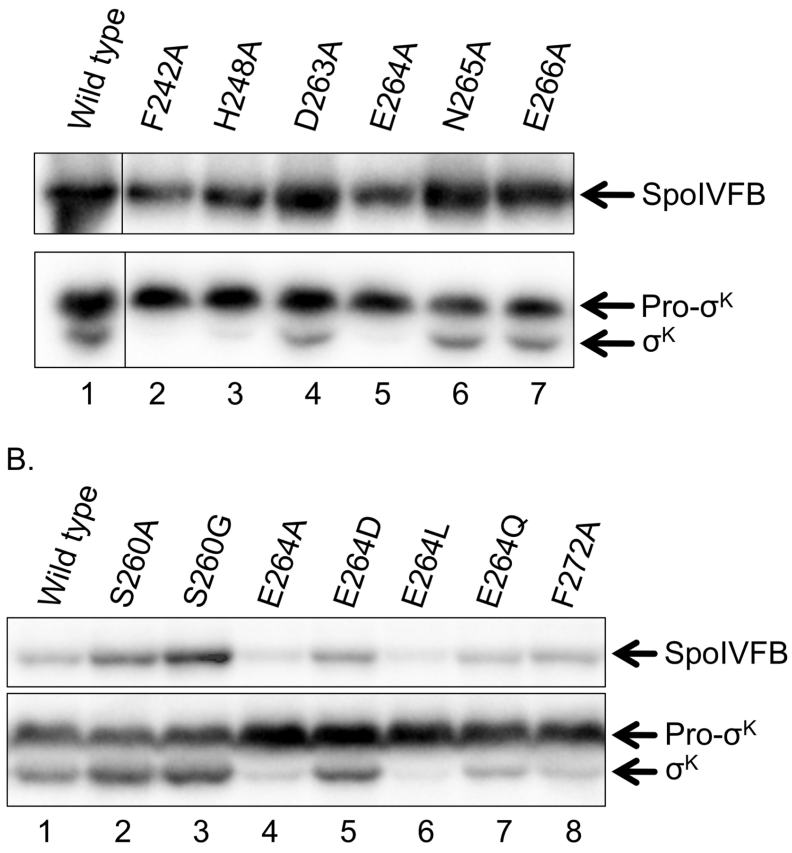

Figure 4.3 Effects of amino acid substitutions in the SpoIVFB CBS domain on cleavage of Pro-σ^K. Wild-type or variant cytTM-SpoIVFB-$FLAG_2$-His_6 was coexpressed with Pro-σ^K(1-127)-His_6 in *E. coli*, and samples collected at 2 h after induction were subjected to immunoblot analysis with anti-FLAG (top) or anti-His (bottom) antibodies. **(A)** Effects of alanine substitutions. **(B)** Effects of additional substitutions.

E264A, E264L strongly impaired Pro-σ^K(1-127) cleavage and appeared to reduce accumulation of SpoIVFB. Taken together, the results of single amino acid substitutions demonstrate the importance of three highly conserved residues in the CBS domain for SpoIVFB activity and/or stability. However, two residues in predicted nucleotide-binding motifs, D263 and S260, tolerated non-conservative alanine (and glycine in the case of S260) substitutions, perhaps indicating a novel mode of nucleotide binding.

Epitope tags on SpoIVFB or deletion of the CBS domain prevent Pro-σ^K cleavage

Prior to the work of this dissertation, the antibodies against the C-terminal interdomain linker and CBS domain of SpoIVFB, which our group had generated [36], had not been used to detect SpoIVFB in immunoblots of *B. subtilis* whole-cell extracts. We therefore attempted to express epitope-tagged SpoIVFB in *B. subtilis* in order to facilitate subsequent testing of the effects of amino acid substitutions in this protein, including measurement of protein accumulation by immunoblot analysis. A plasmid integration construct was generated that introduces a $FLAG_2$-His_6 tag identical to that at the C-terminal end of the *E. coli* overexpression plasmids described above. In addition, a CBS domain deletion, SpoIVFB(1-224), was generated with and without the $FLAG_2$-His_6 tag. These plasmids were introduced into *B. subtilis* for chromosomal integration via single-crossover homologous recombination. The resulting strains were starved to induce sporulation and samples were collected at 2, 4 and 8 h poststarvation for immunoblot analysis. Using antibodies against the FLAG epitope, no signal was detected in the wild-type control strain at 2 or 4 h, as expected, but a strong cross-reacting species was observed at 8 h (Fig. 4.4A). The species is apparently a σ^K-dependent protein since it only appears after significant processing of Pro-σ^K to σ^K in wild type and it is not present in the Δ*spoIVFAB* control strain lacking the *spoIVF* operon and therefore unable to cleave Pro-σ^K. Despite accumulation of SpoIVFB-$FLAG_2$-His_6, the tag prevented detectable cleavage of Pro-σ^K in sporulating *B.*

Fig. 4.4

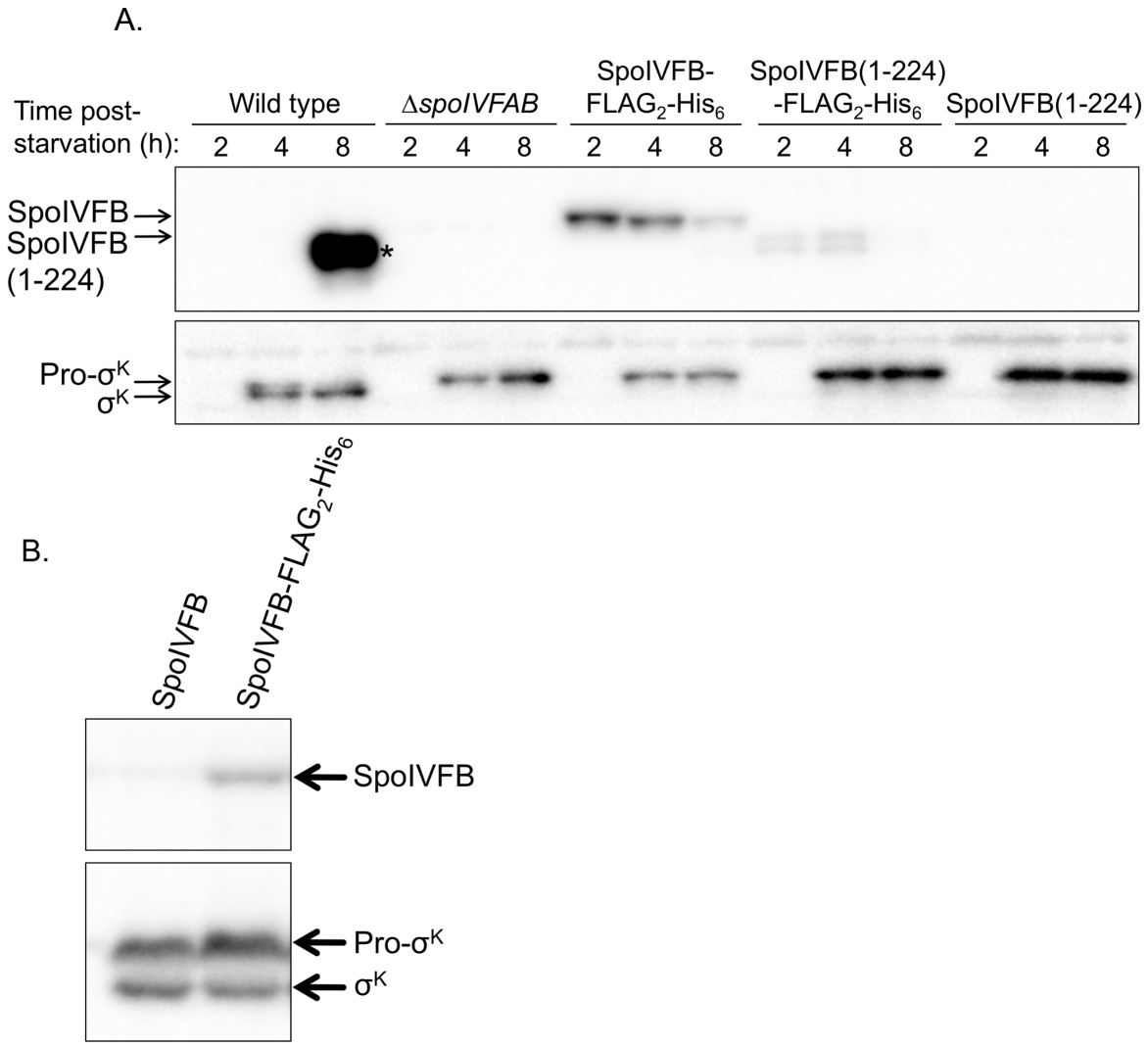

Figure 4.4 Tagging SpoIVFB with $FLAG_2$-His_6 prevents Pro-σ^K processing during sporulation of *B. subtilis* but not during growth of *E. coli.* **(A)** Effects of tagging SpoIVFB and deleting the CBS domain in *B. subtilis*. Plasmids were generated for chromosomal insertion of SpoIVFB-$FLAG_2$-His_6, SpoIVFB(1-224)-$FLAG_2$-His_6, or SpoIVFB(1-224) at the native *spoIVFB* locus. The resulting strains were starved to induce sporulation, along with the wild-type parent and a *spoIVF* null mutant as controls. Samples were collected at 2, 4 and 8 h poststarvation, and subjected to immunoblot analysis using antibodies against the FLAG epitope (top) or Pro-σ^K (bottom). The expected positions of migration for SpoIVFB, SpoIVFB(1-224), Pro-σ^K, and σ^K are indicated. A highly abundant species that cross-reacts with the FLAG antibody is apparent at 8 h wild type (*). **(B)** Effect of tagging SpoIVFB in *E. coli*. cytTM-SpoIVFB or cytTM-SpoIVFB-$FLAG_2$-His_6 were coexpressed with Pro-σ^K(1-127)-His_6. Samples collected at 2 h after induction were subjected to immunoblot analysis with anti-His antibodies.

subtilis. This result was surprising given the activity of cytTM-SpoIVFB-FLAG$_2$-His$_6$ on Pro-σ^K(1-127)-His$_6$ upon coexpression in *E. coli* (Fig. 4.3). No processing of Pro-σ^K was apparent by SpoIVFB(1-224)-FLAG$_2$-His$_6$ which lacks the CBS domain, although accumulation was reduced compared to SpoIVFB-FLAG$_2$-His$_6$ and a breakdown product appeared to be generated, suggesting instability (Fig. 4.4A). The strain designed to produced SpoIVFB(1-224) lacking the CBS and without tags also showed no detectable Pro-σ^K processing, of course accumulation of this SpoIVFB variant could not be determined because even the available SpoIVFB antibodies are against the CBS domain. Interestingly, it was shown recently that a yellow fluorescent protein (YFP) tag on SpoIVFB lacking the CBS domain allowed some Pro-σ^K processing in sporulating *B. subtilis*, although processing was severely inhibited [25]. The YFP tag appears to stabilize SpoIVFB lacking the CBS domain in a way that allows partial activity.

The apparent inactivity of SpoIVFB-FLAG$_2$-His$_6$ in sporulating *B. subtilis* (Fig. 4.4A) raised the question of whether the FLAG$_2$-His$_6$ tag inhibits SpoIVFB activity in *E. coli*. A plasmid with a translation stop codon before the tag exhibited very similar activity as tagged SpoIVFB (Fig. 4.4B). Obviously, there are numerous differences between coexpression in growing *E. coli* and expression from the native chromosomal location and promoter in sporulating *B. subtilis* that may account for the different outcomes (see Discussion).

Since the FLAG$_2$-His$_6$ tag prevented SpoIVFB from cleaving Pro-σ^K detectably in sporulating *B. subtilis*, the antibodies against the C-terminal linker and CBS domain of SpoIVFB, were affinity-purified and used to measure accumulation of SpoIVFB variants in sporulating *B. subtilis* by immunoblot analysis as described [24].

Many substitutions impair SpoIVFB accumulation in sporulating *B. subtilis*

The effects of substitutions in the SpoIVFB CBS domain were assessed by ectopically integrating mutant versions of the *spoIVFAB* operon into the chromosome of *B. subtilis* deleted

Fig 4.5

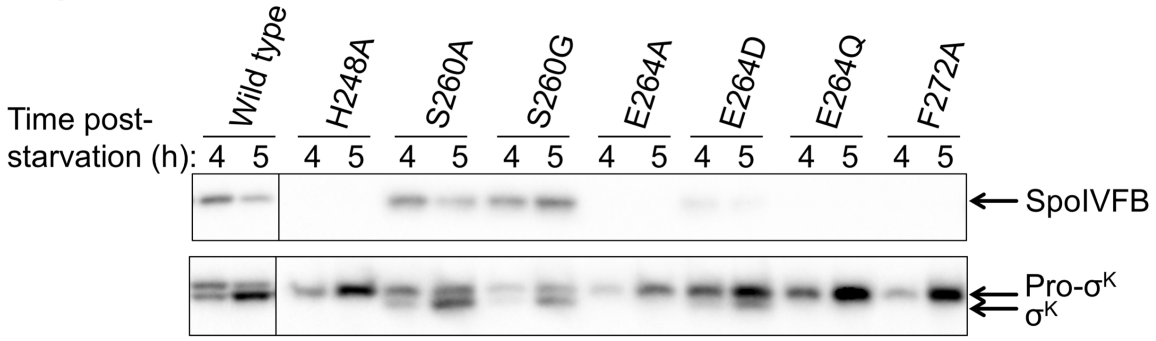

Figure 4.5 Effects of substitutions in the SpoIVFB CBS domain during *B. subtilis* sporulation. *B. subtilis* with a wild-type *spoIVFAB* operon, or a deletion of it at the native site and a version designed to express the indicated SpoIVFB variant protein from the ectopic *amyE* site, were starved to induce sporulation. Samples collected at the indicated times poststarvation were subjected to immunoblot analysis with antibodies against SpoIVFB (top) or Pro-σ^K (bottom).

for the endogenous *spoIVFAB* operon, and inducing sporulation by nutrient starvation. Surprisingly, most amino acid substitutions in the CBS domain greatly reduced or prevented detectable accumulation of the SpoIVFB variant (Fig. 4.5). This apparent instability contrasts with the apparent stability of many of these variants in *E. coli* (Fig. 4.3), although as noted above, accumulation of the H248A and E264A variants appeared to be reduced in *E. coli* (Fig. 4.3A). Even the conservative E264D and E264Q variants and the F272A variant, which accumulated normally in *E. coli* and cleaved Pro-σ^K(1-127) (Fig. 4.3B), failed to accumulate detectably in sporulating *B. subtilis* (Fig. 4.5). These results mirror those observed for several single-residue substitutions in the interdomain linker (residues 197-222) of SpoIVFB [24]. Apparently, both the linker and the CBS domain contribute to stability of SpoIVFB, in addition to their roles in substrate interaction and enzymatic activity [24] (Fig. 4.3). Exceptions to the instability created by CBS domain substitutions were the S260A and S260G variants, which also allowed normal Pro-σ^K processing (Fig. 4.5). Hence, a serine at position 260 is not essential for SpoIVFB activity, even though S260 is predicted to be part of an ATP-binding motif (Fig. 4.2A). As noted above, this could mean that S260 is not required for ATP binding or that alanine or glycine at this position allows SpoIVFB activity without ATP binding.

Taking together the effects of substitutions in the SpoIVFB CBS domain analyzed in *E. coli* (Fig. 4.3) and *B. subtilis* (Fig. 4.5), we conclude that three highly conserved residues (F242, H248, E264) are important for activity and may play a role in ATP binding, and that at least H248 and E264, as well as F272 are crucial for stability during sporulation.

Suppressors of SpoIVFB H248A and E264A variants that restore sporulation and partially restore protein accumulation, map to intriguing residues

To further investigate the lack of accumulation of SpoIVFB variants in sporulating *B. subtilis* (Fig. 4.5), a suppressor screen was performed. Because processing of Pro-σ^K is

Fig 4.6

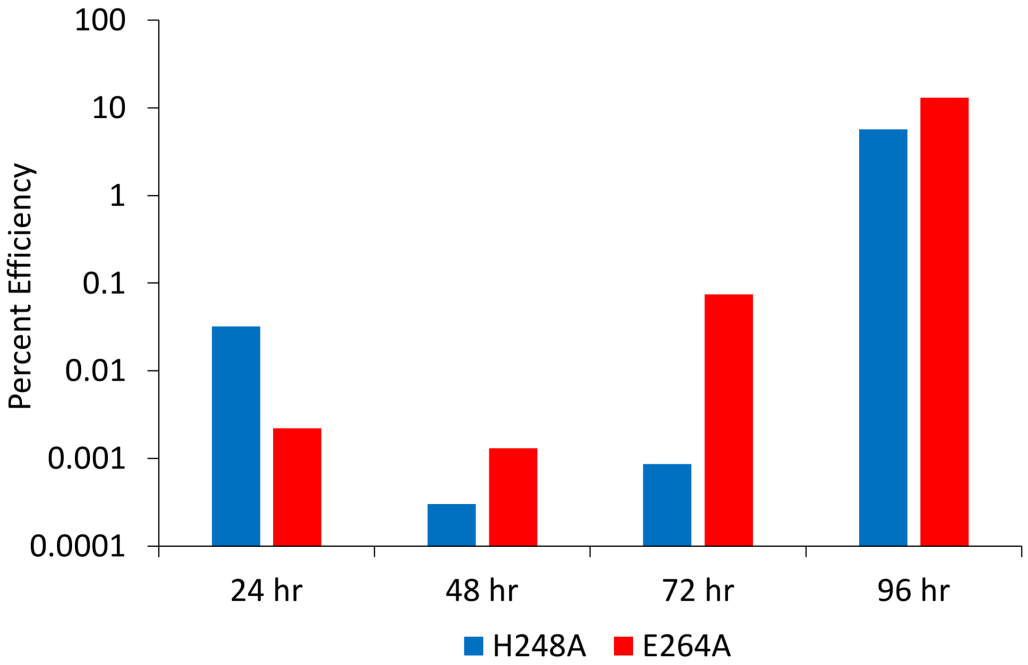

Figure 4.6 Sporulation efficiency of cultures repeatedly passaged after selection for spores. *B. subtilis* strains designed to express SpoIVFB H248A or E264A variants were induced to form spores by nutrient exhaustion and heat treated after 24 h in five rounds of selection. Sporulation efficiency was measured after each round, except the fifth round (owing to contamination on the enumeration plates). Data represent a single replicate.

required for the final stages that generate stress-resistant spores, it may be possible to select for spontaneous mutations that bypass effects of CBS domain substitutions. Such isolates were generated by repeatedly passaging cultures through starvation to induce sporulation and heat treatment at 80°C. Cells that are not spores are killed by heat treatment while suppressor mutants that form spores survive. The strains designed to express SpoIVFB H248A or E264A were subjected to five rounds of sporulation and heat treatment, resulting in recovery from a low sporulation efficiency of ~0.001% after two rounds (48 h) to an efficiency of ~5-13% after four rounds (96 h) (Fig 4.6). A wild-type strain sporulates at nearly 100% efficiency [24]. Heat-resistant isolates were identified after each round of sporulation and heat treatment. The *spoIVFB* gene of isolates was amplified using PCR and the DNA was sequenced. Intragenic suppressor mutations were the target of this screen. While it was possible that extragenic suppressors (e.g., a mutation in a gene coding for a protease, allowing accumulation of the SpoIVFB variant protein) could be isolated, intragenic suppressors were most likely to provide a rationale for future experiments aimed at stabilizing SpoIVFB variants (in order to evaluate effects on Pro-σ^K processing activity). Among the apparent intragenic suppressors, mutations resulting in substitutions at three positions (H206, L227, S260) were found repeatedly. Each occurred in combination with both H248A and E264A, in some cases with mutations in other residues, but combinations of mutations that would result in substitutions at more than one of the three positions were common, especially in isolates from round 4 and 5 of the screen. We chose several such isolates for further analysis. The most common substitutions at the three positions were H206Y, H206S, L227P, and S260N. Isolates with combinations of these substitutions were starved to induce sporulation and samples were subjected to immunoblot analysis. These isolates accumulated the variant SpoIVFB proteins, but not to the extent that wild-type SpoIVFB accumulates (Fig. 4.7). There appeared to be a very small amount of Pro-σ^K

Fig 4.7

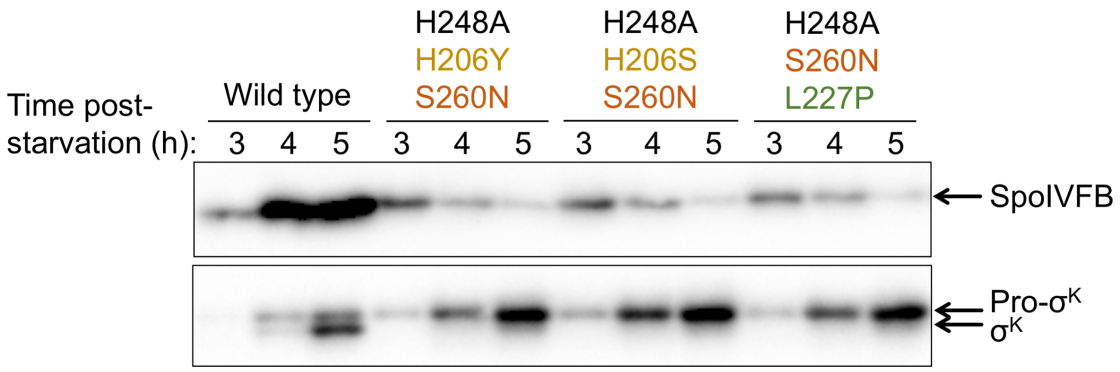

Figure 4.7 Representative *B. subtilis* isolates that suppress the sporulation defect caused by the SpoIVFB H248A substitution were starved to induce sporulation and samples collected at the indicated times poststarvation were subjected to immunoblot analysis with antibodies against SpoIVFB (top), or Pro-σ^K (bottom).

processing, consistent with the observation that very little σ^K is required for efficient sporulation [37].

H206 is in the interdomain linker of SpoIVFB, and L227 and S260 are in the CBS domain (Fig. 4.2A). Intriguingly, SpoIVFB H206A was shown previously to greatly impair Pro-σ^K(1-127) cleavage upon coexpression in *E. coli*, but did not impair Pro-σ^K processing in sporulating *B. subtilis* [24]. Also, several substitutions near H206 (i.e., V207M) or L227 (i.e., L221V, V235I) appeared to improve the thermostability of SpoIVFB in the absence of SpoIVFA [14]. Coincidentally, S260 of SpoIVFB was already a target of this research (Fig. 4.3B and 5) for reasons mentioned above. The repeated appearance of S260N substitutions, as well as H206Y, H206S, and L227P substitutions, in suppressor isolates strongly suggests that these substitutions located in the SpoIVFB linker and CBS domain can partially suppress the destabilizing H248A substitution in the CBS domain (Fig. 4.7).

Discussion

ATP binding induces conformational change in the SpoIVFB active site

Since the observation that SpoIVFB activity *in vitro* is ATP-dependent [12], there has been little published work addressing the role of ATP binding in regulating SpoIVFB function. It was proposed that the CBS domain induces a conformational change in SpoIVFB based on the understood role of other CBS domains [12]. Here, a crosslinking assay between the SpoIVFB active site residue E44C and residue K24 near the Pro-σ^K cleavage site demonstrated such a conformational change. A short (4.4 Å) chemical crosslinker formed less crosslinks in the presence of 1 mM ATP than in its absence (Fig. 4.1A). These results suggest that the conformational change occurring upon ATP binding moves SpoIVFB E44 and Pro-σ^K K24 farther apart. What could this conformational change be? In a recent study, a proposed conformational change occurs following SpoIVFB activation by SpoIVB-dependent cleavage of

SpoIVFA [25]. An F66A mutation was proposed to lock SpoIVFB in the active state and sidestep inhibition by SpoIVFA and BofA, since the requirement for SpoIVB was relieved [25]. This conformational change was modeled after potential open and closed conformations observed in the only known crystal structure of an IMMP [38]. Moreover, this conformational change appeared to control binding of Pro-σ^K to SpoIVFB [25]. Also, a CBS deletion in SpoIVFB-YFP was still partially active for Pro-σ^K cleavage, albeit still dependent on SpoIVB to relieve inhibition by SpoIVFA and BofA [25]. Hence, the CBS domain is not essential for cleavage. In contrast, SpoIVB is essential to relieve inhibition of SpoIVFB and allow it to cleave Pro-σ^K. Therefore, it seems likely that SpoIVB causes a different, perhaps larger, conformational change in SpoIVFB, than does ATP binding to the CBS domain. Nevertheless, testing the effects of the F66A substitution in SpoIVFB using crosslinking approaches is an important future direction.

The ATP dependence of crosslinking is less pronounced for a longer 8.8 Å crosslinker (Fig. 4.1A), suggesting that the conformational change is limited in distance. However, the apparent small change in conformation may be a consequence of using inactive SpoIVFB E44C. By blocking the cleavage cycle, the full range of conformational changes that occur upon ATP binding and Pro-σ^K processing may not be revealed. The E44C substitution is, however, necessary for the present assay, because wild-type SpoIVFB would process Pro-σ^K and release σ^K, whereas SpoIVFB E44C allows purification of the complex with Pro-σ^K. Future work aimed at detecting conformations of SpoIVFB in the absence of inactivating substitutions may allow a better understanding of the complete reaction cycle.

AMP inhibits conformational change induced by ATP

In addition to ATP binding, a number of CBS domains also bind AMP or other nucleotides in order to sense the energy status of the cell [34]. Perhaps the best understood

example of adenine-nucleotide binding is AMP kinase (AMPK). AMPK has several CBS domains that bind AMP, ADP and ATP. In doing so AMPK monitors the cellular energy status and controls catabolic and anabolic processes that relate to ATP generation or consumption. For a review of the current AMPK literature see ref [39]. ATP and AMP binding to SpoIVFB may have an analogous role. Evidence from this work suggests that AMP inhibits the effect of ATP binding on a conformational change within the active site of SpoIVFB (Fig. 4.1C). ADP does not appear to play a role, however further work with ADP may be worthwhile in case a more nuanced role has escaped our detection. Through binding AMP and ATP, SpoIVFB may sense the cellular energy status, ensuring the MC is ready for σ^K activity.

It seems likely that differential binding of AMP and ATP to the CBS domain regulates SpoIVFB activity. A different effect on Pro-σ^K processing was observed after treatment with the ionophore FCCP than with the translation inhibitor chloramphenicol (see Chapter 3). This was despite very similar reductions of ATP concentration after each treatment. Perhaps these treatments have differing effects on AMP concentration, generating a physiological difference that ATP-dependent luciferase activity could not detect.

Why might it be advantageous for SpoIVFB to regulate Pro-σ^K processing based on energy status? Perhaps the σ^K regulon requires a particular energy state to successfully finish sporulation. In the absence of the right energy state, incomplete σ^K activity may lead to weak or immature spores that cannot survive the same environmental stressors as normal spores. According to this model, ATP and AMP binding may constitute a check for the expected energy state, ensuring that the MC is prepared for the final stages of sporulation. Further work is required to measure the binding constant for AMP and determine the physiological conditions under which AMP and ATP ratios regulate SpoIVFB.

Amino acids in the SpoIVFB CBS domain are critical for Pro-σ^K cleavage upon coexpression in *E. coli* and for SpoIVFB stability in sporulating *B. subtilis*

The effects of amino acid substitutions were not entirely consistent when introduced into *E. coli* and *B. subtilis* systems. In the *E. coli* co-expression system, we found that a number of SpoIVFB residues had interesting effects on Pro-σ^K(1-127) cleavage. F242A, H248A, and E264A substitutions all had drastic effects on cleavage, although there was slightly less SpoIVFB accumulation (Fig. 4.3A). SpoIVFB S260A and S260G accumulated well and cleaved Pro-σ^K(1-127) normally (Fig. 4.3B) despite S260 appearing to be located in an ATP-binding motif (Fig. 4.2A). E264D appeared to be a fully functional SpoIVFB substitution in *E. coli* (Fig. 4.3B) and considering the conservative nature of the substitution this was unsurprising. In contrast, with the exception of the S260 substitutions and E264D, there was very little accumulation of SpoIVFB and no Pro-σ^K processing observed for the other substitutions during *B. subtilis* sporulation (Fig. 4.5). Even processing by SpoIVFB E264D was greatly reduced. Why were the results of SpoIVFB substitutions so different in *B. subtilis*?

Expression of SpoIVFB in *E. coli* versus *B. subtilis* is different in numerous ways. First, the complement of proteases present in exponentially growing *E. coli* and sporulating *B. subtilis* is likely to be very different. Second, expression of SpoIVFB under T7 RNAP control in *E. coli* is likely much higher than expression from the native promoter in *B. subtilis*. Perhaps the SpoIVFB variants made in *E. coli* are just as unstable but production is so high that proteases cannot keep up, allowing the variants to accumulate. Third, the *E. coli* expression construct produces SpoIVFB with an additional N-terminal transmembrane segment called cytTM, from a rabbit cytochrome P450, and also creates a c-terminal $FLAG_2$-His_6 epitope tag. CytTM enhances accumulation of SpoIVFB in *E. coli* and the epitope tag allows easy detection [12,40]. Neither cytTM nor the tag are present in *B. subtilis*. Fourth, Pro-σ^K(1-127) was the substrate in *E. coli*, whereas full-length Pro-σ^K was the substrate in *B. subtilis.* It remains to be tested

whether these differences, especially cytTM, merely allow increased expression, or stabilize SpoIVFB in *E. coli*.

It is worth noting that substitutions in SpoIVFB [24] or Pro-σ^K [35] have produced inconsistent results in the *E. coli* and *B. subtilis* systems in previous studies. In the context of this study, methods to assess the secondary structure of SpoIVFB variants such as CD spectral analysis of purified protein may provide insight into whether observed instability *in vivo* may reflect improper folding. Conceivably, impaired ATP binding by variants could cause partial unfolding and increased protease susceptibility *in vivo*. Coexpressing a SpoIVFB variant with Pro-σ^K(1-127) in *E. coli* and purifying the SpoIVFB·Pro-σ^K(1-127) complex [35], then testing in the crosslinking assay described in this work may shed light on the effects of ATP binding. Also, efforts are underway in our group to improve the purification of SpoIVFB and Pro-σ^K(1-127) [35], and the ATP-dependent *in vitro* cleavage assay reported previously [12], which may provide another approach to test activity of the SpoIVFB variants reported here. Studying SpoIVFB by heterologous expression in *E. coli* and by expression in sporulating *B. subtilis* can provide a better understanding than either system alone, and biochemical approaches can shed additional light.

Substitutions in the SpoIVFB CBS domain have similar effects as substitutions in the interdomain linker of SpoIVFB

The phenomenon of SpoIVFB substitutions dramatically impairing Pro-σ^K(1-127) cleavage in *E. coli*, despite considerable accumulation, but accumulating very little when made in sporulating *B. subtilis*, was observed previously with substitutions in the interdomain linker [24]. Taken together the previous results and the results of this work suggest that the linker and the CBS domain play critical roles in stabilizing SpoIVFB in addition to their roles in substrate interaction and, in the case of the CBS domain, ATP binding [12,24].

Recently it was reported that SpoIVFB forms a homotetramer in complex with two Pro-σ^K subunits [32]. A molecular homology model of this 4:2 complex was generated based in part on constraints from *in* vivo disulfide crosslinking and *in vitro* chemical crosslinking experiments followed by mass spectrometry [24]. This model proposes an antiparallel arrangement of the four CBS domains. To accommodate packing of the four membrane domains of the SpoIVFB tetramer, the linkers of two monomers stretch across the MC cytoplasm-facing "bottom" of the CBS domain tetramer, precluding interaction with Pro-σ^K [24]. The linkers of the other two monomers interact with Pro-σ^K. These two different proposed roles of the linkers may explain why substitutions in some linker positions impact both Pro-σ^K cleavage and SpoIVFB stability. Linker residues may form critical contacts with CBS domains, as well as with SpoIVFB membrane domains and Pro-σ^K.

Conversely, CBS domain residues may contact linker residues, or they may contact another CBS domain or Pro-σ^K, or form part of the proposed ATP/AMP binding pocket. Hence, substitutions in the CBS domain may have multiple effects. Interpretation of the effects of CBS domain substitutions would likely benefit from future work aimed at determining the structure of the SpoIVFB CBS domain tetramer with and without nucleotides present, a feat achieved by several groups for a broad diversity of CBS domains [23], and by one group for an IMMP CBS domain tetramer [41]. By exploring the strategies and best practices utilized by other groups, a focused plan may allow successful structural determination of the SpoIVFB CBS domain tetramer and more direct evidence of the roles played by key residues.

Tagging SpoIVFB can be problematic in *B. subtilis*

B. subtilis strains designed to express SpoIVFB lacking the CBS domain and with or without a C-terminal $FLAG_2$-His_6 tag were generated. Neither strain processed Pro-σ^K (Fig. 4.4A). The tagged version migrated as expected but showed a possible breakdown product.

Because this tag inactivated full-length SpoIVFB, the tag may inactivate SpoIVFB(1-224). Accumulation of the untagged SpoIVFB(1-224) cannot be assessed because existing SpoIVFB antibodies were produced against the purified CBS domain [36]. These results contrast with recent findings that a different CBS domain deletion mutant encoding SpoIVFB(1-222)-YFP has limited activity on Pro-σ^K [25]. It is unlikely that an additional two-residue deletion from SpoIVFB would restore limited activity, rather, the YFP tag likely stabilizes the fusion protein. It was previously established that SpoIVFB is stabilized by a GFP fusion in some sporulation mutants when untagged SpoIVFB is unstable [42]. Biochemical approaches to explore how deletion of the CBS domain affects SpoIVFB structure, conformation, and activity, using methods mentioned above, may be fruitful.

Epitope tags often can facilitate research. In the absence of good antibodies, a tag can allow detection of proteins by immunoblotting, or localization by microscopy in the case of GFP. A tag can facilitate the purification of proteins, for instance by cobalt or nickel affinity with His tags. The ability to purify a protein opens the possibility to measure interactions of the native protein or variants with known interacting proteins using pull-down assays, or to identify novel interacting proteins using pull-down/mass spectrometry approaches. Various epitope tags have been used with SpoIVFB and Pro-σ^K in *E. coli* expression systems [12,17]. Recently the tag most often used by our group is the $FLAG_2$-His_6 tag [12,24,32,33,35]. Prior to the purification of a SpoIVFB antibody [24] we fused $FLAG_2$-His_6 to the C-terminal end of SpoIVFB in *B. subtilis* using a plasmid insertion construct, but the tag appeared to inhibit Pro-σ^K processing (Fig. 4.4A). In light of this result we tested whether tagged SpoIVFB activity in *E. coli* is lower than that of untagged SpoIVFB. Cleavage activity on coexpressed Pro-σ^K(1-127) was similar (Fig. 4.4B). The reason for this difference between *E. coli* and *B. subtilis* could again be due to the presence of cytTM on SpoIVFB in the *E. coli* system conferring activity by an unknown mechanism, or could be due to unappreciated consequences of tagging the C-terminus of

SpoIVFB with $FLAG_2$-His_6 in the environment of the *B. subtilis* MC cytoplasm during sporulation. Other potential reasons are mentioned above.

The purification of SpoIVFB antibodies provided a better method for detecting SpoIVFB variants in *B. subtilis* (Fig. 4.5) [24]. In *E. coli*, our evidence indicates that the $FLAG_2$-His_6 tag on the C-terminal end of SpoIVFB is inconsequential (Fig. 4.4B).

Suppressors stabilize SpoIVFB variants with destabilizing substitutions

The apparent instability of SpoIVFB variants in *B. subtilis* was surprising. In order to expand from these results a suppressor screen was performed by selecting for populations that acquire increased ability to form spores. Repeated passaging of strains carrying the E248A or H264A substitution produced populations of *B. subtilis* with increased ability to form spores by several orders of magnitude. Isolates carrying additional mutations in *spoIVFB* were detected by DNA sequencing and three residues of SpoIVFB were commonly substituted, H206, L227, and S260, strongly suggesting that substitutions at these positions can act as intragenic suppressors of the destabilizing E248A or H264A substitutions.

H206 was substituted to serine or tyrosine residues in different isolates. Interestingly, H206 was independently found to be important for cleavage of Pro-σ^K in *E. coli*, but not *B. subtilis* [24]. An H206A substitution blocked Pro-σ^K (1-127) cleavage in *E. coli*, but neither H206A nor H206F impaired processing of Pro-σ^K during *B. subtilis* sporulation. The apparent suppressing substitutions H206S and H206Y create polar side chains near the beginning of the interdomain linker, but it is not clear how this would stabilize the CBS domain with an E248A or H264A substitution. For these and the other apparent intragenic suppressors, genetic reconstruction experiments are needed. For example, expression of SpoIVFB H248A H206S in the *spoIVF* null mutant background is necessary to eliminate possible confounding effects of

Fig. 4.8

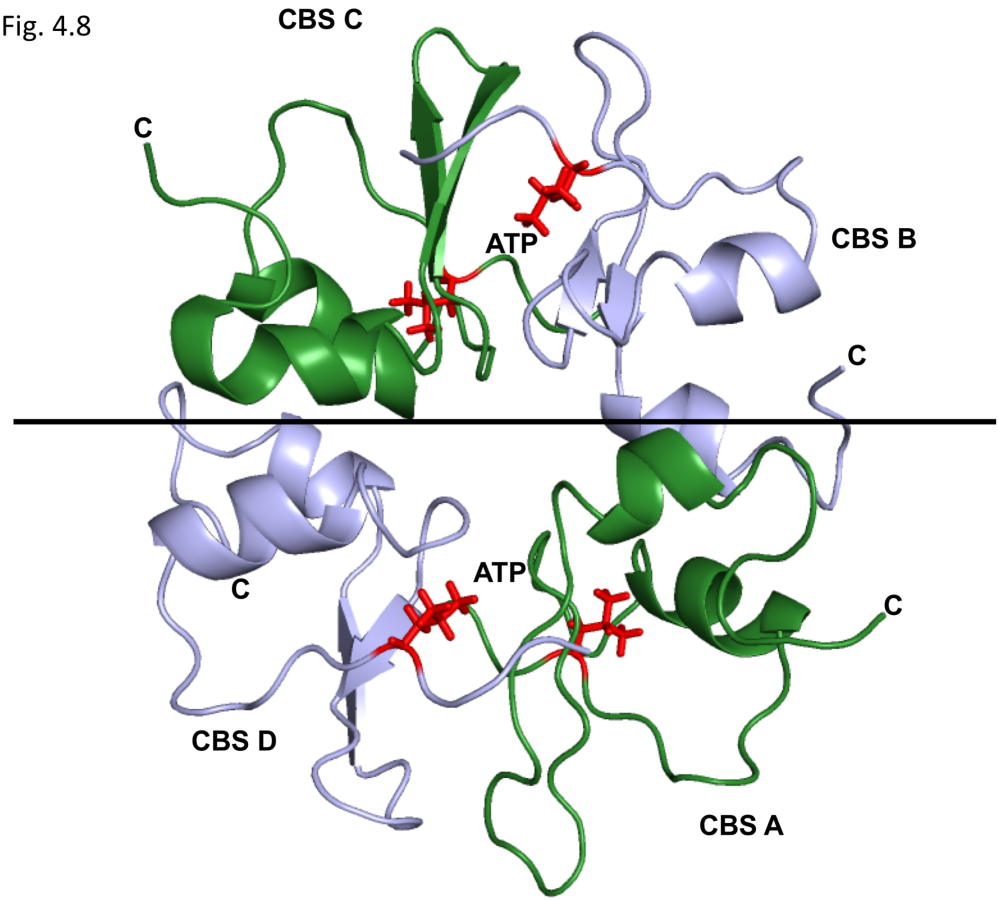

Figure 4.8 Location of L227. The homology model shown in Figure 1C is rotated slightly to emphasize locations of L227 (red) the proposed ATP-binding site in each CBS domain pair.

other mutations in *spoIVFB* or elsewhere in isolates from the suppressor screen. Likewise, the H206S substitution can be tested alone or in combination with other destabilizing SpoIVFB variants. Since the linker and Pro-σ^K make significant contacts [24], H206 substitutions may alter enzyme-substrate interactions. Alternatively, perhaps these substitutions allow flexibility that can mitigate instability. Ultimately, purification of SpoIVFB variants and biochemical analyses will be necessary to better understand SpoIVFB stability.

Another apparent suppressor was L227P (Fig. 4.7). L227 is part of **β**1 in the predicted CBS domain (Fig 2A). In a homology model of the SpoIVFB tetramer [24], L227 is located above and below the proposed ATP-binding pocket (Fig. 4.8). Perhaps L227P substitutes for interactions with ATP/AMP. Both H248A and E264A alter putative ATP/AMP binding motifs in the CBS domain (Fig 2A). By recreating an adenine-nucleotide-binding site, L227P may stabilize SpoIVFB via ATP/AMP binding.

S260N may similarly suppress instability by recreating an ATP-binding motif. S260 is part of the GQKLSQLD sequence predicted to interact with the 2' and/or 3' hydroxyls of ribose (Fig. 4.2A). S260N may shift the motif, creating an asparagine end and using S255 to reconstitute the serine. This would not conserve the proper spacing or critical glycine of the motif. However, neither SpoIVFB activity nor stability were fully restored in the isolates tested (Fig. 4.7). Additional S260 changes were tested in this work (Fig. 4.3B and 5). S260A and S260G were both generated in *E. coli* and *B. subtilis* and in both cases SpoIVFB activity was conserved despite S260 being part of a proposed ATP/AMP binding motif. Perhaps S260A and S260G provide flexibility that allows SpoIVFB to mimic conformational changes in the CBS domain that normally occur upon ATP binding.

Our results suggest that substitutions at several positions in the SpoIVFB interdomain linker and CBS domain may counteract instability caused by substitutions in the CBS domain. Two residues, L227P and S260N, may create novel ATP-binding motifs, while the H206S and H206Y substitutions may provide additional stability to the SpoIVFB tetramer. Testing these

possibilities with an ATP-binding assay such as the one that relies on crosslinking with AMAS (Fig 4.1) will be an important future direction. Other substitutions to residues in the linker and CBS domain have previously stabilized SpoIVFB. In a screen to isolate suppressors of a temperature-sensitive *spoIVFAΔ91* mutant, substitutions at sites 207 (linker), 221, 235, and 273 (CBS domain) were found to reconstitute SpoIVFB activity at both 30°C and 37°C [14,43]. These substitutions appeared to stabilize a 6-transmembrane configuration of SpoIVFB as opposed to a 4-transmembrane conformation, as determined by PhoA/LacZ fusions [43]. These findings, taken together with ours, seem to converge on the idea that the linker and CBS domain play a critical role in maintaining SpoIVFB structure.

Conclusions

This work has contributed exciting new understanding of ways that SpoIVFB might use ATP/AMP binding to regulate activity. These findings may apply directly to other CBS domain-containing IMMPs. Crosslinking detected movement of a residue in the active site of SpoIVFB relative to a residue near the cleavage site of Pro-σ^K. This apparent conformational change is modulated by ATP and AMP binding. We further showed that residues predicted to be in conserved ATP or AMP binding motifs are critical for Pro-σ^K(1-127) cleavage in *E. coli* and for SpoIVFB stability in *B. subtilis*. Suppressor isolates which restore SpoIVFB accumulation were found to carry additional substitutions in SpoIVFB that may generate new ATP-binding sites or promote SpoIVFB stability in general. This work has provided novel findings and avenues for future research that will contribute significantly to general knowledge of IMMPs and their regulation.

APPENDICES

APPENDIX A

Contributions to another publication

I have contributed to the following publication during my dissertation work.

Zhang Y, Halder S, Kerr RA, Parrell D, Ruotolo B, Kroos L. Complex formed between intramembrane metalloprotease SpoIVFB and its substrate, Pro-σ^K. J Biol Chem. 2016;291: 10347–62. doi:10.1074/jbc.M116.715508

My contributions to this work included performing stepwise photobleaching on *Bacillus subtilis* containing a SpoIVFB-GFP fusion. Total internal reflection fluorescence (TIRF) microscopy was used to visualize SpoIVFB complexes during sporulation over time. As imaging continued individual subunits of SpoIVFB photobleached resulting in a measurable drop in fluorescence intensity. Using this technique a tetramer of SpoIVFB subunits were consistently determined by observing four photobleaching events. These findings supported other data from the publication demonstrating SpoIVFB forms a tetrameric complex. For further information the publication can be found at the citation above.

APPENDIX B

Contributions to another publication

I have contributed to the following publication during my dissertation work.

> Halder S, **Parrell D**, Whitten D, Feig M and Kroos L. Interaction of intramembrane metalloprotease SpoIVFB with substrate Pro-σ^K. 2017. *PNAS Plus* 114 (50):E10677–E10686.

My contributions to this work included affinity purifying SpoIVFB antibodies, generating amino acid substitutions to SpoIVFB in *B.* subtilis and performing sporulation with the resulting strains. Samples were collected and immunoblot analysis with antibodies against SpoIVFA, SpoIVFB and Pro-σ^K were performed. I also carried out dilution plating and enumeration of these cultures for calculating sporulation efficiency. Finally, I contributed significantly to generating figures and the editing of this manuscript.

REFERENCES

REFERENCES

1. Kroos L. The *Bacillus* and *Myxococcus* Developmental Networks and Their Transcriptional Regulators. Annu Rev Genet. 2007;41: 13–39. doi:10.1146/annurev.genet.41.110306.130400

2. Ben-Yehuda S, Losick R. Asymmetric cell division in *B. subtilis* involves a spiral-like intermediate of the cytokinetic protein FtsZ. Cell. 2002;109: 257–266. doi:10.1016/S0092-8674(02)00698-0

3. Thompson LS, Beech PL, Real G, Henriques AO, Harry EJ. Requirement for the cell division protein DivIB in polar cell division and engulfment during sporulation in *Bacillus subtilis*. J Bacteriol. 2006;188: 7677–7685. doi:10.1128/JB.01072-06

4. Iber D, Clarkson J, Yudkin MD, Campbell ID. The mechanism of cell differentiation in *Bacillus subtilis*. Nature. 2006;441: 371–374. doi:10.1038/nature04666

5. Imamura D, Kuwana R, Kroos L, Feig M, Takamatsu H, Watabe K. Substrate specificity of SpoIIGA, a signal-transducing aspartic protease in Bacilli. J Biochem. 2011;149: 665–671. doi:10.1093/jb/mvr027

6. Flanagan KA, Comber JD, Mearls E, Fenton C, Wang Erickson AF, Camp AH. A Membrane-embedded amino acid couples the SpoIIQ channel protein to anti-sigma factor transcriptional repression during *Bacillus subtilis* sporulation. J Bacteriol. 2016;198: 1451–1463. doi:10.1128/JB.00958-15

7. Kroos L, Kunkel B, Losick R. Switch protein alters specificity of RNA polymerase containing a compartment-specific sigma factor. Science. 1989;243: 526–529. doi:10.1126/science.2492118

8. Yu Y-TTYTN, Kroos L. Evidence that SpoIVFB is a novel type of membrane metalloprotease governing intercompartmental communication during *Bacillus subtilis* sporulation. J Bacteriol. 2000;182: 3305–9. doi:10.1128/JB.184.19.5393-5401.2002

9. Rudner DZ, Fawcett P, Losick R. A family of membrane-embedded metalloproteases involved in regulated proteolysis of membrane-associated transcription factors. Proc Natl Acad Sci U S A. 1999;96: 14765–70. doi:10.1073/pnas.96.26.14765

10. Urban S. Making the cut: Central roles of intramembrane proteolysis in pathogenic microorganisms. Nat Rev Microbiol. 2009;7: 411–423. doi:10.1038/nrmicro2130

11. Kroos L, Akiyama Y. Biochemical and structural insights into intramembrane metalloprotease mechanisms. Biochim Biophys Acta - Biomembr. doi:10.1016/j.bbamem.2013.03.032

12. Zhou R, Cusumano C, Sui D, Garavito RM, Kroos L. Intramembrane proteolytic cleavage of a membrane-tethered transcription factor by a metalloprotease depends on ATP. Proc Natl Acad Sci. 2009;106: 16174–16179. doi:10.1073/pnas.0901455106

13. Cutting S, Oke V, Driks A, Losick R, Lu S, Kroos L. A forespore checkpoint for mother cell gene expression during development in *Bacillus subtilis*. Cell. 1990;62: 239–250.

14. Cutting S, Roels S, Losick R. Sporulation operon *spoIVF* and the characterization of mutations that uncouple mother-cell from forespore gene expression in *Bacillus subtilis*. J Mol Biol. 1991;221: 1237–1256. doi:10.1016/0022-2836(91)90931-U

15. Ricca E, Cutting S, Losick R. Characterization of *bofA*, a gene involved in intercompartmental regulation of pro-σ^K processing during sporulation in *Bacillus subtilis*. J Bacteriol. 1992;174: 3177–84. Available: http://www.ncbi.nlm.nih.gov/pubmed/1577688

16. Rudner DZ, Losick R. A sporulation membrane protein tethers the pro-σ^K processing enzyme to its inhibitor and dictates its subcellular localization. Genes Dev. 2002;16: 1007–1018. doi:10.1101/gad.977702

17. Zhou R, Kroos L. BofA protein inhibits intramembrane proteolysis of pro-σ^K in an intercompartmental signaling pathway during *Bacillus subtilis* sporulation. Proc Natl Acad Sci U S A. 2004;101: 6385–90. doi:10.1073/pnas.0307709101

18. Wakeley PR, Dorazi R, Hoa NT, Bowyer JR, Cutting SM. Proteolysis of SpoIVB is a critical determinant in signalling of Pro-σ^K processing in *Bacillus subtilis*. Mol Microbiol. 2000;36: 1336–48. doi:10.1046/J.1365-2958.2000.01946.X

19. Cutting S, Driks A, Schmidt R, Kunkel B, Losick R. Forespore-specific transcription of a gene in the signal transduction pathway that governs Pro-σ^K processing in *Bacillus subtilis*. Genes Dev. 1991;5: 456–66. doi:10.1101/GAD.5.3.456

20. Zhou R, Kroos L. Serine proteases from two cell types target different components of a complex that governs regulated intramembrane proteolysis of pro-σ^K during *Bacillus subtilis* development. Mol Microbiol. 2005;58: 835–846. doi:10.1111/j.1365-2958.2005.04870.x

21. Campo N, Rudner DZ. A branched pathway governing the activation of a developmental transcription factor by regulated intramembrane proteolysis. Mol Cell. 2006;23: 25–35. doi:10.1016/j.molcel.2006.05.019

22. Baykov AA, Tuominen HK, Lahti R. The CBS domain: A protein module with an emerging prominent role in regulation. ACS Chem Biol. 2011;6: 1156–1163. doi:10.1021/cb200231c

23. Ereño-Orbea J, Oyenarte I, Martínez-Cruz LA. CBS domains: Ligand binding sites and conformational variability. Arch Biochem Biophys. 2013;540: 70–81. doi:10.1016/j.abb.2013.10.008

24. Halder S, Parrell D, Whitten D, Feig M, Kroos L. Interaction of intramembrane metalloprotease SpoIVFB with substrate Pro-σ^K. Proc Natl Acad Sci USA. 2017;114: E10677–E10686. doi:10.1073/pnas.1711467114

25. Ramírez-Guadiana FH, Rodrigues CDA, Marquis KA, Campo N, Barajas-Ornelas R del C, Brock K, et al. Evidence that regulation of intramembrane proteolysis is mediated by

substrate gating during sporulation in *Bacillus subtilis*. PLOS Genet. e1007753. doi:10.1371/journal.pgen.1007753

26. Harwood CR, Cutting SM. Molecular biological methods for *Bacillus*. Chichester ;New York: 1990. https://www.worldcat.org/title/molecular-biological-methods-for-bacillus/oclc/21482555

27. Shimotsu H, Henner DJ. Construction of a single-copy integration vector and its use in analysis of regulation of the *trp* operon of *Bacillus subtilis*. Gene. 1986;43: 85–94. doi:10.1080/10548408.2013.751272

28. Sterlini JM, Mandelstam J. Commitment to sporulation in *Bacillus subtilis* and its relationship to development of actinomycin resistance. Biochem J. 1969;113: 29–37.

29. Notredame C, Higgins DG, Heringa J. T-coffee: A novel method for fast and accurate multiple sequence alignment. J Mol Biol. 2000;302: 205–217. doi:10.1006/jmbi.2000.4042

30. Drozdetskiy A, Cole C, Procter J, Barton GJ. JPred4: A protein secondary structure prediction server. Nucleic Acids Res. Oxford University Press; 2015;43: W389–W394. doi:10.1093/nar/gkv332

31. Lu S, Halberg R, Kroos L. Processing of the mother-cell sigma factor, σ^K, may depend on events occurring in the forespore during *Bacillus subtilis* development. Proc Natl Acad Sci U S A. 1990;87: 9722–6.

32. Zhang Y, Halder S, Kerr RA, Parrell D, Ruotolo B, Kroos L. Complex formed between intramembrane metalloprotease SpoIVFB and its substrate, Pro-σ^K. J Biol Chem. 2016;291: 10347–62. doi:10.1074/jbc.M116.715508

33. Zhang Y, Luethy PM, Zhou R, Kroos LLK. Residues in conserved loops of intramembrane metalloprotease Spoivfb interact with residues near the cleavage site in pro-σ^K. J Bacteriol. 2013;195: 4936–4946. doi:10.1128/JB.00807-13

34. Scott JW, Hawley SA, Green KA, Anis M, Stewart G, Scullion GA, Norman D, Hardie G. CBS domains form energy-sensing modules whose binding of adenosine ligands is disrupted by disease mutations. J Clin Invest. 2004;113: 274–284. doi:10.1172/JCI19874

35. Zhou R, Chen K, Xiang X, Gu L, Kroos L. Features of Pro-σ^K important for cleavage by SpoIVFB, an intramembrane metalloprotease. J Bacteriol. 2013;195: 2793–806. doi:10.1128/JB.00229-13

36. Kroos L, Yu YT. Regulation of sigma factor activity during *Bacillus subtilis* development. Curr Opin Microbiol. 2000;3: 553–560. doi:S1369-5274(00)00140-5

37. Lu S, Kroos L. Overproducing the *Bacillus subtilis* mother cell sigma factor precursor, Pro-σ^K, uncouples σ^K -dependent gene expression from dependence on intercompartmental communication. J Bacteriol. 1994;176: 3936–43. Available: http://www.ncbi.nlm.nih.gov/pubmed/8021176

38. Feng L, Yan H, Wu Z, Yan N, Wang Z, Jeffrey PD, et al. Structure of a site-2 protease

family intramembrane metalloprotease. Science. 2007;318: 1608–12. doi:10.1126/science.1150755

39. Hardie DG, Lin S-C. AMP-activated protein kinase - not just an energy sensor. F1000Research. 2017;6: 1724. doi:10.12688/f1000research.11960.1

40. Saribas AS, Gruenke L, Waskell L. Overexpression and purification of the membrane-bound cytochrome P450 2B4. Protein Expr Purif. 2001;21: 303–309. doi:10.1006/prep.2000.1377

41. Schacherl M, Gompert M, Pardon E, Lamkemeyer T, Steyaert J, Baumann U. Crystallographic and biochemical characterization of the dimeric architecture of site-2 protease. Biochim Biophys acta Biomembr. 2017;1859: 1859–1871. doi:10.1016/j.bbamem.2017.05.006

42. Doan T, Rudner DZ. Perturbations to engulfment trigger a degradative response that prevents cell-cell signalling during sporulation in *Bacillus subtilis*. Mol Microbiol. 2007;64: 500–511. doi:10.1111/j.1365-2958.2007.05677.x

43. Green DH, Cutting SM. Membrane topology of the *Bacillus subtilis* Pro-σ^K processing complex. J Bacteriol. 2000;182: 278–285. doi:10.1128/JB.182.2.278-285.2000

44. Fort P, Errington J. Nucleotide Sequence and Complementation Analysis of a Polycistronic Sporulation Operon, spoVA, in Bacillus subtilis. Microbiology. 1985;131: 1091–1105. doi:10.1099/00221287-131-5-1091

45. Youngman P, Perkins JB, Losick R. Construction of a cloning site near one end of Tn917 into which foreign DNA may be inserted without affecting transposition in Bacillus subtilis or expression of the transposon-borne erm gene. Plasmid. 1984;12: 1–9. doi:10.1016/0147-619X(84)90061-1

CHAPTER 5: Conclusions and Future Directions - The Future is Bright for Understanding IMMPs

The IMMP field has grown significantly in the past decade. A number of prominent IMMPs from model organisms (RseP, SpoIVFB and RasP) have allowed strides to be made toward answering fundamental mechanistic questions. Importantly, these findings have been applied successfully to a number of pathogen models [1,2] (Chapter 1). This expansion of IMMP models and especially their role in regulating pathogenesis underscores the importance of pursuing better understanding of IMMP function. In this work we have expanded the study of two IMMPs (RasP and SpoIVFB) from the model organism *B. subtilis* and in doing so have contributed to fundamental knowledge about IMMP function. In this concluding chapter, key findings from this work will be reviewed in the context of potential future directions and outstanding questions in the field.

RasP as a model for molecular biology and molecular evolution

Significant progress was made toward understanding RasP proteolysis, as well as toward establishing tools to study RasP [3]. One major accomplishment was the refinement of heterologous expression systems for studying RasP and its substrates, RsiW and FtsL, in *E. coli*. The most beneficial strategies included fusing RasP to cytTM and the first transmembrane segment of SpoIVFB, tagging potential substrates with His_6-MBP, tagging SpoIVFB with $FLAG_2$-His_6 for immunoblot detection, and generating an inactive RasP E21A construct as a negative control. With these refinements in hand, RasP-dependent disappearance of RsiW and FtsL was demonstrated upon coexpression in *E. coli* [3]. The reason processed substrates disappear in *E. coli* is still an outstanding question since testing of a *clpP* mutant in *E. coli* proved uninformative; however, a more expansive screen of *E. coli* protease mutants might reveal the protease(s) causing disappearance. An intriguing extension of the work in *E. coli* will be to

carefully test the prevailing “size exclusion” or “molecular sieve” model for substrate recognition [4]. We found that some non-substrate transmembrane proteins coexpressed with RasP also disappeared, like proper substrates of RasP [3], suggesting that RasP may have promiscuous activity on transmembrane proteins of the proper size. To further test this model, chimeric constructs of non-RsiW transmembrane helices with the full-length and site-1-processed extracellular domains of RsiW, as well as fusions of the RsiW transmembrane domain with extracellular regions of varying size, will allow more direct testing of whether the PDZ domain acts as a passive size exclusion filter or requires specific recognition sequences.

RasP was the third IMMP to be purified and exhibit activity on a physiological substrate [3]. In this assay, site-1 cleavage of RsiW was necessary for RasP cleavage, as shown by comparing full-length and truncated RsiW constructs. FtsL however, was not processed *in vitro,* despite apparent processing in *E. coli* [3,5]. The failure of *in vitro* processing *in vitro* may reflect the absence of a conserved factor that is present in both *E. coli* and *B. subtilis*. The cell division protein DivIC may be this factor. DivIC was reported to stabilize FtsL [6], and homologs of DivIC are present in *E. coli* [7]. Perhaps DivIC, or a shortened form if analogous site-1 cleavage is required, plays a role, not just for stabilization of FtsL *in vivo*, but also for recognition as a substrate by RasP. Purified DivIC could be added to *in vitro* reactions with RasP and FtsL to test whether DivIC is required for processing. Recovered processing would suggest that DivIC and FstL remain associated following release from the divisome, promoting RasP cleavage.

Another interesting future direction related to FtsL is exploring RasP localization. The role of RasP during extramembrane stress is unlikely to require a specific subcellular localization of RasP. However, FstL processing and the role of RasP during cell division makes a strong case for possible subcellular localization of RasP to the divisome. FstL associates with DivIC and several other divisome proteins and is localized to the division septum [6,8,9]. Perhaps RasP is diffuse in the membrane while cells are not dividing or during extracellular stress, but localizes to the division septum during cell division to better act on FtsL. Generating

a GFP fusion to RasP may allow these questions to be addressed, and provide a better understanding of how dynamic IMMP localization is based on required functions.

Lastly, RasP and its homologous protein in *E. coli* RseP have given rise to the discovery of several other PDZ domain-containing IMMPs. Equally diverse have become the number of substrates and physiological responses these IMMPs appear to mediate. This newfound diversification of IMMPs and their function presents an exciting opportunity to study enzyme/substrate evolution. Using phylogenetic analysis of RasP homologs, or the diverse anti-sigma factor and FtsL-like substrates, it may be possible to understand what bacterial processes derived from similar processes in other bacteria. The potential advantages of this are several fold. Such knowledge may expedite the identification of processes in emerging pathogens. Existing knowledge from one system may provide more confidence in deciding which methods are best to study homologous systems. Conservation analysis could allow rapid detection of highly conserved and potentially critical regions of homologous proteins. In addition to these advantages, researching the relationships of diverse enzyme/substrate pairs will allow the study of enzyme/substrate co-evolution. Identifying critically conserved interaction surfaces of IMMPs will direct researchers to important regions to target for studies of structure and function, or to more effectively detect critical regions/interactions to target when designing inhibitors of IMMPs and their substrates. As more gene and genome sequences become available these types of analyses should become increasingly important and accessible.

SpoIVFB and the SpoIIQ-SpoIIIA channels: from conformational change to multicomplex structures

With help from a wealth of literature background and established methods, significant discoveries related to ATP/AMP binding to SpoIVFB (Chapter 4) and regulation by cellular levels of adenine nucleotides (Chapter 3) emerged. Using a mono-Cys complex of SpoIVFB E44C and Cysless Pro-σ^K, and chemical crosslinkers, a conformational change responsive to

ATP and AMP was inferred (Chapter 4). To expand from these results, a number of promising experiments could take advantage of the crosslinkable complex. For instance, recent evidence suggests that an F66A substitution in SpoIVFB results in constitutively active SpoIVFB (without the need for SpoIVB to relieve inhibition by BofA and SpoIVFA) [10]. What happens when an F66A substitution is introduced into the crosslinkable complex? One possibility is that the complex will be locked into one conformation despite the presence of ATP or AMP. Perhaps crosslinking by AMAS will be no different with or without ATP. On the other hand, if the F66A substitution allows Pro-σ^K binding, but ATP-binding to the CBS domain still plays a role in positioning the substrate for cleavage, perhaps AMAS crosslinking will remain sensitive to ATP and AMP. An additional crosslinking experiment to test for conformational change would involve testing for the proposed open and closed conformations of SpoIVFB. Movements of SpoIVFB transmembrane (TM) helices one and six are proposed to create open and closed conformations of SpoIVFB [10,11]. TM-1 and TM-6 residues in close proximity in the closed conformation could be substituted to residues providing the required chemistry for crosslinking. A crosslinker of the proper length to crosslink the closed conformation, but not the open conformation would be used. Residues in TM-1 and TM-6 within close proximity would be determined using a molecular homology model [12]. Chemical crosslinkers of distances greater and smaller than AMAS and Sulfo-SMCC exist, so customization of the required conditions is possible based on the expected movement distances. If successful, this strategy could be adapted to other regions of the complex where conformational changes might occur, for instance in the CBS domain.

Another major result was the discovery that highly conserved residues in the SpoIVFB CBS domain (Chapter 4) and interdomain linker [12] are important for cleavage of Pro-σ^K(1-127) upon coexpression in *E. coli*. A surprising result was that substitutions at these residues render SpoIVFB unstable in sporulating *B. subtilis*. This result makes the effects of substitutions

difficult to interpret. A potential solution is to determine the structure of the interdomain linker and CBS domain. CBS domains are well-studied, and a wealth of structural studies have demonstrated methods effective for crystallization [13]. Yet, crystallization of an IMMP dimer of tandem CBS domains proved challenging [14]. Through careful consideration of the literature a plan using best practices may yield a structure of the SpoIVFB CBS domain and/or the CBS+ATP and CBS+AMP structures. Achieving these structures may determine the role of critical residues more precisely, and demonstrate whether the CBS domain takes on alternate conformations in the presence of different nucleotides. Many CBS domain-containing proteins undergo conformational change due to nucleotide binding [13,15]. Understanding different conformations of the CBS domain will generate new hypotheses about how ATP/AMP binding translates into regulating other conformational changes in SpoIVFB, and SpoIVFB activity.

The work described in this dissertation also involved developing an *in vivo* ATP sensor which used luciferase activity to monitor cellular ATP levels (Chapter 3). The ATP levels in the MC and FS compartments changed significantly over the course of sporulation. ATP levels also changed in the presence of mutations disrupting production of proteins that are part of a proposed “feeding tube” or channel (Chapter 3). These experiments established that channel destruction upon engulfment completion during normal sporulation, or mutational disruption of channels, likely causes the ATP level to rise in the MC, supporting the notion that one or more molecules impacting cellular ATP levels are transferred from the MC to FS. What could this molecule(s) be? In order to address the identity of the channel substrate recent innovations in both mass spectrometry and computational capabilities may provide exciting new opportunities in the form of untargeted metabolomics [16,17]. Untargeted metabolomics of wild-type *B. subtilis* and a channel disrupting mutant (e.g., *spoIIIAA*) during sporulation could possibly identify metabolites whose concentrations differ because of channel activity. Once metabolites of interest are identified, genetic approaches targeting components of the corresponding metabolic pathways could be used to probe involvement in sporulation and specifically in

relation to channel function. Defining channel-dependent metabolic pathways would contribute to better understanding of how channels control FS gene expression after engulfment.

Another question to address using mass spectrometry would be whether ATP, ADP and AMP levels relate to SpoIVFB activity. Chapter 3 demonstrates that ionophores and chloramphenicol can lower ATP levels significantly during sporulation. Despite causing similar changes in the ATP level, the effects of the two types of treatment on SpoIVFB activity were different (Chapter 3). We proposed that a difference in cellular ATP versus other adenine nucleotide levels may comprise a change in energy status that the CBS domain would measure. Considering the effect of AMP on ATP-dependent crosslinking of the SpoIVFB·Pro-σ^K complex described in Chapter 4, AMP may be the other nucleotide that reports the cellular energy status. However, luciferase only uses ATP, so a different approach is needed to measure AMP levels. By measuring AMP levels after each treatment using mass spectrometry, it may be possible to gain further evidence that a difference in the AMP level can regulate SpoIVFB activity. This method of testing would lose the advantage of cell-type specific measurements meaning it would be difficult to differentiate the contribution of the MC or FS to any differences.

Finally, it is an exciting time to study large macromolecular complexes. Improvements in cryoelectron microscopy (cryo-EM) and cryoelectron tomography (cryo-ET) have enabled the study of proteins and protein complexes at resolutions that were previously unattainable. The channels connecting the FS and MC are reminiscent of bacterial secretion systems [18,19] and are good candidates for study via cryo-ET. A number of individual channel protein structures have been solved recently, either by crystallography or single-particle cryo-EM [20–24]. Utilizing cryo-ET on whole cells, to solve the structure of entire channel complexes in the inner and outer FS membranes presents an exciting opportunity to solve the native structure. The channels appear to form additional interactions with other important protein complexes during sporulation [25]. These inter-complex interactions may be weak, or transient, and difficult to reconstitute *in vitro*, making cryo-ET experiments with whole cells an attractive approach. Cryo-

ET of whole cells is not without its difficulties; however, new technology and instrumentation are enabling rapid expansion of the field [26]. Indeed, a number of bacterial secretion systems have been studied in their native membrane environment using cryo-ET [27]. Better understanding the channels of sporulating *B. subtilis* will contribute new knowledge of a specialized secretion system that carries out intercellular communication.

Closing remarks

The work described in this dissertation has benefitted greatly from the established genetics, methodologies, and rich literature base of the *B. subtilis* field. I thank all of those who came before me, and those who more directly provided strains, antibodies or advice. Our findings have contributed broadly to advancing fundamental understanding of IMMP function, but also have contributed to a better understanding a number of ongoing questions more narrowly about sporulation of *B. subtilis*. A great amount of work lies ahead in the pursuit of understanding IMMP function and sporulation, but doing so will undoubtedly result in the continued development of exciting new techniques, and the explanation of novel biological concepts and phenomena. I look forward to what the future has in store for the study of IMMPs and sporulation.

REFERENCES

REFERENCES

1. Schneider JS, Glickman MS. Function of site-2 proteases in bacteria and bacterial pathogens. Biochim Biophys Acta - Biomembr. 2013;1828: 2808–2814. doi:10.1016/j.bbamem.2013.04.019

2. Urban S. Making the cut: Central roles of intramembrane proteolysis in pathogenic microorganisms. Nat Rev Microbiol. 2009;7: 411–423. doi:10.1038/nrmicro2130

3. Parrell D, Zhang Y, Olenic S, Kroos L. *Bacillus subtilis* intramembrane protease RasP activity in *Escherichia coli* and in vitro. J Bacteriol. 2017;199. doi:10.1128/JB.00381-17

4. Hizukuri Y, Oda T, Tabata S, Tamura-Kawakami K, Oi R, Sato M, et al. A structure-based model of substrate discrimination by a noncanonical PDZ tandem in the intramembrane-cleaving protease RseP. Structure. 2014;22: 326–336. doi:10.1016/j.str.2013.12.003

5. Bramkamp M, Weston L, Daniel RA, Errington J. Regulated intramembrane proteolysis of FtsL protein and the control of cell division in *Bacillus subtilis*. Mol Microbiol. 2006;62: 580–591. doi:10.1111/j.1365-2958.2006.05402.x

6. Wadenpohl I, Bramkamp M. DivIC stabilizes FtsL against RasP cleavage. J Bacteriol. American Society for Microbiology Journals; 2010;192: 5260–5263. doi:10.1128/JB.00287-10

7. Villanelo F, Ordenes A, Brunet J, Lagos R, Monasterio O. A model for the *Escherichia coli* FtsB/FtsL/FtsQ cell division complex. BMC Struct Biol. 2011;11: 28. doi:10.1186/1472-6807-11-28

8. Buddelmeijer N, Beckwith J. A complex of the *Escherichia coli* cell division proteins FtsL, FtsB and FtsQ forms independently of its localization to the septal region. Mol Microbiol. 2004;52: 1315–1327. doi:10.1111/j.1365-2958.2004.04044.x

9. Ghigo JM, Beckwith J. Cell division in *Escherichia coli*: role of FtsL domains in septal localization, function, and oligomerization. J Bacteriol. 2000;182: 116–29. doi:10.1128/JB.182.1.116-129.2000

10. Ramirez-Guadiana FH, Rodrigues CDA, Marquis KA, Campo N, Barajas-Ornelas RDC, Brock K, et al. Evidence that regulation of intramembrane proteolysis is mediated by substrate gating during sporulation in *Bacillus subtilis*. PLoS Genet. 2018;14(11):e1007753. doi: 10.1371/journal.pgen.1007753.

11. Zhou R, Cusumano C, Sui D, Garavito RM, Kroos L. Intramembrane proteolytic cleavage of a membrane-tethered transcription factor by a metalloprotease depends on ATP. Proc Natl Acad Sci. USA 2009; 106: 16174–16179. doi:10.1073/pnas.0901455106

12. Halder S, Parrell D, Whitten D, Feig M, Kroos L. Interaction of intramembrane metalloprotease SpoIVFB with substrate Pro-σ^K. Proc Natl Acad Sci. USA. 2017; 114: E10677–E10686. doi:10.1073/pnas.1711467114

13. Ereño-Orbea J, Oyenarte I, Martínez-Cruz LA. CBS domains: Ligand binding sites and conformational variability. Arch Biochem Biophys. 2013;540: 70–81. doi:10.1016/j.abb.2013.10.008

14. Schacherl M, Gompert M, Pardon E, Lamkemeyer T, Steyaert J, Baumann U. Crystallographic and biochemical characterization of the dimeric architecture of site-2 protease. Biochim Biophys acta Biomembr. 1859: 1859–1871. doi:10.1016/j.bbamem.2017.05.006

15. Baykov AA, Tuominen HK, Lahti R. The CBS domain: A protein module with an emerging prominent role in regulation. ACS Chem Biol. 2011; 6: 1156–1163. doi:10.1021/cb200231c

16. Vinayavekhin N, Saghatelian A. Untargeted Metabolomics. Current Protocols in Molecular Biology. Hoboken, NJ, USA: 2010. p. 30.1.1-30.1.24. doi:10.1002/0471142727.mb3001s90

17. Meyer H, Weidmann H, Lalk M. Methodological approaches to help unravel the intracellular metabolome of *Bacillus subtilis*. Microb Cell Fact. 2013;12: 69. doi:10.1186/1475-2859-12-69

18. Doan T, Morlot C, Meisner J, Serrano M, Henriques AO, Moran CP, et al. Novel secretion apparatus maintains spore integrity and developmental gene expression in *Bacillus subtilis*. PLoS Genet. 2009;5: e1000566. doi:10.1371/journal.pgen.1000566

19. Camp AH, Losick R. A novel pathway of intercellular signalling in *Bacillus subtilis* involves a protein with similarity to a component of type III secretion channels. Mol Microbiol. 2008;69: 402–417. doi:10.1111/j.1365-2958.2008.06289.x

20. Meisner J, Maehigashi T, Andre I, Dunham CM, Moran CP, Jr. Structure of the basal components of a bacterial transporter. Proc Natl Acad Sci USA. 2012;109(14):5446-51. doi: 10.1073/pnas.1120113109.

21. Zeytuni N, Hong C, Flanagan KA, Worrall LJ, Theiltges KA, Vuckovic M, et al. Near-atomic resolution cryoelectron microscopy structure of the 30-fold homooligomeric SpoIIIAG channel essential to spore formation in *Bacillus subtilis*. Proc Natl Acad Sci USA. 2017; 114(34):E7073-E81. doi: 10.1073/pnas.1704310114.

22. Rodrigues CD, Henry X, Neumann E, Kurauskas V, Bellard L, Fichou Y, et al. A ring-shaped conduit connects the mother cell and forespore during sporulation in *Bacillus subtilis*. Proc Natl Acad Sci USA. 2016;113(41):11585-90. doi: 10.1073/pnas.1609604113.

23. Zeytuni N, Flanagan KA, Worrall LJ, Massoni SC, Camp AH, Strynadka NCJ. Structural characterization of SpoIIIAB sporulation-essential protein in *Bacillus subtilis*. J Struct Biol. 2018;202: 105–112. doi:10.1016/j.jsb.2017.12.009

24. Levdikov VM, Blagova E V., McFeat A, Fogg MJ, Wilson KS, Wilkinson AJ. Structure of components of an intercellular channel complex in sporulating *Bacillus subtilis*. Proc Natl Acad Sci. USA 2012;109: 5441–5445. doi:10.1073/pnas.1120087109

25. Kroos L, Akiyama Y. Biochemical and structural insights into intramembrane metalloprotease mechanisms. Biochim Biophys Acta - Biomembr. 2013;1828: 2873–2885. doi:10.1016/j.bbamem.2013.03.032

26. Briegel A, Jensen G. Progress and potential of electron cryotomography as illustrated by its application to bacterial chemoreceptor arrays. Annu Rev Biophys. 2017;46: 1–21. doi:10.1146/annurev-biophys-070816-033555

27. Rapisarda C, Tassinari M, Gubellini F, Fronzes R. Using cryo-EM to investigate bacterial secretion systems. Annu Rev Microbiol. Annual Reviews; 2018;72: 231–254. doi:10.1146/annurev-micro-090817-062702